The Structure of a Supernova-dominated Cloudy Interstellar Medium

Stephen Richard Heathcote

Ph. D.

Edinburgh University

1983

ABSTRACT

The interstellar medium in our Galaxy is highly inhomogeneous and is kept in a highly disturbed state by the large input of energy by supernova explosions. Under such circumstances, supernova remnants and interstellar clouds co-exist in a symbiotic relationship the parameters of each being determined by those of the other through the agency of the various interactions between them.

I here develop a simple model of such a supernova dominated cloudy interstellar medium (SDC-ISM). Although based on the work of McKee and Ostriker (1977) it has been extended in several important respects. This model is subjected to an exhaustive parameter search in order to locate the boundaries of its domain of validity and to establish the sensitivity of the model to its various input parameters.

This representation of the SDC-ISM is then combined with a simple model of the structure of the galaxy constructed within the framework of the spiral density wave theory. It is shown that the high temperature component of the ISM is ubiquitous both within the spiral arms and in the interarm region. It then follows that the strong spiral shock assumed can only be supported if quite restrictive conditions are imposed on the galactic supernova rate and the interstellar gas density.

During this investigation the need for a more detailed description of the dynamical interaction between an SNR shock and an interstellar cloud was identified. To meet this need I have constructed a highly approximate but simple model of this process which is then used to explore the behaviour of a cloud exposed to conditions prevalent in the SDC-ISM. I find that having been shocked a cloud is rarely allowed sufficient time to return to pressure equilibrium with its surroundings before encountering a second shock. The disruption of a cloud by its passage through a blast wave is found to be quite effective and the half life of clouds cannot greatly exceed the mean interval between shocks striking a given cloud.

DECLARATION:

This thesis has been composed entirely by myself. The work presented was performed in collaboration with my thesis supervisor Dr. P.W.J.L. Brand and has been published jointly by us (Brand and Heathcote 1982; Heathcote and Brand 1983; appended here to) I have made a major contribution to all of this work, specifically:

Chapter 1 and Chapter 2 are entirely my own work.

Chapter 3 stems from initial ideas of PWJLB substantially developed by myself. The work described was performed entirely by me with consultation from PWJLB.

Chapter 4 is based on work performed jointly by myself with PWJLB. My contribution to this work was very considerable.

Chapter 5 is based on work entirely performed by myself but with consultation from PWJLB.

Chapter 6 is entirely my own work.

ACKNOWLEDGEMENTS

This thesis stems from a long and fruitful collaboration between myself and Dr. Peter Brand. For his continual advice and encouragement and many deep insights both as co-author and supervisor I owe him a great debt of gratitude.

My friends and colleagues both from the Department of Astronomy and the Royal Observatory, have over the years contributed greatly to my understanding of the problems examined. They have also provided a friendly atmosphere of co-operation in which it has been a pleasure to work.

This thesis owes its existence to the "hypersonic" typing fingers of Jane Gough who successfully translated my eccentric version of English into the approved form and cheerfully put up with even the most horrid of my equations.

Finally to my parents I owe everything. As a small token of my appreciation of their continued support over the years I gratefully and affectionately dedicate this work to them.

CONTENTS

1. THE PRESENT CONCEPTION OF THE INTERSTELLAR MEDIUM

The interstellar medium (ISM) is a promiscuous admixture of several "phases", distinguished primarily by their temperature, density and degree of ionisation. Energetic phenomenae, most notably supernova explosions and hypersonic stellar winds, play a dramatic role in determining the thermodynamic, kinematic and morphological properties of this system. The ISM is highly turbulent and is frequently agitated by the passage of strong shock waves. Mass exchange between the phases occurs on quite a short time scale.

This picture of a "violent interstellar medium" (McCray and Snow, 1979) has been developed primarily as a result of observational and theoretical advances over the past decade and represents a radical re-assessment of our perception of the ISM (Spitzer 1982). The purpose of the present work is to examine the consequences of this new insight for our theoretical understanding of the morphology of the ISM both on the large scales associated with galactic spiral structure and at the level of individual interstellar clouds.

Up to the beginning of the 1970's it was generally felt that most observations could be accommodated within a simple model of the ISM in which cool ($T \sim 10^2 K$) rather dense ($n \sim 10 cm^{-3}$) atomic hydrogen clouds were distributed at random through a uniform warmer ($T \sim 10^4 K$) tenuous ($n \sim 0.1 cm^{-3}$) and partially ionised intercloud medium. A theoretical explanation

for co-existence of two such diverse components was provided by the elegant 'two-phase' model of Field, Goldsmith and Habing (1969). They considered the thermal equilibrium of interstellar gas heated by a (hypothetical) steady homogeneous flux of cosmic rays and found that such a system possesses only two equilibrium states. For plausible values of the heating rate and interstellar pressure these two phases were found to have parameters quite similar to those observed. As reviewed by Dalgarno and McCray (1972), broadly similar results have subsequently been obtained from models employing a wide variety of different combinations of steady heating mechanisms, and also from time dependent models in which some or all of the energy input occurs in random bursts of short duration.

The possibility of a phase of the ISM substantially hotter than the intercloud medium was raised as early as 1956 by Spitzer in his seminal paper on the galactic corona (Spitzer 1956). He pointed out that since the postulated intercloud medium would only have a scale height $\sim$500pc in the galactic gravitational field it could not possibly provide sufficient pressure for the containment of apparently normal interstellar clouds observed at distances from the galactic plane of a kiloparsec or more. He thus proposed that the halo of our galaxy is pervaded by a hot ($T\sim10^6$K) extremely tenuous ($n\sim10^{-3}$cm^{-3}) plasma. Spitzer was able to suggest a number of mechanisms capable of heating gas to such temperatures and was able to demonstrate that its cooling would be suff-

iciently slow to permit its persistence for several million years even in the absence of continued heating. In speculating upon the possible consequences of such a component Spitzer foreshadowed many of the theoretical advances of the past decade.

Nevertheless, the suggestion of a hot phase remained no more than an interesting speculation, until the early 1970's when rocket and satellite observations of the soft X-ray ($h\nu \lesssim 1$Kev) background and of the UV absorption lines of highly ionised species, most notably O^{5+}, conclusively demonstrated its existence. It is now apparent that such a 'coronal' plasma occupies between 20% and 80% of the interstellar volume in the galactic disk, at least near the sun (Kraushaar 1977, 1979; Jenkins 1978 a,b), and that this component extends to a distance above the galactic plane of a few kiloparsec (Savage and de Boer 1981).

Over the same period it has become increasingly apparent that the ISM is far from quiescent. A large number of independent optical UV and radio studies indicate the common occurrence of interstellar 'clouds' with velocities considerably in excess of 20Kms^{-1}. Further, following the realisation (Brand and Zealey 1975) that arcuate and filamentary structures are common in the ISM, many giant ($\gtrsim 10^2$pc), shell like features have been identified both in our own galaxy (Heiles 1979 ; Hu 1981) and in other nearby galaxies (Meaburn 1983; Brinks 1981). Many of these show systematic

velocities indicative of expansion. They are often found to be associated with clusters of young luminous (OB) stars and in a few cases are coincident with regions of enhanced soft X-ray emission. This all provides dramatic evidence for the crucial role played by extremely energetic events in determining the state of the ISM.

These observational developments have been closely paralleled by theoretical efforts to understand the origin of the hot component. Supernova explosions (Cox and Smith 1974), hypersonic stellar winds (Castor, McCray and Weaver, 1975), collisions between high velocity clouds and the galactic disk (Tenorio-Tagle 1980, 1981) and the expansion of HII regions into asymmetric environments (Tenorio-Tagle 1982) can all lead to the injection of large amounts of kinetic energy ($E \gtrsim 10^{50}$ergs) into the ISM on a fairly short time-scale and are capable of excavating large cavities. All of the first three will in so doing generate copious quantities of shock heated coronal plasma. Straight forward energetics arguments (See § 2) demonstrate that supernovae must be the dominant source of the coronal gas although the other mechanisms may play an important subsidiary role.

Soon after the discovery of the hot component Cox and Smith (1974) showed how the overlapping of supernova remnants (SNR) could lead to the development of a network of interconnected cavities permeated by hot plasma. They demonstrated that for even quite modest supernova rates such a 'tunnel system'

could grow to occupy 10% or more of the galactic disk.

Subsequent work has stressed the importance of the inhomogeneous nature of the ISM. At the simplest level an SNR in a low density medium can grow to much greater size than one in denser surroundings. This growth is little affected by the presence of denser inclusions; the SNR blast wave simply flows around them. Consequently any warm intercloud component should be rapidly destroyed and replaced by a hot coronal plasma which might then occupy 50% to 80% of the disk volume (McKee and Ostriker 1977, Cox 1979, 1981).

At a more subtle level the interactions between SNR and clouds do have important consequences for both. Collisions between SNR blast waves and clouds accelerate the clouds (McKee, Cowie and Ostriker 1978) and inject a substantial amount of mechanical energy into them. Thermalization of this mechanical energy via the mediation of the clouds' magnetic field may provide a significant source of cloud energy (Cox 1979). Material can be removed from the clouds both directly by 'ablation' as the cloud passes through the blast wave (Heathcote and Brand 1983) and by 'evaporation' driven by thermal conduction across the boundary between the cloud and the hot coronal plasma (McKee and Cowie 1977, Cowie and McKee 1977). The corollary of all this is that clouds are of vital importance in the dissipation of SNR energy both in their direct role as sinks of mechanical energy and because by adding new material to the hot interior

they markedly increase the rate at which it radiates. This 'symbiotic' relationship between clouds and SNR is essential in moderating the tendency of SNR to process all of the interstellar gas to ever higher temperatures. It is also probably instrumental in determining the overall state of the ISM.

Other important advances have come in our understanding of the relationship between hot gas in the galactic disk and halo. As already mentioned the scale height of the hot component is $\gtrsim$1Kpc, much greater than the disk thickness $\sim$250pc. Thus in the absence of back pressure from hot halo gas the disk gas tends to flow upward into the halo. Depending on conditions at the disk-halo boundary and the extent of any additional heating by for instance halo supernovae, the result can either be a static corona as originally envisioned by Spitzer, a steady wind (Mathews and Baker 1971) or a galactic fountain(Shapiro and Field 1976) in which radiative cooling of the rising gas leads to condensation into new (warm) clouds which subsequently return ballistically to the disk.

These various theoretical ingredients have been incorporated into quite extensive global schemes for the ISM by McKee and Ostriker (1977) and Cox (1979, 1981). Although differing in detail - McKee and Ostriker stress the importance of thermal evaporation as a moderator for SNR heating while Cox invokes a combination of 'cloud crushing' and radiative

cooling and recirculation via a galactic fountain - they are very similar in broad outline. In both, the fundamental substrate of the ISM is a highly connected supernova generated hot component; this provides the pressure necessary to contain denser, warm and cold inclusions, embedded within it. In both, interactions between the clouds and the hot component provide a feedback mechanism which closely regulates the equilibrium state of the ISM. Both models are quite successful in reproducing the gross observed characteristics of the ISM and although a number of serious problems and disagreements remain they do provide a valuable framework for further development. I will here refer to this broad conceptualisation of the ISM as the 'supernova dominated cloudy interstellar medium' (SDC-ISM) picture.

In the present work I will extend the SDC-ISM concept in two important directions.

The major thrust of this thesis seeks to include the present view of the ISM within the framework of contemporary ideas on galactic structure. To date all SDC-ISM models have been concerned with conditions appropriate to the solar neighbourhood. I will here examine how the properties of the ISM change from point to point in the galaxy and in particular I ascertain its response to passage through a spiral arm. This is not only of great intrinsic interest but can also provide vital inputs into present models for the generation and maintenance of spiral structure.

In the secondary investigation, I examine the interaction between an individual interstellar cloud and an SNR blast wave, a problem central to the SDC-ISM models, in rather more detail than has previously been employed.

Throughout, the emphasis is on the application of simple physical principles to obtain approximate solutions to the problems involved. Much of the work described is directed toward locating the boundaries in parameter space within which particular representations of the ISM are self consistant or particular processes dominate over others. The state of the ISM is affected by a great many complex and imperfectly understood physical processes taking place simultaneously. Further our knowledge of many of the observational parameters is at best rudimentary. Thus while detailed numerical computations of highly idealised systems may provide vital insights into the basic phenomina - for instance the work described in Chapter 5 would not have been possible without reference to the detailed numerical work of Woodward (1976, 1979) - analytical calculations providing even only order of magnitude estimates of the properties of more realistic systems are still of great value.

In Chapter 2 I will briefly review the various energy sources which have been proposed to drive the 'violent' ISM and demonstrate that on purely energetic grounds the ISM is most likely supernova dominated. In chapter 3 a simple model of the SDC-ISM based primarily on the work of McKee and Ostriker (1977) is developed and the bounds of

its 'domain of validity' are established by means of a fairly exhaustive parameter search. In Chapter 4 this model is combined with a simple representation of our galaxy and the interplay between an SDC-ISM and spiral structure is investigated for the first time. In Chapter 5 I turn to a more detailed investigation of the state of an individual interstellar cloud exposed to the chaos prevalent in a violent ISM. Finally Chapter 6 summarises the main results and conclusions and suggests avenues for future investigation. Appendix A deals with some of the more formal aspects of the SDC-ISM model.

2 The Energetics of a Violent ISM

As outlined in Chapter 1 a hot ($T \sim 10^5 - 10^6$K), tenuous ($n \sim 10^{-3}-10^{-2}$ cm^{-3}) plasma is believed to occupy between 20% and 80% of the volume of the galactic disk (Kraushaar 1977, 1979; Tanaka & Bleeker 1977; McCray & Snow 1979; Jenkins 1978 a,b; Sanders et al 1983; McCammon et al 1983). Material at temperatures near the lower end of this range is also known to occur at distances from the galactic plane of a few killoparsec (Savage & de Boer 1981, York 1982); whether it is accompanied by hotter gas and what its relationship to the hot disk gas may be, is still a matter of controversy (Songaila 1981; Hartquist & Snijders 1982). Because of the abrupt rise in the radiative cooling rate at a temperature $\sim 10^4$K, such a plasma cannot be heated by any of the conventional steady heating sources (Dalgarno & McCray 1972); such conditions are, however, to be expected behind strong shock waves propagating through the ISM (Chevalier 1977; McKee & Hollenbach 1980).

At the same time interstellar gas velocities in excess of 20 kms^{-1} are ubiquitous and values as high as 100 kms^{-1} are not uncommon (McCray & Snow 1979). Many giant ($\sim 10^2$pc) shell like features have been recognised in our galaxy (Heiles 1979; Hu 1981; Olano 1982) and other nearby galaxies (Meaburn 1983; Brinks 1981; Graham & Lawrie 1982). The measured expansion velocities of some of these imply kinetic energies $\sim 10^{51} - 10^{53}$ ergs. Typical formation energies of

up to $\sim 10^{54}$ ergs are inferred in the most extreme cases, irrespective of whether this is provided by a single extremely energetic event or, as seems more probable, multiple events of lower energy.

Together these two observational data lead to the concept of the 'violent interstellar medium' (McCray & Snow 1979) in which various energetic events either singly or in concert drive strong shocks through the interstellar gas keeping all of it in a highly disturbed condition, heating some of it to the observed high temperatures and forming the observed giant shells.

In the present Chapter I will review the various energy sources which have been proposed to power the 'violent' ISM with particular emphasis on the total amount of thermal and kinetic energy they can each supply. I will thus show that supernovae are the major source of the thermal energy of the hot phase and that their contribution to the kinetic energy of bulk motion is greater than or comparable to that from all other sources taken together. I will also compare the total energy inputs to the likely rate of energy dissipation and hence show that the supernova energy input is probably necessary, and certainly sufficient for the maintenance of the violent ISM.

The major results of this section are summarised in table 2-1 which lists the total, thermal and kinetic energy input per unit area projected onto the galactic plane, for each of

the sources considered together with estimates of the dissipation rate of both thermal and kinetic energy. The galactic radius is taken to be 15 kpc and the quoted values are averaged over the whole of the galactic area. It is convenient to divide the sources into those confined to the spiral arms (arm population) and those with a more uniform distribution ('disk' population).

2.1 Arm population sources

Massive stars (here defined to be all those which produce type II supernovae i.e. $M \gtrsim 8M_{\odot}$; spectral types earlier than about B3) can inject energy into the ISM in three ways

(i) by the expansion of their HII region

(ii) by the impact of their hypersonic stellar winds

(iii)by exploding as type II supernovae

It is of course the most massive of these stars (together with their HII regions) which delineate the spiral arms. Even the lower mass members of the group have lifetimes $\lesssim 10^7$ years, much less than the galactic rotation period, and are consequently strongly concentrated in the arms.

Most, possibly all, of these high mass stars are members of OB associations or clusters (Miller and Scalo 1979) and form within giant molecular clouds (See Elmegreen et al 1978 for a review of this process). Expanding HII regions (Whitworth 1979, Bally 1980, Mazurek 1980), stellar winds (Shull 1980a)

and supernovae from the shortest lived most massive association members (Wheeler and Bash 1977, Wheeler et al 1980, Shull 1980b) undoubtedly all play a role in the dispersal or disruption of the parent molecular cloud. This both renders the OB association visible and permits access to the general lower density ISM by the energy subsequently released.

Once this occurs the combined stellar winds and supernova explosions of the remaining cluster members will probably lead to the generation of a large shell filled with plasma, shock heated to coronal temperatures (Bruhweiler et al 1980, Elmegreen 1980, Tomisaka et al 1981; see also § 3.1). The total available energy is easily able to account for even the largest observed supershells. Evidence for the occurrence of this process is clearly seen in the Orion (Reynolds and Ogden 1979, Cowie et al 1979), Cygnus (Abbott et al 1980) and Carina (Cowie et al 1981, Seward and Chlebowski 1982) associations. OB associations are not gravitationally bound and hence slowly disperse, also members of a binary system can be ejected at high velocity when the system is disrupted by the explosion of the other member. Consequently, a significant fraction of the lower mass members can escape the association supershell to go supernova in the ambient ISM (Bruhweiler et al 1980).

In order to compare directly the contribution to the total energy injected by massive stars from each of the three

mechanisms I will compute the mass averaged energy input

$$E_i = \int_{m_l}^{m_u} E_i(m)\dot{n}_*(m)dm \Big/ \int_{m_l}^{m_u} \dot{n}_*(m)dm \qquad 2.1\text{-}1$$

where $E_i(m)$ is the energy injected by stars of mass m through process i. The stellar birthrate function $\dot{n}_*(m)$, is assumed to have the standard form $\dot{n}_*(m) \propto m^{-(1+x)}$ and a value of $x \sim 1.6$ is adopted, appropriate for massive stars (Lequeux 1980, Miller and Scalo 1979, Garmany et al 1982). The upper m_u and lower m_l mass limits are taken to be $8M_\odot$ and $80M_\odot$ respectively. Where necessary I have employed mass-luminosity-radius relationships and stellar lifetimes from stellar evolutionary models including mass loss (de Loore et al 1978, Chiossi et al 1978).

2.1.1 HII Region Expansion

Ultimately the kinetic energy liberated by the expansion of the HII region surrounding an OB star derives from the stellar Lyman continuum flux. Each photoionisation releases an energy $\sim kT_*$ (T_* is the stellar colour temperature, see Kahn and Dyson 1965) so a star emitting S_* Lyman continuum photons per second deposits a total energy $E_{HII} \sim S_* kT_* t_*$ in the ISM over its lifetime, t_*. This ranges from $\sim 2 \times 10^{49}$ ergs for a B0 star to $\sim 3 \times 10^{52}$ ergs for an O5 star. Most of this energy is, however, lost by recombination and radiative cooling so that only a small fraction remains to drive bulk motions of the gas. Further, the

velocities achieved are small, comparable to the sound speed in the warm $H^+ \sim 10 Kms^{-1}$, and the environs of OB stars are invarably sufficiently dense that the shocks driven into the ISM are radiative and large quantities of hot gas are never created.

When an HII region forms around a single star, or a compact group of stars in a uniform medium its evolution follows the classical pattern reviewed by Mathews and Odell (1967). As soon as the stellar UV flux switches on, a highly supersonic (weak R type) ionisation front rushes out into the ambient medium leaving it warm and ionised but relatively undisturbed. Geometrical dilution and recombination in the ionised interior reduce the flux reaching the ionisation front, so it continually decelerates, until the radius approaches that of the equilibrium Strömgren sphere at which by definition recombinations just balance the stellar flux. The warm ionised gas in the HII region is now over pressured with respect to its surroundings and thus tends to expand. As the interior density falls the recombination rate (αn_e^2) also falls so that a larger volume can be kept ionised. The result is that a subsonic (weak D type) ionisation front, preceded by a strong isothermal shock is driven into the ambient medium, the two fronts being separated by a narrow region of highly compressed neutral gas. This expansion phase is considerably longer than the initial ionisation stage and continues until either pressure equilibrium is achieved with the surroundings or (more likely)

the exciting star goes supernova. Only about 1% of the energy deposited by ionisation gets converted to kinetic energy of the dense shell (Spitzer 1978).

This picture is somewhat modified if the exciting star(s) form near the edge of the parent molecular cloud (Tenorio-Tagle 1982). If during either phase of the evolution, part of the ionisation front reaches the cloud boundary then it will rush outward into the lower density surroundings. This sets up a large pressure discontinuity between the ionised cloud material and the now ionised intercloud medium. In response to this a strong isothermal shock is driven into the intercloud medium followed by a fan of supersonically flowing ionised cloud material which eventually spreads out to produce an extended and tenuous HII region. As a result of this extra 'champagne phase' a somewhat larger fraction ~3% of the injected thermal energy can be converted to kinetic energy.

Taking values of S_* and T_* from the work of Panagia (1973) I estimate a mass averaged injected energy $\sim 4 \times 10^{50}$ erg, and hence assuming a 3% efficiency, an average kinetic energy $\sim 10^{49}$ erg is liberated per star. The rate of kinetic energy input per unit area simply obtained by multiplying by the rate of type II supernovae (§4.2.3) is then $\sim 0.1\text{-}1 \times 10^{39}$ erg pc^{-2} yr^{-1}. Spitzer (1978) obtained essentially the same result by estimating the energy input by the number of OB stars required to produce the observed

thermal radio continuum flux.

2.1.2 Stellar Winds

Stellar winds occur to a greater or lesser degree in all stars (Cassinelli 1979), however it is only for the more massive and luminous OB stars that the energy contributed to the ISM becomes significant, approaching in the most extreme cases that of a supernova (Conti 1978, 1982, Conti and McCray 1980).

For main sequence, giant and supergiant stars having luminosities in the range $10^3 L_\odot$ - $10^7 L_\odot$ mass loss rates are well represented by the empirical relationship

$$\dot{M}_W \simeq 1.6 \times 10^{-16} (L/L_\odot)^{1.73} M_\odot yr^{-1} \qquad 2.1\text{-}1$$

(Garmany et al 1981, Abbott et al 1980, 1981 Snow 1982). Terminal velocities are found to be typically ~ 3 times the photospheric escape velocity, so that

$$V_W \simeq 2\times10^3 \left\{ \left(\frac{M}{M_\odot}\right) \left(\frac{R}{R_\odot}\right)^{-1} \left[1-2.7\times10^{-5} \left(\frac{L}{L_\odot}\right) \left(\frac{M}{M_\odot}\right)^{-1} \right] \right\}^{\frac{1}{2}} \text{kms}^{-1} \qquad 2.1\text{-}2$$

(Abbott 1978). Thus the wind luminosity, $L_W \equiv \frac{1}{2}\dot{M}_W V_W^2$ and the total energy injected, $E_W \equiv L_W t_*$ over the stellar lifetime, t_*, range from $L_W \sim 5 \times 10^{34}$ ergs^{-1}, $E_W \sim 10^{49}$ erg for a B0 star to L_W 6 x 10^{36} ergs^{-1}, $E_W \sim 6 \times 10^{50}$erg for an O5 star. For Wolf-Rayet stars, believed to be a stage in the evolution of the most massive ($M \gtrsim 40 M_\odot$) OB stars (e.g. de Loore 1982) the mass loss rate is $\sim 3 \times 10^{-5} M_\odot yr^{-1}$

independent of luminosity. This leads to $L_w \sim 6 \times 10^{37} ergs^{-1}$ and $E_w \sim 7 \times 10^{50} erg$ over the ~ 0.4 Myr duration of the Wolf-Rayet phase (Barlow et al 1981).

Several workers have discussed the evolution of the bubble blown in the ISM by such hypersonic winds (See Dyson 1981 for a review). Because the initial ionisation of the stellar HII region is very rapid the evolution of the stellar bubble takes place within the HII region. Conversely, the subsequent expansion of the HII region takes place sufficiently slowly that it can probably be ignored. Very soon after its onset the stellar wind interacts with its own mass of interstellar gas and a characteristic two shock structure develops in the flow, dividing it into four zones. Nearest the star is a small region of freely expanding stellar wind. The wind is decelerated by an inward facing shock beyond which is an extensive zone of shock heated stellar wind. A contact discontinuity separates this from a shell of shocked interstellar gas bounded by an outward facing shock which advances into the undisturbed ambient medium. The shocked interstellar gas cools quite early to form a dense shell. At first the shell is kept fully ionised by the stellar UV flux, however, for sufficiently high ambient density it may become optically thick in the Lyman continuum so that parts of it re-combine. Ultimately the expansion of the bubble stops when pressure equilibrium is achieved with the surroundings or the star goes supernova. Throughout the evolution $\sim 45\%$ of the total mechanical energy, $L_w t$, injected

by the wind is stored as thermal energy in the hot cavity while ~20% is stored as kinetic energy of the shell.

I estimate that $\langle E_w \rangle \sim 1 \times 10^{50}$ erg, uncertain by about a factor of two. Slightly over half of this total is provided by stars with $M > 40 M_\odot$ during their brief but extremely energetic Wolf-Rayet phase. The rate of energy input per unit area is then $\sim 0.8 - 8 \times 10^{39}$ erg pc^{-2}yr^{-1}. A broadly similar value has been obtained by Abbott (1982), on the basis of counts of massive stars within 3kpc of the sun, and the same stellar wind data.

2.1.3 Type II Supernovae

The total galactic supernova rate is between 0.01 yr^{-1} and 0.1 yr^{-1} about half of which is due to type II supernovae (§ 4.2.2). The energy per supernova is $\sim 10^{50}$-10^{51} erg. This leads directly to a total rate of energy input per unit area of 4-40x10^{39} erg pc^{-2}yr^{-1}.

The evolution of SNR and their interactions with the ISM are discussed extensively in section 3.

Type II supernovae resulting from stars which escape from the association supershell will essentially follow the classical evolutionary sequence for isolated SNR (most such stars will have sufficiently low masses that the effects of their own stellar winds can be completely ignored). Briefly there

is a short initial phase during which the supernova ejecta expand freely into the ISM which terminates when the ejecta mass and swept up mass are comparable. Subsequently, the remnant expands adiabatically until the temperature falls sufficiently for radiative losses to become important. Cooling then proceeds extremely rapidly near the remant's edge and a dense shell forms, which continues to plough out into the ISM, driven by its momentum and the pressure of the gas in the interior, which remains very hot. Ultimately the shell's velocity becomes comparable to the RMS cloud velocities in the surroundings and the shell loses its identity. The remaining hot cavity, however, survives for an appreciable period before being encroached upon by the surrounding colder gas. Overall $\sim 45\%$ of the initial energy is stored as thermal energy of the cavity gas while $\sim 3\%$ resides in the kinetic energy of the shell.

For an SNR occurring within an association supershell the SNR blast wave will expand extremely rapidly until it meets the dense shell surrounding the bubble, when a strong radiative shock will be driven into the shell. Subsequently the evolution will be essentially the same as in the conventional snow plough phase although the dominant contribution to the shell momentum is provided by the stellar winds. For simplicity I will assume the energy conversion efficiences are the same as in the classical model.

2.1.4 Field Star Radiation Pressure

The possibility that the radiation pressure from a single cluster acting upon interstellar dust, collisionally coupled to the gas might generate an expanding shell was originally proposed by O'Dell et al (1967). More recently Elmegreen and Chiang (1982) have discussed the ability of radiation pressure from field stars to enlarge a pre-existing (dust-depleted) cavity generated by for instance supernovae or stellar winds. The important point is that, for shells having radii larger than a few times the photon mean free path, the nett field star radiation pressure is outward directed and increases with increasing radius so that such a cavity grows at an ever increasing rate. By the time radiation pressure becomes important the contribution from field stars would far outweigh that from any central cluster. They propose that shells with initial radii $\sim 10^2$pc could grow to kiloparsec sizes in about 10^8 years, the maximum possible size being determined by Rayleigh-Taylor or gravitational instabilities. Such large shells could have kinetic energies $\sim 10^{52}$ ergs by the end of their evolution.

To obtain an extreme upper limit on the total kinetic energy input from this mechanism I assume that every OB association born creates such a shell*

---

* The remnants of single field supernovae evolving in the hot component of the ISM can reach the required size however (i) In an inhomogeneous ISM most of the dust resides in the clouds which are only slightly disturbed by the hot component SNR, so a dust cleared cavity is not produced (ii) by the time radiation pressure becomes important hot component SNR are already on the point of overlapping so there is little opportunity for further radiation-pressure driven growth.

There are $\sim$4000 OB associations in the galaxy (Blitz 1978). So adopting a lifetime $\sim 2 \times 10^7$yr (Blaauw, 1964) implies that OB associations and hence by supposition wind driven shells are born at a rate $\sim 4 \times 10^{-13} pc^{-2}$. From the results of Elmegreen and Chiang (1982) I estimate that shells formed at this rate can grow to R $\sim$500pc before overlapping at which radius their energy will be $\sim 10^{51}$ ergs. This leads to an energy injection rate per unit area $\sim 4 \times 10^{38}$erg $pc^{-2} yr^{-1}$. Decreasing the formation rate so as to permit greater shell sizes would marginally decrease the total energy input.

2.2 Disk population sources

2.2.1 Type I supernovae

Although the origin of type I supernovae is controversial (C.F. Oemler & Tinsley 1979; Tammann 1982) they do have a fairly uniform distribution over the galactic disk. As already noted (§ 2.1.3) they liberate energies $\sim 10^{50}$-10^{51} erg and occur at a rate $\sim 5 \times 10^{-3}$-5×10^{-2} yr^{-1}. The evolution of their remnants and the energy conversion efficiencies will be as described for isolated type II supernovae above.

2.2.2 High Velocity Clouds

By definition high velocity clouds are simply any neutral hydrogen feature seen at a velocity too large to be explained by galactic rotation models, typically $|V| \gtrsim 100$ kms^{-1} (e.g. Hulsbosch 1979). Although some may represent gas in distant warped spiral arms (Heiles 1975) or the result of local explosive phenomenae (Weaver 1979), the bulk are probably infalling material at large distances from the galactic plane (Oort and Hulsbosch 1978). Such clouds may have condensed out of the galactic fountain (Bregman 1980) or have been torn out of the Magellanic Clouds by tidal interaction (Mirabel 1981) or be primordial in origin.

Tenorio-Tagle (1979, 1980) has proposed that collisions between high velocity clouds and the galactic disk might generate large coronal gas filled cavities. A collision

with a cloud of mass $\sim 10^2$-$10^4 M_\odot$ and a velocity $\sim 250 kms^{-1}$ would liberate $\sim 10^{50}$-10^{52}ergs. The effect of this large energy input into a small volume is essentially identical to that of a supernova explosion and I adopt the conversion efficiencies already quoted for that case. Since the observed mass flux onto the plane is a few solar masses per year (Hulsbosch 1975) the total energy input in this way is limited to about 3×10^{39}erg $pc^{-2}yr^{-1}$.

2.2.3 Dwarf M Flare Stars

Coleman and Worden (1976, 1977) have suggested that the flares and winds of dwarf M stars may provide a significant energy input into the ISM. They estimate that each flare star liberates $\sim 1 \times 10^{37}$erg yr^{-1} which together with a space density of $6 \times 10^{-2} pc^{-3}$ and an effective thickness of 300pc for dwarf M stars (Reid and Gilmore 1982 and private communication) leads to a total energy injection rate of $\sim 4 \times 10^{38} pc^{-2}yr^{-1}$.

2.2.4 Planetary Nebulae

The local birthrate of planetary nebulae is $\sim 50 - 180 \times 10^{-11}$ $pc^{-2}yr^{-1}$ depending on the adopted distance scale (Cahn and Wyatt 1978). Assuming an average ejected mass $\sim 0.5 M_\odot$ (Tinsley 1978) and a typical ejection velocity of $30 kms^{-1}$ (Osterbrock 1974) leads to an energy input $\sim 2 \times 10^{36}$ $- 1 \times 10^{37}$erg $pc^{-2}yr^{-1}$.

2.2.5 'Galactic Flares'

Sturrock and Stern (1980) have proposed, by analogy with solar flares, that the twisting of the galactic magnetic field resulting from differential rotation leads to the sudden release of energy due to magnetohydrodynamic or resistive instabilities. They suggest that such 'galactic flares' might heat the corona and estimate an energy input rate corresponding to $\sim 7 \times 10^{38}$ erg $pc^{-2} yr^{-1}$.

2.3 Energy Losses

2.3.1 Hot Component Radiative Cooling

First, to show that an energy source is necessary to maintain the hot component I essentially repeat Spitzer's (1956) argument but employ more recent (larger) values for the radiative cooling rate. The radiative cooling timescale is given by

$$t_{rad} = \frac{3}{2} \frac{\xi k T}{n(H) \Lambda}$$

where Λ is the cooling function defined so that the total radiative cooling rate per unit volume is $n^2(H)\Lambda$, ξ is the number of free particles per hydrogen nucleus and the other symbols have their usual meanings. For the regime appropriate for the observed hot phase, $\Lambda \simeq 6.2 \times 10^{-19}$ erg cm^3 s^{-1} $T_h^{-0.6}$ (Raymond et al 1976).

Hence

$$t_{rad} \simeq 97 \text{Myr} \left(\frac{n_h}{10^{-3} cm^{-3}} \right)^{-1} \left(\frac{T_h}{10^6 K} \right)^{1.6} \qquad 2.3\text{-}1$$

$$10^5 K \leq T_h \leq 4 \times 10^7 K$$

Thus taking, say, $T_h \sim 10^6$K $n_h \sim 3 \times 10^{-3}$cm^{-3} as typical of the observed hot component $t_{rad} \sim 32$Myr. A primordial origin for the bulk of the hot component is thus unlikely.

To obtain an estimate of the energy input necessary to maintain the hot phase, consider a column through the ISM perpendicular to the galactic plane. If f_h is the volume filling factor of the hot gas in the disk and $2H_d$ is the effective thickness of the disk, then,

$$\dot{E}_{rad} \simeq -4.33\times10^{37}\,\text{erg pc}^{-2}\text{yr}^{-1}\,\beta f_h \left(\frac{n_h}{10^{-3}\text{cm}^{-3}}\right)^2 \left(\frac{T_h}{10^6\text{K}}\right)^{-0.6} \left(\frac{H_d}{150\text{pc}}\right) \qquad 2.3\text{-}2$$

The factor $\beta \gtrsim 1$ is included to take into account the enhancement of the radiative loss rate due to density variations both in the hot component itself and at the interface between the hot component and cooler inclusions. Again inserting typical values the energy loss rate from the disk is $\dot{E}_{rad} \sim -4\times10^{38}$ erg pc^{-2}yr^{-1} βf_h

As already noted the equilibrium scale height of the hot component is very much larger than the disk thickness so that hot gas will tend to flow upward into the halo. If a static corona results then equation 2.3-2 applies with H_d replaced by the half-thickness of the corona and $f \sim 1$. Conversely if a galactic wind or fountain results the energy flux it carries out of the disk must be added to the value of $\dot{E}_{rad}$ for the disk. This will be given by

$$\dot{E}_{wind} \simeq -\frac{3}{2} f \nu(f) c_h^3 n_h$$

$$\simeq -3.6\times10^{39} \text{erg pc}^{-2}\text{yr}^{-1} f_h \nu(f_h) \left(\frac{n_h}{10^{-3}\text{cm}^{-3}}\right)\left(\frac{T_h}{10^6 \text{K}}\right)^{1.5}$$

where C_h is the sound speed in the hot component and $\nu(f)$ is the ratio of the effective flow speed in the disk to C_h. If $f_h \sim 1$ so that the halo and disk are well connected then $\nu \sim 1$; if $f_h \sim 0.2$ so that the hot gas has to 'bubble' up through cooler material then $\nu \sim (L/H_d)^{\frac{1}{2}}$ where L is the radius of a typical bubble. Thus adopting the same typical parameters $\dot{E}_{wind}$ lies between $\sim 1 \times 10^{40}$ erg pc^{-2}yr^{-1} ($f \sim 1$) and $\sim 2 \times 10^{38}$ erg pc^{-2}yr^{-1} ($f \sim 0.1$, $L/H_d \sim 0.3$ say).

2.3.2 Cloud-Cloud Collisions

A crude estimate of the rate of energy loss by cloud-cloud collisions can be obtained as follows. Scalo and Pumphrey (1982) have shown on the basis of simulation of supersonic cloud collisions that the effective mean free path for the collisional dissipation of a cloud's kinetic energy is between 5 and 10 times the geometric mean free path. This essentially results from the preponderance of oblique collisions which dissipate relatively little kinetic energy. With the idealisation that the diffuse clouds are spheres of radius R_{cl} then their mean space density is

$$N_{cl} \simeq \bar{n}_{cl} \left(\frac{4\pi}{3} R_{cl}^3 \; n_{cl}\right)^{-1}$$

where n_{cl} and $\bar{n}_{cl}$ are respectively the density of an individual cloud and the smeared out density provided by all diffuse clouds. Adopting $R_{cl} \sim 2$pc $\bar{n}_{cl} \sim 30\text{cm}^{-3}$ and $\bar{n}_{cl} \sim 1\text{cm}^{-3}$

(Spitzer 1978; Knude 1979; 1981; Crovisier 1981) leads to $N_{cl} \sim 1 \times 10^{-2}$ and a geometrical mean free path of ~ 20pc. Then assuming a one dimensional velocity dispersion of 6 kms^{-1} (Spitzer 1978) leads to an energy density of 9×10^{45}erg pc^{-2}, a collisional dissipation time of 7-14 Myr and hence an energy dissipation rate of $6\text{-}12 \times 10^{38}$ erg $pc^{-2}yr^{-1}$.

2.4 DISCUSSION

As is clear from the results of the foregoing summarised in Table 2-1, supernovae do play a dominant role in the energetics of the ISM. In the spiral arms they supply over 80% of the thermal energy available to the hot component, the remainder being supplied by the stellar winds of the more massive supernova progenitors. They make a roughly equal contribution with expanding HII regions to the kinetic energy input. In the interarm region they are essentially the only energy source; high velocity clouds at most supply a comparable amount of energy and that only if the supernova rate is near the minimum suggested value.

When the available supply of energy is compared with the demands it is clear that within the rather large uncertainty of the estimates a state of balance can certainly be achieved. In the absence of an energy input from supernovae stellar winds alone, could meet the demands of disk radiative cooling and a weak fountain if β and f_h are both small and together with HII regions could meet the kinetic energy drain. However, if $\beta > 1$ and $f_h \sim 1$ as seems likely a supernova contribution is obligatory. This forms the basis of the idea of a supernova dominated ISM which will be taken up in the subsequent chapters.

TABLE 2-1 VIOLENT ISM : ENERGETICS

PROCESS	Energy/ event (erg)	Rate ($pc^{-2}yr^{-1}$)	Total Energy (10^{39}erg $pc^{-2}yr^{-1}$)	Thermal Energy (10^{39}erg $pc^{-2}yr^{-1}$)	Kinetic Energy (10^{39}erg $pc^{-2}yr^{-1}$)	Effective Thickness (pc)
A) Sources:						
Arm Population						
HII Region Expansion	4×10^{50}	$(1-10)\times10^{-11}$	3-30		0.1-1	
Stellar Winds	1×10^{50}	"	0.8-8	0.4-4	0.17.1.7	
Type II Supernovae	5×10^{50}	"	4-40	2-20	0.12-1.2	
Field Star Radiation Pressure	1×10^{51}	4×10^{-13}	0.4		0.4	
Disc Population						
Type I Supernovae	5×10^{50}	$(1-10)\times10^{-11}$	4-40	2-20	0.12-1.2	
Dwarf M Flare Stars	1×10^{37}erg yr^{-1}	36 pc^{-2}	0.4	0.18	$\lesssim$ 0.08	750
Planetary Nebulae	$\gtrsim 5\times10^{45}$	$(50\times180)\times10^{-11}$	0.002-0.01		0.002-0.01	300
High Velocity Clouds	$10^{50}-10^{52}$	$(0.05-5)\times10^{-11}$	$\lesssim$3	$\lesssim$ 1.4	$\gtrsim$ 0.1	
Galactic Flares			0.7	0.7		

TABLE 2.1 Cont.

Energy event	Rate	Total Energy	Thermal Energy	Kinetic Energy	Effective Thickness
B) Sinks:					
Thermal Energy					
Disk Radiative Cooling			$-0.4\beta f_h$		
Halo: radiative cooling			-2.1β		
Halo: Wind/Fountain: Free Flow	$(F_h \sim 1)$		-10		
Halo: Wind/Fountain: Diffusive Flow	$(F_h \sim 0.1)$		-0.3		
Kinetic Energy					
Cloud-Cloud Collisions				-1.2	

3. A Simple Model of the SDC-ISM

3.1 Introduction

In this chapter I will describe a simple model of the SDC-ISM. In essence it is based on that originally proposed by Mckee and Ostriker (1977, hereinafter MO) in which the interstellar clouds are supposed to be embedded in and contained by a hot, low density, SNR generated plasma. Interactions between the clouds and the ensemble of SNR are supposed to control the equilibrium properties of the joint system by means of a feedback process. The particular mechanism postulated for this by MO was the thermal evaporation of the clouds leading to enhanced radiative cooling of the SNR. Striking a balance between the net rate of supernova energy input and its dissipation then fixes the interstellar pressure which in turn determines the properties of the cloud population and in particular the rate at which they can be evaporated. The equilibrium solution is then found by demanding self consistency between the resulting evaporation rate and that used in determining the matrix pressure.

The MO scheme is here extended to include an explicit treatment of the dynamical response of the clouds to being overrun by the SNR blast wave in order to assess the consequency of this important complicating influence on the evaporation rate and the resulting state of the SDC-ISM.

In addition, in view of the uncertainty over the extent to which the evaporation rate can be suppressed by the clouds magnetic field, I also construct a variant model. In this the postulated properties of the cloud population are the same as those considered by MO but the feedback mechanism is supposed to operate via the process of 'cloud crushing' discussed by Cox (1979) which is expected to dominate over radiative cooling if evaporation is completely suppressed.

In the remainder of this section I briefly review the important physical processes thought to operate in the SDC-ISM. Section 3.2 presents the full description of the evolution of an evaporation dominated SNR with special emphasis on the role of cloud dynamics. Section 3.3 presents the corresponding description of SNR evolution in the non-evaporative case. The cloud model used in both schemes is briefly summarised in section 3.4 while section 3.5 explains the method used to find the equilibrium solutions. In section 3.6. I submit the resulting models to a fairly exhaustive parameter search in order to determine the boundaries of their domain of validity and establish the sensitivity of the results obtained from them to the values of the parameters characterising the model. Finally section 3.7 summarises the main results of this chapter.

3.1.1 SNR Evolution

For the present purposes we may regard the complex series of events which occur in the envelope of the incipient supernova (see e.g. Chevalier 1981) as a 'black box' the effect of which is to eject a mass of cool material M_{ej}, with a velocity V_{ej}, into the ISM. For type I supernovae $M_{ej} \sim 0.25M_{\odot}$ and $V_{ej} \sim 20000$ kms^{-1} while for type II supernovae $M_{ej} \sim 5M_{\odot}$ and $V_{ej} \sim 5000$ kms^{-1}, in either case the kinetic energy released E_o is $\sim 10^{51}$ ergs. The precise sequence of events by which this prodigious input of energy becomes shared with an ever increasing mass of interstellar gas and is eventually dissipated, depends in a quite straightforward and well understood way on the pressure and density of the ambient medium, and in a much more subtle and complex way upon its degree of inhomogenity.

The simplest possible case, that of an initially homogeneous isotropic ambient medium, has been intensively studied both by means of simple analytic approximations and detailed numerical simulations (see Kahn 1975, Chevalier 1977 and McKee 1982 for reviews). Typically an SNR in such a medium will follow a simple five stage evolutionary sequence:

(i) Initially the ejecta expand almost freely into the ambient medium and act as a piston which drives a strong shock into the ISM. As more and more interstellar material is swept up by the outward going shock, the ejecta decelerate and a reverse shock is driven into them heating them to considerably temperatures;

the decelerating flow is Rayleigh-Taylor unstable (Gull 1973, 1975) leading to mixing of ejecta and interstellar matter. By the time the ejecta have interacted with a few times their own mass of interstellar gas, their initial kinetic energy will have been almost entirely thermalised and transferred to the swept up gas (Gull 1973, 1975).

(2) The shocked interstellar gas is intensely hot and radiates only very inefficiently by bremsstrahlung; consequently the flow is virtually adiabatic. The ensuing evolution is then well approximated by the Sedov (1959) similarity solution, which describes the expansion into a uniform medium of the adiabatic blast wave initiated by a point explosion. During this stage 72% of E_o is stored as thermal energy and 28% as kinetic energy. The density profile in the remnant interior is extremely strongly peaked near the shock front; about 67% of the total remnant mass lies outside $0.9R_S$.

(3) As the adiabatic expansion reduces the pressure driving the shock its velocity decreases and hence the immediate post-shock temperature falls. For temperatures below $\sim 4 \times 10^7$K the radiative cooling rate increases rapidly as the temperature decreases. Consequently the radiative cooling time behind the shock ultimately becomes shorter than the dynamical timescale for the remnant (Cox 1972). Catastrophic cooling sets in just behind the shock leading to the formation of a

cool dense shell which contains about half the remnants mass and almost all the kinetic energy $\sim 0.28 E_o$ (Rosenburg & Scheuer 1972; Chevalier 1974; Falle 1975, 1981; Preite-Martinez 1981). The interior of the remnant is filled with material which passed through the shock prior to the cooling epoch, was more strongly shock heated and hence can remain hot long after the formation of the shell. About $0.45 E_o$ will be stored as thermal energy in the interior (Kahn 1976).

(4) The shell will continue to expand under the influence of its own momentum and the pressure of the hot gas in the interior. Its expansion is approximately described by the pressure modified snow-plough solution. Oort 1951; McKee and Ostriker 1977; See Appendix A2). The kinetic energy of the shell decreases as $(R_c/R)^2$ while the thermal energy of the interior decreases as $(R_c/R)^5$ during this phase. The expansion of the remnant ultimately ceases when pressure equilibrium is achieved with the ambient medium.

(5) The end result of the preceeding stages is a large cavity filled with hot tenuous plasma. This fossil SNR will have a lifetime against both cooling (Kahn 1975) and re-invasion by surrounding cool gas (Cox & Smith 1974) which is considerably larger than the total duration of stages (1) to (4).

Even for a uniform medium this pattern will be somewhat modified when the density is very high or very low. At

the densities encountered in the cores of molecular clouds $n_o \sim 10^4 cm^{-3}$ even bremsstrahlung cooling may be sufficiently rapid to dominate the energetics at early times. There is then no adiabatic stage (2) and the SNR enters the snow plough phase (4) directly from the free expansion phase (1) (Wheeler et al 1980; Shull 1980). Conversely if the ambient density is very low $\lesssim 10^{-2} cm^{-3}$ the pressure of the ambient medium may become comparable with the interior pressure before radiative cooling. In that case the outer shock will degenerate into a spherical sound wave and no dense shell will form (Cox 1979; Cox & Franco 1981; Cox & Anderson 1982). The end result of the SNR's evolution will however still be the generation of a long lived bubble of hot tenuous plasma.

Supernovae can only rarely evolve into the homogeneous medium assumed in the classical model, however. The progenitors of type II supernovae are young massive OB stars ($M \gtrsim 8M_\odot$). As described in § 2.1 all such stars form in groups or associations within high density molecular clouds. The most massive ($M \gtrsim 20M_\odot$) members of such association can substantially modify their surroundings both through the action of their expanding HII regions and their powerful stellar winds. It is expected that the result will be the formation of a large wind blown bubble around the association filled with a hot tenuous plasma (Bruhweiler et al 1981; Kafatos et al 1981; Tomisaka et al 1981;

Tenorio-Tagle et al 1982). This shell will be further enlarged as successively less massive association members reach the end of their lives and explode as supernovae. OB associations are generally not bound gravitationally and consequently will slowly disperse. In addition members of binary systems can be ejected at high velocity when their companion goes supernova. Consequently 30 - 60% of all OB stars can probably escape from the confines of the 'association supershell' before themselves going supernova.

Even supernova of type I and those supernovae of type II which escape their parent OB association will still explode in a highly inhomogeneous environment. As outlined in Chapter 1 the ISM typically consists of a hot ($T \sim 10^6 K$) low density ($n \sim 5 \times 10^{-3} cm^{-3}$) matrix through which are distributed cooler ($T \sim 10^2 - 10^4 K$) denser ($n \sim 0.1 - 30 cm^{-3}$) inclusions which contain the bulk of the mass. Our knowledge of SNR evolution in such a medium is still rather incomplete; simple analytical description have been given by McKee and Ostriker (1977; hereinafter MO) and Cox (1979) while a numerical computation has been performed by Cowie et al (1981).

If supernovae are distributed at random through such a medium the majority will occur directly in the matrix. The free expansion phase will then occur essentially as above. Even when supernovae occur in typical cold neutral clouds ($n \sim 30 cm^{-3}$, $N \sim 30 M_\odot$) their remnants will generally reach

the cloud boundary after blast wave formation, but long before the onset of cooling. Complex dynamical phenomina will occur at break-out (Falle & Garlick 1982; Bodenheimer et.al. al 1983) but these should die away by the time the SNR has interacted with a few times the clouds' mass of ambient material.

For "matrix supernovae", and for "cloud supernovae" well after break-out, the blast wave phase will also qualitatively resemble that in the classical model. A high velocity shock will be driven into the hot matrix with much slower shocks driven into the clouds since for a fixed driving pressure the shock velocity is proportional to $n_o^{\frac{1}{2}}$; the envelope of the disturbance in the hot component will be roughly spherical. However, mass, momentum and energy exchange with the embedded clouds will take place and must play a significant role in the remnants evolution.

The behaviour of a cloud struck by an SNR blast wave will be discussed in detail in Chapter 5 so I will here only summarise the consequences of the collision for the SNR. During the interaction work is done on the cloud both to compress it (Cox 1979) and to accelerate it in the down-stream direction (McKee et al 1978); part of the energy of the blast wave is also "scattered" from the cloud in the form of acoustic waves (Spitzer 1982). From elementary considerations the fraction of the initial explosion energy consumed by cloud compression, integrated over the

lifetime of an SNR, will be on the order of a few times the cloud filling factor, with the bulk of the energy being dissipated in the lowest density (most easily compressed) component. Consequently if material with a density $\sim 0.1 - 1\ cm^{-3}$ fills an appreciable fraction (~ 0.3-0.6) of the interstellar volume then "cloud crushing" will compete with radiative cooling as the dominant mode of SNR energy dissipation. Cloud acceleration and acoustic wave generation each dissipate a more modest fraction of the explosion energy - a few tenths times the cloud filling factor.

Because of the large temperature gradient across their interface, electron thermal conduction can carry a large heat flux from the SNR interior into the cooler embedded clouds. As a result the clouds 'evaporate': material in their outer layers is heated and diffuses into and is assimilated by the hot ambient medium (McKee & Cowie 1977; Cowie & McKee 1977; see § 3.2.1).

The extent to which a magnetic field in the cloud can reduce the importance of evaporation is highly controversial. The conductivity perpendicular to a magnetic field is limited by the small electron giro radius and is consequently vanishingly small under interstellar conditions. McKee & Ostriker (1977) have, however, argued that the field geometry required to completely 'quench' evaporation from the whole cloud is highly improbable; mass exchange between components of the ISM which must occur even in the absence

of evaporation should ensure a high connectivity. The evaporation rate would then only be slightly reduced below that found in the absence of a magnetic field. Conversely, Cox (1979) has argued that relative motions between a cloud and the hot gas should wrap the field lines around the cloud entirely suppressing the evaporation. In what follows I will adopt an agnostic point of view and consider the consequences of both view points.

If evaporation of the embedded clouds is not significantly inhibited by the magnetic field, then it can make a dominant contribution to the mass in the interior of SNR evolving in the hot matrix, provided its density is $\lesssim 10^{-2} cm^{-3}$. The expansion law of such evaporation dominated SNR was first discussed by MO; subsequently Chiéze and Lazereff (1981) have given a similarity solution for this case. Cowie et al 1981 have given a full numerical treatment of the problem including several effects omitted from the earlier analytical calculations. Evaporation considerably modifies the temperature and density structure within the remnant from that in the Sedov solution. The evaporation rate is a strong function of temperature ($\dot{m} \propto T^{5/2}$) and hence tends to smooth out temperature gradients leading to an almost uniform interior temperature. Similarly since in an evaporation dominated SNR the immediate post-shock density is much less than the mean interior density, both the density and pressure peak at a point in the interior rather than at the edge of the remnant. In the similarity

solution the density peak occurs at ~0.7 of the blast wave radius. When allowance is made for the complete destruction and "sweeping out" of clouds originally near the explosion site this effect is even more pronounced; in the numerical simulation the local number density of clouds and hence the density of evaporated material peak at ~0.5 of the blast wave radius.

As a result of the enhancement of the average density by evaporation together with the dissipation of some of the explosion energy through cloud crushing, the SNR cools at a much earlier epoch than would an SNR in a homogeneous medium of the same density as the hot matrix. In addition cooling occurs and the dense shell forms in the interior of the SNR at the location of the density maximum rather than at the edge of the remnant. The subsequent expansion of the shell is qualitatively like that in the standard snow plough solution. The shock at the outer boundary of the remnant is unaffected by events in the cooling zone and continues to expand as before until eventually its driving pressure drops to that in the ambient medium and it decays into a spherical acoustic wave.

When evaporation is completely suppressed cloud crushing alone may still be sufficient to allow the remnant to cool radiatively before the external pressure becomes important provided the filling factor of readily compressed clouds is fairly large (Cox 1979; Cowie et al 1981).

3.1.2 Interactions and the Maintenance of a Global Hot Phase

Up to this point it has been assumed that SNR remain isolated from one another. However as first noted by Cox and Smith (1974) the longevity of the fossilised remants left by earlier explosions, implies that they must commonly be encountered by the expanding shock front of a new SNR. When this occurs, the blast wave of the young SNR will propagate preferentially into the old cavities' tenuous interior, re-heating and re-pressurising it, and thus forestalling its destruction.

To quantify the importance of this effect Cox and Smith introduced the porosity parameter Q(R) which measures the sum of the fractional volumes of all SNR smaller than some radius R. If supernovae occur at random at a volumetric rate S and their remnants expand spherically such that $R \propto t^{\eta}$ then,

$$Q(R) = \frac{4\pi}{3} \left(1 + 3\eta\right)^{-1} R^3 St \qquad 3.1\text{-}1$$

The volume filling factor of all such overlapping but <u>not interacting</u> SNR is

$$f = 1 - \exp\left[-Q(R) \right] \qquad 3.1\text{-}2$$

If interactions cause the 'rejuvenation' of old remnants as discussed by Cox and Smith then this is somewhat of an underestimate.

Cox and Smith assumed the ISM to be uniform with a mean density $\sim 1\,cm^{-3}$ and hence estimated a radius $\sim$40pc and

a total lifetime $\sim$4Myr for fossil SNR. Reasonable values for the galactic supernova rate then imply Q $\sim$0.1. They suggested that interactions would then occur sufficiently often that the ISM would be permeated by extensive branching chains of interconnected cavities, occupied by a hot low density plasma, periodically reheated by energy from new supernovae percolating through the network. Smith (1977) demonstrated the generation and maintenance of such a tunnel network by means of a Monte-Carlo simulation. This employed the results of evolutionary models of isolated SNR but incorporated a realistic description of both the processes leading to interconnection of intersecting SNR and the propagation of shocks through the chain of low density cavities. The, as yet rather limited, attempts to elucidate the details of SNR interaction by means of 2D hydrodynamic codes (Ikeuchi 1978; Jones et al 1979; Bodenheimer et al 1983) confirm the likely importance of rejuvenation and the general features of the interaction process suggested by Smith.

Subsequently, MO have pointed out that when due account is taken of the observed clumping of the interstellar gas into cold dense clouds the value of Q expected for the galaxy approaches unity. The interstellar clouds then become isolated islands of high density gas embedded in and confined by an all pervading high temperature plasma. MO have presented a detailed description of the thermodynamics and kinematics of the ISM under such circumstances in which

the 'symbiotic' relationship between the clouds and SNR is supposed to determine the equilibrium properties of the joint system.

MO suppose that ionising photons emitted by the hot gas, and by unshielded hot stars, heat and photoionise the outer layer of the clouds generating an extensive partially ionised warm corona around each. This has the important effect of increasing surface area of each cloud and thus enhances the rate at which they lose mass to the hot phase as a result of thermal evaporation. It is then supposed that the mass loss from clouds engulfed by young SNR evolving in the hot matrix is sufficiently rapid that radiative cooling occurs before the SNR reaches pressure equilibrium with its surroundings and before it grows to a size much greater than the vertical extent of the cloud system; material can then be returned to the high density phase via the process of cool shell formation. The pressure of the hot matrix material is then determined by the balance between the rate of energy input by supernovae and its dissipation via evaporation enhanced radiation. Given this pressure and the requirement of pressure equilibrium between the components, the properties of the cloud ensemble are fixed once the total mass of cloud material, and the amount of uv flux available to keep the cloud coronae warm and ionised, are specified. In particular the cloud parameters which fix the rate of evaporation are determined. The system will then be in equilibrium if the mass loss rate that the cloud population can support

matches that required to fix the matrix pressure.

Using values for the various input parameters of the model selected as being appropriate for the solar neighbourhood, MO were able to determine the properties of this equilibrium state in an internally self consistent manner. They were further able to demonstrate a generally good degree of agreement between the gross properties of the observed ISM and those predicted by the model.

In Section 3.3 I will develop a varient of the model of MO which would be appropriate if evaporation were completely suppressed by the clouds magnetic fields. Under these circumstances 'cloud crushing' would replace radiative cooling as the main sink for the SNR energy input (Cox 1979). The scheme discussed by MO is simply adapted to accommodate such a situation and I will show that very similar results to those of MO can be obtained provided only that the filling factor of warm cloud coronae is fairly large.

Habe et al (1981) have discussed the approach of an initially uniform density ISM to an equilibrium state similar to that obtained by MO. They did this by numerically solving a set of somewhat idealised coupled equations describing the exchange of mass between components of the ISM, due to evaporation, ionisation SNR shock heating and dense shell formation. They found that for a range of values of the input parameters close to those selected by MO an equilibrium

state was achieved on a timescale $\sim$1 - 3 Myr.

Because the scale height of gas at a temperature $\sim 10^5$ - 10^6K in the galactic gravitational field is several kil oparsec much greater than the thickness of the cloud population, hot gas generated in the galactic plane naturally tends to flow upward out of the disk. When the porosity Q is small as considered by Cox and Smith the hot gas can only "bubble up" out of the disk by displacing overlying cold gas (Jones 1973); when it is large as suggested by MO open channels will exist through which hot disk gas can freely stream into the halo. The fate of this rising gas depends on its initial temperature and density and the efficacy of any additional heating sources such as type I supernovae in the halo (Chevalier & Oergerle 1979; Habe & Ikeuchi 1980). If the disk gas is cool enough to be bound ($T \lesssim 10^6$K) and is sufficiently tenuous that its radiative cooling can be ignored gas can build up in the halo until its back pressure is sufficient to prevent further outflow and a static corona as originally envisioned by Spitzer (1956) results; if it is initially hot enough to be unbound or halo heating is sufficient to subsequently make it so, then there will be a galactic wind (Matthews & Baker 1971). When the density is sufficient that the gas can cool before reaching its scale height then a galactic fountain results (Shapiro & Field 1976; Bregman 1980; Kahn 1981); the rising hot gas cools and

condenses into clouds which subsequently fall back into the galactic plane, possibly giving rise to some of the observed high velocity clouds. Chevalier and Oergerle demonstrate that this latter possibility probably describes the current situation in our galaxy.

Cox (1979, 1981) has presented an alternate model of the SDC-ISM in which the properties of a warm component mechanically heated by 'cloud crushing' in SNR conspire with the operation of a galactic fountain to provide the same sort of phase control proposed by MO. Like MO, Cox supposes that the fundamental substrate of the ISM is a supernova generated hot tenuous plasma the pressure of which confines the cooler denser cloud components. Cox argues that a significant fraction of the Pdv work done by SNR on the interstellar clouds they overrun can be fed in part through the mediation of the clouds magnetic field into chaotic turbulent motions. Dissipation of this turbulence then leads to heating of the clouds. Cox then demonstrates that provided the matrix pressure is below a certain critical value, this mechanical heating mechanism is able to keep a substantial fraction of the clouds in a warm intermediate density state. Again mechanical ablation and evaporation of the clouds supplies material to the hot phase but Cox assumes this takes place at too low a rate to force SNR to cool within the disk (evaporation is supposed greatly inhibited by the clouds magnetic field), Instead the fraction ($\sim \frac{1}{2}$) of their energy not dissipated by cloud crushing is supposed to drive

a galactic fountain; radiative cooling and recirculation of material by the fountain then plays the same role as dense shell formation in the MO scheme.

Cox finds that the critical pressure below which a warm component can exist corresponds to a critical rate of SNR energy input and hence to a maximum value of the mass flux which the fountain can carry. The fountain flux may exceed this level by an arbitrary amount; the warm phase then ceases to exist, because it cools faster than it is heated, and the ISM consists of the hot matrix plus embedded cold clouds. However, whenever the mass flux falls short of this value, material returned to the disk by the fountain accumulates in the warm phase increasing its volume occupancy. This in turn increases the supply of material to the fountain raising the pressure to a value just short of the critical condition. Thus according to Cox's model conditions in a galaxy will always adjust so that the fountain flux is comparable with or in excess of the critical value.

Interestingly Cox finds that the rate of supernova energy input in the galaxy is just that required to drive such a limiting weak fountain. He also finds that a variety of observational constraints can only be met within the context of the fountain model, if the fountain is indeed weak. Further he suggests that far from being a coincidence, a variety of processes act both during the formation of galaxies

and their subsequent evolution, to ensure that they will always settle down into the weak fountain mode.

In the final analysis, although differing in detail the models of MO and Cox are extremely close in spirit. Indeed as discussed by Cox in the weak fountain limit the distinction between the two becomes largely one of semantics. Cox's model is, of intention, the more general and as a result does not seek to make specific predictions about the parameters of the ISM.

3.2 Evolution of a hot component SNR with Evaporation

3.2.1 Cloud dynamics and the evaporation rate

The evaporation of a static spheroidal cloud immersed in a hotter, stationary medium has been discussed under a variety of circumstances in a series of papers by McKee, Cowie and co-workers (Cowie & McKee 1977, McKee & Cowie 1977, Cowie & Songaila 1977, Balbus & McKee 1982, Cowie & Songaila 1983). The resulting mass loss rate can conveniently be written as,

$$\dot{m}_{ev} = 4\pi a_{cl}^2 \rho_h C_h F(\lambda_e/a_{cl}) \qquad 3.2\text{-}1$$
$$\simeq 3.6 \times 10^{18} gs^{-1} (a_{cl}/pc)^2 (n_h/10^{-3}cm^{-3})(T_h/10^6K)^{\frac{1}{2}} F(\lambda_e/a_{cl})$$

Where a_{cl} is the radius of a sphere having the same volume as the cloud, and ρ_h, n_h, T_h and C_h are respectively the mass density, hydrogen number density, temperature and isothermal sound speed in the hot medium. The dimensionless function F depends on the ratio of the mean free path for electron energy exchange in the ambient medium, $\lambda_e \simeq 3.2 (T_h/10^6K)^2/(n_h/cm^{-3})$, to the clouds dimensions.

When the classical conductivity (Spitzer 1962) is appropriate and radiative cooling of the evaporating gas is negligible, $F \simeq 3.68 \phi \lambda_e/a_{cl}$ (Cowie & McKee 1977) so that,

$$\dot{m}_{ev} \simeq 2.75 \times 10^{19} gs^{-1} \phi (T_h/10^6K)^{5/2} (a_{cl}/pc) \qquad 3.2\text{-}2$$

The constant ϕ is the product of two terms. The first, $\phi_g \gtrsim 1$, is a geometrical factor which is unity for spherical

clouds and depends weakly on the eccentricity according to (deduced from Cowie & Songaila 1977),

$$\phi_g = \frac{1}{2}\frac{e}{(1-e^2)^{1/6}}\left\{\frac{\pi}{4} - \tan^{-1}\left[\left(\frac{1-e}{1+e}\right)^{\frac{1}{2}}\right]\right\}^{-1} \qquad 3.2\text{-}3\ (a)$$

$$\phi_g = \frac{e}{(1-e^2)^{\frac{1}{3}}}\left\{\left|\mathrm{Log}\left[\left(\frac{1-e}{1+e}\right)^{\frac{1}{2}}\right]\right|\right\}^{-1} \qquad 3.2\text{-}3\ (b)$$

For oblate and prolate spheroids respectively. The relationships 3.2-3 are illustrated in Fig 3.2-1. The second term, $\phi_m \sim 1$, is introduced in the spirit of the discussion of § 3.1 to allow for partial quenching of the thermal conduction by magnetic fields.

When $\lambda_e \gtrsim a_{cl}/2$ the assumption of classical conductivity breaks down, the heat flux is limited by the density of electrons available to carry it (saturated conduction), and $F \sim 3.4\phi(\lambda e/a_{cl})^{3/8}$. Conversely, when $\lambda_e \lesssim 0.02\ a_{cl}$, radiative cooling in the conductive interface becomes so rapid that the direction of the flow is reversed and material condenses onto the cloud (McKee & Cowie 1977); in this regime $F \sim -\ 6\times10^{-2}$ (Cowie & Songalia 1983). Since the cloud radius at which radiation becomes important is only a Factor ~25 times larger than the radius at saturation, while interstellar clouds have a range of at least a factor of 50 in size, at any time an SNR may contain clouds in all three regimes. However, for the cloud spectra adopted here the evaporation rate is in general controlled by the smallest clouds. An SNR as a whole will thus be considered to be in the saturated regime when the radius of the smallest clouds it contains are comparable to λ_e and so on.

Application of these results to the case of a cloud overrun by an SNR blast wave will be complicated both by the effects of the flow of the hot material over the cloud and by the

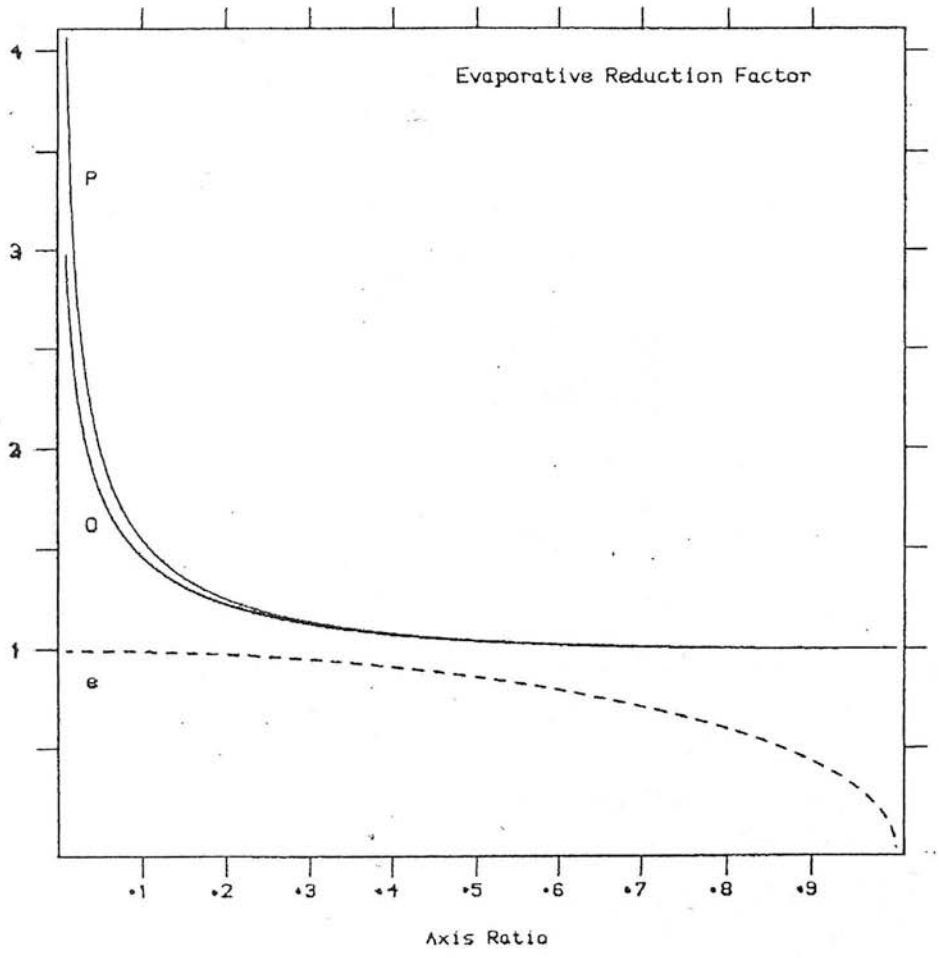

Figure 3.2-1 The evaporative reduction factor ϕ solid lines for prolate (P) and oblate (O) spheroidal clouds as a function of minor to major axis ratio. The dashed line (e) shows the cloud eccentricity for reference.

dynamical response of the cloud to being shocked.

When the cloud and ambient medium are in relative motion viscous stripping and surface instabilities(both Kelvin-Helmholtz and Rayleigh-Taylor) will also remove material from the cloud. The rates of these processes of dynamical ablation have been estimated for the case of rigid clouds immersed in a steady flow by Nulsen (1982). Not surprisingly, since viscosity and thermal conductivity result from closely related microscopic processes the rates of viscous stripping and evaporation are similar, both processes saturate together and both are similarly inhibited by magnetic fields.*

When the classical viscosity is appropriate and the flow past the cloud is laminar the rate of mass loss due to viscous stripping corresponds to $F \sim 1.1 \phi \lambda_e / a_{cl}$; this is just $\sim \frac{1}{3}$ of the corresponding classical evaporation rate and can conveniently be incorporated into equation 3.2-2 by appropriate choice of ϕ.

The assumption of laminar flow breaks down when the Reynolds number, $R_e \simeq 2.8 \, (a_{cl}/\lambda_e)(V/C_h)$ for flow velocity V, exceeds about 30 (Batchelor 1967). When the flow is also subsonic with respect to the cloud, mass loss due to turbulent processes (short wavelength Kelvin-Helmholtz modes) will be important, Nulsen finds $F \simeq \frac{1}{4} \, V/C_h$ for this process so that

---

*Strictly viscous stripping saturates when the ion mean free path is comparable to the cloud dimensions, however, the ion and electron mean free paths are of comparable magnitude. Although the ion giro radius exceeds that of the electron by the ratio of their masses suppression of transport processes perpendicular to the magnetic field is still almost total under interstellar condition.

the mass loss rate will be $\sim R_e/40\phi$ times the classical evaporation rate of equation 3.2-2 (note however, that $R_e \gtrsim 30$ and $V/C_h \lesssim 1$, imply $\lambda_e/a_{cl} \lesssim 9\times10^{-2}$ close to the condition for the supression of evaporation by radiative cooling). In the supersonic flow regime a stationary bow shock forms upstream of the cloud. Consequently there exists a small region of subsonic flow near the stagnation point at the front of the cloud where turbulent processes can operate. However, the flow field at the sides of the cloud will be supersonic (Currie 1974) and the Kelvin-Helmholtz instability will be suppressed (Gerwin, 1968; §5). Hence an upper limit to the resulting mass loss rate will be $F \lesssim 1/8$. Consequently unless substantially supressed by the magnetic field evaporation will be the dominant mode of mass loss until late epochs in SNR evaluation when $a_{cl} \gg \lambda_e$.

Numerical studies of the collision of shock waves with compressible interstellar clouds (Woodward 1976, 1979, Nittmann et al 1982; see §5) suggest that the most important role of fluid dynamical instabilities (predominantly Rayleigh-Taylor but also Kelvin-Helmholtz for subsonic collisions) is in promoting large scale deformation and eventual fission of the cloud. The effect of this is to greatly increase the effective surface area of the cloud (plus fragments) enhancing the rate of evaporation.

The surface pressure experienced by a cloud which is overrun

by an SNR blast wave will increase sharply as the shock passes and then slowly decline as the remnant expands. As discussed in detail in §5 the clouds response to this changing surface pressure is extremely complex even under the most idealised circumstances (Heathcote & Brand 1983). The cloud first collapses rapidly and then re-expands more slowly; ultimately the cloud must re-achieve pressure equilibrium on a timescale of order a few times the clouds sound speed crossing time t_{cl}. The importance of the cloud dynamics for the evaporation rate depends on the relative magnitudes of the characteristic timescales governing the various processes, which are summarised in table 3.2-1.

In general the timescale for evaporative flow in the cloud, t_{flow} is very much shorter than t_{cl} (Cowie & McKee 1977). Consequently the cloud can be treated quasi-statically and the instantaneous evaporation rate will be given by equation 3.2-1 with appropriate choice of F. If $t_{cl} \gg t_{SNR}$ the mean interval between successive young SNR overrunning a given cloud or if evaporation plays an important role in SNR dynamics for a period $\min\left[t_c, t_{es}\right] \ll t_{cl}$ or if clouds completely evaporate in a time $t_{ev} \ll t_{cl}$, then we can regard the cloud radius as a constant determined by the time averaged pressure it experiences. In the converse case, the cloud must remain close to pressure equilibrium with its immediate surroundings and the cloud radius, and consequently the evaporation rate, will change as the pressure in the SNR evolves. To account for this I will assume,

$$a_{cl}(P) \propto P^{-\omega} \qquad 3.2\text{-}4$$

Except for the least dense clouds struck by the highest velocity blast waves the post shock cooling time in the cloud $t_{c,cl} \ll t_c$, and the cloud can be regarded as isothermal, so that $\omega = \frac{1}{3}$, neglecting magnetic support; adiabatic clouds would have $\omega = 5/9$. For the photoionised cloud coronae of MO an additional complication is that the ionisation state may change in response to changes of density if the recombination timescale $t_{rec} \ll t_{cl}$. From the conditions of pressure equilibrium, ionisation balance and conservation of ionising flux (equations 3.3-1, 3.5-1 and 3.5-4) I find,

$$X = (1 + y)^{-\frac{1}{2}} \qquad 3.2\text{-}5$$

$$z = \frac{1}{y}\left[\frac{(1+y)^{\frac{1}{2}} + 1}{(1+y)^{\frac{1}{2}} - 1}\right]$$

Where X is the fractional ionisation z is the normalised cloud radius $z \equiv a_{cl}/(3\alpha_{rec}/4\pi J\sigma_H^2)$ and y is the normalised pressure $y = P/(1.1KT_{cl}.2\pi J\sigma_H/\alpha_{rec})$ and the other quantities are defined in §3.5 These relationships are shown in Fig. 3.2-2. Over the range of $0.25 \lesssim X \lesssim 1.0$ anticipated for the ISM the relationship of a_{cl} to P can adequately be represented by a power law of slope $\omega \sim 1.8$.

Unfortunately conditions in the ISM conspire to ensure that t_{cl}, t_{SNR}, t_{ev}, t_c, t_{es} and t_{rec} are all of comparable magnitude so that none of these cases is likely to be

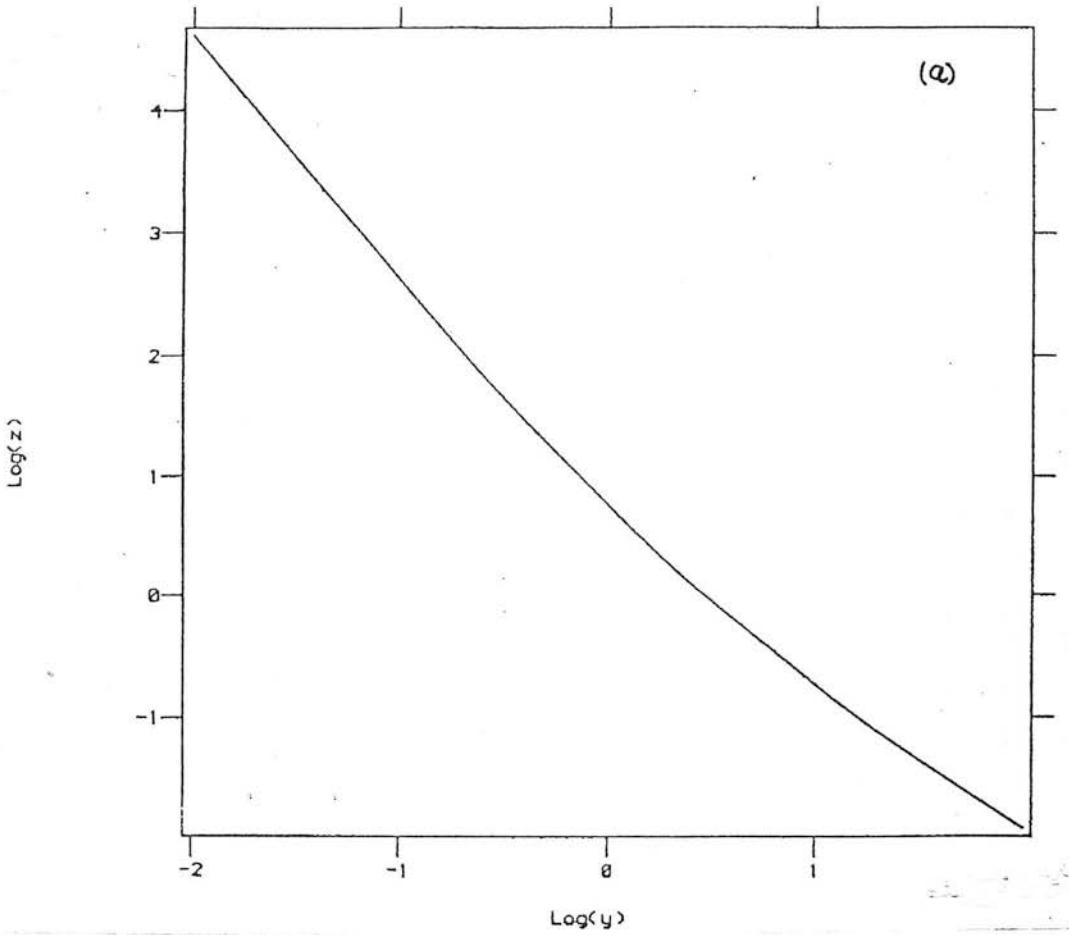

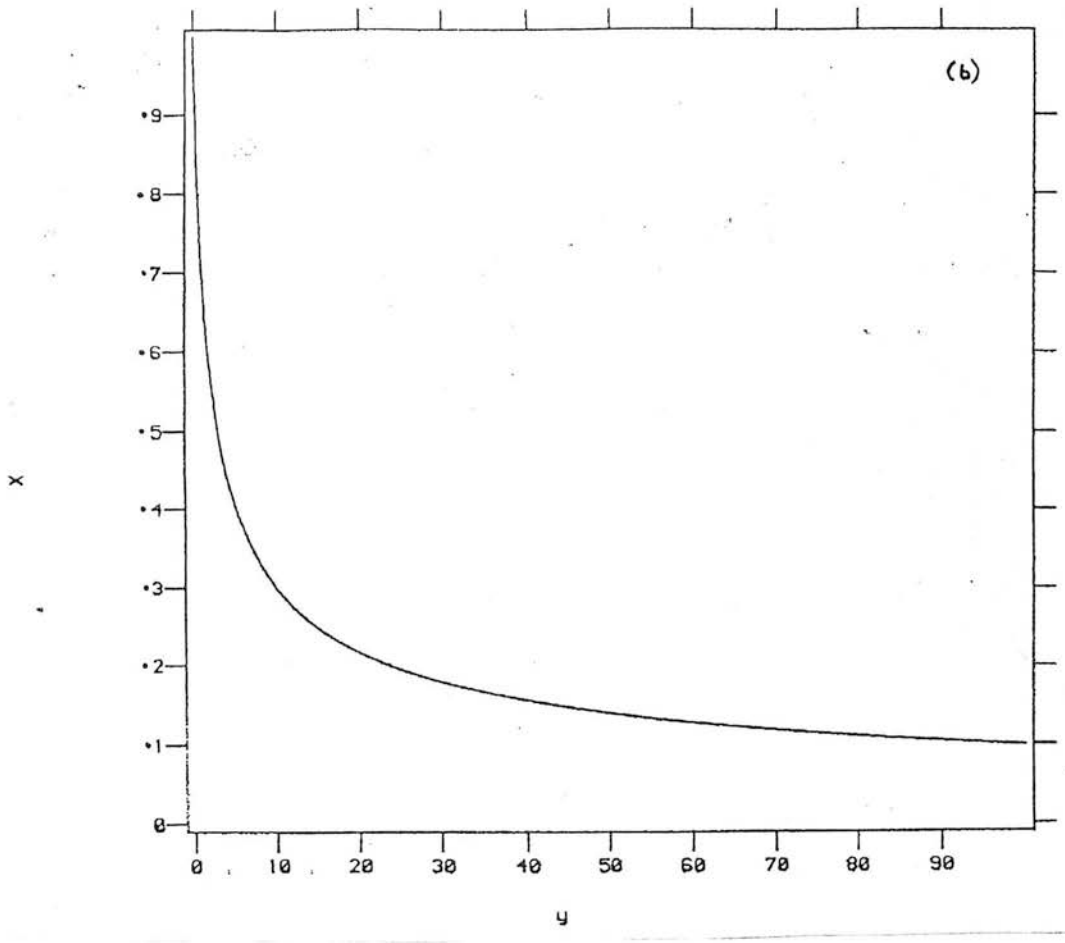

Figure 3.2-2 (a) normalised cloud radius z as a function of normalised pressure Y. Both axes are logarithmic. (b) ionisation fraction x as a function of normalised pressure Y. See text for the definition of these quantities.

applicable in detail. Nevertheless, I will employ equation 3.2-4 with $\omega = 0$, $\frac{1}{3}$ and 1.8 in order to provide a general indication of the way in which the evaporation rate is affected by cloud dynamics. In what follows these three cases will be referred to as case I (dynamics frozen), case II (ionization frozen) and case III.

In order to describe the evaporation rate of the ensemble of interstellar clouds it is convenient to introduce the evaporation parameter*

$$\chi \equiv N_{cl}\dot{m}_{ev}/T_h^{5/2} = 2.75 \times 10^4 \text{gs}^{-1}\text{K}^{-5/2}\text{pc}^{-3}\phi\left(\frac{N_{cl}}{\text{pc}^{-3}}\right)\left(\frac{\langle a_{cl}\rangle}{\text{pc}}\right) \qquad 3.2\text{-}6$$

where N_{cl} is the total number of clouds per unit volume and the angular brackets represent an average over the whole ensemble of clouds. In writing the second form it is explicitly assumed that the classical evaporation rate 3.2-2 is appropriate for all clouds which contribute significantly to the average.

---

* The evaporation parameter χ defined here differs from the parameter Σ introduced by MO. The two quantities are related by

$$\left(\frac{\chi}{\text{gs}^{-1}\text{K}^{-5/2}\text{pc}^{-3}}\right) = 2.89 \times 10^{-6}\text{gs}^{-1}\text{K}^{-5/2}\text{pc}^{-1}\alpha\left(\frac{\Sigma}{\text{pc}^2}\right)^{-1}$$

TABLE 3.2-1 Characteristic Timescales for Various Processes

Evaporative flow: - $t_{flow} \equiv \frac{4\pi a_{cl}^3 \rho_h}{\dot{m}_{ev}} \simeq 3 \times 10^2 \text{yr} \left(\frac{a_{cl}}{\text{pc}}\right)^2 \left(\frac{n_h}{10^{-3}\text{cm}^{-3}}\right) \left(\frac{T_h}{10^6\text{K}}\right)^{-5/2}$

Complete cloud evaporation: - $t_{ev} \equiv \frac{4\pi a_{cl}^3 \rho_{cl}}{\dot{m}_{ev}} \simeq 3 \times 10^5 \text{yr} \left(\frac{a_{cl}}{\text{pc}}\right)^2 \left(\frac{n_{cl}}{\text{cm}^{-3}}\right) \left(\frac{T_n}{10^6\text{K}}\right)^{-5/2}$

Dynamical response:- $t_{cl} \equiv \frac{a_{cl}}{c_{cl}} \simeq 1 \times 10^6 \text{yr} \left(\frac{a_{cl}}{\text{pc}}\right)\left(\frac{c_{cl}}{\text{kms}^{-1}}\right)^{-1}$

Cooling time of cloud shock:- $t_{cool,\,cl} \equiv \frac{3}{4} \frac{kT_{cl,sh}}{n_{cl}\Lambda(T_{cl,sh})} \simeq 6 \times 10^2 \text{yr} \left(\frac{V_{cl,sh}}{10^2\text{kms}^{-1}}\right)^{3.2} \left(\frac{n_{cl}}{\text{cm}^{-3}}\right)^{-1} V_{cl,sh} > 60\text{kms}^{-1}$

$$\simeq 6 \times 10^4 \text{yr} \left(\frac{V_{cl,sh}}{20\text{kms}^{-1}}\right)^{-5} \left(\frac{n_{cl}}{\text{cm}^{-3}}\right)^{-1} \quad 20 \leqslant V_{cl,sh} \leqslant 60$$ [58]

$$\simeq 3 \times 10^5 \text{yr} \left(\frac{V_{cl,sh}}{10\text{kms}^{-1}}\right)^{-1} \left(\frac{n_{cl}}{\text{cm}^{-3}}\right)^{-1} \quad V_{cl,sh} \leqslant 20\text{kms}^{-1}$$

Recombination time:- $t_{rec} \equiv \frac{1}{n_e \quad _{rec}} \simeq 1 \times 10^5 \text{yr} \left(\frac{n_e}{\text{cm}^{-3}}\right)^{-1}$

SNR repetition time:- $t_{SNR} \equiv \left(\frac{4\pi}{3} R^3 S\right)^{-1} \simeq 2.4 \times 10^6 \text{yr} \left(\frac{R}{100_{\text{pc}}}\right)^{-3} \left(\frac{S}{10^{-13}\ \text{pc}^{-3}\ \text{yr}^{-1}}\right)^{-1}$

SNR pressure evolution time:- $t_p \equiv \frac{P_s}{\partial P_s / \partial t}$

SNR Cooling time:- $$t_c \equiv \frac{E_{th}}{(dE_{th}/d_t)_{R_{ad}}} \simeq 4.5 \times 10^5 \text{yr} \left(\frac{E_o}{10^{51}\ \text{erg}}\right)^{-0.14} \left(\frac{\bar{\chi}}{10^{2}\ \text{gs}^{-1}\text{K}^{-\text{sh}}\ \text{pc}^{-3}}\right)^{-0.64}$$

Evaporation dominance time:- $$t_{es} \simeq 1.25 \times 10^8 \text{yrs} \left(\frac{E_o}{10^{51}\ \text{erg}}\right)^{\frac{1}{2}} \left(\frac{\bar{\chi}}{10^{2}\ \text{gs}^{-1}\text{K}^{-5/2}\ \text{pc}^{-3}}\right)^{\frac{2}{3}} \left(\frac{n_h}{10^{-3}\ \text{cm}^{-3}}\right)^{-1}$$

3.2.2 Evolution of an evaporative SNR

Adiabatic Phase

In order to treat the evolution of an evaporative SNR I adopt the following simplifying assumptions:

1. The SNR is presumed large enough to contain many clouds so that the SNR-cloud interaction can be treated statistically; this requires $R_s \gtrsim N_{cl}^{\frac{1}{3}} \sim 10\ pc$.
2. Both the low density ambient medium and the clouds are supposed smoothly and isotropically distributed so that spherical symetry is appropriate; large scale inhomogeneities due to the finite thickness of the cloud system and the action of previous and neighbouring supernovae are thus ignored requiring that R_s be less than the smaller of the cloud scale height, H_{cl}, and the radius at which SNR interact, R_{ov}.
3. During the adiabatic phase the pressure of the ambient medium is taken to be negligible compared to that in the SNR interior so that the blast wave is strong; the necessary condition is $R_c \ll (3E_{th}/2P_o)^{\frac{1}{3}}$.
4. The dynamical effects of the clouds, in particular the loss of energy due to cloud crushing and acceleration, are neglected; strictly this requires $f_{cl} \ll 1$ but as discussed in Appendix A1 even when $f_{cl} \lesssim 1$ the gross features of the SNR's evolution are not seriously misrepresented.
5. The evaporation rate is assumed to be given by equation 3.2-2, valid when the classical conductivity is appropriate, with the effects of cloud dynamics approximated

by equation 3.2-4; however, in Appendix A1 it is shown that the reduction of the evaporation rate due to saturation and complete cloud destruction at early epochs does not seriously effect the late time evolution.

The rate at which mass is added to the SNR by evaporation can then be conveniently written,

$$\dot{m}_{ev} = \frac{4\pi}{3} R_s^3 \; \bar{\chi}(R_s) \; \bar{T}^{5/2} \qquad (3.2\text{-}7)$$

where $\bar{T} \equiv (2\bar{\mu}E_{th}/3kM)$ is the mass averaged temperature in the remnant interior. The evaporation parameter $\bar{\chi}$ which varies with R_s due to the pressure dependence of a_{cl} (equation 3.2-4) is defined by,

$$\bar{\chi} = \chi(\bar{P}) \int_0^1 \left(\frac{\chi(P)}{\chi(\bar{P})}\right) \left(\frac{T}{\bar{T}}\right)^{5/2} d\left[\left(\frac{R}{R_s}\right)^3\right] \equiv \chi(\bar{P}) \; \phi_{SNR}$$

where the subscript s is used to denote quantities evaluated immediately behind the SNR shock and $\bar{P} = (E_{th}/2\pi R_s^3)$ is the volume averaged pressure in the SNR.

When the mass of evaporated material greatly exceeds the mass of swept up ambient gas a straightforward extension of the work of MO (Appendix A) leads to the dependence of the remants age and the enclosed mass upon R_s,

$$t = 0.85 M_{yr}\left[\left(\frac{\eta}{\alpha}\right)^7 \frac{1}{1-\eta}\right]^{1/6}\left(\frac{\bar{\chi}(R_s)}{10^2 gs^{-1}K^{-5/2}pc^{-3}}\right)^{1/6}\left(\frac{E_o\varepsilon}{10^{51}\,ergs}\right)^{-1/6}$$

$$\times \left(\frac{R_s}{10^2 pc}\right)^{5/3}$$

$$m = 3.84 \times 10^3 M_\odot\left[\left(\frac{\eta}{\alpha}\right)\frac{1}{1-\eta}\right]^{\frac{1}{3}}\left(\frac{\bar{\chi}(R_s)}{10^2 gs^{-1}K^{-5/2}pc^{-3}}\right)^{\frac{1}{3}}\left(\frac{E_o\,\varepsilon}{10^{51}\,ergs}\right)^{\frac{2}{3}}$$

$$\times \left(\frac{R_s}{10^2 pc}\right)^{4/3} \qquad (3.2\text{-}8)$$

$$\bar{\chi}(R_s) = \bar{\chi}(R_o)(R_s/R_o)^{3\omega}$$

In this expression $\eta = 6/(10 + 3\omega)$; the overall time dependence of R_s is $R_s \propto t^{\eta}$. The constants α and ε are respectively the ratio of the expansion velocity to the mass averaged isothermal sound speed in the SNR interior, $(3E_{th}/2M)^{\frac{1}{2}}$. and the ratio of the thermal to total energies E_{th}/E_o.

The numerical values of α, ε and ϕ_{SNR} depend on the runs of density, temperature, velocity and cloud number density within the remnant, which in turn depend in a complex manner on the value of ω, and how effective thermal conduction is in smoothing the temperature profile. However as discussed in Appendix A1 the dependence is quite weak so that even drastic modification of the internal structure leads to only small changes in the values of these parameters. Furthermore, this insensitivity suggests that equation

(3.2-8) will be a far better approximation to the expansion law of SNR in a realistic ISM than might be supposed from the crudity of the assumptions, especially those relating to the physics of the cloud shock interaction, made in its derivation. In Appendix A1 I estimate $1.5 \lesssim \alpha \lesssim 3$ $0.5 \lesssim \varepsilon \lesssim 1$ and $\frac{1}{2} \lesssim \phi_{SNR} \lesssim 2$; for ease of comparison with the work of MO I will adopt $\alpha = 2.5$, $\varepsilon = 0.7$ and $\phi_{SNR} = 1$, as assumed by them, as the standard values.

Following MO I define the SNR cooling time to be,

$$t_c = \frac{3}{2} \frac{k}{\beta} \frac{\bar{T}}{\Lambda(\bar{T})} \left(\frac{4\pi}{3} \frac{R^3 \bar{\mu}}{M} \right) \qquad (3.2\text{-}9)$$

where Λ is the radiative cooling coefficient for an optically thin plasma of cosmic abundances and in collisional ionisation equilibrium, which for $10^5 K \lesssim T \lesssim 4 \times 10^7 K$ is approximately $\Lambda(T) \simeq 6.2 \times 10^{-19}$ erg cm^3 $T^{-0.6}$ (Raymond, Cox & Smith 1976). The radiative cooling enhancement factor, β, exceeds unity due to three effects. Firstly, since the radiative cooling rate varies as the square of the gas density, inhomogeneities within the remnant lead to an enhancement by a factor,

$$\beta_{SNR} \equiv \left(\frac{T_s}{\bar{T}} \right)^{-0.6} \int_0^1 \left(\frac{\rho}{\rho_s} \right)^2 \left(\frac{T}{T_s} \right)^{-0.6} \left[d\left(\frac{R}{R_s} \right)^3 \right]$$

Again β_{SNR} depends only weakly on the runs of density and temperature within the remnant and will typically be ~ 2. Secondly as discussed by McKee and Cowie (1977), radiation from gas in the evaporative flow around the embedded clouds can considerably increase the net cooling rate, the major contribution coming

from gas with $T \sim 10^5$K near the peak of the cooling curve. Clearly the importance of this effect must decline as the temperature of the ambient medium itself approaches 10^5K. Consequently as the temperature at the cooling point will be found to be typically $\sim 10^6$K the enhancement due to this process is limited to only modest values; from the results of McKee and Cowie (1977) I estimate $\beta_{ev} \lesssim 2$. Finally the ionisation state of both the newly shocked ambient gas and the material injected by evaporation, will lag its temperature and consequently it cools at a rate greater than that in collisional equilibrium. The magnitude of this effect is uncertain due to the absence of detailed calculation of the non-equilibrium cooling rate for the evaporated gas, which by assumption makes up the majority of remnants mass, however, it is unlikely to exceed a factor ~ 2. MO assumed a rather high overall value $\beta \sim 10$, while their later numerical study (Cowie, McKee & Ostriker 1981) led to $\beta \sim 1$ at the time of cooling. However, this latter value explicitly ignores the effects of non-equilibrium ionisation on the cooling rate and McKee (1982) has therefore, argued that the larger value is more likely correct. Recognising the large degree of uncertainty in this parameter I conservatively adopt $1 \lesssim \beta \lesssim 10$.

Substituting from 3.2-8 into 3.2-9 straightforwardly leads to expressions for the age, radius, mass and other parameters of the SNR at the cooling point in terms of $\bar{\chi}_c$ the value of

the evaporation parameter at that epoch. For ease of reference these expressions are summarised in Table 3.2-1, while the power law dependences of these parameters upon R_s expressed in terms of their values at cooling are given in Table 3.2-3. When calculating volume averages over the ensemble of SNR as in §3.2.3 it is more convenient to have the parameters expressed in terms of the porosity parameter $Q \equiv 4\pi R^3 st/3(1 + 3\eta)$ and its value at the cooling point Q_c. Such expressions are listed in Tables 3.2-2 and 3.2-3.*

---

* Note that in the corresponding expressions given by MO the exponents of α in the equations for t_c and $\dot{R}_c$ are incorrect.

TABLE 3.2-1 Conditions at the cooling point in terms of χ_c

$$R_c = 140 \text{ pc } (\alpha/\eta)^{61/64} (1-\eta)^{31/64} \beta^{-15/32} (\varepsilon E_o/10^{51}\text{ erg})^{1/64} (\bar{\chi}_c/10^2 \text{gs}^{-1}\text{K}^{5/2}\text{pc}^{-3})^{-31/64}$$

$$t_c = 1.5 M_{yr} (\alpha/\eta)^{27/64} (1-\eta)^{41/64} \beta^{-25/32} (\varepsilon E_o/10^{51}\text{ erg})^{-9/64} (\bar{\chi}_c/10^2 \text{gs}^{-1}\text{K}^{5/2}\text{pc}^{-3})^{-41/64}$$

$$\dot{R}_c = 74 \text{ K}_{ms}^{-1} \alpha (\alpha/\eta)^{-15/32} (1-\eta)^{-5/32} \beta^{5/16} (\varepsilon E_o/10^{51}\text{ erg})^{5/32} (\bar{\chi}_c/10^2 \text{gs}^{-1}\text{K}^{-5/2}\text{pc}^{-3})^{5/32}$$

$$M_c = 6.1 \times 10^3 M_\odot (\alpha/\eta)^{-15/16} (1-\eta)^{5/16} \beta^{-5/8} (\varepsilon E_o/10^{51}\text{ erg})^{11/16} (\bar{\chi}_c/10^2 \text{gs}^{-1}\text{K}^{-5/2}\text{pc}^{-3})^{-5/16}$$

$$\bar{n}_c = 1.5 \times 10^{-2} \text{cm}^{-3} (\alpha/\eta)^{-123/64} (1-\eta)^{-75/64} \beta^{25/32} (\varepsilon E_o/10^{51}\text{ erg})^{41/64} (\bar{\chi}_c/10^2 \text{gs}^{-1}\text{K}^{-5/2}\text{pc}^{-3})^{73/64}$$

$$\bar{T}_{hc} = 4.1 \times 10^5 \text{K} (\alpha/\eta)^{-15/16} (1-\eta)^{-5/15} \beta^{5/8} (\varepsilon E_o/10^{51}\text{ erg})^{5/16} (\bar{\chi}_c/10^2 \text{gs}^{-1}\text{K}^{-5/2}\text{pc}^{-3})^{5/16}$$

$$(10^{-13}\text{pc}^{-3}\text{yr}^{-1}(1+3\eta)Q_c/S) \equiv 1.7 (\alpha/\eta)^{105/32} (1-\eta)^{67/32} (\varepsilon E_o/10^{51}\text{ erg})^{-6/64} (\bar{\chi}_c/10^2 \text{gs}^{-1}\text{K}^{-5/2}\text{pc}^{-3})^{-67/32}$$

TABLE 3.2-2 Conditions of the cooling point in terms of Q_c

$$R_c = 120\ \mathrm{pc}\ (\alpha/\eta)^{13/67}\beta^{5/134}\ (\varepsilon E_o/10^{51}\ \mathrm{erg})^{5/134}\ (10^{-13}\mathrm{pc}^{-3}\mathrm{yr}^{-1}\ (1+3\eta)\ Q_c/S)^{31/134}$$

$$t_c = 1.3 M_{yr}\ (\alpha/\eta)^{-39/67}\beta^{-15/134}\ (E_o/10^{51}\ \mathrm{erg})^{-15/134}\ (10^{-13}\mathrm{pc}^{-3}\mathrm{yr}^{-1}\ (1+3)\ Q_c/S)^{41/134}$$

$$\dot{R}_c = 78\ K_{ms}^{-1}\ (\alpha/\eta)^{-15/67}\beta^{10/67}\ (\varepsilon E_o/10^{51}\ \mathrm{erg})^{10/67}\ (10^{-13}\mathrm{pc}^{-3}\mathrm{yr}^{-1}\ (1+3\eta)\ Q_c/S)^{-5/67}$$

$$M_c = 5.6 \times 10^3 M_o\ (\alpha/\eta)^{30/67}\beta^{-20/67}\ (\varepsilon E_o/10^{51}\ \mathrm{erg})^{47/67}\ (10^{-13}\mathrm{pc}^{-3}\mathrm{yr}^{-1}\ (1+3\eta)\ Q_c/S)^{10/67}$$

$$\bar{n}_c = 2 \times 10^{-2}\mathrm{cm}^{-3}\ (\alpha/\eta)^{-9/67}\beta^{-55/134}\ (\varepsilon E_o/10^{51}\ \mathrm{erg})^{79/134}\ (10^{-13}\mathrm{pc}^{-3}\mathrm{yr}^{-1}\ (1+3\eta) Q_c/S)^{-73/134}$$

$$\bar{T}_{hc} = 4.4 \times 10^5 \mathrm{K}\ (\alpha/\eta)^{-30/67}\beta^{20/67}\ (\varepsilon E_o/10^{51}\ \mathrm{erg})^{2-/67}\ (10^{-13}\mathrm{pc}^{-3}\mathrm{yr}^{-1}(1+3\eta)\ Q_c/S)^{-10/67}$$

$$(\bar{P}_c/k) = 2.1 \times 10^4 \mathrm{Kcm}^{-3}\ (\alpha/\eta)^{-39/67}\beta^{-15/134}\ (\varepsilon E_o/10^{51}\ \mathrm{erg})^{119/134}\ (10^{-13}\mathrm{pc}^{-3}\mathrm{yr}^{-1}(1+3\eta) Q_c/S)^{-93/134}$$

$$\bar{\chi}_c = 131 \mathrm{gs}^{-1}\mathrm{K}^{-5/2}\mathrm{pc}^{-3}(\alpha/\eta)^{105/67}\beta^{-70/67}\ (E_o/10^{51}\ \mathrm{erg})^{-3/67}\ (10^{-13}\mathrm{pc}^{-3}\mathrm{yr}^{-1}(1+3\eta)\ Q_c/S)^{-32/67(1-\eta)}$$

TABLE 3.2-3 SCALING WITH R AND Q

Adiabatic Phase

$$R = R_c(Q/Q_c)^{\eta/(3\eta + 1)}$$

$$t = t_c(R/R_c)^{1/\eta} = t_c(Q/Q_c)^{1/(3\eta + 1)}$$

$$\dot{R} = \dot{R}_c(R/R_c)^{(\eta - 1)/\eta} = \dot{R}_c(Q/Q_c)^{(\eta - 1)/(3\eta + 1)}$$

$$M = M_c(R/R_c)^{2(1 - \eta)/\eta} = M_c(Q/Q_c)^{2(1 - \eta)/(3\eta + 1)}$$

$$n = n_c(R/R_c)^{(2 - 5\eta)/\eta} = n_c(Q/Q_c)^{(2 - 5\eta)/(3\eta + 1)}$$

$$T_h = T_{hc}(R/R_c)^{2(\eta - 1)/\eta} = T_{hc}(Q/Q_c)^{2(\eta - 1)/(3\eta + 1)}$$

$$P = P_c(R/R_c)^{-3} = P_c(Q/Q_c)^{-3/(3\eta + 1)}$$

$$\chi = \chi_c(R/R_c)^{-(6 - 10\eta)/\eta} = \chi_c(Q/Q_c)^{-(6 - 10\eta)/(3\eta + 1)}$$

Post-Cooling Phase

$$R = R_c(Q/Q_c)^{\eta'/(3\eta' + 1)}$$

$$t = t_c(R/R_c)^{1/\eta'} = t_c(Q/Q_c)^{1/(3\eta' + 1)}$$

$$\dot{R} = \dot{R}_c(\eta'/\eta)(R/R_c)^{(\eta' - 1)/\eta} = R_c(\eta'/\eta)(Q/Q_c)^{(\eta' - 1)/\eta'}$$

$$n = n_c(1 - \delta)(R/R_c)^{-3} = n_c(1 - \delta)(Q/Q_c)^{-3\eta'}$$

$$T_h = T_{hc}(R/R_c)^{-2} = T_{hc}(Q/Q_c)^{-2\eta'/(3\eta' + 1)}$$

$$P = P_c(1 - \delta)(R/R_c)^{-5} = P_c(1 - \delta)(Q/Q_c)^{-5\eta'/(3\eta' + 1)}$$

Post Cooling Evolution

At the cooling point a fraction $\delta \sim \frac{1}{2}$ of the mass contained in the remnant condenses into a dense shell, and the mean pressure and density in the remnant fall to a fraction $(1 - \delta)$ of their immediate pre-cooling values. Since for $10^5 K \lesssim T_c \lesssim 2 \times 10^7 K$ the interstellar gas is thermally unstable shell formation will be extremely rapid.

The majority of the work described here was completed before the publication of Cowie et al's (1981) numerical study. Consequently it was assumed, following MO, that the shell formed at the edge of the remnant. The SNR then evolves as a "pressure driven snowplough". As discussed in Appendix A2 after shell formation the expansion law can then be approximated by $R \propto t^{\eta'}$ with $2/7 \lesssim \eta' \lesssim 1$. The upper bound on η' corresponds to the case where the initial mass of the shell is so great that the forces acting on it are negligible compared to its inertia. It then expands at constant velocity. The lower bound corresponds to the opposite limit where the mass of the shell is dominated by the ambient gas which it sweeps up. Since the interior pressure declines rapidly with decreasing radius ($P \propto R^{-5}$) the external pressure becomes rather suddenly important at a radius $R_D \simeq R_c (P_o/(1 - \delta)P_c)^{1/5}$. Subsequently the shell continues to expand driven by its stored momentum. If the shell remained intact the expansion of the remnant would then drive the interior pressure below that of the ambient medium until the pressure differential so generated was

sufficient to halt (and indeed reverse) its motion. However the decclerating shell will be Rayleigh-Taylor unstable and hence will break up the resulting fragments continuing to expand at constant momentum.

Conversely, if the dense shell forms in the SNR interior as indicated in the computation of Cowie et al, then the dynamics of the (adiabatic) shock bounding the SNR, and the dense cooled shell are largely uncoupled. The reduction in the interior pressure due to cooling will only be communicated to the outer shock after about a sound crossing time for the remnant $\sim \alpha t_c/\eta$ which is typically much greater than the time required for the completion of the remnants expansion. Consequently the SNR as a whole continues to expand more or less as in the adiabatic phase* so that $\eta' \simeq \eta$. Eventually the immediate post shock pressure falls to the ambient pressure at a radius $R'_E \simeq R_c (P_o/P_c)^{\frac{1}{3}}$ and the outer shock degenerates into a spherical sound wave. The evolution of the dense shell will be somewhat complicated, since the pressure and density of the medium into which it advances, the outer part of the remnant, decreases with time as the outer shock expands. However, the time scale for the outer shock to decay into

---

* An observationally interesting possibility is that for ambient densities somewhat higher than considered by Cowie et al, but still low enough that SNR are evaporation dominated, radiative cooling may eventually set in behind the outer shock leading to an SNR with two concentric cool dense shells.

a sound wave will be much shorter than the characteristic expansion timescale of the shell so that the snowplough solutions discussed in Appendix A2 will still be crudely applicable.

Thus in either case the outer boundary of the remnant expands according to $R \propto t^{\eta'}$; the power law dependences of other quantities of interest upon R and Q are given in Table 3.2-3. For simplicity, the end of the post cooling expansion phase and the onset of the "disruption phase" will be taken to occur when the remnant reaches the appropriate "pressure equilibrium radius" R_E or R'_E: the prescription for the determination of the ambient pressure adopted in § 3.2.3 makes this epoch equivalent to that at which interaction with remnants of similar age become probable as is appropriate for a supernova dominated ISM. It is assumed that the average conditions within the SNR do not change significantly beyond this epoch. This ignores the effects of continued radiative cooling which tends to lower the temperature and pressure in the SNR and the effects of further mass exchange with the enclosed clouds which changes the density. However, for the conditions in the ambient medium/old SNR found below the timescales for both processes are long compared to the mean interval which elapses between successive SNR overrunning a given point.

3.2.3 Average Conditions in the Hot Matrix

Following MO I will assume that SNR came into pressure equilibrium with their surroundings and cease expanding when interactions with other SNR of comparable age become common. This will be taken to occur when the porosity parameter $Q = 1$. The radius age and expansion velocity at the point of overlap can then be obtained directly by substituting $Q = 1$ in the relationships in Table 3.2-3. As discussed in § 3.2.2 I will further assume that conditions within the SNR cease to change after the epoch of overlap so that the temperature, density and pressure in the ambient medium are set equal to their values for an SNR when $Q = 1$.

The average of any quantity, F taken over the entire ensemble of SNR will then be given by,

$$\langle F \rangle \equiv \int_0^\infty F(Q) e^{-Q} dQ = \int_0^1 F(Q) e^{-Q} dQ + F(Q = 1)/e \qquad 3.2\text{-}9$$

The average pressure, temperature and density of the hot component obtained in this way are shown in Figure 3.2-3, as functions of Q_c the porosity parameter at the cooling point, for various choices of the exponents in the pre-cooling and post-cooling expansion laws $\eta = 6/(10 + 3\omega)$ and η' . In all cases the value of the mass fraction incorporated in the shell δ has been taken as $\frac{1}{2}$.

In the simple representation of the cloud dynamics employed here the cloud radius varies with pressure according to

a $\propto P^{-\omega}$. In §3.5 'typical' values of the properties of the cloud population will be defined purely as a computational convenience, as being those values which would obtain if all the clouds were in equilibrium with the average hot component pressure $\langle P \rangle$. Clearly the volume average properties of the cloud ensemble are observationally of more relevance. In Figure 3.2-4 I show the ratio of the volume averaged cloud radii, filling factors and line of sight separation to their typical values, again as functions of Q_c, η and η'.

Note that MO fixed the parameters of the cloud population by assuming the clouds to be in equilibrium at a pressure P_{typ} defined to be the value of the pressure averaged over all supernovae having $0.25 \leq Q \leq 0.75$. This was presumably intended to crudely allow for the effects of the cloud dynamics which are treated explicitly here. The typical pressure of MO is generally lower than the volume average pressure employed here because it excludes the contribution of the youngest adiabatic SNR.

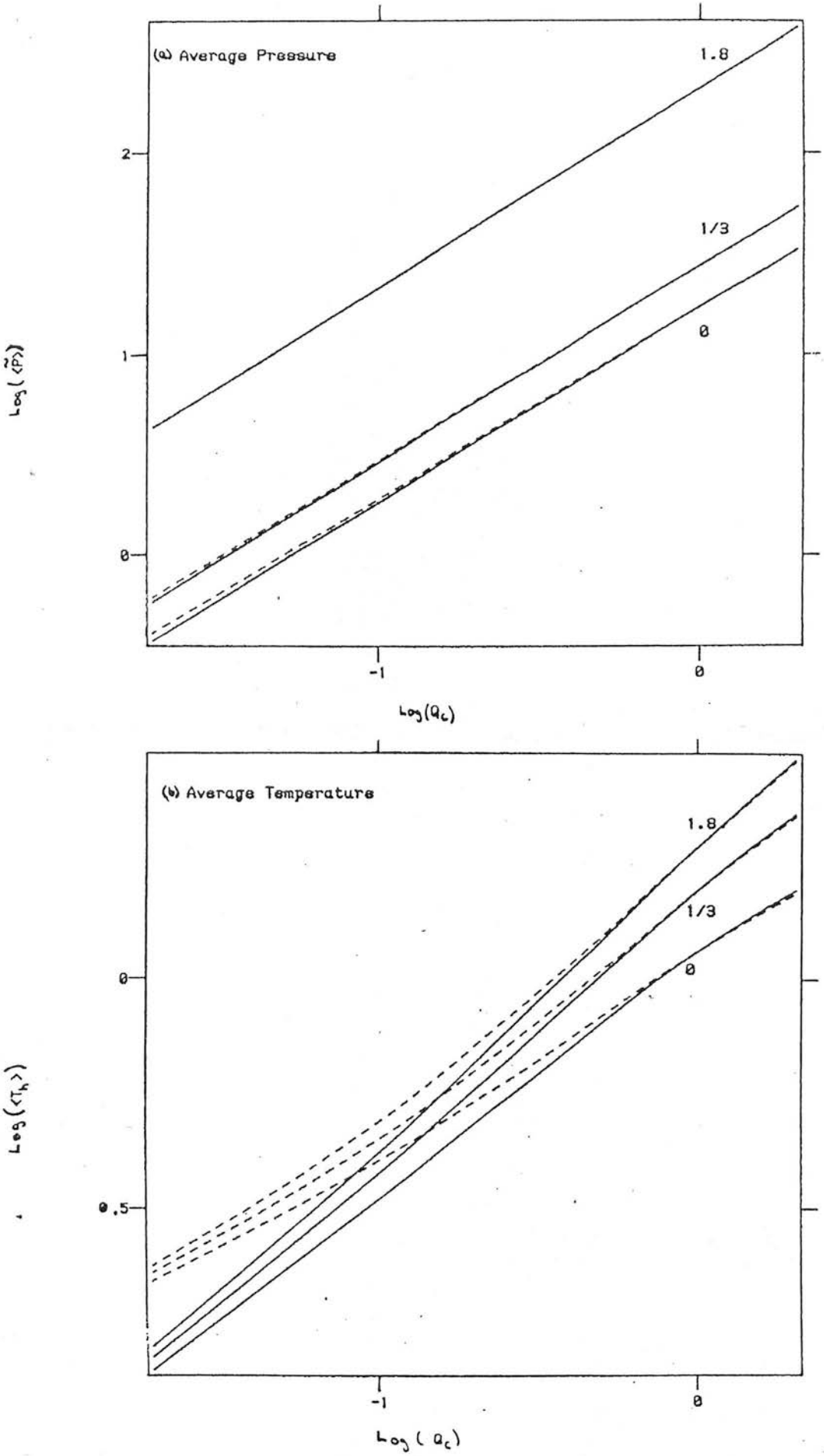

Figure 3.2-5: (a) The Average pressure and (b) the average temperature as functions of Q_c. The various curves are labelled by the cloud compression exponent ω. Solid curves are for $\eta' = 1$ dashed curves for $\eta' = 2/7$.

3.3 The Evolution of Hot Component SNR without Evaporation

The model for the evolution of SNR in the hot matrix presented in §3.2 assumed that the evaporation of embedded clouds plays a dominant role in the early stages of SNR evolution. However, as discussed in §3.1, thermal evaporation may be suppressed if the magnetic field in the interface between the cloud and the hot matrix possesses a suitable geometry. Cox (1979) has examined the evolution of hot component SNR under such circumstances. In particular his calculations show that for this case both the external pressure and interactions with the halo will become important prior to the onset of radiative cooling. He suggested that cloud compression might then be the dominant sink for SNR energy and that this mechanism could represent an important heat source for the clouds. To assess the consequences such a situation might have for the model of the SDC-ISM described here I will construct a simple variant of it in which Cox's scheme for SNR evolution is used in place of the scheme for evaporative SNR presented in §3.2 In the present section I will very briefly summarise the results from Cox's work which will be required here.

Cox obtained an approximate expression for the expansion law of an SNR in an inhomogeneous medium when the external pressure is not negligible by comparison with the pressure in the remnant interior. His treatment assumes that the SNR is spherical and expands at a velocity given by the jump

conditions for an adiabatic shock driven by a pressure,

$$P = P_o + \frac{2}{3}\left(\frac{3}{4\pi}\frac{E_o}{f_B R_B^3}\right) \simeq P_o\left(1 + \frac{5}{4}y\right)$$

which defines the dimensionless parameter y in such a way that the external pressure becomes important when $y \sim 1$*. Here P_o is the pressure in the ambient medium R_B is the shock radius and f_B is the fraction of the volume interior to the SNR shock which is raised to a high pressure by its passage. f_B was assumed to have a value less than unity to allow for the volume occupied by the clouds but somewhat greater than $(1-f_{cl})$ to crudely allow for the effect of their compression on the expansion. In this way Cox obtained an expression for the expansion law which approximates to the Sedov solution for small values of y and to the motion of a sonic wave for large y.

Cox assumed that the expansion of the SNR continued until at $y = y_{max}$, all the explosion energy had been dissipated, and calculated the volume average pressure contributed by the ensemble of SNR as a function of y_{max} in a manner analogous to that described in §3.2.3. The result obtained by Cox can be written,

$$\langle P_h \rangle \simeq 3.3\times10^{-12}\ \text{dyn cm}^{-2}\left[\frac{1}{f_b}\left(\frac{n_h}{10^{-3}\text{cm}^{-3}}\right)^{\frac{1}{2}}\left(\frac{E_o}{10^{51}\text{erg}}\right)\left(\frac{S}{10^{-13}\text{pc}^{-3}\text{yr}^{-1}}\right)\log(2\,y_{max}+1)\right]^{\frac{2}{3}} \qquad 3.3.1$$

---

* Cox denoted this variable by S. The change is made here to avoid confusion with the supernova rate.

where n_h is the density of the hot matrix gas.

He also obtained an expression for the rate of net compressional work done by an SNR on the clouds contained within it. The integral of this quantity from y = 0.1 to y' can be approximately represented by

$$W_{net}(y') \simeq \frac{0.955\, E_o\, (E_o/\langle P_h\rangle)^{\frac{1}{3}}\, n_h^{\frac{1}{2}}}{n_w^{\frac{1}{2}}\, \langle a_w\rangle + 0.228\, (E_o/\langle P_h\rangle)^{\frac{1}{3}} n_h^{\frac{1}{2}}}\, f_w\, (1-(10y')^{-\frac{1}{4}}) \qquad 3.3\text{-}2$$

where f_w is the filling factor of the warm clouds and $\langle a_w\rangle$ is the radius of the warm clouds averaged over the entire population of interstellar clouds (See § 3.4). Equation 3.3-2 has been corrected to allow for the complete compression of the smallest clouds.

In order to determine y_{max}, I will assume for simplicity that all of the explosion energy is consumed by cloud crushing and thus I require $W_{net}(y_{max}) = E_o$. The asymptotic behaviour of the explicit y dependence in equation 3.3-2 together with the rapid decrease of f_w with increasing y, consequent on the increasing pressure results in $W_{net}(y)/E_o$ possessing a maximum near $y \sim 0.3$. When this is combined with the description of the cloud properties given in § 3.4 this implies that the requirement that $W_{net}(y_{max})/E_o = 1$ can only be met if $S^{\frac{2}{3}}/\bar{n} \leq 3.6 \times 10^{-9}$. Conversely if the ambient pressure is to be sufficient to confine the warm

envelopes so that $f_w \leq 1$ then $S^{\frac{2}{3}}/\bar{n} \geq 1.4 \times 10^{-9}$. Obviously these two requirements considerably restrict the range of conditions over which it will be possible to find valid solutions to the model equations in the non-evaporative case.

3.4 Representation of the cloud ensemble

I will adopt the model of the interstellar clouds developed by MO, but incorporate a straightforward extension to allow for the possibility of non-spherical clouds. In this, each cloud optically thick to ionising photons possesses a composite core-envelope structure. The core is cold, dense, and neutral; the more tenuous envelope is kept warm and partially ionised by UV photons emitted by stars and the hot matrix gas. The thickness of the ionised envelope is simply fixed by the requirement that the optical depth for ionising photons is of order unity at its base (the criterion adopted below, equation 3.4-4, implies $\tau_w = 3/2$). The subscripts c and w will be used to distinguish between parameters of the cold cores and the warm envelopes.

For simplicity, I will assume that the warm envelope is a layer of constant depth overlying the cloud core. Then, the condition that the ionisation rate must balance the rate of incoming photons in an optically thick cloud can be written,

$$4\pi^2 \Theta_g \, a_w^2 \, J = \frac{4}{3}\pi (a_w^3 - a_c^3) \zeta \, n_w (1 - X_w) \qquad 3.4\text{-}1$$

where, the small correction required to allow for photoionisation of helium has been neglected. Here a_w and a_c are the radii of spheres enclosing the same volume as the outer boundaries of the core and the envelope respectively, J is the mean intensity of UV ionising photons in the vicinity of the cloud (photons $cm^{-2}S^{-1}Sr^{-1}$) and ζ is the photoionisation

rate per atom for hydrogen. The geometrical factor Θ_g is simply the ratio of the cloud surface area to that of the equivalent volume sphere; this is given in terms of the eccentricity e by

$$\Theta_g = \frac{1}{2}\frac{1}{(1-e^2)^{\frac{1}{3}}}\left[1 + \frac{(1-e^2)}{e}\,\mathrm{Log}\left(\frac{1+e}{1-e}\right)\right] \qquad 3.4\text{-}2$$

$$\Theta_g = \frac{1}{2}(1-e^2)^{\frac{1}{3}}\left[1 + \frac{1}{(1-e^2)^{\frac{1}{2}}}\,\frac{\mathrm{Sin}^{-1}e}{e}\right]$$

for oblate and prolate spheriods respectively, which relationships are illustrated in Fig. 3.4-1. Following MO I assume that at a typical point in the envelope photons are incident from 2π steradians so that $\zeta = 2\pi J \sigma_H$ where σ_H is the effective photoionisation cross section for hydrogen, $\sigma_H \equiv 6.3 \times 10^{-18}\,\mathrm{cm}^{-2} \int_1^\infty \sigma(\nu/\nu_L)\, J(\nu/\nu_L)\, d(\nu/\nu_L)/J$. Hence it follows that,

$$a_w^2\, a_{wb} = a_w^3 - a_c^3 \qquad 3.4\text{-}3$$

where a_{wb}, the radius of the smallest optically thick cloud, is given by,

$$a_{wb} = \frac{3\Theta_g}{2\sigma_H n_w (1 - X_w)} \qquad 3.4\text{-}4$$

In describing the variation of a_w and a_c with cloud mass, M_{cl}, it is convenient to introduce the parameter $a_o \equiv (3M_{cl}/4\pi\rho_c)^{1/3}$ which is the radius the cloud would have if it were all cold. It is then easy to show that, to lowest order in the small quantity $(n_w/n_c) \sim 5 \times 10^{-3}$,

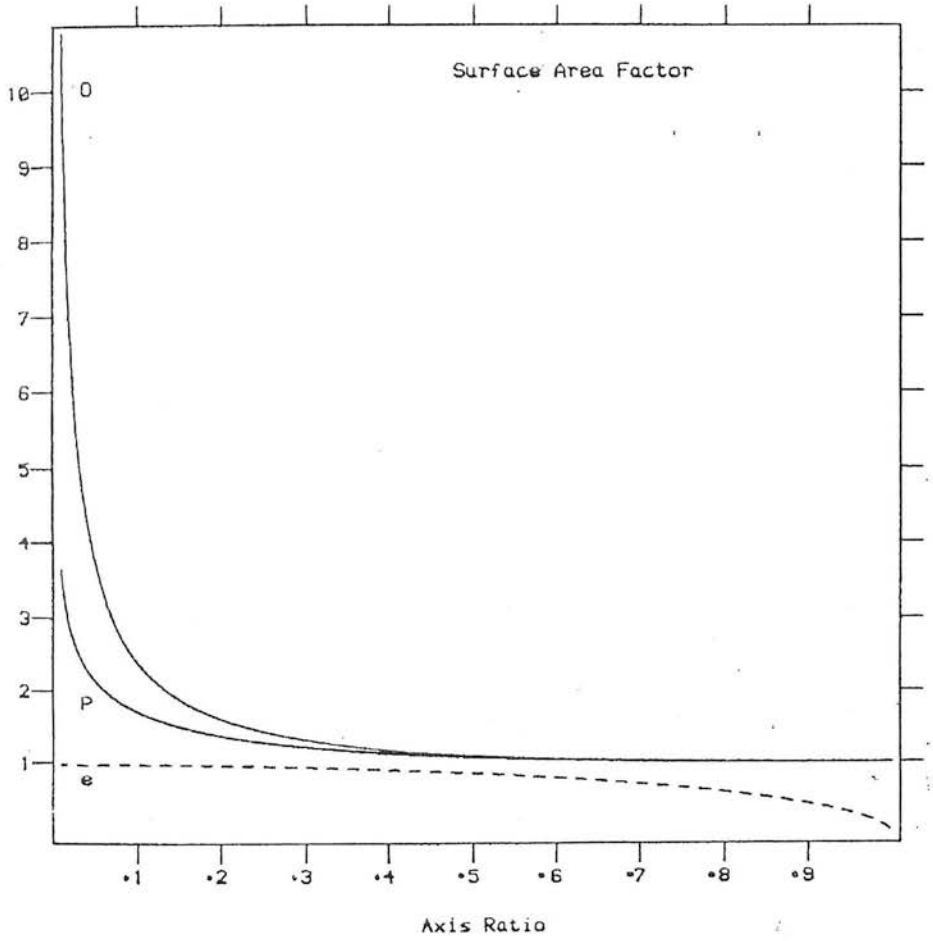

Figure 3.4-1 the surface area correction factor Θ_g (solid lines) for prolate (P) and oblate (O) spheroidal clouds as a function of minor to major axis ratio. The dashed line (e) shows the eccentricity of the cloud for reference.

$$a_w \simeq a_{wb}\left\{1 + \left(\frac{n_w}{n_c}\right)\left[\left(\frac{a_o}{a_{ob}}\right)^3 + \left(\frac{n_c}{n_w}\right)^{\frac{1}{3}}\left(\frac{a_o}{a_{ob}}\right)^2\right]\right\}^{\frac{1}{3}},$$

$$a_c \simeq a_{ob}\left[\left(\frac{a_o}{a_{ob}}\right)^3 - 1\right]^{\frac{1}{3}} \qquad a_o \gtrsim a_{ob} \qquad 3.4\text{-}5$$

$$a_w \equiv a_{wb}\left(\frac{a_o}{a_{ob}}\right), \quad a_c \equiv 0 \qquad a_o < a_{ob}$$

where a_{ob} is the value of a_o for the smallest optically thick cloud. Thus $a_w \sim a_{wb}$ over a wide range of cloud masses ($\frac{1}{2}\, a_{ob} \lesssim a_o \lesssim 5a_{ob}$) beyond which it tends asymptotically to a_o from above; a_c tends rapidly toward a_o from below for $a_o \gtrsim a_{ob}$.

For the present purposes, the properties of the cloud ensemble are completely specified by the four lowest moments of a_w and a_c over the cloud spectrum. In the most general possible model of the SDC-ISM the cloud mass spectrum would be derived self consistently from consideration of the processes which create and destroy clouds, together with those which act to redistribute mass amongst them (fragmentation, coalesence). Such an ambitious scheme is beyond the scope of the present work and, in view of our ignorance of many of the factors which determine the cloud spectrum it is questionable whether such an undertaking is currently practicable or even desirable. Instead a form for the cloud spectrum will be adopted based on the as yet rather primative theoretical models of the cloud spectrum combined with the rather uncertain observational determinations.

Oort (1954) first realised that cloud-cloud collisions occur so frequently - typically every 1 - 10 M_{yr} - that they must play a major role in determining the properties of the cloud ensemble. Subsequently, many attempts have been made to derive the cloud mass spectrum and velocity distribution function from purely collisional models (e.g. Field and Saslaw 1965; Field and Hutchings 1968; Penston et al 1969; Taff and Savedoff 1972, 1973; Kwan 1979; Cowie 1980; Chièze and Lazereff 1980: for a critical review see Hausman 1982). Most such studies assume that all collisions are completely cohesive so that large clouds are built up from small. Clouds which grow to the Jeans mass will undergo gravitational collapse leading to star formation; generally their entire mass is supposed to be returned to the cloud ensemble in the form of small clouds, permitting a steady state solution to be obtained. Generally the resulting equilibrium mass spectrum is a power law $N(m)\ dm \propto m^{-q}\ dm$ with $1.0 \lesssim q \lesssim 1.53$ well away from the upper and lower mass limits (Kwan 1979). However, except for rare low velocity, almost head on impacts, collisions between clouds of comparable mass invariably lead to fragmentation (Kahn 1955; Chièze and Lazeneff 1980; Hausman 1981, 1982) so that at best only the largest clouds can grow by accretion of smaller clouds. It may then be equally plausible to suppose that very large clouds are formed by some process and fragment to give the smaller observed clouds; in this case the mass spectrum is a

steeper power law with $q \sim 3$ (Hausman 1982). In neither case as emphasised by Hausman, can purely collisional models simultaneously reproduce the observed cloud spectrum (see below) and the observed velocity distribution function (velocity approximately independent of mass, at least for the low mass clouds of interest here).

To date the most sophisticated attempt to generalise collisional models, and the one which is most relevant in the present context, is that of Chièze and Lazereff (1980). In this, collisional processes described by realistic collision cross sections and fragmentation probabilities derived from external hydrodynamic calculations, are incorporated within the framework of the MO SDC-ISM scheme. They find that collisions are predominantly disruptive; the smaller clouds are removed by evaporation while the larger clouds grow by accretion of material as they pass through the cold shells of radiative SNR, strict mass balance between these two processes being enforced. They obtain a power law spectrum of $q \sim 1.9$ bounded at low masses at the point where the destruction of clouds by evaporation is balanced by their replacement by the fragmentation products from collisions of larger clouds. Several questions remain about the details of their model. The velocity distribution function is assumed independent of mass; if it were determined self consistantly from the acceleration due to cloud shell collisions alone, momentum conservation implies $V \propto M^{-\frac{1}{3}}$ (MO, McKee et al 1978). Cloud fission

due to interactions between clouds and SNR shocks will be at least as important as cloud collisions for disrupting the smaller clouds (§4.2). It is as yet unclear that accretion of material from SNR shells onto pre-existing clouds is the appropriate mechanism by which evaporated material is returned to the dense phase - new clouds may rather be formed by the thermal instability in the rather broad cooling zone in the interior of evaporative SNR (§5.43). Finally, the parameters of the ambient medium which determine the evaporation rate were simply adopted from the work of MO, rather than being determined self consistantly along with the cloud spectrum; since the resulting cloud spectrum differs little from that assumed by MO this is not a serious objection for the case computed.

Various attempts to determine the cloud mass spectrum have been made observationally. Typically the mass is not obtained directly but is deduced from some other property, for instance column density or extinction, via subsidiary assumptions about the cloud structure and geometry. Table 3.4-1 summarises the results of several such determinations for low mass clouds taken from the literature, expressed as the power law index q together with the range of masses covered, and an indication of the quantity actually measured. Column densities have been converted to mass where necessary by assuming the clouds to be spheres of constant density

independent of mass*.

Taken together the data suggest $q \sim 1.6\text{-}2$ uncertain by at least $\pm$ 0.5 due to the difficulty in converting observed quantities into masses.

In the light of the foregoing I will adopt a power law form for the cloud mass spectrum which in terms of the parameter a_0 becomes,

---

* More generally if the cloud cross section is $\sigma(m) \propto M^a$ and $n(\mathcal{N})d\mathcal{N} \propto \mathcal{N}^b d\mathcal{N}$ then $q \simeq b - (b-2)a$ which is almost independent of a, since b is typically ~ 2.

TABLE 3.4-1 Empirical determinations of the mass spectrum of small clouds

Reference	q	mass range	quantity measured[2]	Note
Knude (1979, 1981)	1.5-1.6	$7M_\odot \lesssim M \lesssim 80M_\odot$	$M(E_{b-y})$	3
Field & Hutchings (1968)	1.65	$1M_\odot \lesssim M \lesssim 24M_\odot$	$M(H^o)$	4,5
	1.85	$280M_\odot \lesssim M \lesssim 1600M_\odot$		
Schwartz & Van Woerden (1974)	1.5	$M \lesssim 100M_\odot$	$M(H^o)$	4,5
Crovisier (1981)	1.8	$0.1M_\odot \lesssim M \lesssim 700M_\odot$	$N(H^o)$	1,5
Hobbs (1974)	2.0	$1.6M_\odot \lesssim M \lesssim 1500M_\odot$	$N(K^o)$	1
Penston et al (1969)	1.5	$20M_\odot \lesssim M \lesssim 2000M_\odot$	$N(C_a^o)$	1,6
Schefler (1969)	2.0 ± 0.3	$M \lesssim 5000M_\odot$	(E_{B-V})	7

Notes to Table

1. Mass range computed from column density range assuming $n_c = 30\ cm^{-3}$ masses scale as n_c^2 .
2. M indicates a direct determination of the mass spectrum. $\mathcal{N}$ indicates measured column density spectrum converted to mass spectrum as described in the text. The quantity in brackets indicates the type of tracer actually used.
3. For 94 small resolved dust clouds with well determined distances within 300pc of the sun.
4. Based on clouds of measured angular size and column density but unknown distance. For reasonable distance distributions the measured value of q is not biased by selection effects.
5. The mass spectrum may differ from that observed due to partial conversion of H^o to H^+ and H_2 at the lower and upper mass limits respectively.
6. Conversion from $\mathcal{N}(C_a^o)$ to $\mathcal{N}(H)$ is uncertain due to variable depletion effects.
7. From statistical analysis of extinction for stars within 2Kpc of the sun.

$$N(a_o)da_o = N_o\, a_o^{-(3q-2)}\, da_o \qquad a_{o1} \lesssim a_o \lesssim a_{ou} \qquad 3.4\text{-}6$$

where the exponent of a_o will be $\sim 2\text{-}4$.

The mass spectrum will be bounded at its upper end at roughly the mass at which clouds cease to be stable against gravitational collapse. Mouschovias and Spitzer (1976) have determined the critical mass for a magnetically supported isothermal* cloud, by combining the results of a virial theorem analysis, with corrections for non-uniform density and magnetic field distributions and non-spherical contraction derived from numerical computations (Mouschovias 1976). Their result can be written as,

$$a_{ou} = 8.0\text{pc}\left(\frac{T_c}{K}\right)\left(\frac{\tilde{P}_{th}}{\text{Kms}^{-3}}\right)^{-\frac{1}{2}}\left[\frac{(1-\delta_B)^{4/3} + 0.16\,\delta_B}{(1-\delta_B)^2}\right]^{\frac{1}{2}} \qquad 3.4\text{-}7$$

---

*Jura (1976) has given a similar analysis for clouds with a realistic temperature structure determined from a specific cloud heating model and neglecting magnetic support. His results are well represented by equation 3.4-7 (for $\delta_B = 0$) when T_e is set equal to the mean temperature derived from the heating - cooling balance at pressure $\tilde{P}_{th}$. Since the heating rate in his model (in common with most such models) is proportional to n while the cooling rate is proportional to n^2, T_c is a decreasing function of $\tilde{P}_{th}$ so that the critical mass declines even more rapidly with pressure than for the case of fixed temperature.

where $\tilde{P}_{th}$ is the thermal pressure in the ambient medium and δ_B is the ratio of the magnetic pressure in the cloud, $\tilde{P}_B \equiv B^2/8\pi k$, to $\tilde{P}_{th}$. Following Mouschovias (1976) the magnetic field will be assumed to scale with density according to $B = B_o n_c^{k}$ with $\frac{1}{3} \lesssim k \lesssim \frac{1}{2}$.

The lower bound to the mass spectrum will occur at the point where clouds are destroyed by, for instance evaporation, faster than they are created. In the absence of a detailed cloud formation model it is difficult to locate this limit precisely. However, as argued by MO clouds without cold cores have such low surface densities ($\lesssim a_{wb} n_w$) that they are readily swept up and assimilated into the dense shells of SNR in the post cooling phase (which have surface densities $\sim Rn_o/3$).

Further, their lifetime against evaporation even in the relatively benign environment of the ambient medium is typically shorter than or comparable with both the SNR cooling timescale and the typical cloud-cloud collision timescale. Thus they are likely to be destroyed faster than they are replaced whether this takes place via cooling processes in old SNR or via fragmentation of larger clouds. I thus assume that,

$$a_{ol} = K_1^{\frac{1}{3}} a_{ob} \qquad 3.4\text{-}8$$

with the expectation that $K_1 \sim 1$. For the specific case

computed by Chièze and Lazereff (1980) the mass spectrum was found to turn down sharply at a mass which would correspond roughly to $K_1 \sim 4$.

For a cloud spectrum of the form 3.4-6 it is straight forward to obtain expressions for the moments of a_w and a_c (equation 3.4-5). In doing so I explicitly assume that $q > 1$ so that the number of clouds decreases with increasing mass, and that the minimum and maximum cloud masses are such that $K_1^{\frac{1}{3}} = (a_{o1}/a_{ob}) \ll (n_c/n_w)^{\frac{1}{3}} \ll (a_{ou}/a_{ob})$. The zeroth moment i.e. the total number of clouds per unit volume is then,

$$N_{c1} = \frac{N_o\, a_{o1}}{3(q-1)}^{-3(q-1)} \left[1 - (a_{o1}/a_{ou})^{-3(q-1)}\right] \simeq \frac{N_o a_{o1}}{3(q-1)}^{-3(q-1)} \qquad 3.4\text{-}9$$

For the moments of the cold core radius I write $\langle a_c^m \rangle = a_{ob}^m\, {}_q^mB_c(y_1, y_u)$ where the ${}_q^mB_c$ are given by,

$${}_q^mB_c \simeq 3(q-1)y_1^{3(q-1)} y_c^{m-3(q-1)} \left[\frac{1}{3(q-1)-m} + \frac{M}{3}\frac{y_c}{(3q+4-m)}\right]$$

$$\simeq \begin{cases} 3(q-1)y_1^{3(q-1)} & m - 3(q-1) < 0 \\ 3(q-1)y_1^{3(q-1)}\, \mathrm{Ln}(y_u/y_c) & m - 3(q-1) = 0 \\ 3(q-1)y_1^{3(q-1)}\, \dfrac{y_u^{m-3(q-1)}}{m-3(q-1)} & m - 3(q-1) > 0 \end{cases} \qquad 3.4\text{-}9$$

Here y is a_o/a_{ob} and y_c is the larger of $K_1^{\frac{1}{3}}$ and unity. Note that for the range $4/3 \lesssim q \lesssim 2$ found above, the lowest three moments of a_c go from being controlled by the largest clouds to being controlled by the smallest. Specifically

for the rather steep $q = 4, K_1 = 2$ spectrum considered by MO $\langle a_c \rangle \simeq 1.76\, a_{ob}$, $\langle a_c^2 \rangle \simeq 4.35 a_{ob}^2$ and $\langle a_c^3 \rangle \simeq 6\ \mathrm{Ln}\ (a_{ov}/a_{o1}) a_{ob}^3$; for an extremely flat $q = 4/3$ spectrum, on the other hand, $\langle a_c \rangle \simeq a_{o1}\ \mathrm{Ln}\ (a_{ou}/a_{oc})$, $\langle a_c^2 \rangle \simeq a_{o1} a_{ou}$ and $\langle a_c^3 \rangle \simeq \frac{1}{2} a_{o1} a_{ou}^2$.

Similarly, for the moments of the warm envelope radius I write $\langle a_w^m \rangle = a_{wb}^m\ {}^m_qB_w$, where the ${}^m_qB_w$ are given by;

$$
\left.
\begin{aligned}
{}^m_qB_w &\simeq \left\{ 1 + \frac{3(q-1)}{m-3(q-1)} \left(\frac{y_1}{y_u}\right)^{3(q-1)} \left[\left(\frac{n_w}{n_c}\right)^{\frac{1}{3}} y_u \right]^m \right\} && m - 3(q-1) \neq 0 \\
&\simeq \left\{ 1 + 3(q-1) y_1^{-3(q-1)}\, \mathrm{Ln} \left[\left(\frac{n_w}{n_c}\right)^{\frac{1}{3}} y_u \right] \right\} && m - 3(q-1) = 0
\end{aligned}
\right\} K_1 \quad 1
$$

3.4-10

$$
\left.
\begin{aligned}
&\simeq \frac{\left\{ m\, y_1^{3(q-1)} - y_1^m + 3(q-1) \left(\frac{y_1}{y_u}\right)^{3(q-1)} \left[\left(\frac{n_w}{n_c}\right)^{\frac{1}{3}} y_u \right]^m \right\}}{(m - 3(q-1))} && m-3(q-1) \neq 0 \\
&\simeq y_1^{3(q-1)} \left\{ 1 - 3(q-1)\, \mathrm{Ln} \left[\left(\frac{n_w}{n_c}\right)^{\frac{1}{3}} \frac{y_u}{y_1} \right] \right\} && m-3(q-1) = 0
\end{aligned}
\right\} K_1 \quad 1
$$

Hence for "steep" spectra such as that considered by MO, $a_w^m \sim a_{wb}^m$ while for "flat" spectra $a_w^m \sim a_{wb}^m + a_c^m$.

In terms of these moments the cloud filling factors and mean intercloud distances are,

$$
f_w = \frac{4\pi N_{c1}}{3} \left(\langle a_w^3 \rangle - \langle a_c^3 \rangle \right) \simeq \frac{4\pi N_{c1}}{3} a_{wb}^3 \ , \quad f_c = \frac{4\pi N_{c1}}{3} a_{wb}^3 \left(\frac{n_w}{n_c}\right) {}^3_qB_c
$$

$$
\lambda_w^{-1} = \pi N_{c1} a_{wb}^2\ {}^2_qB_w \psi_g \ , \quad \lambda_c^{-1} = \pi N_{c1} a_{wb}^2 \left(\frac{n_w}{n_c}\right)^{\frac{2}{3}} {}^2_qB_c \psi_g \qquad 3.4\text{-}11
$$

The geometrical correction factor ψ_g is introduced to allow for the possibility of non-spherical clouds; if the clouds

are oblate or prolate spheroids of eccentricity e and if their major axes are aligned randomly in space then

$$\Psi_g = \frac{1}{2}\ (1 - e^2)^{\frac{1}{3}} + \left(\frac{1 - e^2}{2e}\right)^{\frac{2}{3}} \left|\mathrm{Ln}\left(\frac{1 + e}{1 - e}\right)\right|$$

$$\Psi_g = \left(\frac{1 - e^2}{e}\right)^{\frac{2}{3}} \left|\mathrm{Ln}\left(\frac{1 + e}{1 - e}\right)\right| \qquad 3.4\text{-}12$$

respectively (fig. 3.4-2). Finally, the evaporation parameter which controls SNR evolution in the evaporative case is given by

$$\chi = 2.75 \times 10^4\ \mathrm{gs}^{-1}\mathrm{K}^{-5/2}\mathrm{pc}^{-3}\ \phi\ {}^{1}_{q}B_w \left(\frac{N_{cl}}{\mathrm{pc}^{-3}}\right)\left(\frac{a_{wb}}{\mathrm{pc}}\right) \qquad 3.4\text{-}13$$

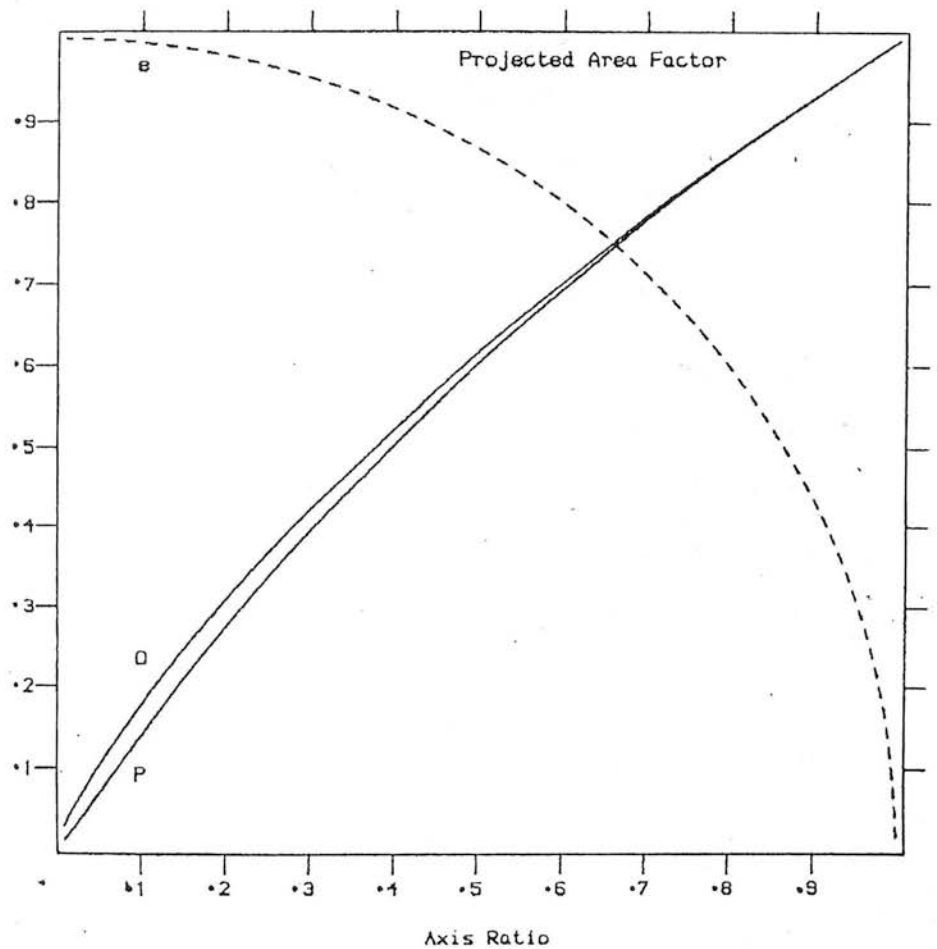

Figure 3.4-2 the projected area correction factor Ψ_g (solid lines) for prolate (P) and oblate (O) spheroidal clouds as a function of minor to major axis ratio. The dashed line (e) shows the eccentricity of the cloud for reference.

3.5 Equilibrium Conditions and Method of Solution

The modeling of SNR evolution (§3.2 and §3.3 for evaporative and non-evaporative SNR respectively) and the representation of the cloud ensemble (§3.4) can now be linked together by means of the conditions of pressure balance, mass balance and ionisation balance to give a self consistent model of the SDC-ISM. The essence of this linkage is straightforward: the pressure in the hot intercloud matrix is determined by the balance between the rate of energy input by supernova explosions per unit volume, $S E_o$, and the rate of its dissipation mediated by interactions with the clouds; given this pressure and the requirement of pressure equilibrium between the components, the properties of the cloud ensemble are fixed if the total amount of gas available to make up clouds $\bar{n}$, and the total UV flux, ε_{uv}, available to keep part of that gas warm and ionised, are also specified; in particular the cloud parameters which fix the rate of SNR energy dissipation (χ for the evaporative case and essentially f_w for the non-evaporative case) are determined; self consistency then requires that their values match those used in determining the matrix pressure. Of course, such self consistent solutions may not exist for all possible values of S, E_o, $\bar{n}$ and ε_{uv} and even if they do the properties of the solution may be such that one or more of the assumptions made in deriving the model is violated; the boundaries of the domain in parameter space within which valid, self-consistent solutions can be found will be located in

§3.6

The applicability of the equation of pressure balance and ionisation balance to a system as chaotic as the SDC-ISM is of course questionable. As briefly discussed in §3.2.1 conditions in the hot matrix fluctuate about their average values on a timescale t_{SNR} (see Table 3.2-1); the cloud components will respond dynamically to these changes on a timescale t_{cl} while the ionisation state of the warm envelopes varies in response to the resulting changes of density on the timescale t_{rec}. When $t_{SNR} \ll t_{cl}$ (case I) it is at least plausible that the parameters of the clouds will take up time independent values and I will assume, perhaps somewhat "naively, that these are dictated by the time average pressure in the external medium (I will further assume that the SDC-ISM constitutes an ergodic system). Conversely when $t_{cl} \ll t_{SNR}$ (Case II) the clouds remain at all times close to pressure equilibrium with their surroundings. If it also happens that $t_{rec} \lesssim t_{cl} \ll t_{SNR}$ (Case III) strict <u>local</u> ionisation equilibrium will also hold. Inevitably reality lies between these extremes (at least for the smaller interstellar clouds); in this middle ground the clouds can never be in local equilibrium and their properties will depend in a complex way upon their experiences over the last few crossing times. Nonetheless, optimistically, one might hope that at least statistically speaking the equilibrium conditions will hold and that the results of model calculations for Cases I, II and III may at least crudely bound those

for a realistic ISM.

It is convenient to refer the values of those parameters of the cloud ensemble which vary with pressure (for Cases II and III) such as the cloud densities radii and filling factors to their values at some fixed pressure, hereinafter referred to as the typical values; a particularly convenient choice for this reference pressure is $\langle \tilde{P}_h \rangle$ the hot component pressure averaged over the ensemble of SNR (equation 3.2-9 and 3.3-1). Given the pressure distribution function it is a straightforward matter to relate the typical values to the observationally more relevant volume average values (§ 3.2.3)*.

In the spirit of the discussion above, the condition of pressure balance will be written,

$$\langle \tilde{P}_h \rangle = 1.1 \ (1 + X_w) \ n_w T_w = 1.1 \ n_c T_c \qquad 3.5\text{-}1$$

where the factor 1.1 allows for the partial pressure of helium (assuming $n(H_e) \sim 0.1\ n(H)$ and $[n(H_e^+)/n(H_e^o)]\ [n(H^+)/n(H^o)] \gg [n(H_e^{2+})/n(H_e^o)]$).

The possibility that clouds may be supported in part by turbulence (e.g. Hobbs 1974, a,b, Dickey et al 1977, 1978,

---

* In particular for Case I the typical and volume average values are identical by definition; for Case II since the ionisation state is constant by definition and I will further assume T_w and T_c to be constant the typical and volume average values of n_w and n_c are identical.

1979 Crovisier 1981, but see Wayte et al 1978 for a counter example) can readily be incorporated by interpreting the temperatures in equation 3.5-1 as the sum of the gas kinetic temperature and the "doppler temperature" $T_D \simeq 130K\ (V_{turb}/kms^{-1})^2/(1 + X)$. Similarly partial support by a magnetic field as discussed by inter alia Cox (1979, 1981) can be included by incorporating in T the further term $T_m \simeq 288K\ (B/\mu G)^2/(1 + X)(n/cm^{-3})$. To the extent that magnetic support requires a magnetic field largely tangential to the cloud surface (or else highly tangled) it is incompatable with efficient thermal evaporation of the cloud and hence is specifically excluded for the evaporative model.

As a simplification I will take T_c and T_w as free parameters (subject to the constraint $T_c \ll T_w$) independent of, for instance, density. Strictly their values should be determined self consistently from a study of the thermal and kinetic energy balance within the clouds and they will then inevitably depend on density as well as other parameters through the heating and cooling rates. To the extent that computations of the time independent heating - cooling balance can be taken as a guide to cloud temperatures the approximation is not too severe for the gas kinetic temperature; the major heat source for the warm component will be photoionisation which necessarily gives T_w independent of density, while the temperature predicted for the cold clouds in most models varies by less than a factor of two over a wide range of densities (see e.g.

Draine 1978, Cox 1979). Alternatively one need only note that measured kinetic temperatures for the majority of cold clouds lie within a factor ~ 2 of the mean value (e.g. Savage et al 1977, Dickey et al 1977, 1978 1979; Crovisier 1981, Mebold et al 1982). Similarly if B is taken to vary with n according to $B \propto n^K$ with $\frac{1}{3} \lesssim K \lesssim \frac{2}{3}$ then $T_m \propto n^{2K-1}$ is also only weakly density dependent. Potentially, the value of T_D may be strongly dependent on the rate of turbulent energy input from SNR shocks and cloud collision as well as the clouds cross section for absorbing this energy. Its value may then be a strong and complex function of many properties of the SDC-ISM. Measurements of cloud velocity dispersions also show rather a large scatter in T_D although this is in part an observational artifact (Crovisier 1981). A more careful treatment than that given here must however await a more detailed understanding of the processes which generate and dissipate supersonic turbulence in interstellar clouds.

It is explicitly assumed that there is no <u>net</u> exchange of mass between the phases (formation of new cloud material in radiative SNR balances evaporation) and that the cloud spectrum is in equilibrium. Thus on a scale much larger than individual SNR the fraction of the total interstellar gas contained in each component is fixed and the cloud number density is a constant. In keeping with the assumptions made in deriving the equations of SNR evolution it is further assumed that on average the ensemble of SNR behaves

as if each of them separately evolved (up to the point of overlap) into a homogoneous and isotropic medium characterised by these globally averaged properties.* The mean hydrogen number density $\bar{n}$ is related to the densities and filling factors of the three components through,

$$\bar{n} = n_c f_c + n_w f_w + n_h \left[1 - (f_c + f_w)\right] \simeq n_c f_c \qquad 3.5\text{-}2$$

since I will show that the warm and hot components contribute only a few percent and a few tenths of a percent of $\bar{n}$ respectively. When combined with the pressure balance equation 3.5-1 this immediately leads to expressions for the cloud number density in terms of the typical value of a_{wb},

$$N_{cl} = \frac{3}{4\pi} \frac{1.1(1 + X_w)}{\langle \tilde{P}_h \rangle} T_w \bar{n} \frac{1}{3 B_c a_{wb}^3} \qquad 3.5\text{-}3$$

Provided the ensemble of warm clouds is optically thick to UV photons the requirement of ionisation equilibrium implies that the mean production rate of ionising photons must just balance the mean recombination rate so that,

$$\mathcal{E}_{UV} = \alpha_{rec} \langle n_w^2 X_w^2 f_w \rangle \equiv \alpha_{rec} \xi n_w^2 X_w f_w \qquad 3.5\text{-}4$$

where the correction factor ξ is unity in Cases I and II and is simply the ratio of the volume average electron

---

This innocent sounding assumption is of course fraught with peril. In the computation of Cowie et al 1981 the partial destruction and sweeping out of clouds from the centre of the SNR produced a cloud depleted cavity surrounded by a shell of enhanced cloud number density. This raises the possibility that even for evaparative models the ISM may be subject to the sort of "cavitation chain reaction"(this time acting on the cloud population) originally invoked by MO as an argument against the non-evaparative models. This may not be serious because the perturbation in cloud number density is of small amplitude.

density $\langle n_e X_w \rangle$ to its typical value for Case III (since mass conservation implies that the combination $n_w F_w$ is invariant). The recombination coefficient α_{rec} will be taken to have its case B value $\alpha_{rec} \simeq 2.6 \times 10^{-13} cm^3 s^{-1} (T/K)^{-0.80}$ for T near $10^4 K$ (Spitzer 1978) since although the envelopes are individually marginally optically thin the ensemble is not.

Equations 3.5-1 to 3.5-4 can now be combined with the equation of SNR evolution (§3.2 and §3.3) and those describing the cloud population (§3.4) to obtain a system of equations relating the problem parameters which can be solved iterativly.

Specifically, for the evaporative model equations 3.5-3 and 3.4-13 combine to give,

$$\bar{\chi}_c = 7.2 \times 10^3 gs^{-1} K^{-5/2} pc^{-3} (1+X_w) \left(\frac{1}{q} B_w / \frac{3}{q} B_c\right) \left(\frac{T_w}{K}\right) \left(\frac{n}{cm^{-3}}\right) \left(\frac{\tilde{P}_h}{K cm^{-3}}\right)^{-1} \left(\frac{a_{wb}}{pc}\right)^{-2} \left(\frac{P_h}{P_c}\right)^{\omega} \qquad 3.5\text{-}5$$

for the value of the evaporation parameter at the cooling point (recall $\bar{\chi}(P) = \bar{\chi}(P_c)(P/P_c)^{-\omega}$). Given a value for this quantity all the other properties of SNR at the cooling point are fixed by the relationships in Table 3.2-1 while the average conditions in the hot component, in particular $\langle \tilde{P}_h \rangle$, are specified by the results of section 3.2-3. Eliminating a_{wb} between equations 3.5-5 and 3.4-4 leads to a quadratic for X_w,

$$\frac{(1-X_w^2)}{(1+X_w)} = 4.4\times10^{-6}\,\theta_g^2\left({}^3_qB_c/q'B_w\right)\left(\frac{T_w}{K}\right)\left(\frac{\langle\tilde{P}_h\rangle}{K\,cm^{-3}}\right)^{-1}\left(\frac{\bar{n}}{cm^{-3}}\right)^{-1}\left(\frac{\chi_c}{gs^{-1}K^{-5/2}pc^{-3}}\right)\left(\frac{\langle\tilde{P}_h\rangle}{\tilde{P}_c}\right)^{-\omega} \qquad 3.5\text{-}6$$

combining the expressions for $\bar{n}$ and ε_{UV} above (equations 3.5-2 and 3.5-4) with the relationships for the moments of the cloud spectrum then leads to,

$$\frac{a_{ob}}{a_{ou}} = K_1^{(q-1)/(2-q)}\left[\frac{1.1}{\xi}\,\frac{X_w^2}{(1+X_w)}\left(\frac{\alpha_{rec}}{cm^3S^{-1}}\right)^{-1}\left(\frac{\varepsilon_{UV}}{cm^{-3}S^{-1}}\right)\left(\frac{\langle\tilde{P}\rangle}{Kcm^{-3}}\right)^{-1}\left(\frac{\bar{n}}{cm^{-3}}\right)^{-1}\left(\frac{T}{K}\right)\right]^{1/3(2-q)} \qquad q<2 \qquad 3.5\text{-}$$

$$Ln\left(\frac{a_{ob}}{a_{ov}}\right) = -\left\{K_1^3\,L_n\left[Max\,(K_1,1)\right] + \left[\frac{\xi}{1.1}\,\frac{(1+X_w)}{X_w^2}\left(\frac{\alpha_{rec}}{cm^3S^{-1}}\right)\frac{\varepsilon_{uv}}{cm^{-3}S^{-1}}\left(\frac{\langle\tilde{P}_h\rangle}{Kcm^{-3}}\right)\left(\frac{\bar{n}}{cm^{-3}}\right)\left(\frac{T}{K}\right)^{-1}\right]\right\} \quad q=2$$

Finally, the system of equations is closed by the expression for a_{ou} (equation 4.4-7) and the relationship between a_{wb} and a_{ob} which can be written, by means of the pressure equilibrium equation as,

$$a_{wb} = \left[(1+X_w)\,\frac{T_w}{T_c}\right]^{\frac{1}{3}}\,a_{ob} \qquad 3.5\text{-}8$$

The problem is now specified by the values of S, E_o, $\bar{n}$ and ε_{UV} together with those of the subsidiary quantities. (see table 3.6-1 for a summary definition of each of these parameters together with bounds on their values) Given an initial guess of the values of a_{wb}, (a_{ou}/a_{ob}), X_w and $\langle\tilde{P}_h\rangle$

the solution proceeds by first solving 3.5-5 for $\bar{\chi}_c$ and hence obtaining a revised value for $\langle \tilde{P}_h \rangle$; an improved value of X_w then follows from 3.5-6 and thence a_{ou} and a_{ob} are obtained from 3.4-7 and 3.5-7 respectively; finally 3.5-8 yields an updated value of a_{wb}. The procedure converges quite rapidly over a large region in parameter space and more importantly is not subject to violent oscilations even when the initial values are badly chosen.

For the non-evaporative case the procedure is closely analogous, however the equations that result are somewhat unwieldy and will therefore not be given here in full. Basically setting $(W_{net}/E_o) = 1$ in equation 3.3-2 and eliminating f_w by means of equation 3.5-3 leads to an expression for y_{max}. The value of y_{max} then determines $\langle \tilde{P}_h \rangle$ by application of equation 3.3-1. The expression for y_{max} can also be inverted to give an expression for a_{wb}; eliminating a_{wb} between this expression and equation 3.5-8 then leads directly to an expression for X_w which is used in place of equation 3.5-6. Equation 3.5-7 for (a_{ob}/a_{ou}) equation 3.4-7 for a_{ou} and equation 3.4-4 for a_{wb} then complete the system of equations. The solution to this set of equations is then obtained in exactly the same way as for the evaporative case.

3.6 Results

3.6.1 'Standard' Case

In the interests of definiteness of presentation I will begin by discussing the results obtained for a specific 'standard' case. In this the SDC-ISM is described by the evaporative model with the cloud dynamics represented by case II, in which the clouds respond dynamically, but their ionisation state remains frozen. The values chosen for all the input parameters in this standard case are listed for ease of reference in Table 3.6-1. These values were selected to coincide as far as possible with those used by MC so as to facilitate a direct comparison with their findings.

Column (2) of Table 3.6-2 lists the values of a number of the more important quantites derived from the model for this standard case. Column (4) of that table gives for comparison the values of these same parameters from MC. The differences between these two sets of results stem entirely from the different treatment of the interstellar pressure. Since the 'typical' pressure employed by them is rather lower than the average pressure employed here, they predict fewer larger clouds of lower density; consequently they obtained a smaller value of the evaporation parameter and hence SNR reach a larger size before cooling and adiabatic SNR have a larger filling factor in their model.

TABLE 3.6-1 The Parameters of the Model

Parameter	Standard Value		Range
Controlling Parameters:			
Supernova rate	$(S/10^{-13}\,pc^{-3}\,yr^{-1})$	1.0	0.1 - 10
Explosion energy	$(E_o/10^{51}\,erg)$	1.0	0.1 - 10
Mean total density	$(\bar{n}/cm^{-3})$	1.0	0.1 - 100
Ionising photon emissivity	$(\varepsilon_{uv}/10^{-15}\,cm^{-3}\,s^{-1})$	2.0	0.2 - 20
Parameters of the SNR:			
Ratio of blast wave velocity to mass averaged isothermal sound speed	α	2.5	1.5 - 3
Radiative cooling enhancement factor	β	10	1 - 10
Fraction of E_o stored as thermal energy	ε	0.7	0.5 - 1.0
Mass fraction included in dense shell	δ	0.5	-
Exponent of pre-cooling expansion law	$\eta = 6/(10+3\omega)$	6/11	3/5, 6/11, 0.39
Exponent of post cooling expansion law	η'	0.4	2/7 - 1
Cloud compression exponent	ω	$\frac{1}{3}$	0, $\frac{1}{3}$, 1.8

TABLE 3.6-1 Cont.

Parameter		Standard Value	Range
Parameters of the Cloud Population:			
Exponent of mass spectrum	q	2	4/3 -2
Evaporation efficiency factor	$\phi = \phi_g \phi_m \phi_{SNR}$	$\frac{1}{3}$	.1 - 1
Surface area correction factor	Θ_J	1	1 - 10
Ratio of smallest cloud mass to that of smallest optically thick cloud	K_1	2	0.5 - 10
Temperature of cold cores	(T_c/K)	80	40 - 160
Temperature of warm envelopes	(T_w/K)	8000	7000 - 10000
Magnetic field for $n = 1cm^{-3}$	$(B_o/\mu G)$	0.5	0.25 - 1.5
Exponent of magnetic field-density relationship	k	0.4	$\frac{1}{3}$ - $\frac{1}{2}$

TABLE 3.6-2 Results of Various Models for Standard Values of the Controlling Parameters

Parameters	(1) Case I	(2) Case II	(3) Case III	(4) MO	(5) Non Evaporative
q_c	0.25	0.11	0.78	0.51	Y max = 0.18
(R_c/pc)	128	156	206	181	R max = 268
$(\langle \tilde{P}_h \rangle /kcm^{-3})$	5700	5700	4700	7900 (P_{typ} = 3600	3750
$(\langle T_h \rangle /K)$	$3.6x10^5$	$3.8x10^5$	$4.0x10^5$	$4.6x10^5$	-
$(\tilde{\kappa}_c /gs^{-1}K^{-5/2}pc^{-3})$	240	230	140	110	-
(N_{cl}/pc^{-3})	$2.6x10^{-2}$	$2.5x10^{-2}$	$1.1x10^{-2}$	$5.9x10^{-3}$	$6.7x10^{-3}$
$(\langle a_w \rangle /pc)$	1.0	1.0	1.4	2.1	1.98
f_w	0.1	0.1	0.14	0.23	0.22
(λ_w/pc)	12	12	13	12	12
(n_w/cm^{-3})	0.4	0.4	0.32	0.25	0.25
X_w	0.6	0.6	0.65	0.68	0.68
(a_{ol}/pc)	0.23	0.23	0.33	0.48	0.48
(o_u/pc)	10	10	12	10	8.9

TABLE 3.6-2 Cont.

	Case I	Case II	Case III	MO	Non Evaporative
f_c	0.015	0.015	0.018	0.024	0.023
(λ c/pc)	110	110	120	88	106
(n_c/pc)	65	65	53	42	42

The values of the main controlling parameters of the model S, E_{51}, $\bar{n}$ and ε_{uv} may differ considerably from the rather arbitrarily chosen standard values, both as a consequence of observational uncertainty and because of the intrinsic large-scale changes in conditions which result from galactic structure. It is thus necessary to examine the effects such changes will have on the predictionsof the model, and in particular to establish the boundaries of the region in parameter space within which self consistant solutions can be otained. To this end I have performed an extensive grid of model computations for values of each of the controlling parameters covering the entire range which is likely to be encountered.

Figure 3.6-1 illustrates the variation of several of the quantities derived from the model over a cross section through parameter space in which E_o and ε_{uv} are kept fixed at the standard values while S and $\bar{n}$ vary over the range $3 \times 10^{-15} \text{pc}^{-3}\text{yr}^{-1} \leq S \leq 9.5 \times 10^{-13} \text{pc}^{-3}\text{yr}^{-1}$ $0.03 \leq \bar{n} \leq 9.5 \text{ cm}^{-3}$. Each of the quantities are illustrated both by a contour diagram and an isometric plot; the former is better for the extraction of quantitative data while the latter aids visualisation of the qualitative features. In the contour diagram $\bar{n}$ is given as abscissa and S as ordinate; both are plotted on logarithmic scales; contours are drawn at logarithmic intervals. In the isometric plots the scaling along all three axes is also logarithmic. Thus in this depiction a quantity which varied according to

Figure 3.6-1 The variation of the predicted parameters over the S, n plane for the standard model of Table 3.6-1. Successive panels show the following (a) the boundaries of the region in parameter space within which the model is self consistant; the lines representing each of the constraints (See text) are labelled on the side where the condition is violated. The shaded region shows the area where all the principle constraints are satisfied. (b) the porosity parameter for adiabatic SNR Q_c (c) the average pressure ($\langle \tilde{P} \rangle$ / kcm^{-3}) (d) the cooling radius (R_c/pc) (e) and (f) the warm and cold component filling factors (q) the average warm cloud radius ($\langle a_w \rangle$ /pc) (h) the line of sight separation of the warm envelopes (λ_w/pc) (i) the parameter Y = Log (a_{ou}/a_{ol}) which characterises the range of cloud masses (j) the ionisation parameter $Z = (1 + x_w)$ (k) the number density of cloud cores (N_{cl}/pc^{-3}).

The layout of each of the panels (b) - (k) are identical. At left the variation of the parameters is shown on a contour diagram. S is plotted as ordinate and n as abscissa on logarithmic scales. The origin of coordinates is indicated by heavy tick marks. Minor tick marks occur at intervals corresponding to a factor of two. The contour interval is also logarithmic the value of the lowest contour and the contour interval are given in the rubric. This also gives the maximum (M) and minimum (m) values illustrated.

At right the same information is shown as an isometric plot. The scale along all three axes is again logarithmic. The orientation of the plots has been chosen to best exhibit the solution topology the direction in which n and S increase being indicated by arrows.

Figure 3.6-2 As Figure 3.6-1 but for the S, E_{uv} plane. E_{uv} is plotted as abscissa in the contour diagrams.

Figure 3.6-3 As Figure 3.6-1 but for the S, E_o plane. E_o is plotted as abscissa in the contour diagrams.

Figure 3.6-1:

a

PLANE: (S,NBAR)

MODEL: 2

ORIGIN;	S	1.00
	NBAR	1.00
	E51	1.00
	EUV	2.00
PARAMETERS;	ALPHA	2.50
	BETA	10.00
	ETA2	.40
	PHI	.33
	THETA	1.00
	TW	8000.00
	TC	80.00
	B0	2.50
	KAPPA	.42
	KL	2.00

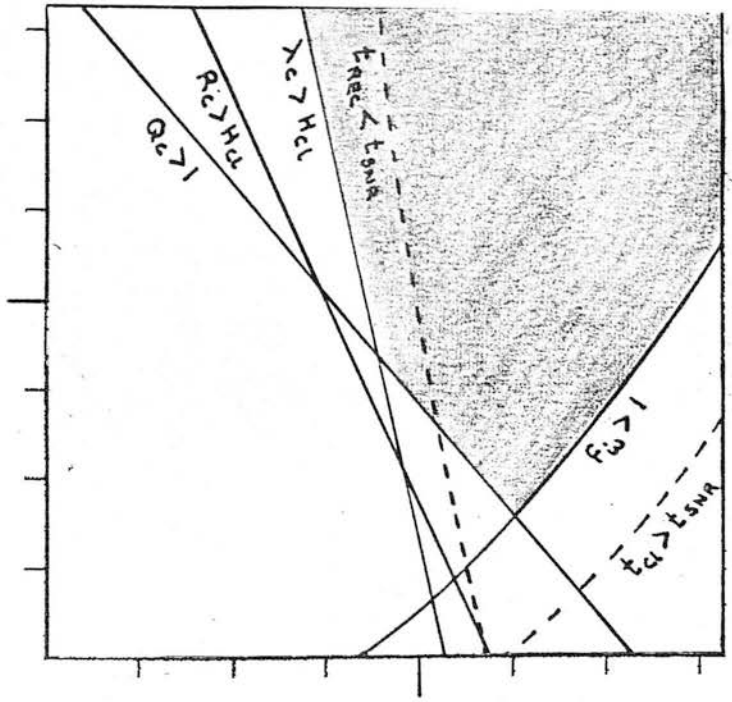

b

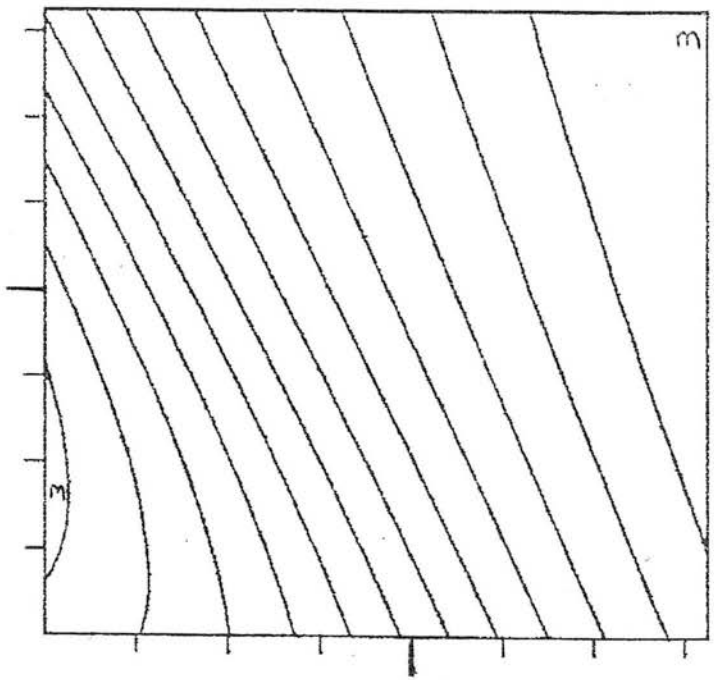

Q

MINIMUM	-2.82
MAXIMUM	3.65
CONTOURS;	
LOWEST	-2.00
INTERVAL	.50

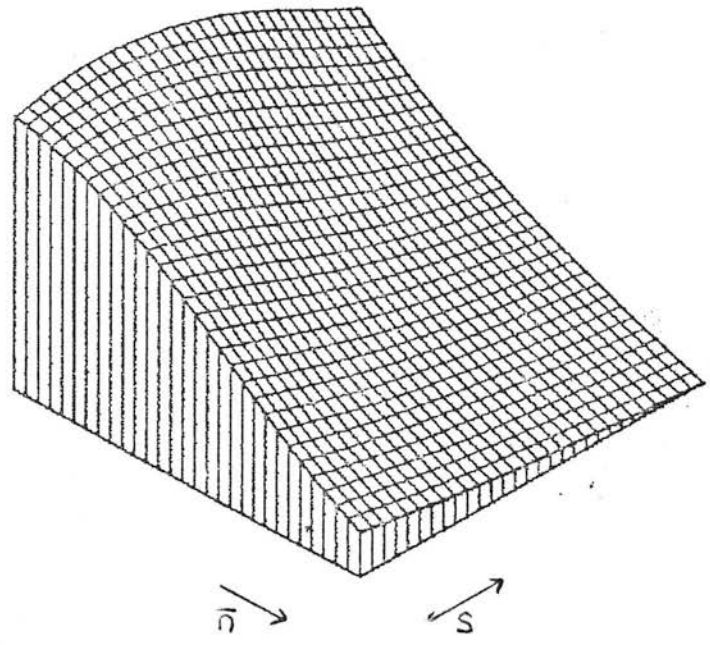

c

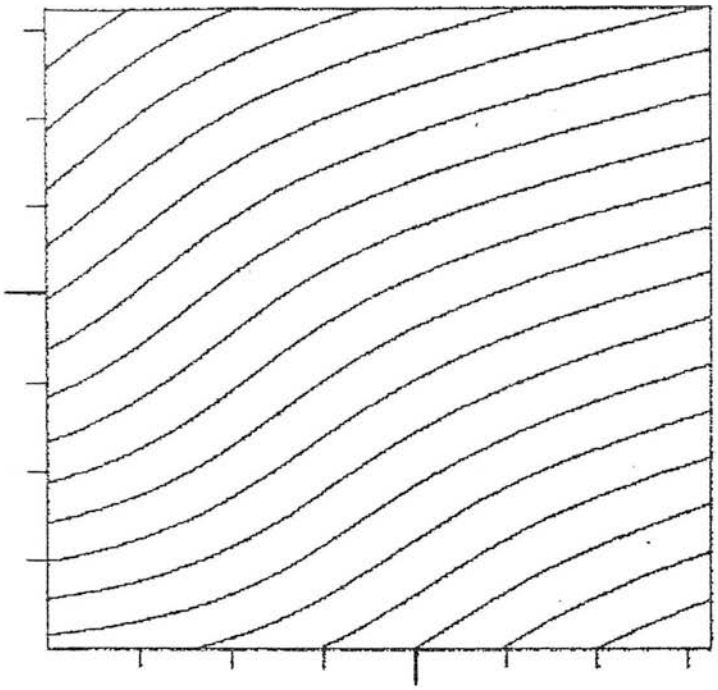

PA

MINIMUM 2.80
MAXIMUM 4.70

CONTOURS;

LOWEST 2.80
INTERVAL .10

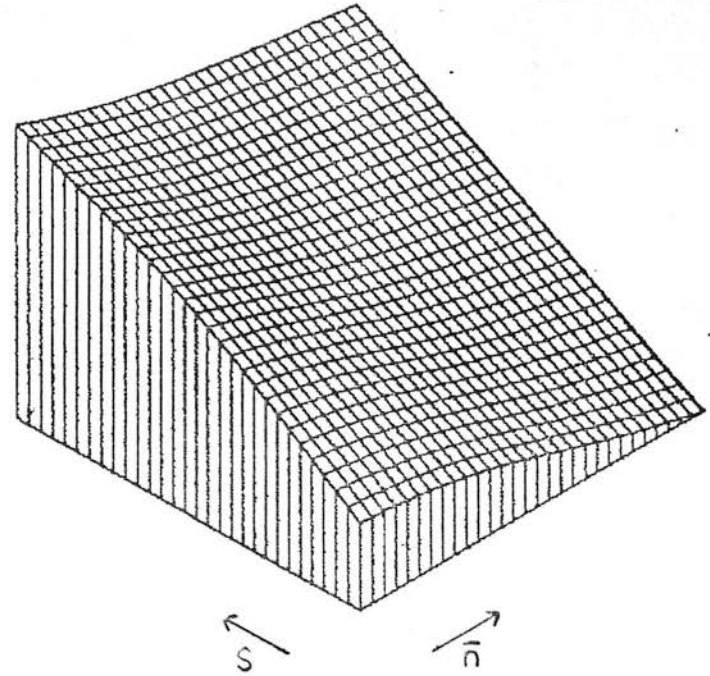

d

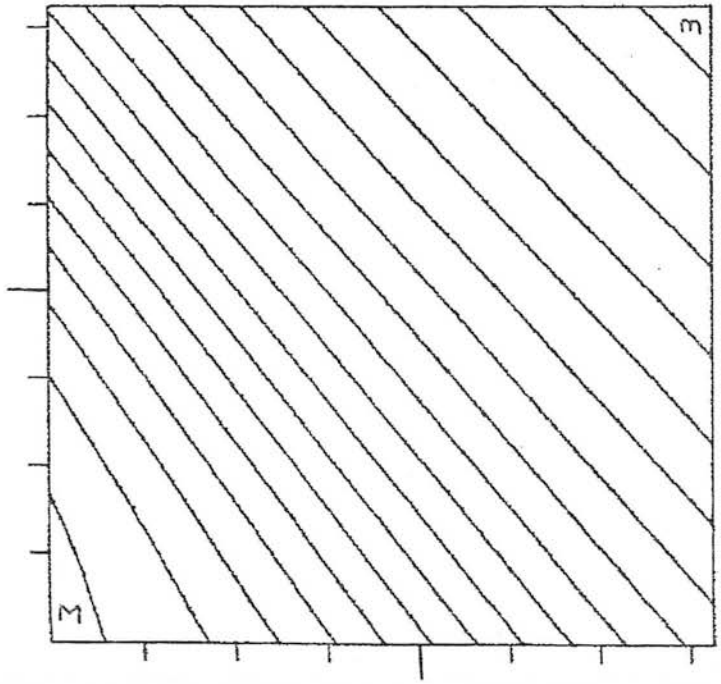

RC

MINIMUM 1.43
MAXIMUM 3.23

CONTOURS;

LOWEST 1.50
INTERVAL .10

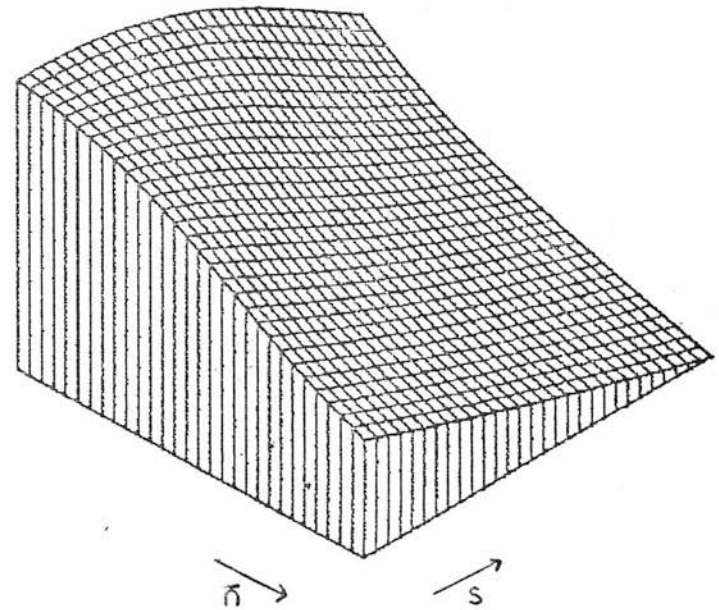

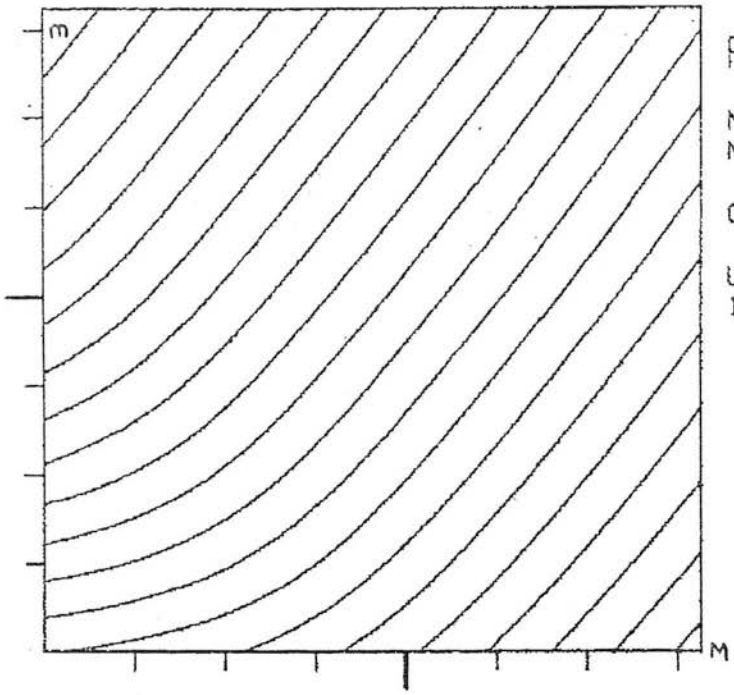

FW

MINIMUM -3.00
MAXIMUM 1.08

CONTOURS;

LOWEST -2.80
INTERVAL .20

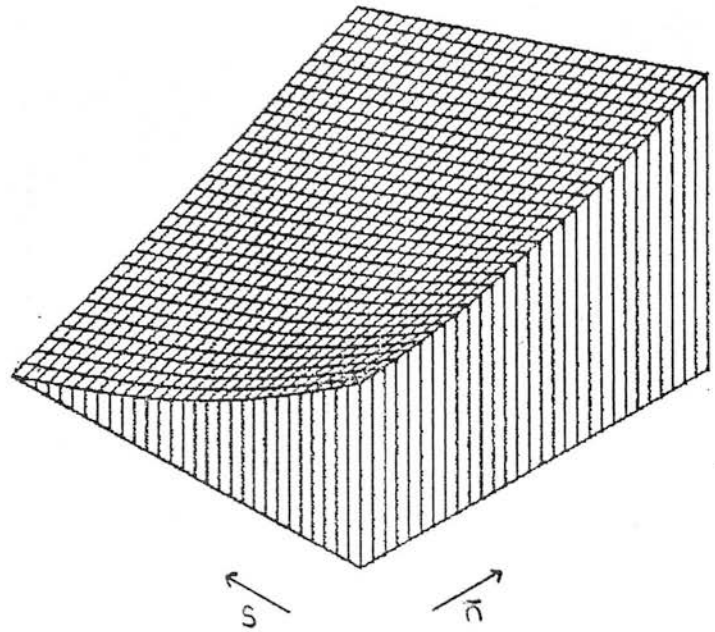

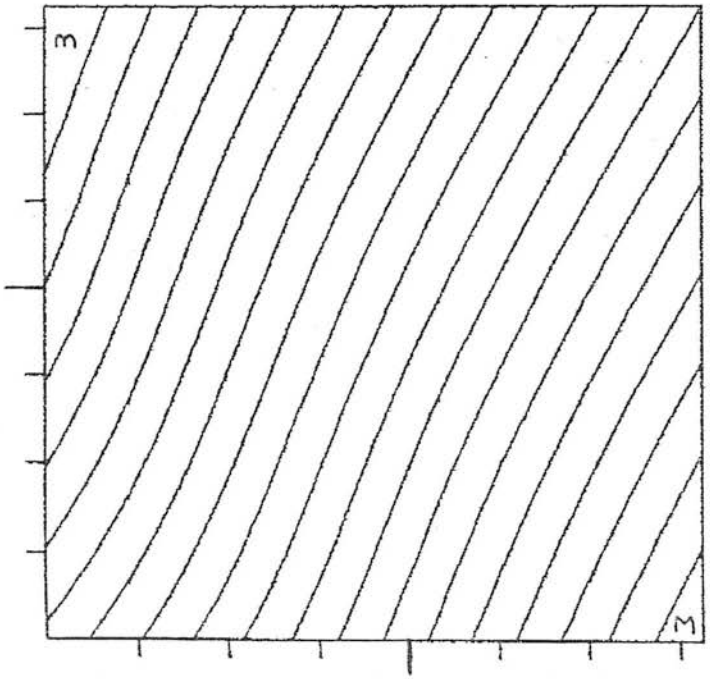

FC

MINIMUM -3.89
MAXIMUM .20

CONTOURS;

LOWEST -3.60
INTERVAL .20

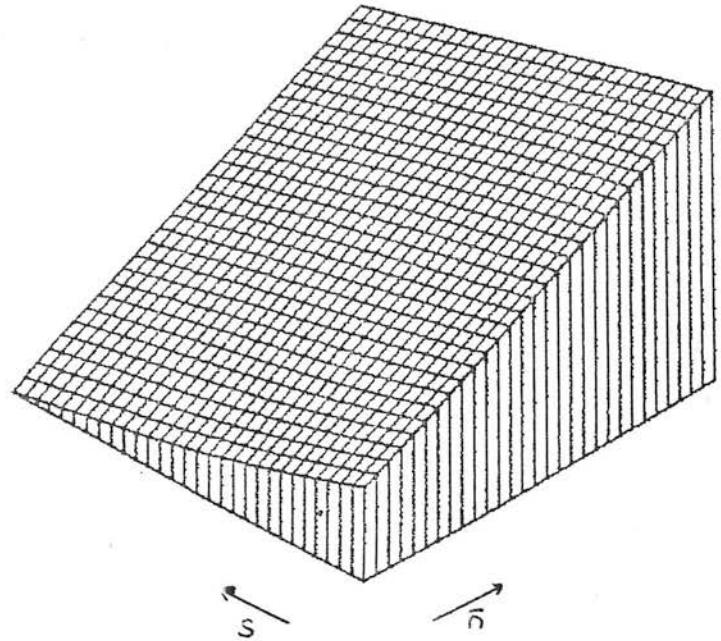

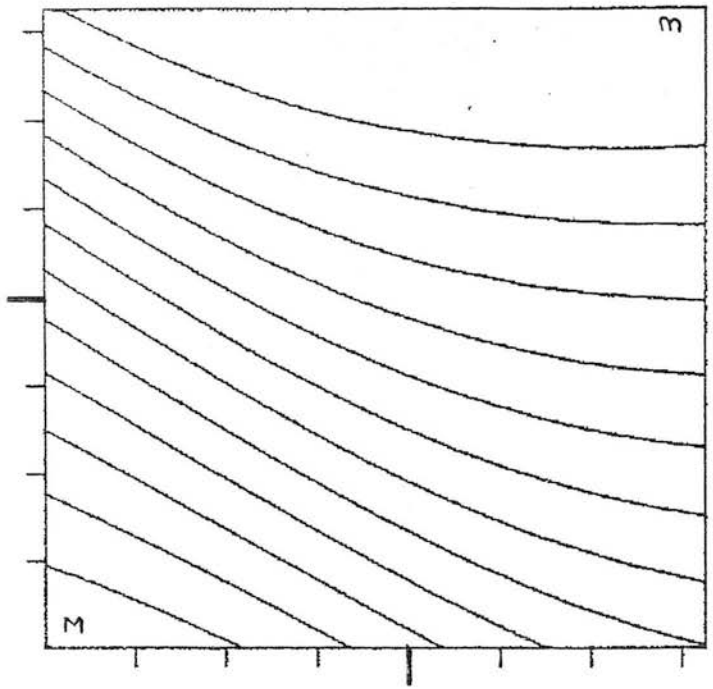

AWB

MINIMUM	-.97
MAXIMUM	1.80
CONTOURS;	
LOWEST	-.60
INTERVAL	.20

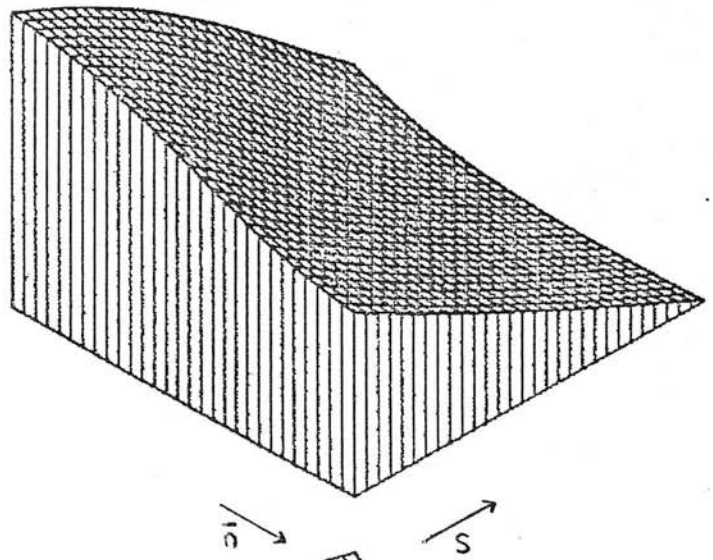

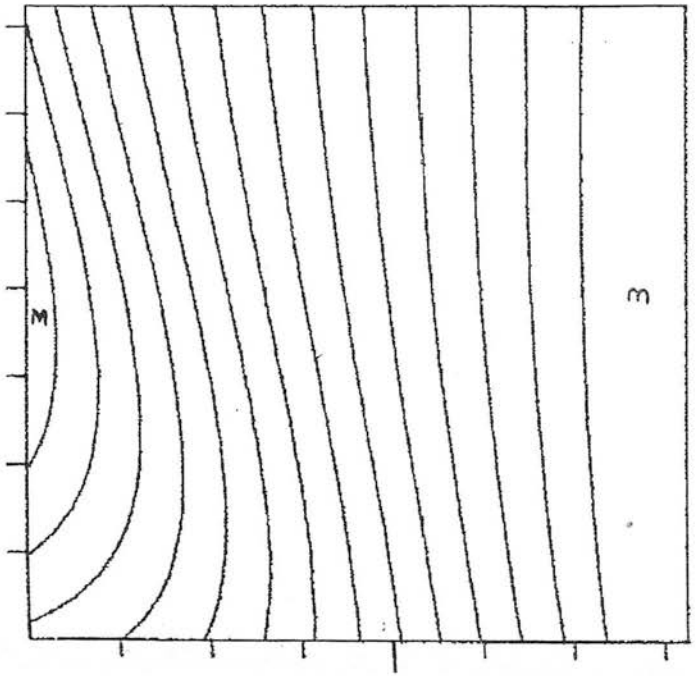

LW

MINIMUM	-.19
MAXIMUM	2.94
CONTOURS;	
LOWEST	.20
INTERVAL	.20

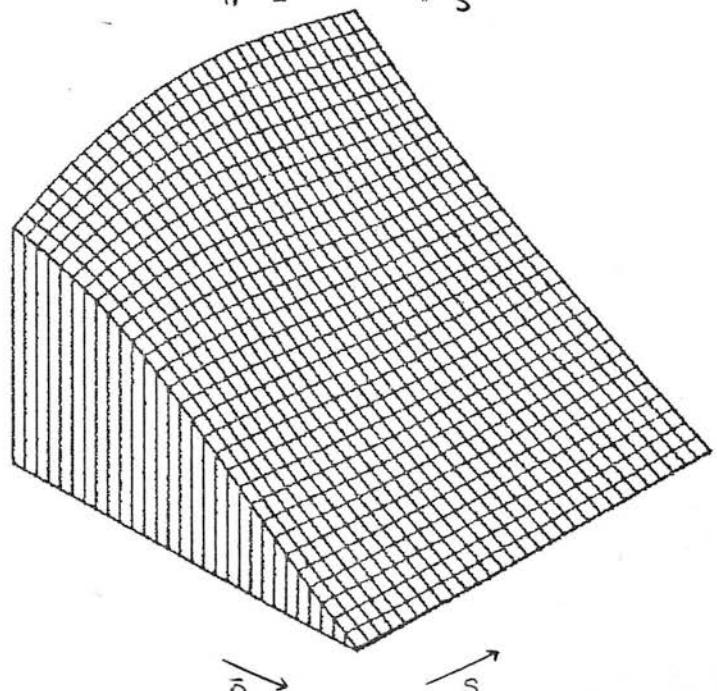

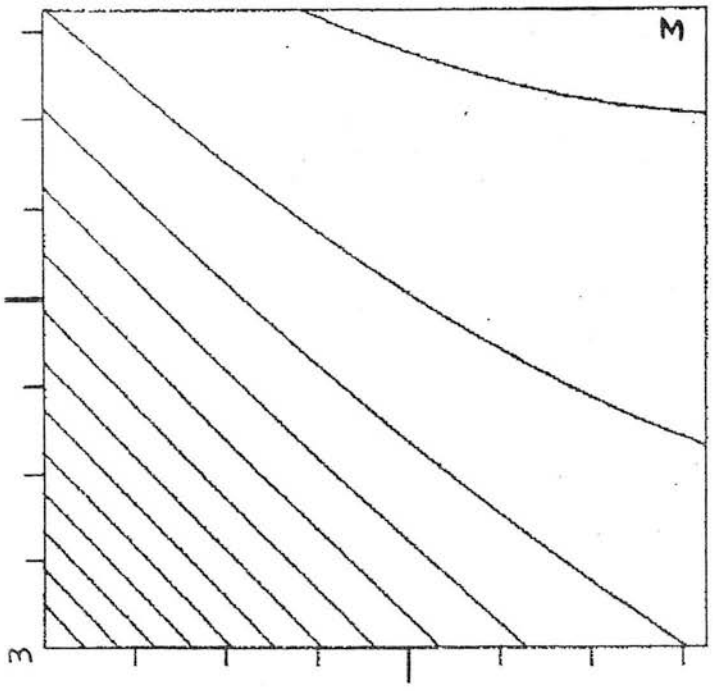

Y

MINIMUM -.62
MAXIMUM .73

CONTOURS;

LOWEST -.50
INTERVAL .10

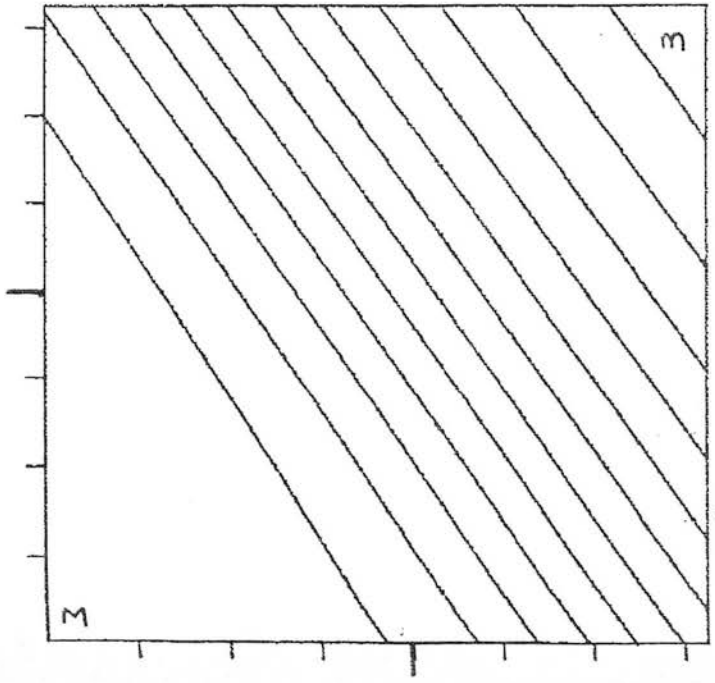

Z

MINIMUM .04
MAXIMUM .30

CONTOURS;

LOWEST .06
INTERVAL .02

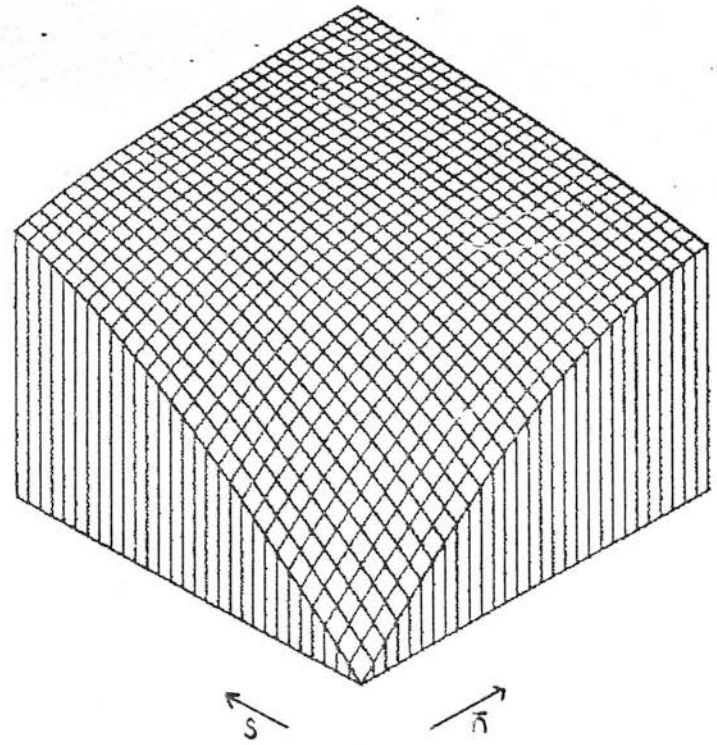

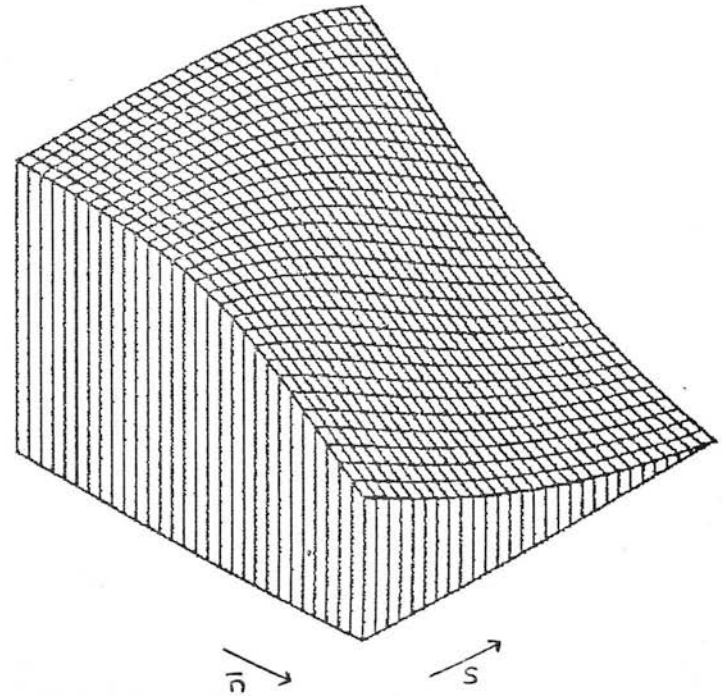

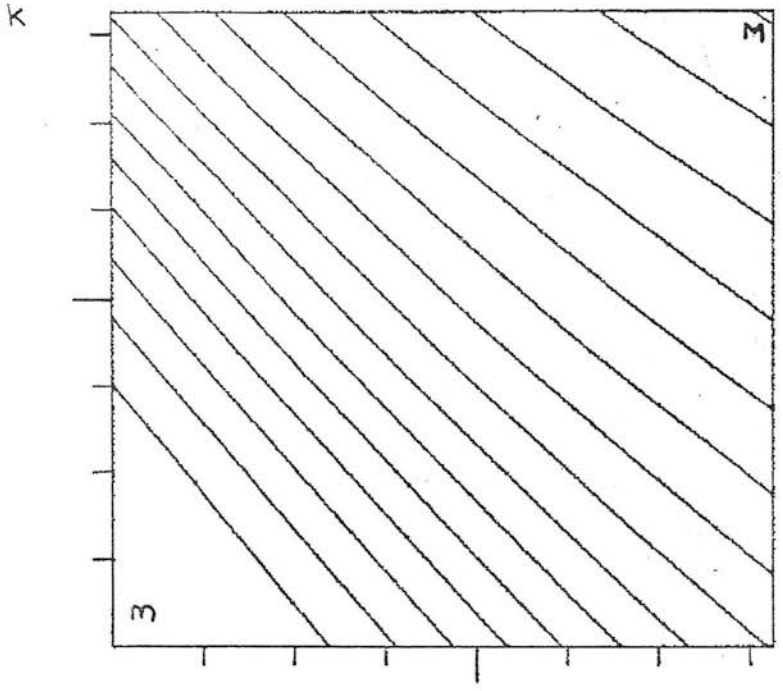

NCL

MINIMUM	-6.44
MAXIMUM	1.57

CONTOURS;

LOWEST	-5.50
INTERVAL	.50

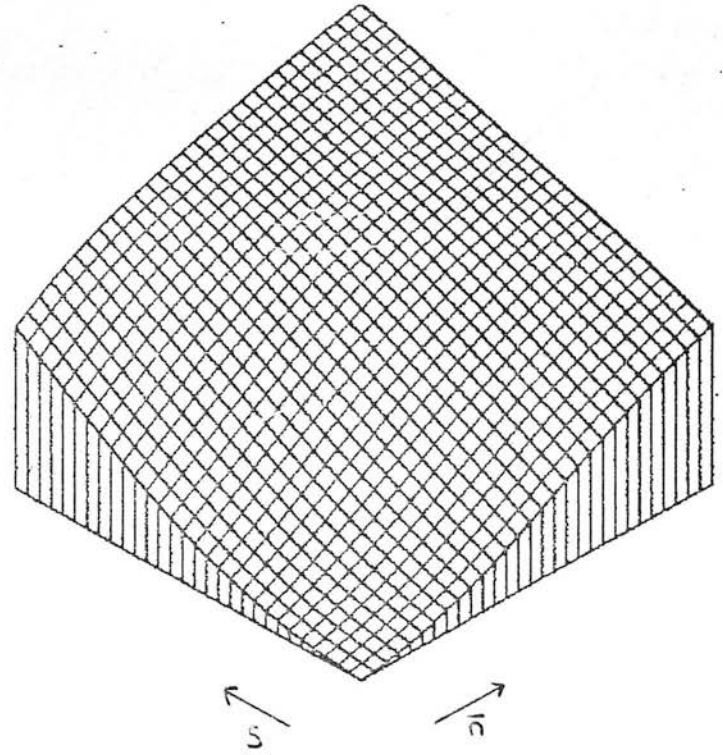

Figure 3.6-2

a

PLANE;	(S,EUV)	
MODEL;	2	
ORIGIN;	S	1.00
	NBAR	1.00
	E51	1.00
	EUV	2.00
PARAMETERS;	ALPHA	2.50
	BETA	10.00
	ETA2	.40
	PHI	.33
	THETA	1.00
	TW	8000.00
	TC	80.00
	B0	2.50
	KAPPA	.42
	KL	2.00

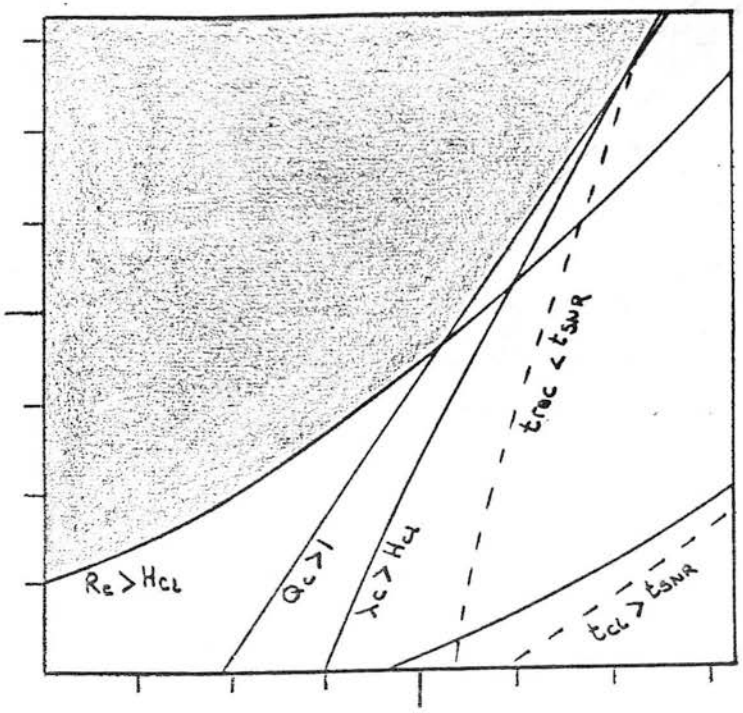

b

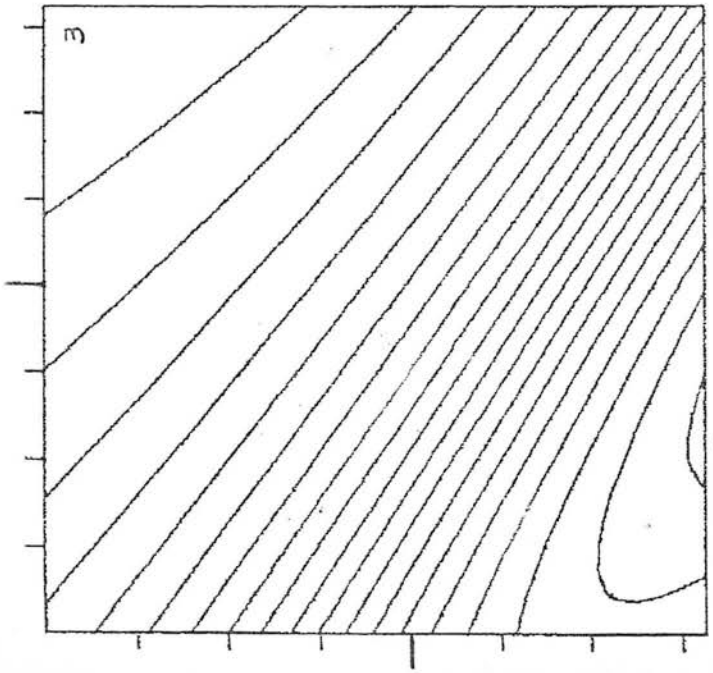

Q

MINIMUM	-1.63
MAXIMUM	2.24
CONTOURS;	
LOWEST	-1.40
INTERVAL	.20

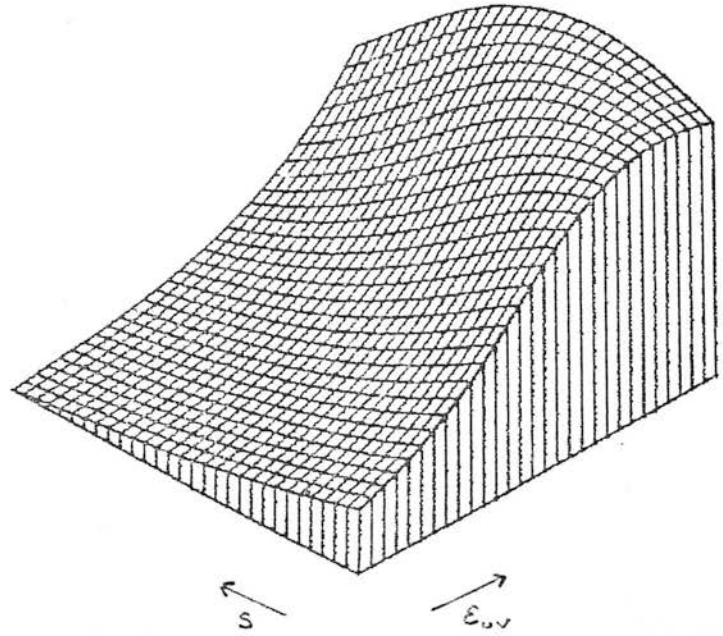

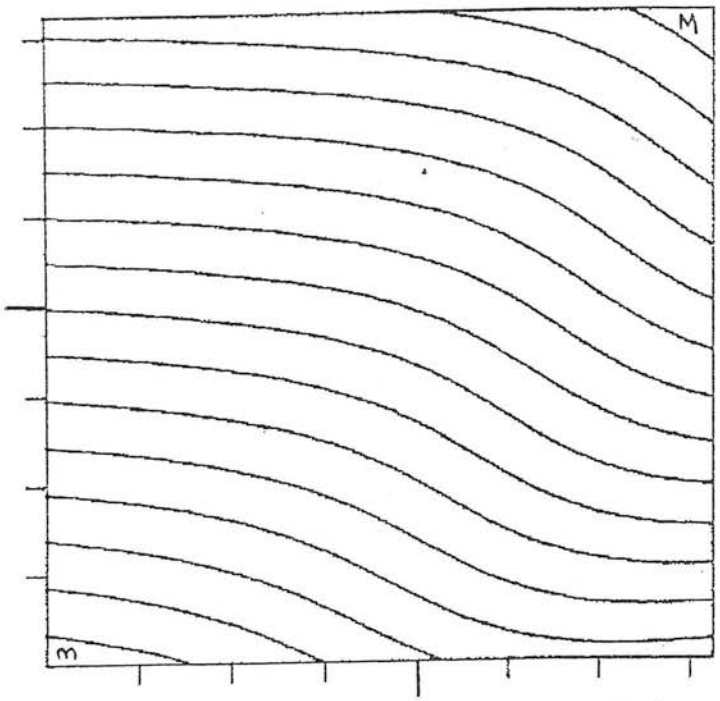

PA

MINIMUM	2.94
MAXIMUM	4.58
CONTOURS;	
LOWEST	3.00
INTERVAL	.10

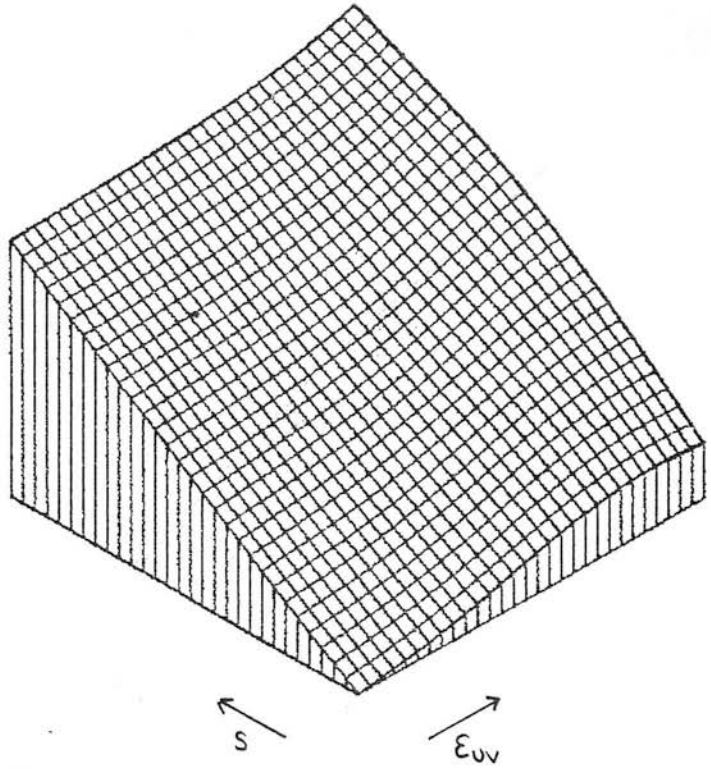

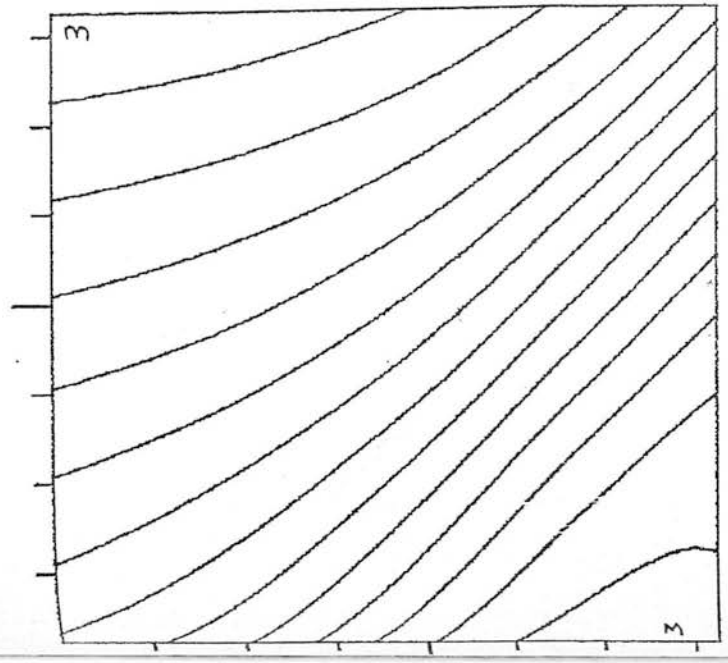

RC

MINIMUM	1.71
MAXIMUM	3.04
CONTOURS;	
LOWEST	1.80
INTERVAL	.10

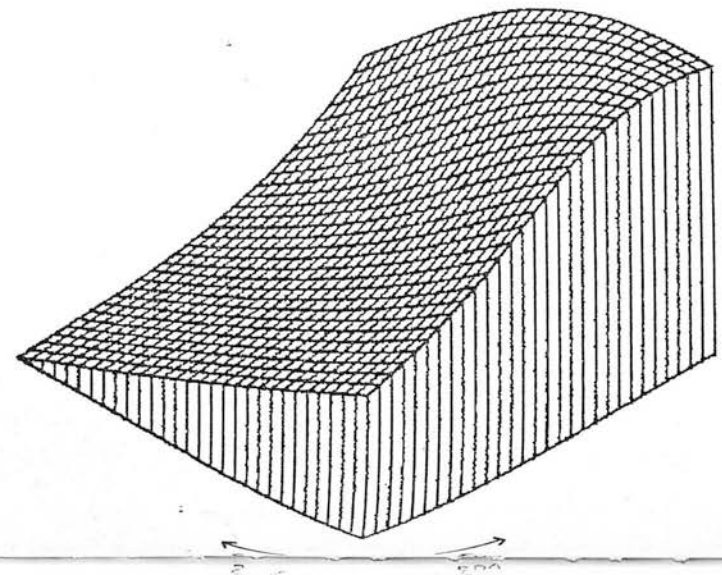

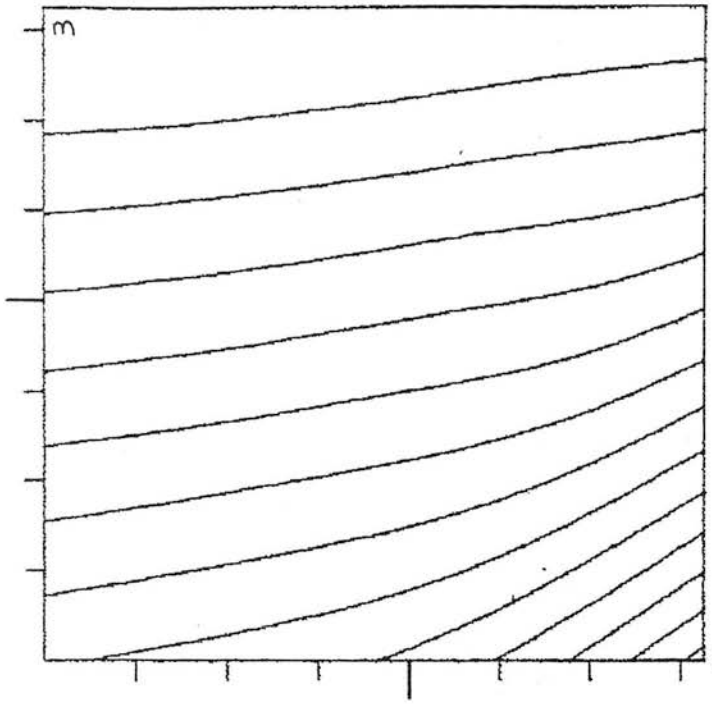

FW

MINIMUM -1.92
MAXIMUM .87

CONTOURS;

LOWEST -1.60
INTERVAL .20

F

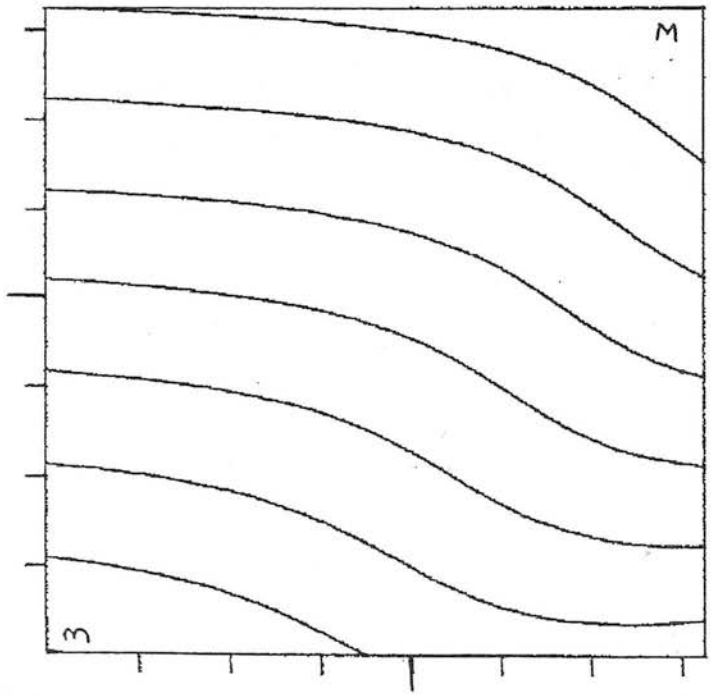

FC

MINIMUM -2.64
MAXIMUM .00

CONTOURS;

LOWEST -2.40
INTERVAL .20

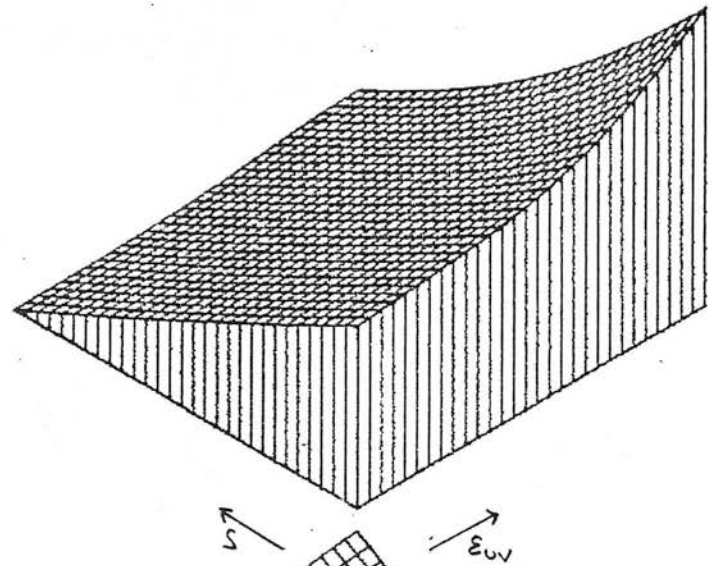

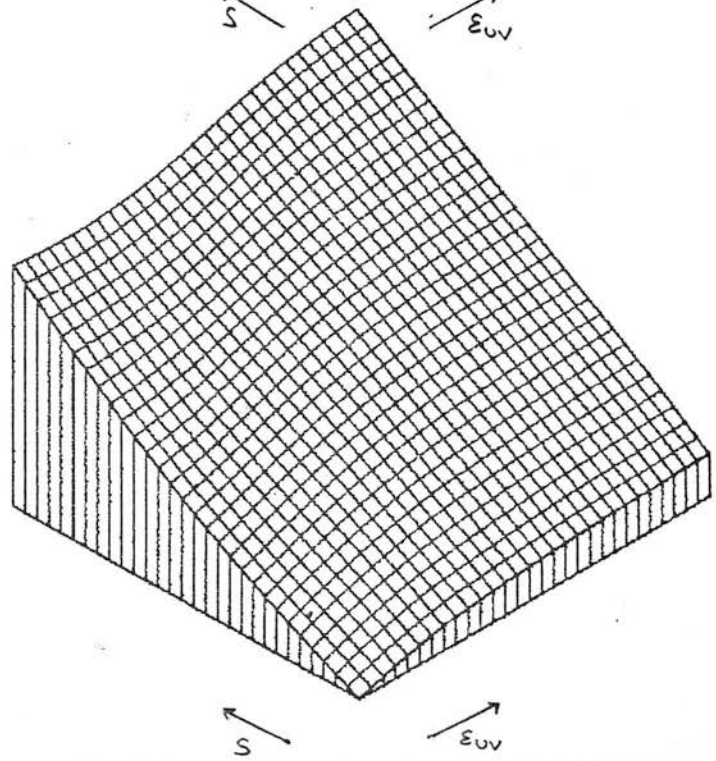

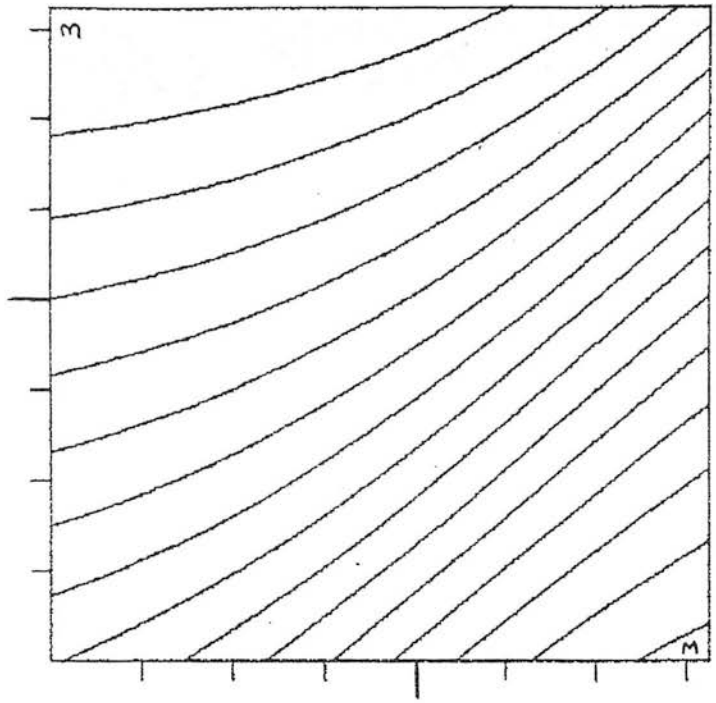

AWB

MINIMUM	-1.12
MAXIMUM	2.08
CONTOURS;	
LOWEST	-.80
INTERVAL	.20

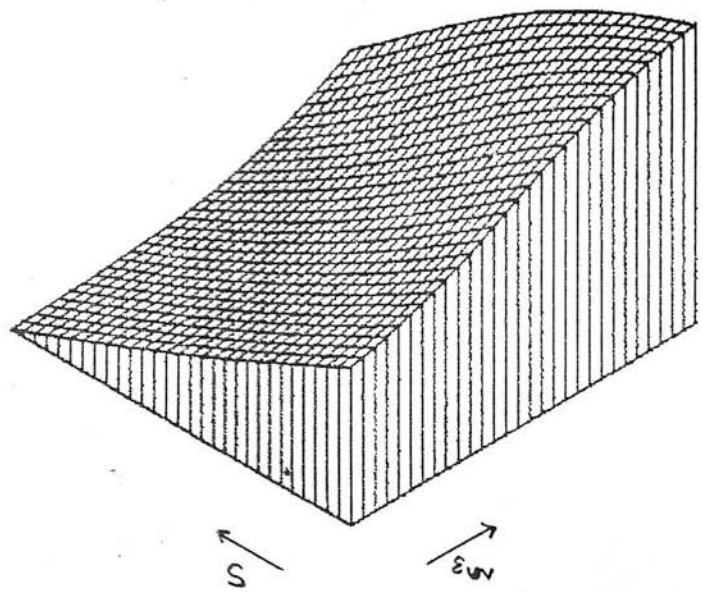

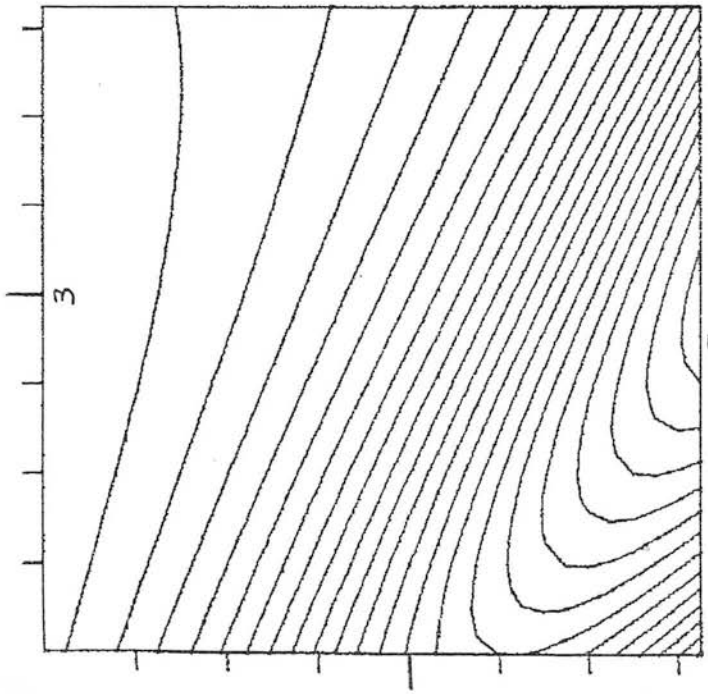

LW

MINIMUM	.91
MAXIMUM	1.98
CONTOURS;	
LOWEST	.95
INTERVAL	.05

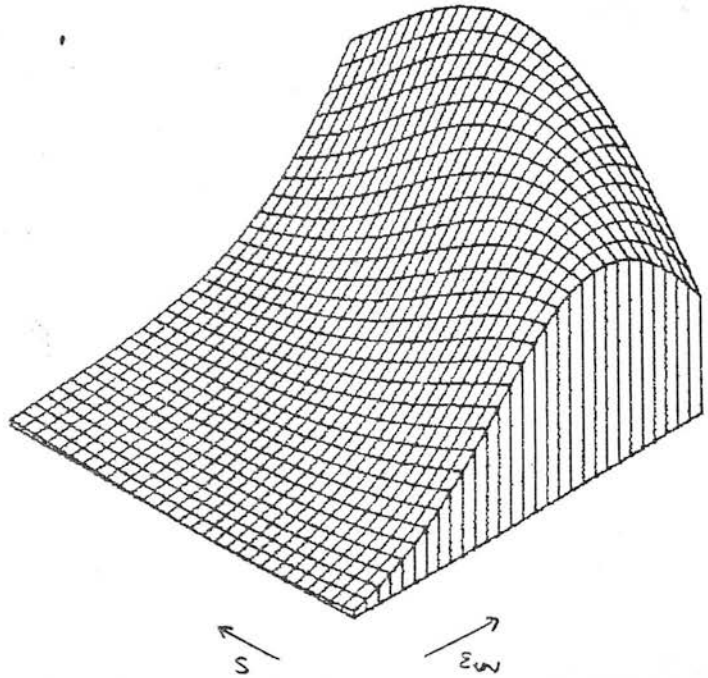

i

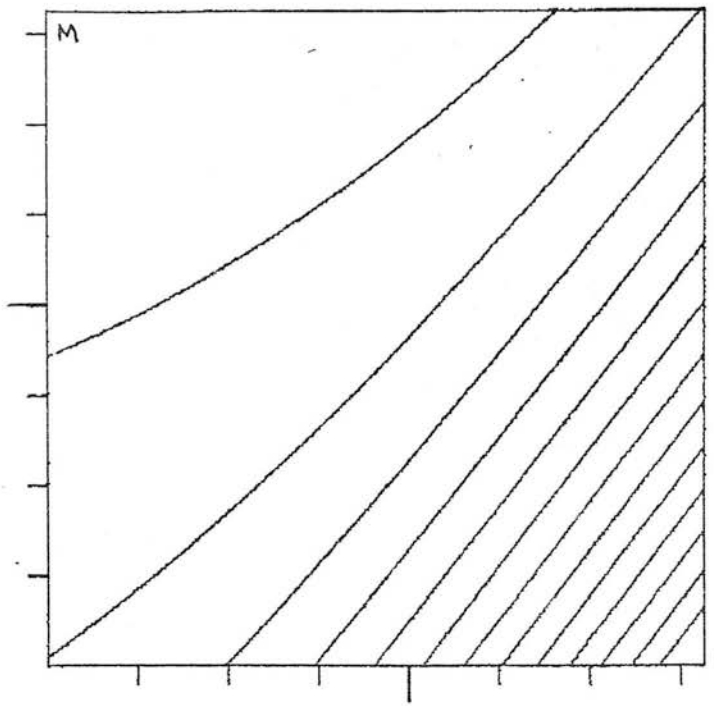

Y

MINIMUM	-.65
MAXIMUM	.78
CONTOURS;	
LOWEST	-.50
INTERVAL	.10

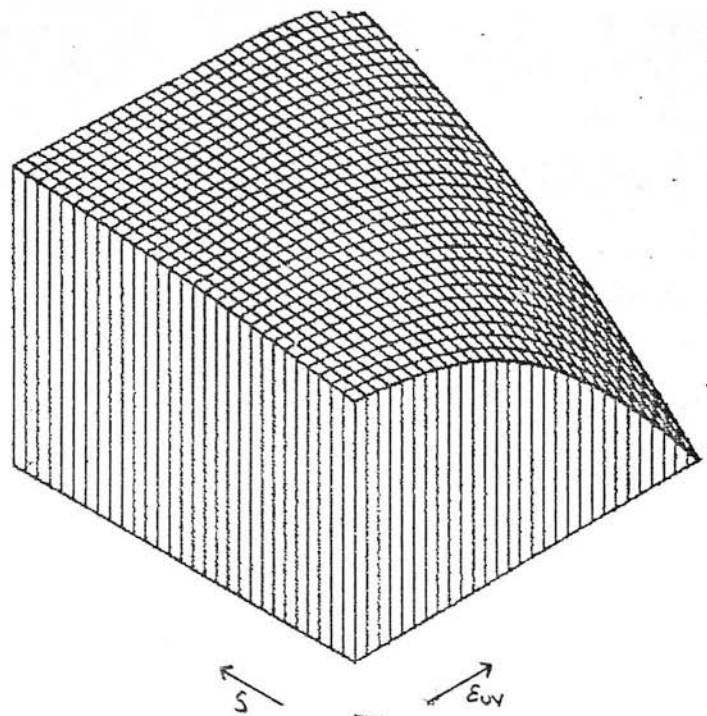

j

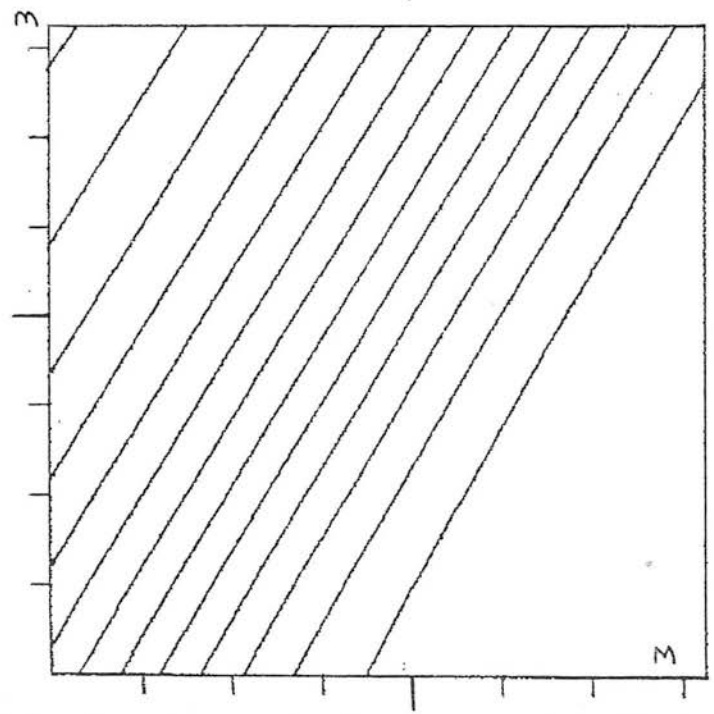

Z

MINIMUM	.04
MAXIMUM	.30
CONTOURS;	
LOWEST	.04
INTERVAL	.02

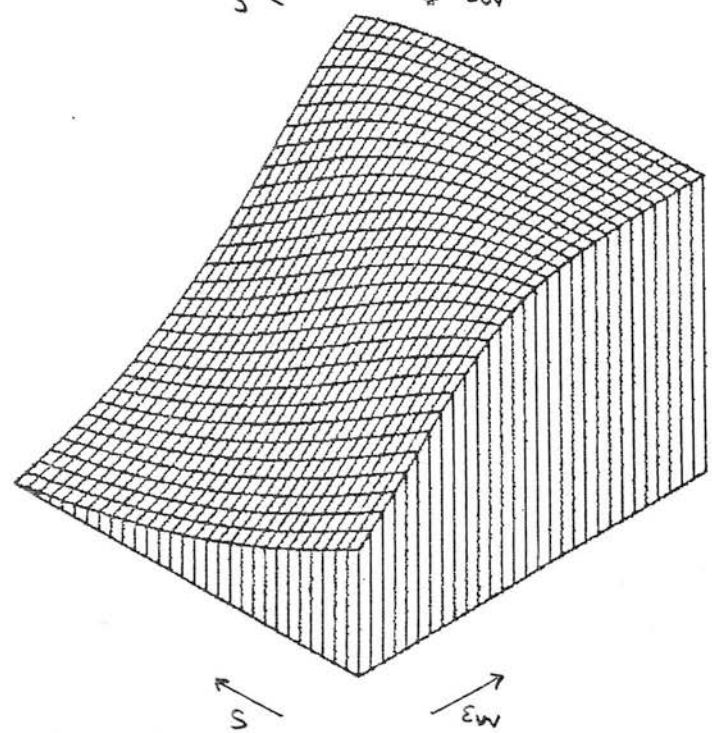

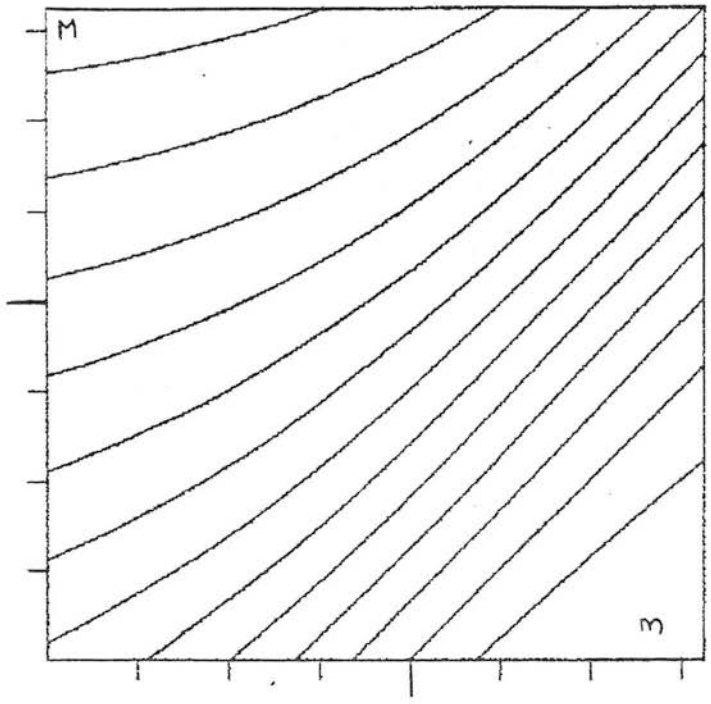

NCL

MINIMUM	-6.02
MAXIMUM	.81

CONTOURS;

LOWEST	-5.50
INTERVAL	.50

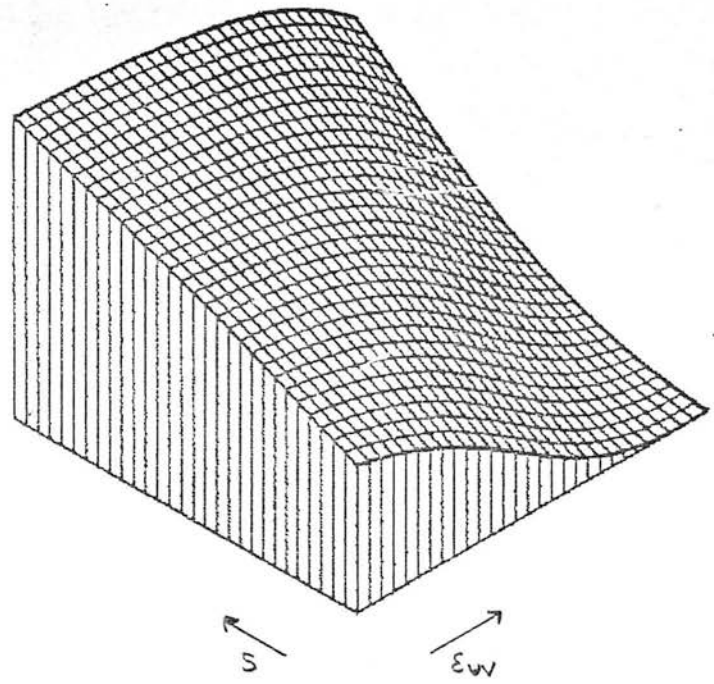

Figure 3.6-3

a

PLANE; (S,E51)

MODEL; 2

ORIGIN;	S	1.00
	NBAR	1.00
	E51	1.00
	EUV	2.00
PARAMETERS;	ALPHA	2.50
	BETA	10.00
	ETA2	.40
	PHI	.33
	THETA	1.00
	TW	8000.00
	TC	80.00
	B0	2.50
	KAPPA	.42
	KL	2.00

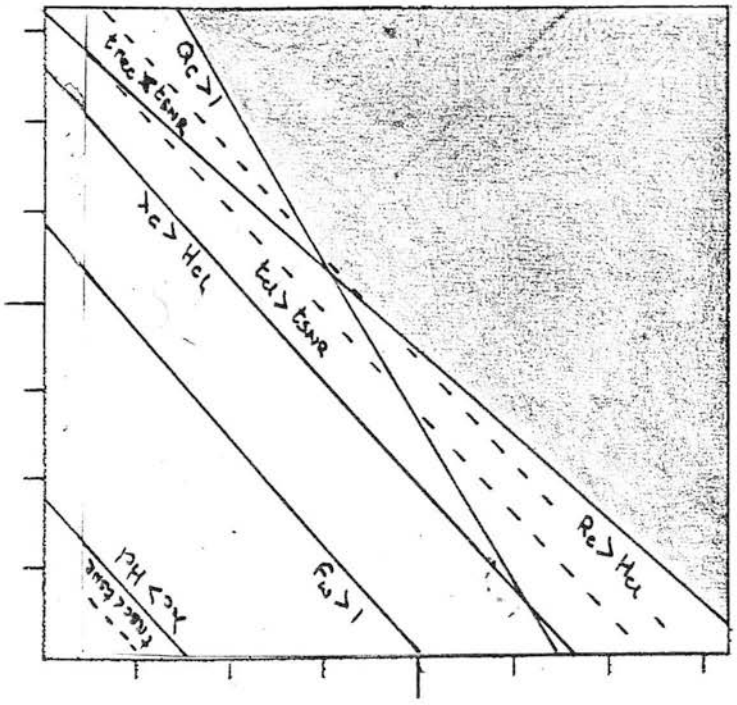

b

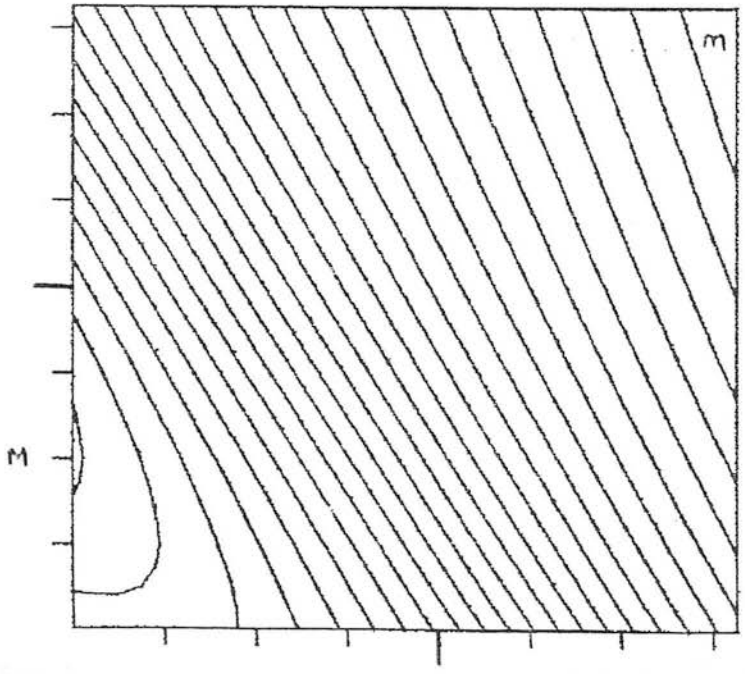

Q

MINIMUM	-2.62
MAXIMUM	2.43
CONTOURS;	
LOWEST	-2.40
INTERVAL	.20

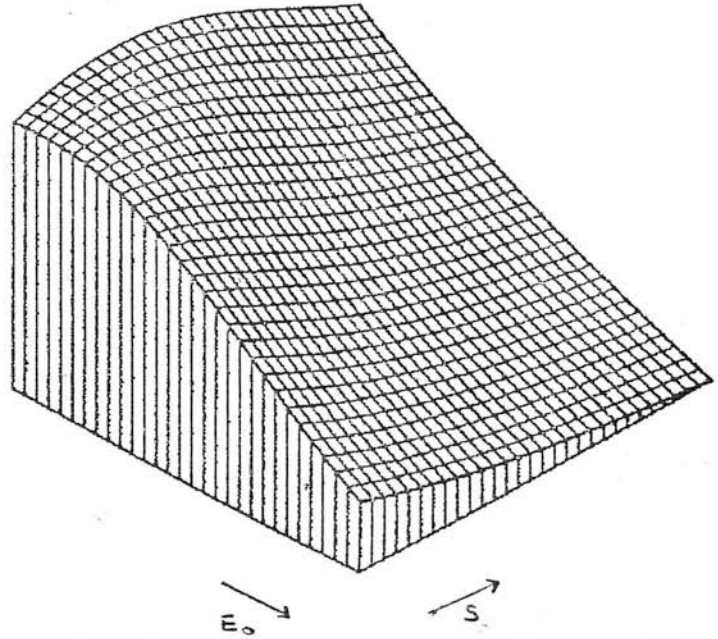

c

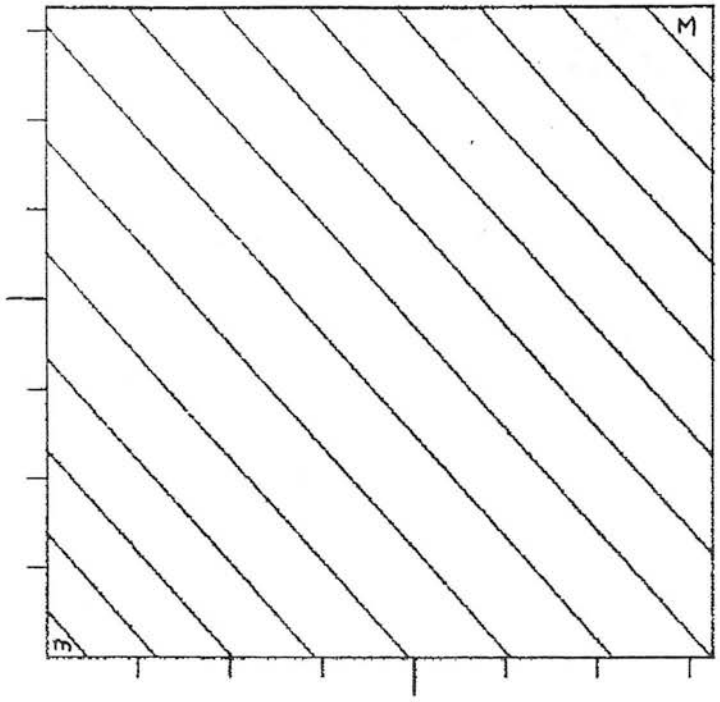

PA

MINIMUM	2.28
MAXIMUM	5.16
CONTOURS;	
LOWEST	2.40
INTERVAL	.20

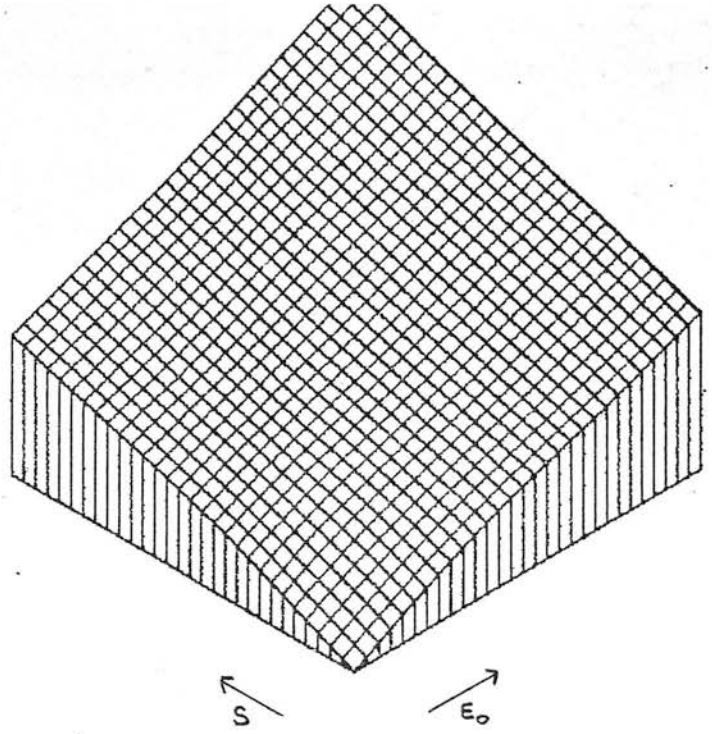

d

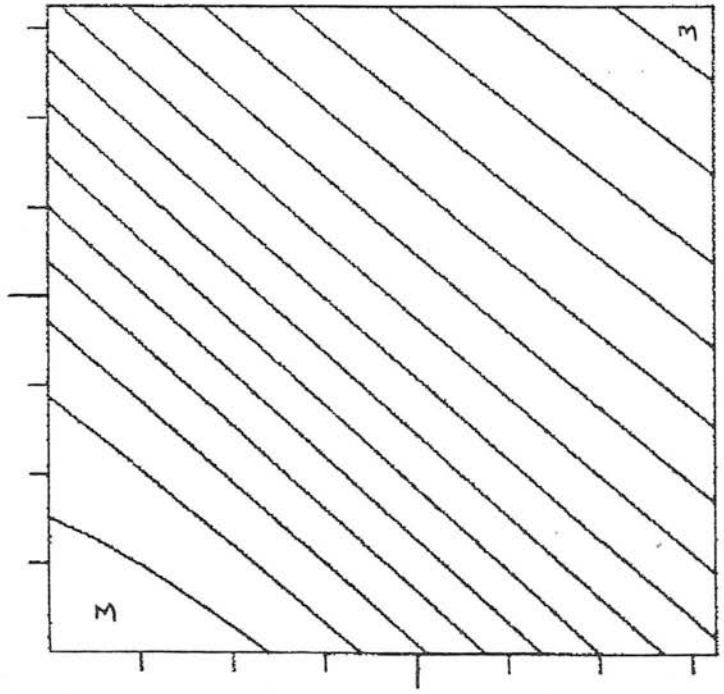

RC

MINIMUM	1.52
MAXIMUM	3.05
CONTOURS;	
LOWEST	1.60
INTERVAL	.10

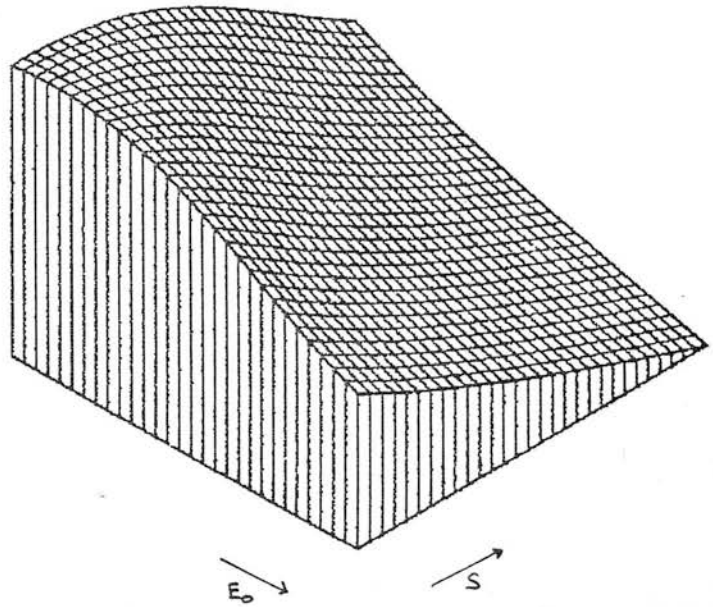

e.

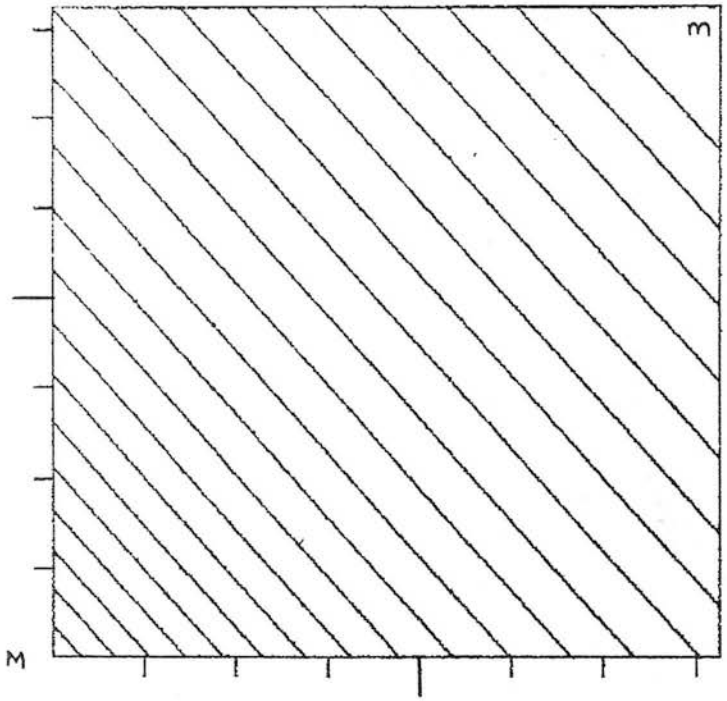

FW

MINIMUM -2.77
MAXIMUM 1.77

CONTOURS;

LOWEST -2.40
INTERVAL .20

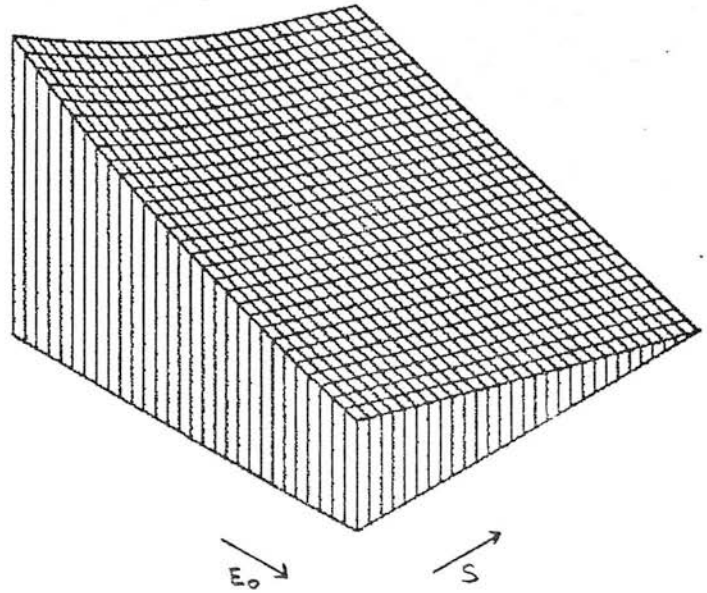

f.

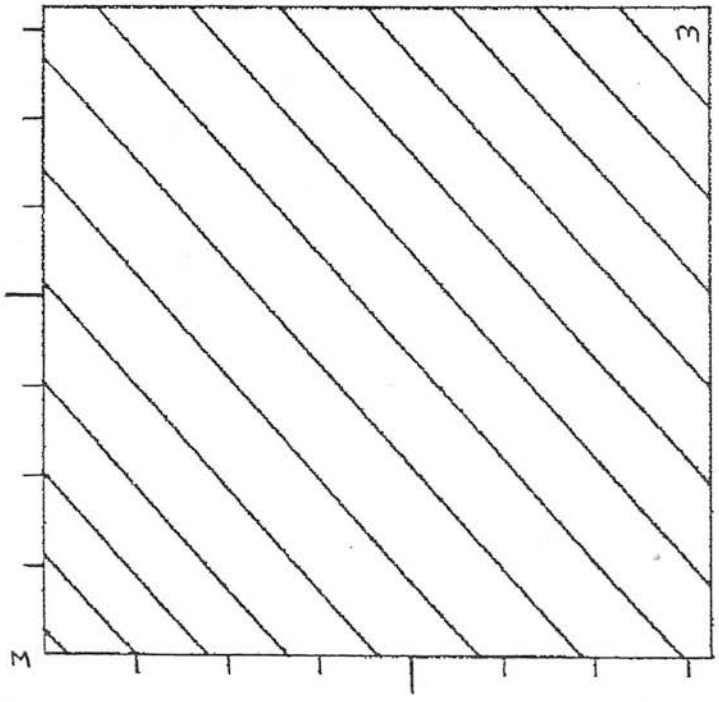

FC

MINIMUM -3.22
MAXIMUM .00

CONTOURS;

LOWEST -3.00
INTERVAL .20

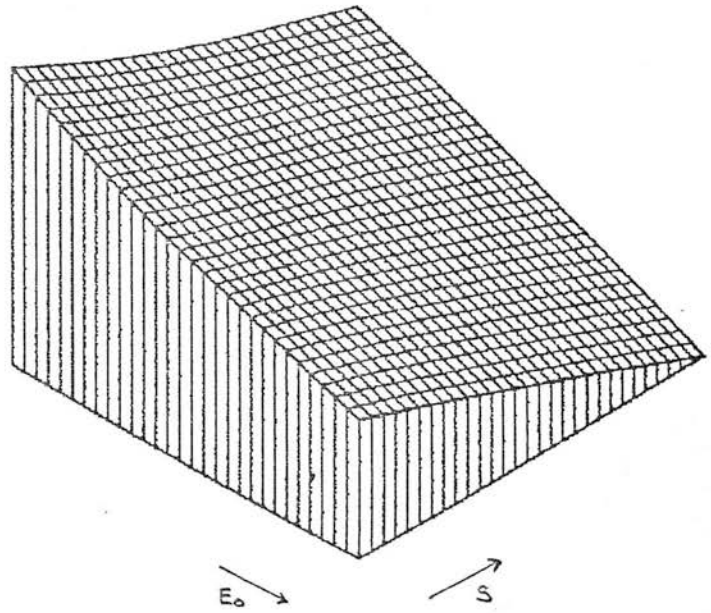

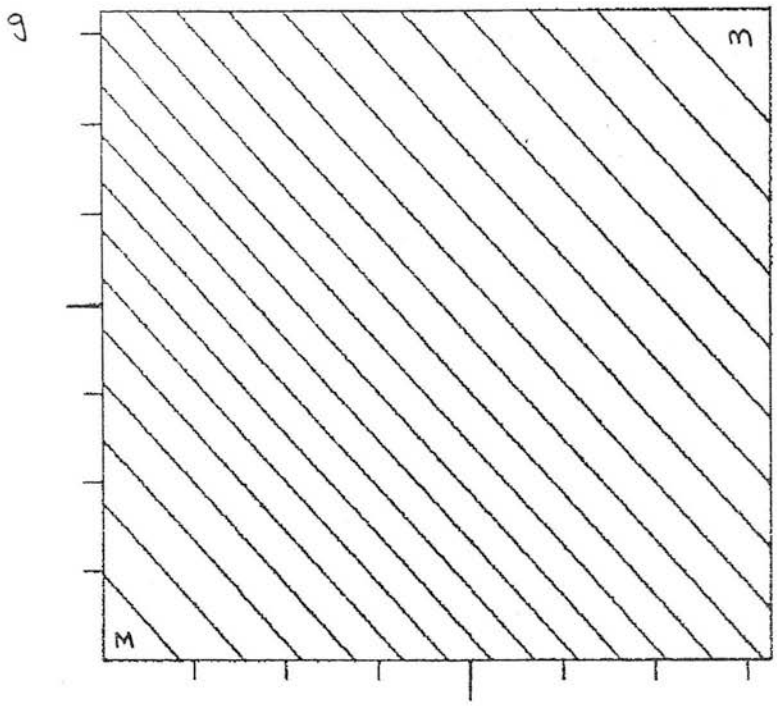

AWB

MINIMUM	-1.89
MAXIMUM	2.61
CONTOURS:	
LOWEST	-1.60
INTERVAL	.20

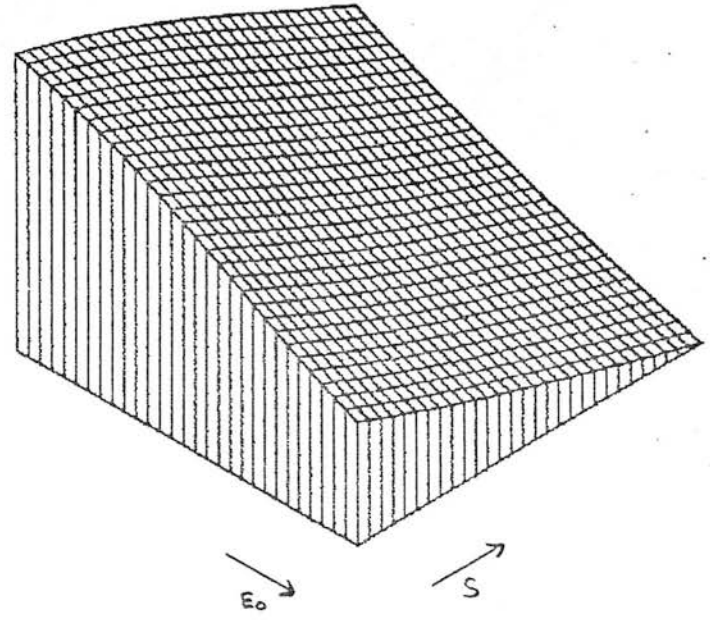

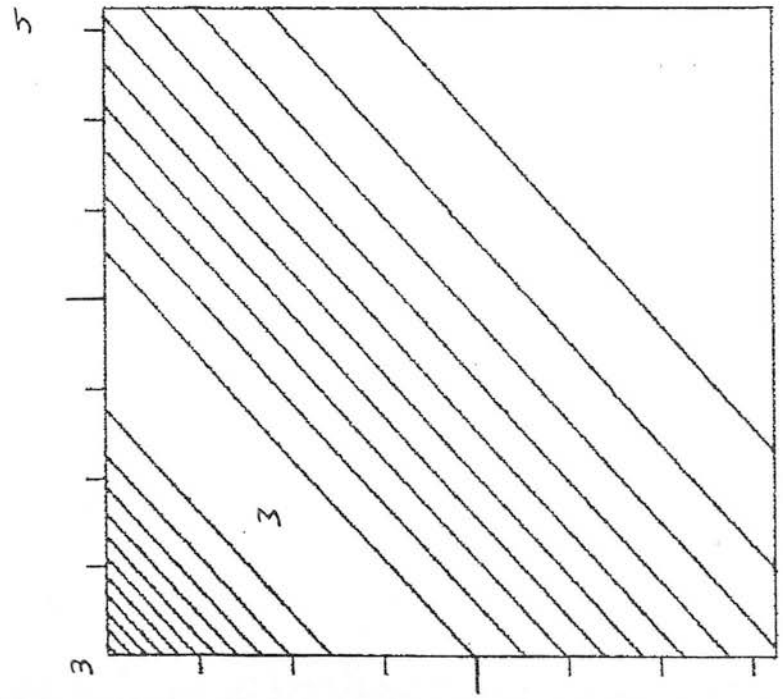

LW

MINIMUM	.97
MAXIMUM	1.53
CONTOURS:	
LOWEST	1.00
INTERVAL	.05

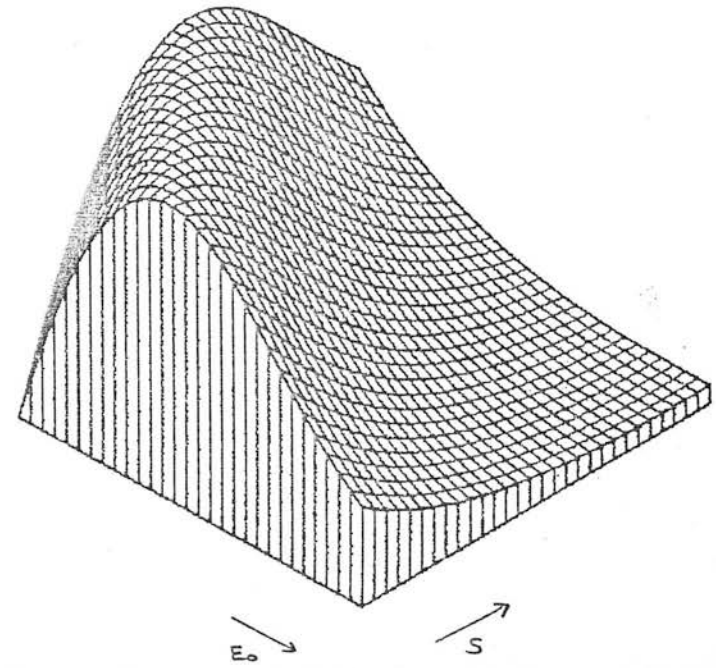

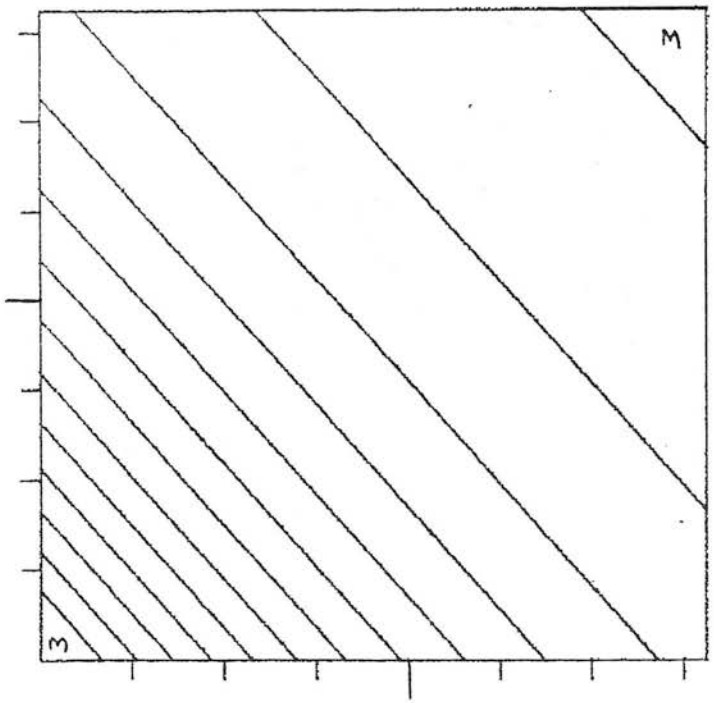

Y

MINIMUM -.58
MAXIMUM .83

CONTOURS;

LOWEST -.40
INTERVAL .10

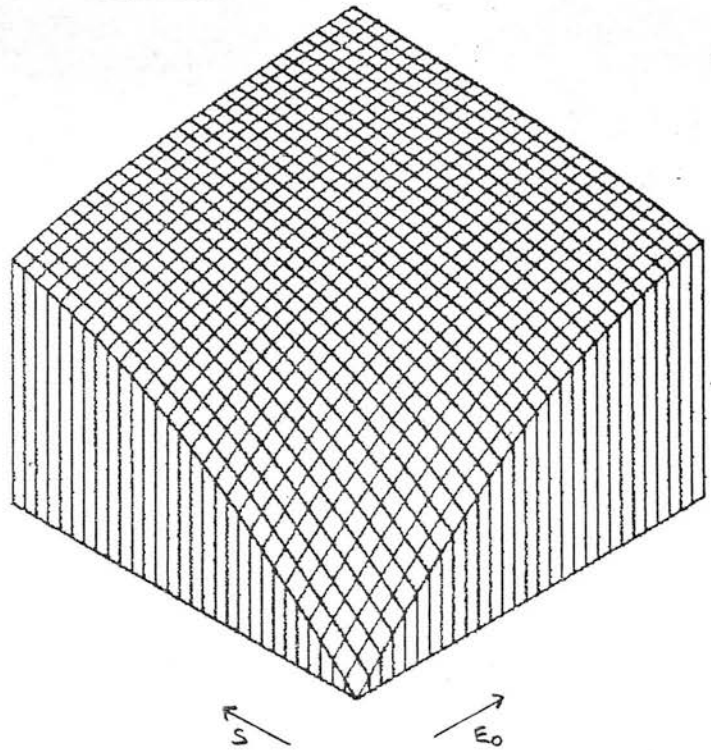

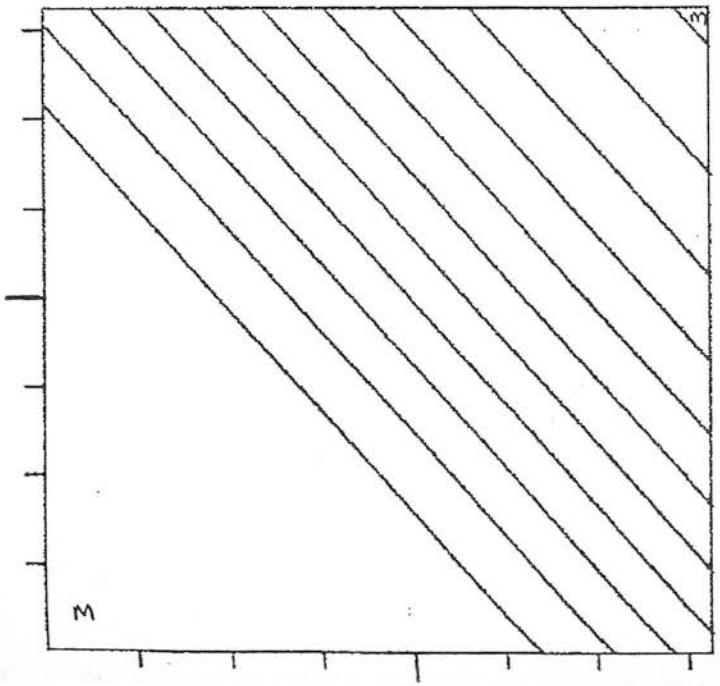

Z

MINIMUM .05
MAXIMUM .29

CONTOURS;

LOWEST .06
INTERVAL .02

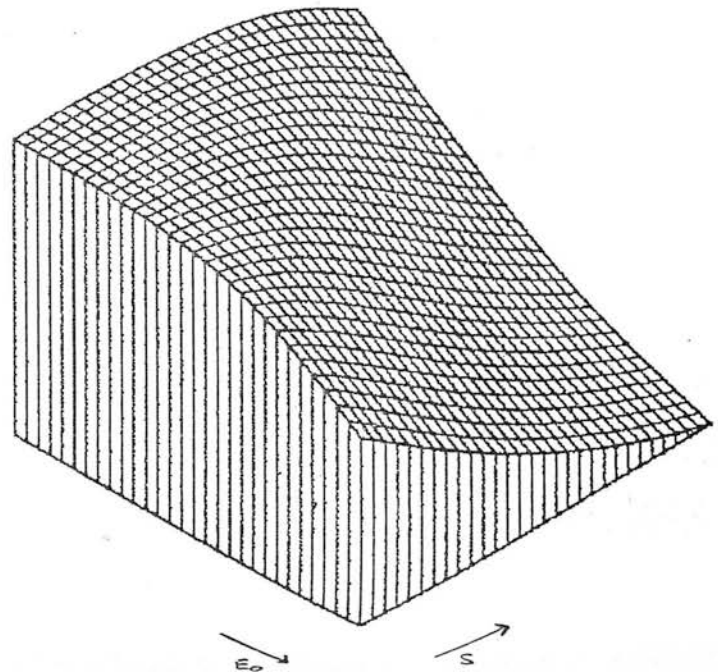

k

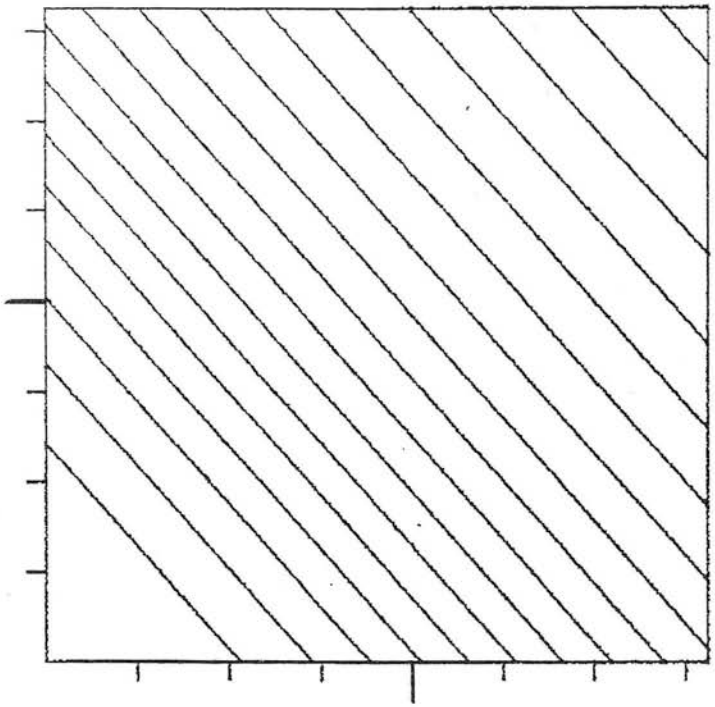

NCL

MINIMUM	-6.68
MAXIMUM	2.28

CONTOURS;

LOWEST	-6.00
INTERVAL	.50

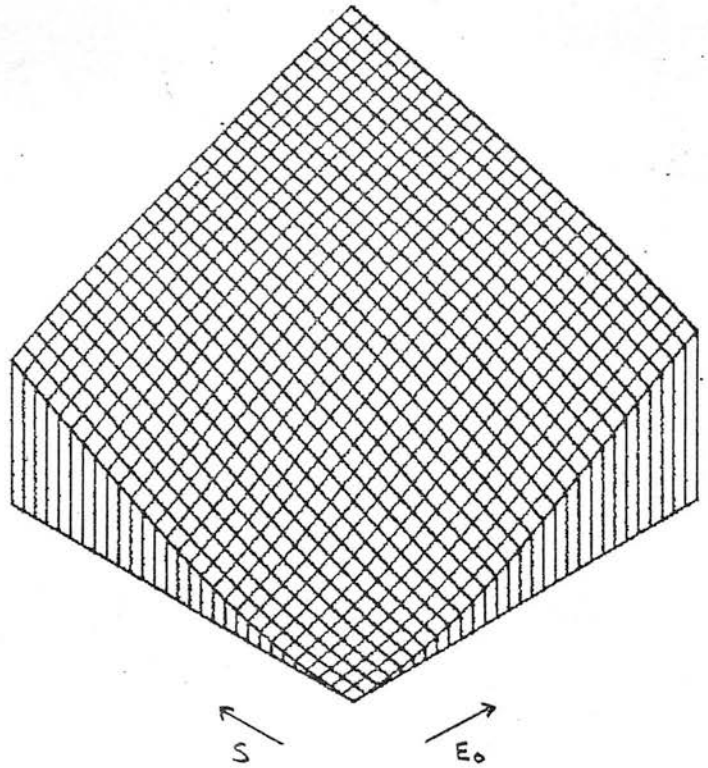

$F(S,\bar{n}) \propto S^{a-b}$ would appear as a set of equispaced straight lines in the contour diagram and as an inclined plane in the isometric plot.

Figure 3.6-2 shows the variation of the same quantities in a cross section in which S and ε_{uv} vary over the ranges $3 \times 10^{-15} pc^{-3} yr^{-1} \leq S \leq 9.5 \times 10^{-13}$ and $6.3 \times 10^{-17} cm^{-3} s^{-1} \leq \varepsilon_{uv} \leq 2.3 \times 10^{-14} cm^{-3} s^{-1}$ respectively while $\bar{n}$ and E_o remain fixed at the standard values. Similarly Figure 3.6-2 is for the section through parameter space in which $\bar{n}$ and ε_{uv} are held constant while S and E_o span the ranges $3 \times 10^{-15} pc^{-3} yr^{-1} \leq S \leq 9.5 \times 10^{-13}$ and 3.1×10^{49} ergs $\leq E_o \leq 9.5 \times 10^{51}$ ergs.

The quantites which are illustrated are; the porosity parameter Q_c which measures the sum of the fractional volumes of all SNR in the adiabatic phase (panel b); R_c the SNR radius at cooling (panel d); the ensemble average interstellar pressure $\langle \tilde{P}_h \rangle$ (panel c); the filling factor of the warm envelopes f_w (panel e) and the cold cores f_c (panel f); the mean warm envelope radius $\langle a_w \rangle$ (panel g) and line of sight separation λ_w (panel h); the quantity $Y = Ln\ (a_{ou}/a_{ol})$ which parameterises the mass range covered by the clouds (panel i); the ionisation parameter $\chi = (1 + X_w)$ (panel j) and; the total number of clouds N_{cl} (panel k). The values of $\langle a_c \rangle$ λ_c and f_c may straightforwardly be calculated from the relationships,

$$\langle a_c \rangle = 0.38\, Z^{-\frac{1}{3}} \langle a_w \rangle, \quad \lambda_c = 6.25\, Z^{\frac{4}{3}} \lambda_w$$

$$n_c = 0.01\, Z\, n_w$$

Similarly other properties of the ensemble of SNR can be calculated using the plotted values of Q_c and the relationships given in §3.2.

These figures illustrate the following general trends:

(1) When S or E_o are <u>increased</u> the average pressure increases ($P \propto SE_o$). Consequently the clouds are smaller ($a \propto P^{-1.8}$), denser ($n \propto P$) and very much more numerous. ($N_{cl} \propto P^{4.4}$). This has the effect of increasing the evaporation parameter ($\chi \propto P^{3.4}$) so that SNR cool both earlier and at smaller radii, although there are more SNR this is more than compensated for by the decrease of R_c, t_c and hence Q_c <u>decreases</u>. This apparently paradoxical result that increasing the energy input leads to earlier energy dissipation can be shown to be an automatic consequence of the evaporative feedback mechanism and the assumption of pressure balance.

(2) When $\bar{n}$ is <u>increased</u> this quite understandably increases the number of clouds ($N_{cl} \propto \bar{n}$) and hence the evaporation parameter, again leading to a smaller value for R_c and a very much reduced filling factor of adiabatic phase SNR. It also leads to an increase in the cloud filling factors and a decrease in the line of sight cloud separations. The small drop in the

pressure due to the decrease in Q_c does lead to a reduction in the average cloud size which in part offsets the direct effect of increasing $\bar{n}$.

(3) When ε_{uv} is <u>increased</u> the size of the smallest cloud is increased (recall that the minimum cloud size is tied to the size of the smallest optically thick cloud in recognition of the easy destruction of clouds without cores). Consequently the number of clouds is considerably decreased as is the evaporation parameter. The SNR thus cool later and Q_c is smaller. The increase of ε_{uv} also increases the fractional ionisation of the warm envelopes.

Note that the trends discussed in (1) and (3)are such as to oppose one another. This has important consequences for the results of the galactic model discussed in §4 where it is plausibly assumed that $\varepsilon_{uv} \propto S$. This means that acceptable model solutions can be obtained over a much greater range of supernova rates than would be possible if S varied alone.

Panel (a) of Figures 3.6-1 to 3.6-3 shows the intersection of the boundaries of the region of validity with the surface in parameter space depicted in the plots. The nature of the lines of constraint are as follows.

(1) When $Q_c > 1$ SNR will commonly overlap and cease their expansion before cooling takes place.

(2) When $R_c > H_{cl}$ the typical cloud scale height, energy and mass exchange with the galactic halo will begin to influence the energy and mass balance of the SDC-ISM.

(3) When $f_w \gtrsim 1$ energy losses due to cloud crushing and the increased retardation of the blast wave by interactions with the clouds will begin to severely modify SNR dynamics. Further, since the estimate of the average pressure ignores the volume taken up by clouds it will begin to give a serious underestimate of the pressure. As discussed in §3.2 these effects are partially compensating, so that the model results should qualitatively hold until values of $f_w \sim 1$ are predicted by the model.

(4) When $\lambda_c \gtrsim H_{cl}$ the galactic disk will become optically thin to ionising photons and a significant fraction of ε_{uv} will begin to 'leak' into the halo.

(5) Formally the condition for the validity of the case II description of the cloud dynamics is that $t_{cl} \ll t_{SNR} \ll t_{rec}$. As already noted in §3.2-1 these conditions can never be truly satisfied in the SDC-ISM; the various descriptions of the cloud dynamics where primarily introduced to assess the effects expected rather than as a rigorous formal description. To give some idea of where the dynamical description is <u>least bad</u> the locci of points along which $t_{cl} = t_{SNR}$ and $t_{rec} = t_{SNR}$ are given.

In light of Cowie et al's (1981) results for the evolution of evaporative SNR the consequences of any violation of the first two of these constraints will not be as serious as was originally supposed by MC. Because radiative cooling and shell formation take place deep in the SNR interior they will be relatively little effected either by interaction of the outer shock with other SNR or its expansion beyond the galactic cloud layer. However, the ISM will be characterised by a high degree of connectivity between the disk and halo and mass and energy exchange will take place. The situation may then be more akin to that discussed by Cox (1981) in which the mass and energy balance of the SDC-ISM are accomplished at least in part by the operation of a galactic fountain. Since these conditions are violated when S and E_o are both small the required energy flux can probably be carried by quite a weak fountain.

When $f_w \sim 1$ the ISM will be more reminiscent of the situation originally discussed by Cox & Smith (1974) where hot SNR generated gas is enclosed in a matrix of warm material.

In the following sections I will discuss the sensitivity of the model to the values of the other parameters. Grids of model calculations similar to those illustrated in Figures 3.6-1 to 3.6-2 have been obtained for each of the representations of the cloud dynamics described in § 3.2.1

and also for the non-evaporative model described in §3.3. In addition a thorough although less detailed set of calculations has been performed covering the expected ranges of each of the other parameters which enter into the model as listed in Table 3.3-1. These show that the gross qualitative features exhibited in Figures 3.6-1 to 3.6-3 and described above are preserved although of course considerable quantitative changes do take place. The major results of this extensive effort are conveniently summarised in Table 3.6-3 which shows the effects of changing each of the model parameters by a factor of two from its standard value, upon each of the derived quantities in a semi-quantitative way. Although derived for case II and for parameter values near those assumed in the standard model the relative magnitudes and direction of variation depicted in this table hold good at essentially all points in parameter space examined.

Table 3.6-3 The sensitivity of the model results to each of the input parameters. Rows (1) - (13) show the effect of increasing each of the named parameters by a factor of 2 on each of the derived quantities. Rows (14) and (15) show the effect of changing the description of the cloud dynamics and Row (16) the effect of adopting the non-evaporative model. The effects are shown semi-quantitatively; upward-pointing (downward pointing) arrows show an increase (decrease) whose magnitude is indicated by the length of the arrow as shown in the key. Although calculated for points here the standard conditions defined in Table 3.6-1 the results shown are qualitatively valid over most of the parameter space explored (See text).

	Q_c	R_c	$\langle \vec{F}_h \rangle$	$\langle T_h \rangle$	$\bar{\chi}$	N_{cc}	q_{wb}	F_w	λ_w	n_w	x_w	q_{ol}	q_{ou}	F_c	λ_c	n_c
(1) S	⇊	↓	↑	·	↑↑	↑↑↑	⇊	↓	·	↑	·	⇊	↓	↓	·	↑
(2) $\bar{n}$	⇊⇊	↓	↓	↓	↑↑	↑↑	↓	↑	⇊	·	↓	↓	·	↑↑	⇊	·
(3) E_o	⇊⇊	↓	↑	·	↑↑	↑↑↑	⇊	⇊	·	↑	↓	⇊	↓	↓	↓	↑
(4) ε_{ov}	↑↑	↑	·	·	⇊	⇊⇊	↑	↑	↑	·	↑	↑	·	·	↑	·
(5) α	↑↑↑↑	↑	↓ !	·	↓	⇊⇊	↑	↑	·	↓	·	↑	·	↑	·	↓
(6) β	↓	·	↓	·	↓	↓	↑	·	·	·	·	↑	·	·	·	·
(7) ϕ	⇊	·	·	·	↑	·	·	·	·	·	·	·	·	·	·	·
(8) Θ	↑↑	↑	·	·	↓	⇊	↑	·	↑	·	·	↑	·	·	↑	·
(9) K_L	↑↑↑	↑	·	↑	⇊	⇊⇊	↑	↓	↑↑	·	↑	↑	·	·	↑	·
(10) T_ω	↑↑↑↑	·	↑	↑	⇊⇊	⇊⇊⇊	↑↑↑	↑↑	↑	⇊	↑	↑↑	·	·	↑↑	·
(11) T_c	↑	·	·	·	·	·	·	·	·	·	·	↑	↑	↑	↓	↑

	Q_c	R_c	$\langle \tilde{R}_h \rangle$	$\langle T_h \rangle$		$\bar{\chi}$	N_{Cl}		a_{w0}	F_w	λ_w	η_w	x_w		a_{01}	a_{00}	F_c	λ_c	η_c
(12) q_v	↑↑↑↑↑	||	↑	↑		↓↓↓	↓↓↓↓↓		↑↑	↓↓	↑↑	.	↑		↑↑	.	↓↓	↑↑↑	↑
(13) B_0	↑↑	.	.	.		↓	↓↓		.	↓	↑	.	.		.	↑↑	.	↑	.
(14) Case I	↓↓	↓	.	.		.	.		.	.	.	.	.		.	.	.	.	.
(15) Case III	↑↑	↑	↓	.		↑	↑↑		↑	↑	.	↓	.		↑	↑	.	.	..
(16) 'Cox'			↓				↓↓		↑	↑↑	.	↓	.		↑	.	↑	.	↓

Key

. $< 2^{1/3}$ | $2^{1/3} - 2^{1/2}$

| $2^{1/2} - 2$ || $2 - 4$

||| $4 - 8$ |||| $8 - 16$

||||| > 16

3.6.2 The Parameters of the SNR Model

The main adjustable theoretical parameters of the SNR model are the ratio of the blast wave velocity to the mass weighted sound speed in the SNR α, the fraction of the explosion energy stored as thermal energy ε the radiative cooling enhancement factor β, and the exponent of the post cooling expansion law η'. Their standard values and anticipated range are listed in Table 3.6.1.

The effect of changing ε is obviously identical to that of changing E_o discussed in the previous section (see row (3) of table 3.6-3). Increasing α (row (5) of Table 3.6-3) has an effect approximately opposite to that of changing E_o (or ε). The pressure decreases so that there are many fewer, larger and more tenuous clouds, consequently $\overline{\chi_c}$ decreases and R_c and Q_c increase. Increasing β has a similar effect although of somewhat reduced amplitude on the properties of the cloud ensemble. However, the direct effect of β on R_c ($R_c \propto \beta^{-0.46}$) and Q_c ($Q_c \propto \beta^{-2.2}$) is sufficiently strong to cause both of them to decrease. The value of η' effects the value of the exponent in the relationship between $\langle \tilde{P} \rangle$ and Q_c relatively slightly consequently changing its value does not modify any of the values predicted by the model at the level of sensitivity shown in Table 3.6-1 and consequently its effect has not been illustrated.

3.6.3 The Parameters of the Cloud Population

Row (12) of Table 3.6-3 shows the effect of changing the slope of the cloud mass spectrum from the value 2 adopted for the standard case to a value of 4/3. These two values just about span the range of possibilities suggested on the basis of the observational and theoretical results summarised in § 3.4. Essentially as the slope of the spectrum is decreased in this way more and more of the interstellar mass is locked up in the largest clouds. The effect of this is just about the same as decreasing the value of $\bar{n}$ by a factor $\sim$3. The total number of clouds decreases greatly while their average size and the line of sight cloud separation increase; the cloud filling factors and the evaporation parameter decrease. Consequently Q_c and R_c increase to such an extent that for the standard values of S, $\bar{n}$ and $\mathcal{E}_{uv}$ SNR no longer cool before overlapping and expanding beyond the confines of the cloud layer. To some extent changing the value of q does change the character of the models. As discussed in § 3.4 the average properties of the cloud ensemble pass from being controlled by the smallest clouds to being controlled by the largest as q decreases from 2 to 4/3. This in turn implies that the properties of the equilibrium state become more and more dependent on parameters such as T_c and B_o which together control the mass of the largest cloud and less and less on K_1 and T_w which control that of the smallest cloud. However, tables similar to Table 4.6-3 have been

constructed for several values of q and they demonstrate that the discussion given here remains essentially valid for q in the range $4/3 < q \lesssim 2$ although not significantly beyond it.

As noted above the lower bound of the cloud mass spectrum is fixed by K_1 and T_w; raising either increases the mass of the smallest cloud. Similarly increasing either T_c or B_o increases the mass of the largest cloud. Either change leads to a reduction in the total number of clouds (for a fixed value of $\bar{n}$), and hence decreases χ and increases Q_c and R_c. Increasing T_c and T_w of course also leads to a decrease of the density of the corresponding component for a fixed value of the pressure; for the warm component this then leads to a greater fractional ionisation.

The remaining parameters of the cloud population are the evaporation reduction factor ϕ and the surface area to volume ratio Θ_g. The first of these essentially only changes the evaporation parameter and consequently Q_c. Increasing the second just increases a_{wb} and this has an effect identical to increasing K_1.

3.6.4 Changing the Description of the Cloud Dynamics

The three different models of the cloud dynamics parameterised by ω lead as discussed in §3.6.2 to rather different expansion laws for the SNR and thus to somewhat different

dependences of the properties of the ensemble of SNR on the value of the evaporation parameter. Essentially the higher the degree of 'compressibility' of the clouds the more the evaporation is reduced at early epochs below that for case I and thus the later cooling will take place. Note that although three discrete values of ω were chosen to typify the different extremes of the cloud dynamical behaviour my treatment of the resulting effects on SNR evolution is valid for arbitrary ω. The resulting equilibrium state of the ISM is also a continuous function of ω. Thus to the extent that the real behaviour of clouds under the chaotic condition of the SDC-ISM may be described by some effective value of ω between 0 and 1.8, its properties will also be somewhere between those predicted from case I and case III.

The results for all three cases for the standard set of parameters are listed in Table 3.6-2 while rows (14) and (15) of Table 3.6-3 show their relative differences. Evidently the predictions for case I and case II are very similar in all respects, the major difference being a somewhat larger porosity and cooling radius for case II. The domains of validity of the two models are also almost coincident. The very much higher degree of compressibility in the case III model does lead to rather more different predictions. Its domain of validity although partly overlapping with those of the other two is displaced toward higher S, $\bar{n}$

and E_o and lower ε_{uv}.

3.6.5 The Non-Evaporative Model

For the reasons discussed in §3.3 the domains of validity of the non-evaporative model is somewhat more restricted than that of the evaporative model. In order that all the explosion energy can be dissipated by cloud crushing $S^{\frac{2}{3}}/\bar{n} \lesssim 3.5 \times 10^{-9}$ while the confinement of the warm envelopes by the matrix pressure requires $S^{\frac{2}{3}}/\bar{n} \gtrsim 1.4 \times 10^{-9}$. When these conditions are satisfied however I find that the predictions of the model are qualitatively quite similar to those of the evaporative model. Results for the standard set of parameters are shown in column (5) of Table 3.6-2 and these are compared with those obtained for the standard case in row (16) of Table 3.6-3. The main differences stem from the somewhat lower pressure of the matrix gas predicted in the non-evaporative model. Consequently the number of clouds and their densities are somewhat smaller and the cloud radii and filling factors are somewhat larger for this case.

3.7 SUMMARY

In this chapter I have developed a simple model of the SDC-ISM based on the work of MO. This model extends on the previous work in three important ways:

(1) by incorporating a highly approximate description of the way a cloud responds to being overrun by an SNR blast wave, I have been able to assess the effects of cloud dynamics on the process of cloud evaporation which lies at the heart of the model.

(2) to assess the effects of the complete suppression of evaporation by the clouds magnetic field I have constructed a variant model in which 'cloud crushing' (Cox 1979, 1981) replaces evaporation enhanced radiation as the dominant sink of SNR energy.

(3) the treatment of the cloud population has been generalised to allow for the possibility of non-spherical clouds and changes in the slope of the assumed mass spectrum.

The model turns out to be remarkably robust : the results obtained from it do not change grossly when quite drastic changes are made to the description of the cloud dynamics; they are not unduly sensitive to the assumption made about the dominant mode of energy dissipation; nor are they greatly altered by changes in the slope of the cloud mass spectrum or the topology of the clouds. The properties of this specific model may therefore be taken with some

confidence, to be typical of SDC-ISM models in general.

The several variants of the model have been subjected to an exaustive parameter search in order to establish the domain in parameter space within which the model is self consistent and to test the sensitivity of its predictions to the very many uncertain free parameters which enter into its formulation. From this I conclude that:

(1) the model remains self consistant when its main controlling parameters the supernova rate S, explosion energy E_o, mean gas density $\bar{n}$ and ionising photon emissivity ε_{uv} vary over quite large ranges near the values believed appropriate to the solar neighbourhood. When S, $\bar{n}$ and E_o are small and ε_{uv} large the model fails because the energy dissipation rate falls below the value necessary to ensure that supernova cool before overlapping and before growing larger than the thickness of the cloud layer. When $\bar{n}$ and ε_{uv} are large and S and E_o are small the pressure of the hot gas is insufficient to contain the warm component of the ISM which grows to full volume occupation. When $\bar{n}$ is small and ε_{uv} large the galactic disk becomes optically thin to the ionising photons, this condition would probably be self-correcting.

(2) the qualitative features of the model remain unaffected by quite major changes of the other input parameters; its quantitative predictions are only moderately

sensitive to the precise values chosen (See Table 3.6-3) and depend on them in a readily understandable way.

4. SPIRAL STRUCTURE AND THE SDC-ISM

4.1 Introduction

Spiral structure is the most striking morphological attribute of galaxies. Spirals make up about $\frac{1}{3}$ of all galaxies (or $\sim$ 60% of all bright galaxies), including of course our own. More importantly in this context, they make up $\sim$ 90% of all those galaxies which at the present epoch both contain a significant amount of interstellar gas and are currently actively engaged in star formation. They thus represent the most important class of systems to which the SDC-ISM scheme might be thought to apply.

To date all investigations of the SDC-ISM have focussed attention on conditions in the solar neighbourhood and have thus made use of appropriate average values of the controlling parameters such as $\bar{n}$, S and ϵ_{uv}. However, the existence of spiral structure implies a modulation in the values of these parameters by about a factor of ten as one passes from arm to interarm regions. Further, the sun lies in the outskirts of the main star forming region in our galaxy so that the controlling parameters will also vary by a similar amount with galactocentric distance. The results of §3 show that this will have a profound influence on the properties of the SDC-ISM so that any discussion based purely on the solar neighbourhood is inevitably rather incomplete.

Equally the influences responsible for the existence of

spiral structure must propagate through and operate on the ISM. In particular the essential visible manifestation of spiral structure is the conversion of interstellar gas into new stars in a rather narrow zone - the spiral arms. Thus it is evident that the phase properties of the ISM must play a crucial role in any theory of spiral structure. To date however, with a few very recent exceptions, models of spiral structure have discussed the ISM within the framework of the Field et al (1969) two phase model, if at all (Shu et al 1972, Biermann et al 1972).

In this chapter I will describe the first, admittedly rather preliminary attempt to incorporate a model of the small scale properties of the SDC-ISM within the global context of the structure of a spiral galaxy similar to our own. In the remainder of this section I present background material on the current theories of spiral structure and the problems entailed for them by the adoption of the SDC-ISM model. In §4.2 a very simple representation of galactic structure is presented from which values of the controlling parameters at any point in a galaxy may be obtained. §4.3 describes the results obtained when this model is combined with the description of the SDC-ISM formulated in §3. §4.4 discusses several consequences which emerge from these calculations.

4.1.1 Theories of Spiral Structure

Spiral structure poses three main problems which any theory for its origin must address:

(i) The majority of galaxies rotate differentally thus material arms would be wound up on a timescale of order a few rotation periods much smaller than the age of the galaxy. Hence any model invoking such material arms must incorporate a mechanism for their rapid creation. The alternative approach (the one normally employed) is to regard the arms, as long lived waves either of stellar and gaseous density or of star formation) which propagate in the galactic disk.

(ii) In general spiral structure exhibits a great deal of overall regularity (Oort 1962; see Kormandy 1982 for a comprehensive and incisive review of galaxy morphology). There exists, however, a considerable variety of structural forms. In particular spirals can be divided into a continuum of classes according to the degree of symetry and continuity of their arms (D. Elmegreen 1981; Elmegreen & Elmegreen 1982). At one extreme are the 'grand design' spirals which possess two smooth symetric arms, extending continuously from the centre to the edge of the visible disk; at the other are the 'flocculent' spirals which consist of a large number of short patchy, ragged, spiral segments which do not join up to make a coherent pattern.

(iii) Spiral structure is predominantly a phenomenon of the

young stars and gas; it is exhibited much less markedly if at all by the old disk stars which make up the majority of the mass. Furthermore, in the 'grand design' spirals the inner edge of the spiral arm is characteristically delineated by a narrow H^{o} ridge, prominant dust lanes and chains of small intense often regularly spaced HII regions. In the proto-typical 'grand design' spiral M51 the ridge line of the radio continuum flux (dominated by synchrotron emission) is also coincident with main dust lanes along the inner edge of the arms (Mathewson et al 1972).

There are two main theories of spiral structure currently prevalent in the literature. The oldest and best developed of these, the density-wave theory of Lin and Shu (1964, 1966) is a purely dynamical scheme (for reviews see e.g. Lin, 1967; Wielen, 1974; Roberts, 1977; Rohlfs, 1977; Toomre, 1977). In this it is supposed that a rigidly rotating, small amplitude spiral perturbation is imposed upon the axisymetric gravitational potential of the galactic disk. This induces departures from circular motion in both the stars and the gas and consequently a spiral purturbation in their density. For a given galactic rotation curve Ω, and a chosen value of the rotation speed of the spiral pattern Ω_p, it is possible to find values of the pitch angle i, and the amplitude of the spiral potential, for which the induced density perturbation is just sufficient to sustain the imposed gravitational potential (Lin & Shu 1964; 1966; Contopoulos 1973; see

Roberts et al 1975 for applications to several galaxies). The density wave is then self supporting.

The magnitude of the induced peculiar velocities are $\lesssim W_{\perp_o} \equiv \tilde{\omega}$ $|(\Omega - \Omega_p)|$ sin i the component of the circular velocity perpendicular to the arm, which is typically $\sim$10 - 20 kms^{-1}. The old stars which make up $\sim$90% of the disk mass have dispersion velocities $\sim$30 - 40 kms^{-1} rather greater than this, ard consequently the density-wave induced in them is of small amplitude and is almost a sinusoidal function of azimuth. Conversely <u>if</u> the interstellar gas has an effective sound speed $\sim$10 kms^{-1} the induced gas flow will be transonic, even for quite modest spiral perturbation; the gaseous response is then highly non linear and shocks will appear in the flow (Fujimoto 1968). This leads to the highly influential, two-armed-spiral-shock (TASS) model of Roberts (1969; see also Shu et al, 1973; Woodward, 1975). Roberts showed that global galactic shocks form parallel to and slightly upstream of each of the underlying density-wave arms in the old stellar population. For $\Omega > \Omega_p$ so that the spiral structure is 'trailing' this corresponds to the inner (concave) edge of the arms leading to the natural association of the spiral shock with the observed H^o ridges and dust lanes of 'grand design' spirals.

When considered within the framework of the Field et al (1969) two phase model a rather elegant and self consistant picture emerges (Shu et al 1972, Biermann et al 1971). The volume-

filling, intercloud component of that model necessarily has the sound speed $\sim$10 kms^{-1} required if it is to respond strongly to the spiral forcing; the coincidence between the magnitude of induced streaming velocity and the sound speed naturally, and possibly universally, follows from the values of atomic constants (Shu et al 1972). Moreover the amplitude of the pressure modulation through the spiral shock somewhat exceeds the range of pressures over which two stable phases can co-exist and consequently the ISM undergoes forced phase transition; the high pressure in the post shock region forces condensation of intercloud material on a timescale comparable with the radiative cooling time, resulting in the formation of a narrow belt of newly formed cloud material, which might be identified with a dust lane; the reverse transition will take place in the low pressure interarm region. Unfortunately as I will discuss in §4.1.2 a simple minded analysis suggests that things are not quite this tidy in a three phase ISM.

Several means by which the TASS wave might lead to the triggering of star formation in the spiral arms have subsequently been considered. Roberts (see also Shu et al 1972) suggested that the large pressure jump behind the galactic shock might push pre-existing clouds beyond the brink of gravitational stability leading to their collapse to form stars; Woodward (1976; 1979; see §5) has investigated this cloud shock interaction in considerable detail. The direct formation

of gravitationally unstable clouds by the forced phase transition has also been invoked (Biermann et al 1972). However the very small wavelengths implied for the thermal instability (Field 1965; Schwartz et al 1972) require that some other process acts to coalesce the new formed clouds into a gravitationally unstable clump. Mouscovias et al (1974) have shown how the passage of a spiral shock can considerably increase the growth rate of Parker's (1966) magnetic Rayleigh-Taylor instability which might then provide such a long range collection mechanism. This idea has gained new force with the realisation that the majority of star formation occurs within giant molecular cloud complexes (GMC) which are unlikely to be substantially affected by the passage of a spiral shock (B. Elmegreen 1978; Elmegreen et al 1979). Blitz & Shu (1980) have suggested that the masses and sizes of nearby GMC are consistant with their having been formed by the Parker instability. Alternatively B. Elmegreen (1979, 1982a, b) has suggested that the collection mechanism is predominantly gravitational, the magnetic field only playing a secondary role; GMC then form by hierachical fragmentation of the dust lane. In this way he explains the occurrence of chains of GMC in our galaxies and the quasi-regular spacing of regions of active star formation along the arms of external galaxies like 'beads on a string' (See Elmegreen & Elmegreen 1983). Alternatively if GMC are long lived and grow from smaller clouds by collisions (Scovile & Hersh 1979; Kwan 1979; Cowie 1981) they may themselves respond strongly to the spiral potential perturbation, since their velocity dispersion is

also $\sim$10 kms^{-1} (Shu 1978; Cowie 1981; Levinson & Roberts 1981; Huntly & Gerola 1981; Roberts et al 1983; Roberts 1983; Kwan & Valdes 1983). Star formation would then occur either directly as a result of shock compression in cloud-cloud collision or by gravitational collapse of those clouds which grow beyond their Jeans mass; the enhancement of star formation in the arms then results from the higher cloud density and consequently higher collision rate which occurs there (Norman & Silk 1980: Levinson & Roberts 1981; Kwan & Valdes 1983).

Since density wave theory was originally formulated to circumvent the 'winding dilemma' mentioned above it is somewhat ironic that the major unsolved problem of the theory concerns the maintenance of the spiral wave against various dissipational processes. Firstly, radial transport of the energy of the spiral wave is inevitable, the group velocity being typically comparable with the sound speed (Toomre 1969). For galaxies which rotate rigidly a standing wave can be set up by reflecting spiral waves between corotation (where $\Omega = \Omega_p$) and the nuclear bulge, and the density wave may then be steady (Mark 1976, 1977). However, for galaxies which rotate very differentially there exists a radius interior to corotation at which the stellar epicyclic frequency exactly matches the period of the spiral forcing (inner Lindblad resonance). Spiral waves will be strongly attenuated as they pass through this region, their energy being coupled into random stellar motion. The density wave will then decay on a timescale

comparable to the sound travel time from corotation to the nucleus, which is typically only a few times the rotation period at corotation (Feitzinger & Schmidt-Kaler 1980). Secondly the irreversible processes associated with the galactic spiral shock inevitably imply damping of the spiral wave, the time constant being once more only a few rotation times (Kalnajs 1972; Roberts & Shu 1973; Feitzinger & Schmidt-Kaler 1980). In the face of this a number of mechanisms have been proposed to replenish the energy of the spiral wave of which the most important invoke periodic forcing by a bar (Toomre 1969) or 'oval disortion' (Sanders & Huntly 1976) or by interactions with companions (Toomre 1982).

The second theory of spiral structure, the stochastic self propagation star formation (SSPSF) model proposed by Mueller and Arnett (1976) and extended by Gerola, Seiden and co-workers (Seiden & Gerola 1982, Seiden 1983 and references therein) is essentially phenomonological. By contrast with the density wave theory in which star formation is a by product of spiral structure the SSPSF model views spiral structure as a by product of star formation! The basic idea of the model as originally formulated is very simple: Consider an initial cluster of young massive OB stars whose expanding HII regions, strong stellar winds and eventual explosion as supernovae drive shocks into the surrounding ISM as discussed in §2. There is then a definite probability that these shocks will stimulate the formation of a new OB

cluster in a nearby gas cloud 'Elmegreen & Lada 1977; Elmegreen et al 1978; Herbst & Assousa 1977) which in turn drives shocks into the neighbouring ISM etc. Differential rotation then stretches the resulting aggregate of young clusters into a spiral pattern.

In the earliest models the probability that an existing OB cluster could stimulate the formation of a cluster in a neighbouring region was just taken as a constant P_{st}; it was also assumed that once an OB cluster formed in a region its susceptibility to further star formation would be reduced for some time. Even with these simple assumptions it proved possible to generate simulated galaxies showing a striking resemblance to the more irregular and 'flocculent' spirals Mueller & Arnett 1976; Gerola & Seiden 1978; Seiden & Gerola 1979). However, because the SSPSF process is fundamentally one of percolation this could only be done if P_{st} was confined within a very restricted range; for too small a value star formation dies out while for too large a value the whole disk turns into stars. This problem can, however, be removed by a more careful treatment of the role of the ISM (Mueller & Arnett 1976; Seiden et al 1982). In this the gas is divided into 'active gas' which is capable of forming stars and 'inactive' gas which is not; P_{st} is then assumed to be proportional to some power of the density of 'active gas', and it is further supposed that the process of star formation converts all the 'active gas' into 'inactive gas', which is only allowed to return to the active

state after some time delay. This results in a feedback mechanism by which an overly high local rate of star formation deactivates all the available gas thus reducing the star formation rate, which is hence kept fixed near the value required for good spiral structure.

As a by product the model then also generates apparent spiral ordering in the ISM; the distribution of the 'inactive gas' closely mimics that of the active star formation regions while that of the 'active gas' is like its 'negative image.' When the observed radial distributions of H^o and H_2 are compared with those predicted for the 'active' and 'inactive' gas it is found that they should be equated with H^o and H_2 (or more probably GMC) respectively (Seiden 1983 a,b). This seemingly paradoxical result can be understood if the SSPSF theory is reinterpreted as one of stochastic self propagating molecular cloud formation as envisioned by B. Elmegreen (1981) with star formation regarded as an inevitable but not necessarily instantaneous consequence of the cloud formation process (Seiden 1983b).

On the principle that when two processes can operate they probably do, it would seem appropriate to consider the behaviour of galaxies in which star formation occurs both through the action of the large scale galactic shocks of the TASS scheme and through the SSPSF process (Mueller & Arnett 1976; Gerola & Seiden 1979). As would be anticipated when stars predominantly form in the spiral shock, the

resulting galaxy exhibits the characteristic global ordering and bilateral symetry of the 'grand design' spirals but with a substantial degree of local disorder superimposed. Jensen et al (1981) present compelling evidence for the co-existence of a galactic shock and stochastic processes in M83. Conversely when the stochastic star formation dominates, a characteristically irregular galaxy results, but with some residual bilateral symetry resulting from the TASS wave. Kaufman (1979 a, b, 1981) has given a simple phenomonological model for the profile of the star formation rate behind a spiral density-wave shock including the presence of successive generations of stars born by sequential star formation. Comparing the results of this with the observed distribution of HII regions she finds that $\sim$10% - 70% of all OB stars form directly in the spiral shock in our galaxy while in M33 this fraction is $\sim$6% - 50% the large range resulting from uncertainty over the period which must elapse between successive generations of stars.

The sequence of spiral galaxies from 'flocculent' to 'grand design' might then be viewed as a sequence of increasing dominance of the spiral shock (Elmegreen & Elmegreen 1982). Support for this view comes from the appearance of galaxies in the near IR where the light of the old disk stars dominates. In the 'grand design' spirals the underlying red arms are rather smooth and continuous and have been plausibly identified as the density wave in the old disk stars, which supports the spiral potential (Schweizer 1976). In the

'flocculent' spirals the red arms are just as chaotic as the blue arms (D. Elmegreen 1981) as would be expected from the SSPSF models. Additional evidence comes from the statistics of occurrence of 'grand design' and 'flocculent' spirals (Kormandy & Norman 1979; Elmegreen & Elmegreen 1982). It is found that most barred spirals ($\sim$75%) and most unbarred spirals with companions or which are members of groups ($\sim$67%) are grand design spirals. Amongst isolated, unbarred galaxies most ($\sim$68%) are 'flocculant' spirals while in those which show 'grand design' structure it is predominantly confined to the region interior to the inner Lindblad resonance. Overall $\sim$69% of all spirals show 'grand design' structure. Consequently it appears that 'grand design' structure, and by inference dominant spiral density waves, are ubiquitous wherever means are plausibly available for their excitation and maintenance. When these are absent the structure is flocculent and can result from the SSPSF mechanism alone.

The view of our understanding of spiral structure presented here may be rather optimistic. In particular none of the mechanisms for maintaining density waves are fully understood while our understanding of the process of sequential star formation (cloud formation?) is still little beyond the level of vigorous hand waving! Nevertheless it probably provides an adequate framework for what follows.

4.1.2 Is the SDC-ISM Compatible with Spiral Shocks?

In bringing together the TASS model for galactic structure and the SDC-ISM picture it is important to recognise that a basic incompatibility may exist between the two concepts. As first recognised by Scott et al (1977) the hot gas which fills most of the interstellar volume has such a high sound speed ~ 120 Kms^{-1} that its response to the spiral potential will be negligible. Thus on a simple minded analysis the SDC-ISM cannot support a global spiral shock and the density wave theory would be bereft of its most attractive features. Further the kinematic lifetime of the spiral wave would become much less than a galactic rotation period imposing an impossible burden on any mechanism for its maintenance. There are five possible responses to this dilemma.

(i) it might be argued that in 'grand design' spirals the interstellar pressure is so high that SNR are for the most part isolated, leaving warm gas as the main volume filling component. While this possibility cannot be absolutely excluded either observationally or theoretically it certainly raises more questions than it solves.

(ii) we may abandon density wave theory altogether; however SSPSF process alone cannot account for all the observed properties of spiral galaxies and there is as yet no obvious alternative theory.

(iii) The hot phase might be confined to the spiral arms

where the supernova rate is high with a phase transition to a predominantly warm ISM occurring in the interarm region (Scott et al 1977, Reinhardt & Schmidt-Kaler 1979; Blitz & Shu 1980). This apparently plausible suggestion is based on the false premiss that the supernova rate is negligible (i.e. zero) in the interarm region. In fact I will show in §4.4 that while S is certainly reduced this is more or less compensated for by the lower value of $\bar{n}$ in the interarm region, and the hot gas filling factor is if anything rather larger than in the arms.

(iv) The effective accoustic speed of the composite of warm and hot gas which makes up the SDC-ISM might be low enough to support the TASS wave (Weigandt & Schmidt-Kaler 1980). This possibility will be examined further in §4.4.

(v) Since the dispersion velocity of the interstellar clouds is $\sim$10 kms^{-1}, the cloud component alone may respond strongly and non-linearly to the spiral potential (Shu 1977; Cowie 1981; Levinson & Roberts 1981; Huntly & Gerola 1981; Roberts et al 1983; Roberts 1983; Kwan & Valdes 1983).

Either of these two last possibilities would leave the prediction of the TASS model qualitatively intact. The sound speed of the composite ISM must obviously be higher than that of the warm component alone so that the amplitude of its response will be somewhat weaker, for a given potential

purturbation, than that of a smooth warm gas. Similarly the cloud mean free path is sufficiently long compared to the width of spiral arms that it does not behave exactly like a continum and consequently the compression is rather weaker, and occurs over a more extended region, than that normally obtained. Provided the amplitude of the response is kept as a free parameter, however, the results of the usual TASS models can be used as a convenient first approximation to the response of the ISM in either case.

4.2 A Simple Representation of Galactic Structure

The model of the SDC-ISM requires the values of three main controlling parameters $\bar{n}$, S and ε_{uv}. I will here describe a very simple model which gives values of these parameters as functions of galactocentric distance $\tilde{\omega}$ and spiral phase Θ; variations of these parameters with distance from the galactic plane are neglected so that the galactic disk is treated as a uniform slab of finite thickness. The model is formulated within the framework of the TASS model and consequently, in terms of the discussion in §4.1, is applicable to the 'grand design' spirals where direct star formation by the spiral shock is at least comparable in importance to the SSPSF mechanism. It is also constructed, for purely anthropocentric reasons, as a representation of our galaxy, however, extention of the results to other galaxies is fairly straightforward. No attempt to achieve self consistancy between the strength of the spiral shock and the resulting parameters of the SDC-ISM is made; this is done not least because in the light of the discussion of §4.2 it is not at all clear how to do so. The shock strength is thus taken as a free parameter. Discussion of the question of whether such a shock could be supported is postponed to §4.4.

Given values for the controlling parameters at any point the procedure described in §3 can then be used to determine the local properties of the ISM. This presupposes that the ISM remains in a quasi-steady state as S, $\bar{n}$ and ε_{uv} vary slowly

with time and that variation of these parameters on length scales much larger than the typical dimensions of an SNR do not drastically affect local conditions. The gross thermodynamic and kinematic properties of the SDC-ISM can be expected to achieve a quasi-equilibrium state on a timescale comparable with the SNR repetition time, $t_{SNR} \sim 10^6$yr (Smith 1977; Habe et al 1981). For the cloud spectrum the problem is a little more severe. If the cloud spectrum is determined collisionally then the results of Chièze and Lazereff (1980) suggest that the spectrum can adjust on a timescale $\sim 2 \times 10^7$yr essentially the typical cloud-cloud collision time. Obviously since the destruction and formation of the smallest clouds is controlled (by assumption) by SNR adjustment of the lower mass bound should occur on a timescale $\sim t_{SNR}$. Similarly a decrease in the upper mass bound can be accomplished in about a free fall time for the largest clouds $\sim 10^7$yr; an increase in the upper mass bound by collisional coalescence requires a few times longer. Thus the assumption of a quasi-equilibrium state will be valid for timescales 10^7yr much shorter than a galactic rotation period but comparable with the time for flow through a spiral arm. This long relaxation time and the statistical distribution of supernovae will inevitably somewhat blur the parameter distribution obtained. Nevertheless, solutions obtained assuming locally uniform values for S, $\bar{n}$ and ε_{uv} at each point in the disc, should not represent too severe an approximation except near the discontinuities at the passages of the density wave shock and the 'switch on' of the new generation of supernovae.

4.2.1 The Total Gas Density

In the TASS model (Roberts 1969; Shu et al 1972; 1973; Woodward 1975) the ISM supports two shocks which are stationary in a frame rotating at the pattern speed Ω_p of the imposed spiral potential. Successive passages of a parcel of gas located at a mean distance $\tilde{\omega}$, from the galactic centre are thus separated by half the rotation period of the spiral potential,

$$t_{gal}(\tilde{\omega}) = 2\pi / \left[\Omega(\tilde{\omega}) - \Omega_p \right] \qquad 4.2.1$$

where $\Omega(\tilde{\omega})$ is the angular rotation speed of the galaxy. In what follows Ω_p is taken to be 13.5 kms^{-1} kpc^{-1} (Wielen 1974) and I adopt a flat rotation curve such that $\Omega(\tilde{\omega}) = 250\ (\tilde{\omega}/kpc)^{-1}$ kms^{-1} kpc^{-1} which adequately approximates the results of Gordon and Burton (1978) over the region exterior to $\tilde{\omega} \sim 5$kpc which is of primary interest here. Consequently $t_{gal}/2 \sim 2.7 \times 10^8$yr for $\tilde{\omega}$ = 10kpc here taken to be the galactocentric distance of the sun, and drops to $\sim 8.4 \times 10^7$yr at $\tilde{\omega}$ = 5 kpc.

For the present purposes an adequate approximation to the variation of the gas density along a typical stream tube behind a galactic shock is,

$$\bar{n}\ (\tilde{\omega}, \Theta) \simeq \bar{n}_o\ (\tilde{\omega})\ [1 + (C-1) \exp\ (-\Theta/\Theta_o)] \qquad 4.2\text{-}2$$

where Θ is the azimuthal angle ('spiral phase') measured from the position of the shock in the frame corotating with the spiral pattern; the second shock is located at $\Theta = \pi$ and the

density pattern of 4.2-2 is repeated. Typically the angular width of the arm is $\theta_o \sim 0.1$ corresponding to a passage time through the arm $\sim t_{gal}/20$ and a linear arm thickness $\pi\tilde{\omega}/10$ along the stream tube. For simplicity the density contrast or compression ratio C will be taken to be a constant; I will discuss the relationship of C to the parameters of the ISM in §4.4 Equation 4.2-2 will be taken to hold everywhere interior to the corotation radius, which for the values of $\Omega(\tilde{\omega})$ and Ω_p adopted above occurs at $\tilde{\omega}_{CR} \sim 18.5$ kpc, here taken as the edge of the galaxy. In reality of course it must break down interior to the inner Lindblad resonance ($\tilde{\omega}_{ILR} \sim 3 - 4$ kpc) and at each of the countable infinity of "ultraharmonic resonances" which occur at radii exterior to $\tilde{\omega} \sim 11.5$ kpc (Shu et al 1973). The amount of interstellar gas present in these regions is however sufficiently small that the misrepresentation is not too serious.

The constant $\bar{n}_o(\tilde{\omega})$ is obtained by requiring that the azimuthal average of $\bar{n}(\tilde{\omega})$ is equal to its observed value i.e.

$$\langle \bar{n}(\tilde{\omega}) \rangle = \frac{1}{\pi}\int_o^{\pi} \bar{n}(\tilde{\omega}, \theta)\, d\theta \simeq \bar{n}_o \left\{ 1 + (1 - C)\frac{\theta_o}{\pi} \right\} \equiv \bar{n}(\tilde{\omega}, H^o) + 2\bar{n}(\tilde{\omega}, H_2) \qquad 4.2\text{-}3$$

where $\bar{n}(\tilde{\omega}, H^o)$ and $\bar{n}(\tilde{\omega}, H_2)$ are the observed azimuthally smoothed densities of neutral and molecular hydrogen respectively.

While the galactic distribution of H^o is quite well established (Burton 1976) that of H_2 has been the subject of considerable controversy although there are now signs that

a general consensus of opinion is emerging (Lequeux 1981; Liszt 1982; Sanders et al 1983). The problem arises because the galactic distribution of H_2 cannot be determined directly but must be inferred from observations of a surrogate tracer most commonly CO; a series of rather uncertain and much debated steps must then be used to convert the measured CO emissivity J(CO) to the desired quantity $n(H_2)$. Despite the very real controversy about the individual steps entailed in its derivation, the final conversion factor obtained in a wide range of different studies, covering both nearby molecular clouds and those in the galactic interior, all lie within a factor of $\sim$2 of their mean $n(H_2)/J(CO) \sim 0.12$ cm^{-3} K kms^{-1} kpc^{-1} $^{-1}$ (Lizt 1982; Young & Scovile 1982a; Sanders et al 1983). A further potential difficulty is that the observed gradient in the abundance of carbon (Pagel & Edmunds 1981) might lead to a CO-H_2 conversion factor which changes with $\tilde{\omega}$ (Guibert et al 1978; Blitz and Shu 1980). Sanders et al (1983) have advanced cogent arguments which suggest that any such effect must, however, be small and the broad similarities between the calibration constant derived from clouds in the solar neighbourhood and in the galactic interior lend further credence to their view point.

In order to span the full range of possibilities I will consider three different models for $\bar{n}(\tilde{\omega}, H_2)$. These are based on, in order of decreasing H_2 density: (i) the results of Solomon et al (1979; SSS) which employed

$n(H_2)/J(CO) \sim 0.2 [cm^{-3}\ K\ kms^{-1}\ kpc^{-1}]^{-1}$ near the upper end of the likely range; (ii) the results of Gordon and Burton (1976; GB; see also Burton & Gordon 1978) for which the conversion factor employed was equivalent to $N(H_2)/J(CO) \sim 0.08 [cm^{-3}\ K\ kms^{-1}\ kpc^{-1}]^{-1}$; and (iii) model 3 of Guibert et al (1978; GLV) which was obtained from the data of GB by assuming $n(H_2)/J(CO) \sim 0.04 [cm^{-3}\ K\ kms^{-1}\ kpc^{-1}]^{-1}$ at the solar distance varying inversely with the carbon abundance [C/H] taken to be constant at 2.5 times the local value for $\tilde{\omega} \lesssim 8$ kpc and following d Log [C/H] /d $\tilde{\omega}$ = $-0.2\ kpc^{-1}$ exterior to this. Note that the SSS and GB data differ essentially only by the factor ~ 2.5 which results from the different calibration value used. All of these early surveys of the H_2 distribution were based on data from the Northern galactic hemisphere, however, more recent surveys incorporating partial coverage of the southern hemisphere (Robinson et al 1983, Sanders et al 1983) show that the southern and northern distributions are qualitatively the same.

Finally I take the vertical distributions of H^o and H_2 to be gaussians with scale heights of 160pc and 70pc respectively independent of $\tilde{\omega}$ (Jackson & Kellmann 1974; Cohen & Thaddeus 1977; Manchester et al 1983; Sanders et al 1983).

4.2.2 The Supernova Rate

In order to connect the local stellar birthrate $\dot{n}_*$ to the local mean gas density $\bar{n}$, I will adopt $\dot{n}_* \propto \bar{n}^m$ purely as a convenient, although plausible parameterisation*. The motivation for this particular choice, of course, lies in the classic work of Schmidt (1959) who first proposed a relationship of this form and estimated $m \sim 2$ on a variety of empirical grounds. Subsequently, a variety of attempts to "test" Schmidt's law and to determine the value of m from observations have been made. Obviously, only those made recently enough to include estimates of the total gas content, including H_2, are of relevance; some of these are summarised below. It must, however, be stressed from the outset, that all the observational tests refer to quantities averaged

---

* Note that for $m \sim 1$ the parameterisation adopted here leads to a star formation rate which decays exponentially to some low constant value behind the spiral shock on a timescale $\sim 10^7$yrs fixed by the timescale for the density decay. Kaufman's (1979 a,b) phenomenological derivation of the star formation rate profile behind a spiral shock, including secondary stimulated star formation, leads to precisely this form. The decay time is fixed by the efficiency of stimulated star formation and she finds a value $\sim 2.4 \times 10^7$yr from comparison of her model with observed arm widths. Incorporating a different timescale for the drop off of the density and star formation rate into the model, would add another free parameter into a system which already has uncomfortably many, without materially affecting the principal conclusions.

either over large volumes or over time and there is thus no compelling reason for believing they have any bearing on the use of Schmidts law in the strictly local sense implied here.

GLV have used a comparison of the radial and vertical distribution of several tracers of recent massive star formation with that of the interstellar gas (H^o plus H_2) and found $m \simeq 1.3 - 2.5$. A similar study of Smith et al (1978) based primarily on the distribution of HII regions but incorporating constraints derived from considerations of chemical evolution led to a somewhat smaller value in the range $m \simeq 0.5 - 1.0$. For external galaxies the blue luminosity (which presumably derives from young massive stars) is linearly proportional to the current H_2 content both within the disks of individual galaxies (Young & Scovile 1982 a,c; Scovile & Young 1983, Solomon et al 1981) and from galaxy to galaxy over an extremely wide range of luminosities (Young and Scovile 1982b). This suggests $m \sim 1$; since H_2 was the dominant constituent in the star forming regions of the galaxies considered and since the H^o content was almost independent of luminosity it is unclear whether this result applies to the density of H_2 alone or to the total gas density. Not surprisingly earlier results based on the H^o content alone summarised by Madore (1977) lead to a much steeper slope $m \sim 2$. Obviously a serious criticism of these results is that they assume that gas density is the only factor which determines the distribution of the star formation rate; in the context of

the TASS model there are strong reasons for believing that $\dot{n}_*$ should decrease rapidly with increasing radius (Shu 1973) even if the gas density were constant. It may however be argued that the variations of any second parameter(s) would have to be chosen most judiciously in order to reproduce the good agreement between the radial luminosity and gas density profiles found in the external galaxies (Young & Scovile 1982b).

On the other hand Miller and Scalo (1979) have deduced constraints on the stellar birthrate history in the solar neighbourhood by requiring continuity between the initial mass function (IMF) for stars with ages less than and greater than the age of the galaxy. They find that the current stellar birthrate cannot differ from the average birthrate over the age of the galaxy by more than a factor ~ 4. A similar conclusion has been reached by Twarog (1980) from models of the chemical enrichment of the galactic disk. Further Kennicutt (1983) determines current star formation rates for a large sample of disk galaxies which differ little from the rate averaged over their ages. Unless the depletion of the ISM due to star formation is largely offset by, for instance accretion of intergalactic gas the constancy of the stellar birthrate is inconsistent with $m \gtrsim 0.5$. The assumption of a time independent IMF inherent in all these studies may lie at the root of this discrepancy. There is a growing body of evidence which suggests that the IMF varies from place to place even within our galaxy (e.g. Larson 1982, Garmany et al 1982) and may vary with metalicity in external

galaxies (e.g. Terlevich & Melnick 1983). There is also a growing suspicion that high and low mass stars are formed in different locations and by different processes (see Larson 1982).

Guided by the above, but bearing in mind the caveat stated earlier concerning the likely relevance of the observational tests I will construct models with m = $\frac{1}{2}$, 1 and 2. I thus take the rate of supernovae to be given by,

$$S(\tilde{\omega}, \theta) = S_o \bar{n} (\tilde{\omega}, \theta - \theta_*)^m \quad m = \tfrac{1}{2}, 1 \text{ or } 2 \qquad 4.2\text{-}4$$

where $\theta_* = 2 t_*/t_{gal}$ and t_* is the average total lifetime of the progenitors of type II supernovae measured from the start of the process of star formation.* Roughly t_* is the sum of the time required for the collapse of an interstellar cloud plus the time required for contraction onto the main sequence, plus the main sequence evolution time of the supernova progenitor; since the progenitors of SNII have masses $\gtrsim 8M_\odot$ (Chevalier 1981 a,b Wheeler 1981) conservatively adopting a total pre-main sequence evolutionary time $\sim 10^7$yrs (Woodward 1978) implies $10^7 \text{yr} \lesssim t_* \lesssim 3 \times 10^7 \text{yr}$.

The normalisation constant S_o is obtained

---

* This procedure is strictly incorrect in that it fails to distinguish between supernovae of type II which have short lived progenitors and those of type I which are supposed to originate from old disk population objects. However, it does provide an adequate description of the observed azimuthal distribution of supernovae; the constant term $\bar{n}_o$ in equation 4.2-1 leads to a uniform interarm supernova rate with a magnitude close to that observed. This shortcoming could be rectified at the expense of introducing an additional arbitrary constant, however none of my results are materially affected by the simplification.

by equating the integral of the volumetric supernova rate over the galactic disk to the total galactic supernova rate S_{gal}. Estimates of S_{gal} have been obtained by a number of workers using one of four independent methods all of which are however subject to severe selection effects and/or uncertainties due to small number statistics (see Tammann 1982 and Lerche 1981 for reviews):-

(i) The number of galactic supernovae can be estimated from the seven certain supernovae recorded over the last two millenia, after applying large and uncertain incompleteness corrections to allow for galactic extinction, the absence of historical records from the southern hemisphere, omissions from the records etc. (Clark and Stevenson 1977 a,b 1982; Tammann 1982).

(ii) Counts of galactic radio SNR down to some limiting surface brightness can be converted to the number of SNR smaller than some diameter by means of an empirical surface brightness diameter relationship determined from a small number of SNR of "known" distance; adapting an appropriate theoretical model of SNR evolution (usually the Sedov model) and assuming all SNR evolve into a medium of the same density and magnetic field strength then leads to the number of SNR younger than a certain age (Clark & Caswell 1978). The difficulty of course lies in this last step; we do not know the correct evolutionary model to employ (Mathewson et al 1983) and all SNR cannot conceivably be evolving into a medium of the same density.

In general SNR in a low density medium, e.g. the hot matrix, fade much faster than those in a high density medium, or may even escape detection, so the supernova rate obtained in this way will be an underestimate (Kafatos et al 1981, Lozinskya 1980, Tomisaka et al 1980). Higdon and Lingenfelter (1980) have used the data for the very small subset of radio SNR for which independent age estimates are available to determine separate surface brightness age relationships for 'warm phase' and 'hot phase' SNR. They then attempt to self consistently determine the supernova rate and hot component filling factor by modeling the number-surface brightness relationship for all radio SNR. (For a theoretical discussion of the surface brightness diameter relationship for SNR in an SDC-ISM see Blandford and Cowie 1982).

(iii) Under the conservative assumption that there is a one-to-one relationship between supernova explosions and pulsar births the galactic supernova rate can be determined from estimates of the pulsar birth rate. Determination of this latter quantity is, however, rendered uncertain by our ignorance concerning the pulsar distance scale, their true ages and the value of the beaming factor (Taylor & Manchester, 1977; Arnett and Lerche, 1981; Arnaud & Rothenflug, 1980; Lyne, 1982). Further, it remains unclear whether all SNR or just a subset e.g. SNII give rise to pulsars or whether some pulsars can be formed non-explosively.

(iv) Over the past 50 years about 170 supernovae have been recorded in external galaxies. However, it is well established that the supernova rate is a strong function of galactic luminosity and morphological type so that it is necessary to employ a distance limited sample and subdivide the reduced sample according to galaxian type which results in typical sample sizes $\sim$10 (Tammann 1982). The observed rates must be corrected for incompleteness due to internal extinction and (highly uncertain) inclination effects. Further the galaxian type and luminosity of our own galaxy are not particularly well known (de Vaucouleurs 1979).

Table 4.2-1 provides a compilation of recent determinations of S_{gal}, obtained by each of the four methods, selected from the literature. It is not intended to be comprehensive but rather to give a fair estimate of the uncertainties which result from the difficulties inherent in each method. Taken together all the data seem to be consistant with $0.01 yr^{-1} \lesssim S_{gal} \lesssim 0.1 yr^{-1}$; in view of the many difficulties involved in the determination this shows a remarkably high degree of agreement!

The statistics of supernova in external galaxies also provide us with the only available estimate of the relative numbers of SNI and SNII as a function of galaxian type. For our galaxy SNI should make up a fraction $\sim$0.6 of the total (Tammann 1982).

TABLE 4.2-1 The Total Galactic Supernova Rate S_{gal}

Method	Reference	$(S_{gal}/10^{-2}yr^{-1}$	Sample Size	Note
(i) Historical Supernovae				
	Clark & Stevenson (1977b)	~3.3	7	
	Lerche (1981)	$1.7^{+3.0}_{0.7}$	8	
	Tammann (1982)	6.3 ± 2.5	5	
(ii) Radio SNR				
	Clark & Caswell (1976)	$\gtrsim 0.6$	120	
	Caswell & Lerche (1979)	$1.25^{+0.75}_{0.35}$	120	(1)
	Milne (1978)	3.3-2.5	120	(1)
	Higdon & Lingenfelter (1980)	$3.3^{+0.5}_{0.9}$	120	(2)
(iii) Pulsars				
	Taylor & Manchester (1977)	16.7-2.5	~350	
	Arnaud & Rothenflug (1980)	$1.0^{+0.43}_{0.38}$	~350	
(iv) Extragalactic Supernovae				
	Tamman (1982)	4.1 ± 2.5	77 (~10/type) in 400 galaxies	(3)
	Lerche (1981)	$1.4^{+3.6}_{1.4}$		

Notes:

(1) The data have been empirically corrected for the Z dependence of the density and magnetic field but still assume a single component medium.

(2) Corrected for effects of multi-component ISM

(3) Calculated assuming H_o = 50 $kms^{-1}Mpc^{-1}$ for other values multiply by $(H_o/50 kms^{-1}Mpc^{-1})^2$.

4.2.3 The Emissivity of Ionising Photons

Since a large proportion of the total ionising uv flux has its origin either in SNR or the young hot OB stars which are the progenitors of SNII I adopt the following simple parameterisation,

$$\varepsilon_{uv}(\tilde{\omega}, \Theta) = \varepsilon_1 S(\tilde{\omega}, \Theta) + \varepsilon_2 \qquad 5.2\text{-}5$$

where the constant term ε_2 describes the contribution from all old population sources (excluding SNI) in particular the nuclei of density bounded planetary nebulae.

Observational estimates suggest that in the solar neighbourhood SNR of all types, unshielded B stars and planetary nebulae each contribute $\varepsilon \sim 1\text{-}1.5 \times 10^{-15}$ photons $cm^{-3}s^{-1}$ (Salpeter 1979). Potentially the most massive OB stars make a much bigger contribution. From measurements of the diffuse radio continuum emission Mezger (1978) estimates that for the whole annulus $10kpc \lesssim \tilde{\omega} \lesssim 11kpc$ OB stars emit $\varepsilon \sim 4.6 \times 10^{-14}$ photons $cm^{-3}s^{-1}$ of which, however, $\sim 20\%$ comes from stars which are still contained within extremely dense radio HII regions; direct optical counts of OB stars within $\sim 3kpc$ of the sun lead to $\varepsilon \sim 4 \times 10^{-14}$ photons $cm^{-3}s^{-1}$ (Abbot 1982).

The difficulty comes in determining what fraction of this total flux is consumed in the relatively high density region in the immediate vicinity of the source and what fraction is

available to ionise the more general ISM. Mezger (1978) estimates that near $\tilde{\omega} \sim 10$kpc ~ 40-60% of this flux escapes from the 'extended low density HII region'. Similarly local estimates of the fraction of OB stars which are inside optically prominant HII regions suggest that $\sim 50\%$ of the flux escapes from these regions (Torres-Piembert et al 1974; Lynds 1980). However, Elmegreen (1975, 1976 a, b) has shown that even those OB stars situated in the general ISM can quickly surround themselves with an ionisation bounded HII region by photoionising surrounding interstellar clouds; the resulting nebula however would have too low an emission measure to be detected in straightforward optical searches. The extent to which his conclusion is modified by the clearing away of the low density debris by the stars' own stellar wind and by blast waves from nearby SNR is however difficult to assess (See §2). MO took the rather extreme view that no uv flux is provided by OB stars; since only a 5% leak would, however, roughly double the ionising flux I will also consider the effects of allowing a larger contribution from this source.

Based on these considerations I will adapt values of ε_1 between 1.5×10^{61} photons SNR^{-1} (no OB star contribution) and 20×10^{61} photons SNR^{-1} (50% of total OB star flux); I also take $\varepsilon_2 \simeq 1 \times 10^{-15}$ photons cm^{-3} S^{-1}.

4.3 Results

4.3.1 A 'Standard' Case

For purposes of orientation I will begin by considering the results obtained for a specific 'standard' case. In this the SDC-ISM is described by the evaporative model with the cloud dynamics represented by case II ($\omega = \frac{1}{3}$) and a supernova explosion energy $E_o = 5 \times 10^{50}$ ergs was adopted. The theoretical parameters of the SNR and the cloud spectrum were taken to have the standard values defined in Table 3.6.1. In addition the galactic model used the GB density distribution. The values adopted for the other parameters of the galactic model were : galactic supernova rate $S_{gal} = 0.02\ yr^{-1}$: ionising photon emissivities $\varepsilon_1 = 1.2 \times 10^{61}$ photons per SNR (no C star photoionisation) and $\varepsilon_2 = 0.7 \times 10^{-15}$ photons $cm^{-3}s^{-1}$; spiral shock compression C = 5.0 and; exponent of star formation m = 1.0. Subsequent sections will deal with the effects of changing these parameters of the galactic model. For ease of reference table 4.3-1 lists the standard values for all the parameters of the galactic model together with the ranges of values which are considered below.

Figure 4.3-1 shows the variation of a number of parameters of the ISM with spiral phase Θ in the midplane of the galaxy at the galactocentric distance of the sun ($\tilde{\varpi} = 10kpc$). The values of the same quantities at points on the loci

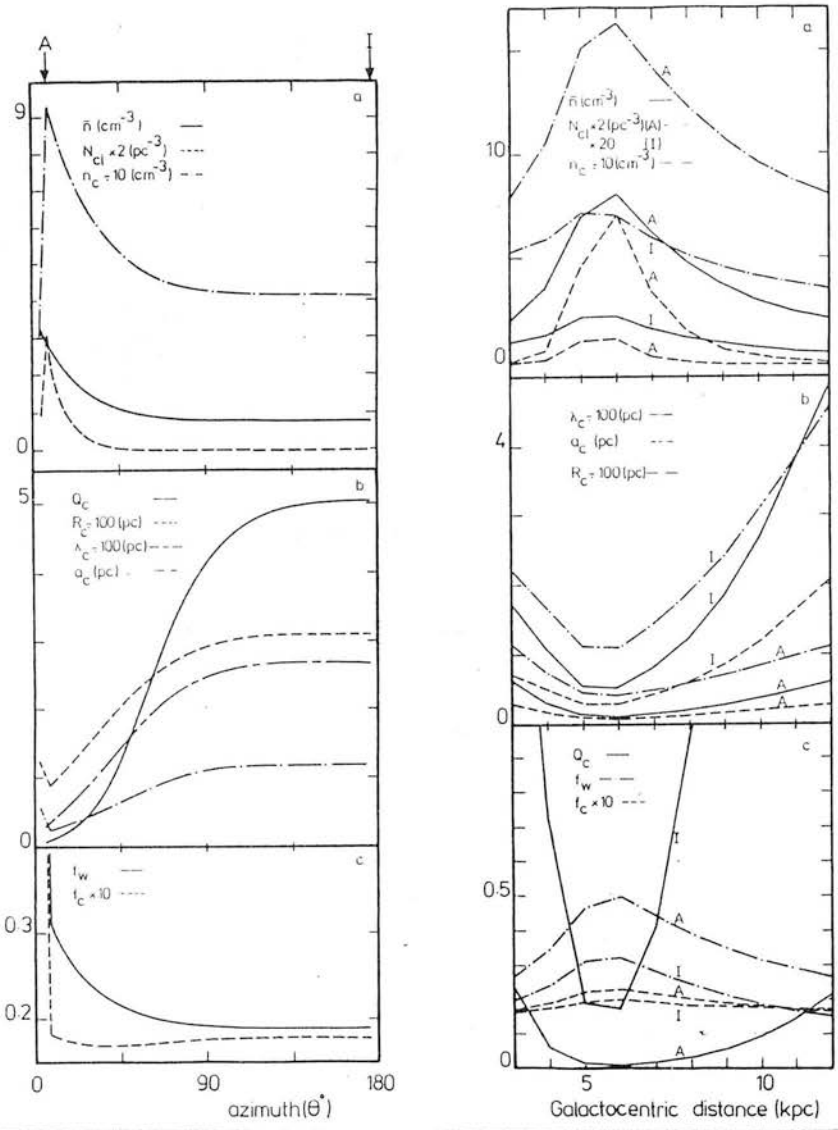

Figure 4.3.1 (Left) Calculated quantities as a function of azimuth θ°, in the midplane of the galaxy at a galactocentric distance of 10 kpc (see text). θ is zero at the position of the density wave shock. The positions at which the 'arm' (A) and (interarm) (I) properties were evaluated are indicated. The properties of the warm envelopes may be estimated from the relationships in the text while $\langle \tilde{P} \rangle \sim 88$ kn$_c$.

Figure 4.3-2 (Right) The same quantities as in Fig. 4.3-1 but plotted as functions of galactocentric distance, $\tilde{\omega}$ (kpc) along the 'arm' (A) and 'interarm' (I) loci.

TABLE 4.3-1 : The Parameters of the Galactic Model

Parameter	Standard Value	Range
Density jump across density wave shock C	5	5-10
Form of gas density distribution (See § 4.2.1)	GB	SSS,GB,GLV
Galactic supernova rate (S_{gal}/yr^{-1})	0.02	0.01-0.1
Exponent of star formation m	1	$\frac{1}{2}$, 1, 2
Ionising photon emissivity parameters ($E_1/10^{61}SNR^{-1}$)	1.2	1-20
($E_2/10^{-15}cm^{-3}s^{-1}$)	0.7	
Density wave pattern speed Ω_p	$13.5 kms^{-1}kpc^{-1}$	
Galactic rotation curve $\Omega(\tilde{\omega})$	$250/W kms^{-1}kpc^{-1}$	
Full width at 1/e height of spiral arm density enhancement θ_o	$\pi/10$	
Time delay between star formation and first supernova t_*	$1x10^7 yr$	

of maximum supernova rate ('arm') and minimum mean density ('interarm') are shown as functions of galactocentric distance $\tilde{\omega}$ in figure 4.3-2. Table 4.3-2 (a) lists the arm and interarm values both for $\tilde{\omega}$ = 10kpc and $\tilde{\omega}$ = 5 kpc, the latter distance being chosen as broadly representative of points in the molecular ring.

Column (1) gives the porosity parameter Q_c, which measures the sum of the fractional volumes of all SNR still in the pre-cooling phase of their evolution while column (2) gives R_c the remnant radius at the cooling epoch. Other parameters of the remnants at the cooling point can be ascertained from the relationships in Table 3.2-2. These quantities especially the former, increase very rapidly with <u>both</u> decreasing $\bar{n}$ and decreasing S, so that they attain their maximum values in the <u>interarm</u> region. It will be recalled from § 3.6 that this apparently paradoxical result is a direct consequence of the evaporative feedback mechanism in the MO scheme; it is not dependent on the details of the galactic model adopted here. Note that for the standard case $Q_c \gtrsim 1$ in the interarm region interior to 4kpc and exterior to 8kpc, so that in these regions SNR frequently overlap before cooling. Similarly in these regions R_c exceeds the scale height of the disk gas $\sim$ 160 pc and energy losses to the halo will begin to play a dominant role in the energy balance of the ISM. Under these circumstances the ISM will be characterised

Table 4.3-2 Properties of the ISM for various values of supernova rate, arm compression ratio, density distribution, and star formation rate. See Section 4.3 for details.

	R (kpc)	$\bar{n}$ (cm^{-3})	S ($10^{-13}\,pc^{-3}\,yr^{-1}$)	Q_c	R_c (pc)	$\langle P\rangle/k$ ($10^4\,K\,cm^{-3}$)	N_{cl} (pc^{-3})	$\langle a_c\rangle$ (pc)	λ_c (pc)	f_c (×100)	n_c (cm^{-3})	$\langle a_w\rangle$ (pc)	λ_w (pc)	f_w	n_w (cm^{-3})
(a) $S_{gal} = 0.02\,yr^{-1}$, $c = 5.0$, $m = 1.0$, GB density law.															
A	5	7.01	10.69	0.01	45	1.32	2.34	0.09	13.5	4.66	150.5	0.28	1.69	0.22	1.04
I	5	2.25	2.86	0.19	112	0.63	0.06	0.30	54.6	3.12	72.1	0.93	6.36	0.19	0.45
A	10	3.04	4.64	0.09	85	0.84	0.18	0.20	38.2	3.17	96.0	0.62	4.52	0.18	0.61
I	10	0.79	0.93	5.06	310	0.37	7.4×10^{-4}	1.19	269.4	1.89	41.6	3.86	28.96	0.18	0.23
(b) $S_{gal} = 0.02\,yr^{-1}$, $c = 10.0$, $m = 1.0$, GB density law.															
A	5	7.79	12.33	0.01	42	1.44	3.27	0.08	12.1	4.76	163.6	0.25	1.51	0.22	1.14
I	5	1.61	2.17	0.48	148	0.56	0.02	0.42	88.4	2.54	63.5	1.32	10.02	0.18	0.38
A	10	4.22	6.68	0.04	65	1.03	0.53	0.14	25.3	3.60	117.3	0.44	3.06	0.19	0.77
I	10	0.57	0.67	18.57	451	0.32	1.4×10^{-4}	2.05	479.6	1.56	36.3	6.70	50.48	0.18	0.19
(c) $S_{gal} = 0.05\,yr^{-1}$, $c = 5.0$, $m = 1.0$, GB density law.															
A	5	7.01	26.73	0.02	39	2.54	4.89	0.06	16.6	2.43	288.3	0.18	2.00	0.12	1.89
I	5	2.25	7.15	0.26	98	1.23	0.11	0.19	69.8	1.62	139.4	0.62	7.89	0.10	0.83
A	10	3.04	11.59	0.13	74	1.63	0.33	0.13	48.9	1.64	185.6	0.41	5.60	0.10	1.12
I	10	0.79	2.32	6.56	266	0.70	1.5×10^{-3}	0.75	335.8	0.99	79.9	2.44	35.70	0.09	0.43
(d) $S_{gal} = 0.02\,yr^{-1}$, $c = 5.0$, $m = 1.0$, SSS density law.															
A	5	16.57	13.38	0.01	28	1.41	16.38	0.06	4.3	10.60	159.5	0.19	0.58	0.43	1.17
I	5	5.32	3.58	0.02	65	0.64	0.49	0.19	16.2	7.32	72.8	0.56	2.04	0.37	0.51
A	10	6.45	5.21	0.02	55	0.81	1.03	0.14	13.3	7.02	91.9	0.43	1.69	0.34	0.65
I	10	1.67	1.04	0.40	168	0.33	0.01	0.63	73.6	4.43	37.7	1.96	8.47	0.31	0.23
(e) $S_{gal} = 0.02\,yr^{-1}$, $c = 5.0$, $m = 2.0$, GB density law.															
A	5	7.01	44.38	0.02	36	3.65	6.90	0.05	18.9	1.69	414.9	0.14	2.24	0.09	2.64
I	5	2.25	3.18	0.20	110	0.68	0.06	0.28	55.9	2.90	77.7	0.88	6.49	0.18	0.48
A	10	3.04	8.34	0.11	77	1.29	0.28	0.15	44.4	2.08	146.3	0.47	5.15	0.12	0.90
I	10	0.79	0.33	6.90	421	0.18	1.7×10^{-4}	2.56	256.9	3.76	20.9	8.31	27.49	0.40	0.11
(f) $S_{gal} = 0.02\,yr^{-1}$, $c = 5.0$, $m = 1.0$, GB density law.				y_{max}	R_{max}										
A	5	7.01	10.69	0.16	79	0.68	1.35	0.14	10.4	9.03	77.7	0.53	0.82	0.86	0.54
I	5	2.25	2.86	0.17	106	0.29	0.02	0.55	44.0	6.82	33.0	2.16	3.21	0.90	0.20
A	10	3.04	4.64	0.18	97	0.42	0.10	0.32	29.5	6.34	48.0	1.22	2.21	0.74	0.31
I	10	0.79	0.93	0.20	140	0.15	1.5×10^{-4}	2.80	234.1	4.54	17.3	11.47	15.67	0.98	0.09

A = Arm condition. I = Interarm condition.

by a high degree of connectivity between disk and halo and energy and mass balance will be accomplished, in part, by the operation of a galactic fountain as discussed by Cox (1981). Although under these circumstances the basic assumptions of the present SDC-ISM model are violated it is expected that the results obtained from it will remain qualitatively although not quantitatively correct.

Column 3 of Table 4.3-2 contains the volume average contribution to the ISM pressure provided by SNR, $\langle\tilde{P}\rangle$. Notice that the behaviour of this parameter is qualitatively similar to that of $\bar{n}$ in this case. In column 4 I give, N_{cl}, the number of cloud centres per cubic parsec. This quantity is largest in the arm region of the molecular ring and falls dramatically with decreasing $\bar{n}$ and S. Notice that the distribution of N_{cl} in both $\tilde{\omega}$ and Θ is significantly more sharply peaked than for instance that of $\bar{n}$. Again this behaviour is a consequence of MCs evaporative feedback mechanism.

Columns 5 - 8 give respectively the mean radius, $\langle a_c\rangle$, filling factor f_c, intercloud distance, λ_c and density, n_c, of the cold cores. Notice that the forms of the variation of $\langle a_c\rangle$, and λ_c are very similar, while the assumption of pressure equilibrium dictates that n_c is simple proportional to $\langle\tilde{P}\rangle$. Columns 9 - 12 give the corresponding quantities: $\langle a_w\rangle$, f_w, λ_w and n_w for the

warm envelopes. Recall that the ratios $\langle a_c \rangle / \langle a_w \rangle$, λ_c / λ_w, f_c / f_w and n_c / n_w are entirely fixed by the assumption of pressure equilibrium and the modelling of the cloud properties, specifically

$$a_w / \langle a_w \rangle = 0.38(1 + x_w)^{-1/3}, \quad \lambda_c / \lambda_w = 6.25(1 + x_w)^{\frac{2}{3}},$$

$$n_w / n_c = 100(1 + x_w), \quad f_w / f_c = 0.02(1 + x_w)^{-1} \ln(M_u / M_l),$$

where x_w is the fractional ionization in the warm envelope and M_u and M_l are the masses of the largest and smallest clouds permitted by the model. Since x_w varies only slightly the first three ratios are almost constant, having in the present case the values ~ 0.3, ~ 8.3 and ~ 0.06 respectively. Conversely M_u / M_l is quite sensitive to the local values of ε_{uv} and $\langle \tilde{P} \rangle$ and hence f_w / f_c varies rather more.

I will now consider the effect on the results of changing the constants in the galactic model from those used to derive Table 4.3-2(a). I have performed calculations employing each of the three density distributions discussed in §4.2.1 for m = 0.5, 1 and 2 and with c and S_{gal} having various values in the range 1 - 10 and 0.01 - 0.1 yr^{-1}, respectively. These show that the gross qualitative features exhibited in Figs. 4.3-1 and 4.3-2 are preserved, even though the absolute values of the derived parameter and the magnitudes of their variation with $\tilde{\omega}$ and θ may change considerably. One important exception to this, however, is that the qualitative behaviour of the filling

factors differs significantly according to the value of m. I will return to this point shortly.

4.3.2 Effect of Changing the Shock Compression Ratio c.

Understandably, the larger the value of c, the larger the contrast between the arm and interarm values of the derived parameters. This tendency is particularly pronounced in the cases of N_{cl} and Q_c and is least prominent for the filling factors. Rather more surprising is the relative insensitivity to the value of c of conditions in the arm region of the molecular ring. These trends are illustrated by the data in Table 4.3-2(b) which were calculated for c = 10.0, the other constants being the same as for Table 4.3-2 (a). The arm-interarm contrasts in N_{cl} and Q_c shown in Table 4.3-2(b) are respectively 4 - 15 times and 3 - 8 times those shown in Table 4.3-2(a). Conversely the values of f_w and f_c at any point are virtually the same in both tables. In the arm region at $\tilde{\omega}$ = 5 kpc the data in these two tables are the same to within ~ 30 per cent and excluding N_{cl} and Q_c brings this difference down to $\lesssim$ 10 per cent. For any individual parameter the difference between the values in the two tables is substantially greater at any other point.

4.3.3 Effect of Changing the Galactic Supernova Rate S_{gal}

Throughout the volume of parameter space examined here if the value of S_{gal} is increased, $\langle \tilde{P} \rangle$, N_{cl}, n_c and n_w

all increase at any point, while R_c, the cloud radii and cloud filling factors decrease. To a fairly good approximation, the ratio of the values of any of these quantities obtained from models differing only in the value of S_{gal}, is both independent of position and of the values of the other constants. The values of Q_c, λ_c and λ_w are almost independent of S_{gal}. At points for which the local value of S exceeds $1 \times 10^{-13} pc^{-3} yr^{-1}$ the value of Q_c increases slightly with S_{gal} while below this the converse is true. Similarly the intercloud distances are slowly increasing functions of S_{gal} wherever $S \gtrsim 0.5 \times 10^{-13} pc^{-3} yr^{-1}$ and are slowly decreasing functions elsewhere. As a specific example Table $4.3\text{-}2^{(c)}$ gives the values obtained for the same values for the constants as in Table $4.3\text{-}2^{(a)}$ except that $S_{gal} = 0.05 yr^{-1}$. Dividing the data in Table $4.3\text{-}2^{(c)}$ by those in Table $4.3\text{-}2^{(a)}$ I obtain the ratios ~ 2 for N_{cl} ~ 0.65 for $\langle a_c \rangle$ and $\langle a_w \rangle$ ~ 0.53 for f_c and f_w, ~ 1.85 for $\langle \tilde{P} \rangle$ n_c and n_w and ~ 0.85 for R_c. These ratios are broadly typical of those obtained for any other pair of models having $S_{gal} = 0.02\ yr^{-1}$ and $S_{gal} = 0.05 yr^{-1}$. In this case the corresponding ratio of the values of Q_c is ~ 1.3 while those of the intercloud distances are both ~ 1.2.

4.3.4 Effect of Changing the Molecular Hydrogen Densities

Essentially the values of $\bar{n}(H_2)$ obtained by SSS only differ from those of GB in being everywhere ~ 2.5 times larger. Thus since in either case $\bar{n}(H^0) \ll \bar{n}(H_2)$, adopting the SSS

values rather than those of GB affects the normalization constant, S_o, of equation 4.2-4 in essentially the same way as decreasing S_{gal}. The consequences of this for the values calculated at any position is of course complicated by the accompanying increase in the local value of $\bar{n}$. I find that the overall effect of this change is to increase the number of clouds, their densities and their filling factors while decreasing Q_c, R_c, the cloud radii and the intercloud distances. Again the ratio of the values obtained from two models differing only in the choice of the density distribution, are approximately independent of the values of the other constants and only change slowly with position. The data in Table $4.3\text{-}2^{(d)}$ were obtained with the same constants as for Table $4.3\text{-}2^{(a)}$ but using the SSS density distribution. The ratios here are ~ 0.1 for Q_c, ~ 10 for N_{cl}, ~ 0.6 for R_c, $\langle a_c \rangle$ and $\langle a_w \rangle$, ~ 0.34 for λ_w and λ_c and ~ 1.1 for n_c and n_w.

The density values derived by GLV are ~ 0.64 and ~ 0.2 times those of GB at 10 and 5 kpc respectively. The consequence of these considerably lower densities is that the cloud evaporation rate per unit volume is commonly insufficient for cooling to occur before the SNRs either overlap or burst out of the disc even in the arm region.

4.3.5 Effect of Changing the Star Formation Exponent, m

For the case m = 2 the results are in general qualitatively

similar to those for m = 1 except that the magnitudes of the arm-interarm and radial contrasts in the various quantities are substantially greater. However, the behaviour of the filling factors is exceptional in this respect. I find quite generally that if m $\simeq$ 1.46 the value of f_w is independent of $\tilde{\omega}$ and θ, while for f_c the same is true at m $\simeq$ 1.73. As has been seen for the case m = 1, below these values the filling factors are higher in the arm region than in the interarm region and have a maximum value in the molecular ring. The converse is true for the case m = 2. Table 4.3-2$^{(e)}$ which gives the results for the same model as Table 4.3-2$^{(a)}$ but with m = 2 illustrates these trends and broadly typifies the results obtained for other cases. For m = $\frac{1}{2}$ the basic trends are consistent with those discussed above. However, generally in this case I find that the value of f_w predicted approaches or exceeds unity everywhere. When f_w is comparable to unity the SNR evolution will be primarily controlled by the cloud component rather than the HIM and the MC scheme is inappropriate. The situation then becomes more reminiscent of the original Cox & Smith (1974) model.

4.3.6 Increasing the O Star Contribution to ε_{uv}

The calculations for the standard case assume that O stars make no contribution to the ionisation of the general ISM because they rapidly surround themselves by an ionisation bounded HII region. However because of the large increase in the value of ε_{uv} which would occur if even only a small fraction of their flux were to escape I have performed a series of calculations assuming various different values for the O star contribution in the spiral arms. As can readily be understood from the discussion of the role of ε_{uv} in §3.6.1 the main consequence of increasing its value is to somewhat increase the size, fractional ionisation and filling factor of the warm envelopes. Consequently the lower mass limit of the cloud spectrum is raised and the clouds are thus considerably fewer leading to a smaller value of the evaporation parameter. This in turn implies a somewhat larger value of Q_c and R_c and a slightly higher interstellar pressure.

As a concrete example suppose that all of the uv flux from O stars that are outside prominent HII regions ($\sim$50% of all O stars) is available to the general ISM. The value of ε_{uv} in the arms is then increased by about a factor of 10. When all the other constants are kept the same as for the standard case of Table 4.3-1(a) Q_c increases by about a factor $\sim$6 and N_{cl} decreases by about a factor $\sim$10 in the arm region throughout the galaxy. The corres-

ponding changes in the other parameters are much smaller the cloud radii and mean separation and the warm component filling factor all increase by a factor 1.5 to 2 while the average pressure and the cloud densities increase by a factor $\lesssim 1.5$ and the cold cloud filling factor decreases by about the same amount. Assuming a rather less extreme 'leak' of C star flux produces a proportionately smaller change in the prediction of the model.

4.3.7 The Non Evaporative Model

As discussed in § 3.3 the supernova energy input can only be consumed by cloud crushing when $S^{\frac{2}{3}}/\bar{n} \lesssim 3.6 \times 10^{-9}$ while the confinement of the warm clouds requires $S^{\frac{2}{3}}/\bar{n} \gtrsim 1.4 \times 10^{-9}$ Wherever these conditions are satisfied for a particular galactic model I find, however, that the behaviour of the derived parameters with $\tilde{\omega}$ and Θ is qualitatively similar to those obtained in the MO model. Quantitatively the 'Cox' calculations lead to pressures typically $\sim \frac{1}{2}$ those obtained from the MO model for the corresponding case. Consequently, N_{cl}, the cloud densities and intercloud distances are smaller while the cloud radii and filling factors are rather larger in the Cox case. Table 4.3-1(f) lists the data for the GB density distribution with $c_* = 5.0$, $m = 1.0$ and $S_{gal} = 0.02 yr^{-1}$ which can be compared directly with the data of Table 4.3-1(a). R_{max} is the SNR radius when $y = y_{max}$. The behaviour of f_w is noteworthy in that it is largest where $\bar{n}$ and S are smallest which differs from the behaviour of f_c. The trends exhibited

in this case are typical of those for other models using the GB or SSS density laws and with m = 1 (bearing in mind the limits discussed above). For models having m = 2 one or both of the above limits are invariably violated at some point in the disc while as in the MO case models having m = $\frac{1}{2}$ generally predict $f_w > 1$ throughout the disc. With the GLV density law the density is too small to permit the complete dissipation of the explosion energy by cloud crushing for any reasonable value of S_{gal}.

4.4 Discussion

4.4.1 The Mach Number of the Spiral Shock

As outlined in § 4.1.2 the central question and that which initially motivated this study, concerns whether or not the ISM possesses properties consistant with the existence of a density wave shock. As discussed there the potential perturbation due to the density wave in the old stellar population can only induce transonic flow in the ISM if the effective acoustic speed $\bar{c}$ is comparable with the component of the circular velocity perpendicular to the spiral pattern $W_{\perp_o}$. Furthermore, although a spiral shock will form whenever the flow contains a sonic point, a narrow zone of strong compression can only be obtained when the unperturbed flow is supersonic (Shu et al 1973; Roberts et al 1975). Thus the criterion for the existance of a strong density wave shock is $W_{\perp_o} > \bar{c}$.

Schmidt-Kaler and Weigandt (1980) have discussed the value of $\bar{c}$ appropriate to a multicomponent medium in the limit of long wavelengths. Writing their result in a more convenient form I obtain,

$$\bar{c} = \frac{c_w c_h}{\left[(1 - f_w)^2 c_w^2 + f_w^2 c_h^2 + f_w(1-f_w)(c_w^2+c_h^2)\right]^{\frac{1}{2}}} \qquad 4.4\text{-}1$$

where c_h is the sound speed in the hot component $\sim$120 kms^{-1} and c_w is that in the warm component which lies between 9.2 and 13.2 kms^{-1} depending on the fractional ionisation.

According to this the effective acoustic speed drops extremely steeply with increasing f_w for $f_w \lesssim 0.2$, beyond which it slowly and asymptotically approaches c_w. Even for quite small values of f_w the warm envelopes are remarkably effective in retarding shocks propagating through the medium.

In Fig. 4.4-1 I show the value of $\bar{c}$ calculated from equation 4.4-1 for the 'interarm' region as a function of $\tilde{\omega}$ in a number of representative cases. This can be compared with the expected run of $W_{\perp_o}$ for the galaxy (Burton 1976; following Roberts, Roberts & Shu 1975). For the MO models if m = 1 or 2 only those employing the SSS density distribution satisfy the criterion $W_{\perp_o} > \bar{c}$ at any point and then only if $S_{gal} \lesssim 0.02 yr^{-1}$. For m = 1 this only occurs in a rather limited region near $\tilde{\omega}$ = 5 kpc; however, for m = 2 the form of the variation of f_w with $\bar{n}$ and S permits the condition to be satisfied over a much larger range in $\tilde{\omega}$ for a given value of S_{gal}. Similarly, for the Cox models the requirement that all the explosion energy be dissipated, necessitates a sufficiently large value of f_w for the existence of a shock, but can only be satisfied when S_{gal} is small and $\bar{n}$ large. As already noted the models with $m = \frac{1}{2}$ predict large values of f_w everywhere and consequently will generally satisfy this criterion.

The point is often made (e.g. Scott et al 1977; Reinhardt & Schmidt-Kaler 1979; Blitz & Shu 1980) that supernovae of type I which predominate in the interarm region may yield a smaller energy per explosion than supernovae of type II.

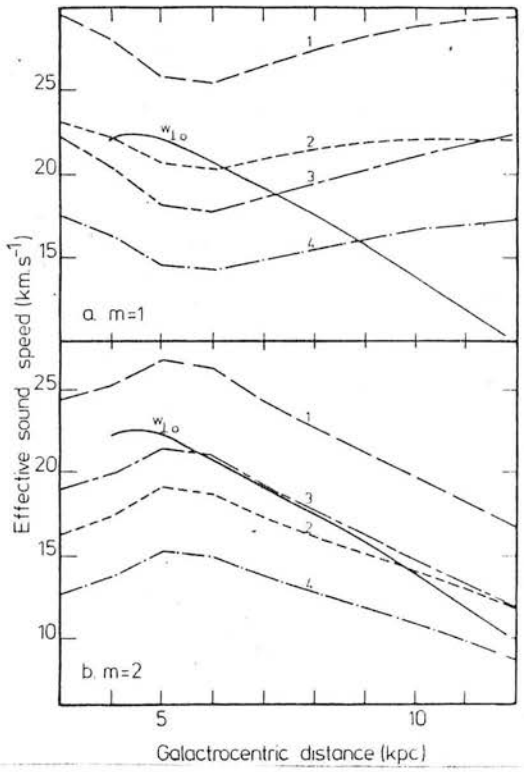

Figure 4.4-1 The effective sound speed $\bar{c}$ (kms^{-1}) of the interarm ISM as a function of galactocentric distance. For both panels a compression factor, c of 5.0 and galactic supernova rate, S_{gal} of 0.02yr^{-1} was employed. For (a) the exponent m of star formation was 1, while for (b) it was 2. The numbered curves were calculated for (1) GB density law $E_o = 5 \times 10^{50}$ erg, (2) SSS density law $E_o = 5 \times 10^{50}$ erg, (3) GB density law $E_o = 2.5 \times 10^{50}$ erg, and (4) SSS density law $E_o = 2.5 \times 10^{50}$ erg. The solid line shows the streaming velocity perpendicular to the spiral arm $W_{\perp o}$ (kms^{-1}) after Burton (1976).

To examine the consequences of this I have performed calculations using a reduced explosion energy for all the supernovae in the interarm region. I find that as would be expected this reduces $\langle \tilde{P} \rangle$ and hence leads to a modest increase in f_w (typically $\sim$70 per cent if E_o is halved to 2.5×10^{50}erg). Nevertheless, contrary to the suggestion of these authors the hot phase continues to be an important constituent of the interarm ISM. The increase in f_w does, however, lead to a decrease in $\bar{c}$ as indicated in Fig 4.11 and a rather less restricted range of models are then able to satisfy the constraint on $W_1/\bar{c}$. In particular it becomes possible for models employing the GB density distribution with m = 1 and $S_{gal} \lesssim 0.02$ to satisfy this criterion in the molecular ring.

Thus it seems that the parameters of the SDC-ISM in the interarm region can be made consistent with the existance of a strong density wave shock, provided only that the supernova rate is near the low end and the gas density near the high end of the ranges suggested for them from observations, judicious adjustment of some of the parameters of the SDC-ISM model (e.g. reducing k_1) could probably be made which would further relax the restrictions slightly. However, the sound speed of the composite of warm envelopes and hot matrix gas would certainly be too high to support the density wave shock if the interarm gas density were <u>much lower</u> or the interarm supernovae rate <u>much higher</u>

than the limits set here.

Even if the intercloud gas is incapable of supporting density wave induced shocks it remains possible that the 'cloud fluid' may be able to do so as has been proposed by Cowie (1980). The details of such a mechanism, however, remain to be worked out. In any case it should be borne in mind that observation both of our own and external galaxies do indicate the existence of a density enhancement associated with spiral arms (e.g. Visser 1980; Cohen et al 1980) so the galactic model may not differ too much from the truth whatever mechanism is ultimately found to be responsible.

4.4.2 Molecular Clouds in the Model

Another interesting question relates to the status of molecular clouds within the model. In modelling the cloud properties I have not included the presence of molecular cores although in calculating $\bar{n}$ I have included the molecular component. As a rough empirical criterion a cloud possesses sufficient self shielding to contain a significant H_2 content when its column density exceeds $\sim 6 \times 10^{20} cm^{-2}$ (Savage et al 1977) i.e. when its core radius exceeds $\sim 194/n_c$ pc. Consequently the numerous small clouds which primarily control the properties of the model never possess molecular cores, so neglecting their presence should not greatly affect the results obtained here. Overall for the

steep cloud spectrum assumed for the models described in this chapter ~ 40% of the ISM mass is contained in clouds with sufficient self shielding to possess molecular cores. That this falls short of the molecular fraction actually observed and tacitly assumed is not however, surprising.

The adopted cloud spectrum was assumed to terminate at the limiting mass given by Mouschovias & Spitzer (1976), corresponding to a radius typically ~10pc in the spiral arms which as has often been noted falls considerably short of the observed length scale of giant molecular cloud complexes (SSS; Stark & Blitz, 1978). On the other hand, the very numerous small clouds found in the arms lead to a typical cloud separation very much smaller than the average separation of the early type stars ~50pc (deduced from Torres-Dembert et al 1974) responsible for much of the ionisation. Thus mutual cloud-cloud shielding might become an important effect. Tentatively, then one might envisage molecular cloud complexes as being agglomerates of many mutually shielding clouds spaced more closely than the average. Such aggregates might form initially through the operation of Elmegreen's (1979, 1981a,b) gravitational mechanism which should operate irrespective of the small scale cloudy structure of the interstellar gas which has to be collected. The enhanced rate of cloud-cloud collisions in the aggregates might then cause the few pre-existing large clouds to quickly grow beyond the gravitational stability limit and collapse to form stars.

Their stellar winds and eventual explosion as supernovae might then lead to further clumping in the ensemble of clouds. They might also provide an energy source for the random turbulent velocities of the population of small cold clouds necessary to prevent the wholesale coalescence and gravitational collapse of the agglomerate (e.g. Norman and Silk 1980; Fleck 1981). Certainly the observation that molecular clouds are inhomogeneous (Silk 1980; Larson 1982) provides some encouragement for such a point of view.

4.4.3 Observational Constraints

It is clearly of considerable interest to examine the observable consequences of the model and to consider what if any constraints can then be imposed upon it. MO compared many predictions of their model with the observed properties of the ISM in the solar neighbourhood, and found reasonable agreement in most respects bearing in mind the highly approximate nature of the model. To the extent that the variants of the MO model presented here, produce results largely concordant with those that they obtained, under similar conditions, their discussion is also applicable to the present case. The considerable dependence of the values predicted for the observable quantities, on the values assumed for the input parameters (§ 3.6) should, however, caution against too literal an interpretation of the model predictions.

Here I will concentrate on predictions relating to the larger scale properties of spiral galaxies. In particular the question of whether the hot component of the ISM is truly ubiquitous or merely a local anomaly can clearly be most easily resolved by studying nearby galaxies.

Ultimately the most unequivocal evidence for a pervasive hot phase in any external galaxy would come from observations of its soft X-ray emission. Following MO the effective soft X-ray opacity of a multiphase medium is approximately given by,

$$\kappa_x \simeq (\lambda_c + 1/n_c\sigma)^{-1} + (\lambda_w + 1/n_w\sigma)^{-1},$$

where σ is the effective cross-section per hydrogen atom (Brown & Gould 1970; the more detailed analysis of Ride & Walker 1977, requires a different cross-section for the cold and warm components however I will neglect this in view of the approximate nature of the calculation). For the MO model I find that the volume average emissivity of the HIM is proportional to S and almost independent of Q_c. It is then straightforward to calculate the relative intensity emitted at a particular energy at each point in the models. In general the S dependence of the emissivity dominates over the increased opacity resulting from larger $\bar{n}$ so that regions of high $\bar{n}$ and S would be expected to be 'bright' at soft X-ray energies. For instance in the Wisconsin groups B band (0.17 keV, Burstein et al 1977) I find from the results of Table 4.3-1 that the ratios of

the arm to interarm intensities are ~1.25 and 1.42 at 5 and 10 kpc respectively. At the higher energy of the M band (0.4 - 0.85 keV) the corresponding ratios are ~2.23 and 1.85. Because most of the soft X-ray flux is emitted by the younger, smaller remnants the actual distribution of flux will inevitably be very irregular. Furthermore, the interpretation of any observations will be complicated by the presence of emission from the galaxies halo as well as 'contamination' by the emission from our own Galaxy.

Another potential tracer of the hot gas and one for which observations already exist is its non-thermal radio emission. Unfortunately the details of the emission mechanism in SNRs remain unclear and in particular depend critically on the geometry of the magnetic field which is as yet unknown (Caswell & Lerche 1979b; Blandford & Cowie 1982). It is therefore not possible to make any useful predictions of its distribution on the basis of the model.

The statistical properties of resolved SNRs may represent a useful probe of the conditions in their vicinity (Higdon & Lingenfelter 1980. Note in particular that the model predicts an increase in the typical remnant size scale with decreasing $\bar{n}$ and S which shows up in the results of Figure 3.3-2 as an increase in remnant size with increasing galactic radius. Such a trend has already been noted for our galaxy both for radio remnants (Jones 1975) and for the giant H^{o} shells reported by Heiles (1979), (Bruhweiler

et al 1980). However, other interpretations of this trend are possible and selection effects are undoubtedly important.

It might seem that observations of the properties of the cold and warm gas in external galaxies might provide a test of the model and hence by inference provide information on the hot phase. Photographic surface photometry can provide information on the distribution of dust and hence gas in nearby galaxies with a linear resolution of tens of parsecs while 21-cm aperture synthesis measurements yield comparable data for H^o alone at rather lower resolution. Unfortunately such observations ultimately can only provide a measurement of the local value of $\bar{n}$ at any point and hence while certainly useful for testing the galactic model they provide only limited information on the properties of the cloud population. In principle the statistical fluctuations in the observed column density provide a measure of N_{cl}; however, because of the large volume elements involved I do not expect the effect to be measurable. A statistical study of individual large (resolved) clouds (Elmegreen 1980) can help to elucidate some features of the model but the insensitivity of the results to the details of the cloud spectrum probably render such data of limited value in testing the model. Similar arguments can also be made with regard to $H\alpha$ observations of the warm envelopes, in addition to which the emission measure predicted from

the warm envelopes is small compared to that from a single normal HII region rendering interpretation difficult.

4.5 Summary

In this chapter I have described the first attempt to elucidate the way in which the global characteristics of a spiral galaxy like our own interact with the small scale properties of a supernova dominated interstellar medium.

The assumptions made in this investigation were: (1) that SNR interact with the inhomogeneous ISM in the manner originally proposed by MO and further developed in Chapter 3; (2) that the pattern of mean total density $\bar{n}$ is similar to that predicted by TASS models; (3) that the local star formation rate and supernova rate are proportional to one another and to some power m of $\bar{n}$.

I conclude that:

(1) The results do not depend strongly on whether evaporation enhanced radiation or cloud crushing is supposed to be the dominant sink of the energy input by supernovae; nor are they grossly affected by changes of detail in the model. Consequently, I confidently expect that similar results would hold for any model of the SDC-ISM.

(2) The theoretical case for a ubiquitous hot phase of the ISM remains strong. Contrary to previous expectation if the hot phase is important in spiral arms it

remains so in the interarm region. This continues to be the case even when due allowance is made for the lower energy of the type I supernovae which predominate in the interarm region.

(3) The results of the model impose strong constraints on the conditions which must prevail in spiral galaxies if the interstellar gas is to support a strong density wave shock. For our own Galaxy if $m \gtrsim 1$ then I require that both the lower estimates of the galactic supernova rate (i.e. $S_{gal} \lesssim 0.02$ and the higher estimates of $\bar{n}$ (i.e. that of SSS) are both correct. **If either condition is not met then the** density wave shock can only be supported if some other mechanism such as that suggested by Cowie (1980) acts to produce a strong density enhancement in the arms. For $m \lesssim \frac{1}{2}$ the model fails because the warm component becomes predominant everywhere. Such a situation would favour density waves. However, in this instance the star formation rate has such a low arm-interarm contrast that blue spiral arms would be imperceptible, and type II supernovae would occur frequently between the arms. I believe that this constitutes a strong observational argument implying that as used here $m > \frac{1}{2}$. This is basically a statement about the shortcomings of the parameterisation of the star formation rate adopted here, rather than about the actual value of m which occurs in Schmidt's law. Since observations suggest the existance of a spiral density wave in the galaxy I conclude that the requisite requirements are

in fact met.

(4) Observationally, it seems unlikely that studies of external galaxies can supply information on the vital question of the ubiquity of the hot phase in the near future.

(5) The high pressure predicted within spiral arms must make the support of giant molecular clouds against self-gravity even more difficult to understand. Conversely, the model predicts a great many small clouds in the spiral arms. Consequently I tentatively propose a clumpy cloud model similar to that of Norman and Silk (1980). However, instead of T Tauri winds I propose that hot phase material separates, pressurizes and possibly drives the motions of the densely packed small clouds.

(6) The mechanisms discussed here may be subject to feedback, in the sense that for instance, supernova overproduction will drive much of the material into the hot phase and eventually reduce the star formation rate. The fact that the results presented (a) describe the state of our own galaxy (and possibly others) fairly well and (b) indicate a narrow range of viable conditions in which the model can sustain itself, may be taken as tentative evidence of such feedback.

5 THE STATE OF CLOUDS IN AN SDC-ISM

5.1 Introduction

As discussed extensively in the foregoing, interactions between SNR and interstellar clouds play a central role in our present conception of the ISM. On the one hand the SNR generate the pervasive, hot but tenuous medium responsible for the pressure confinement of the clouds. In addition SNR are, in one way or another, major sources of both thermal and kinetic energy for the clouds. On the other hand the clouds dissipate SNR energy both in their direct role as energy sinks and by providing new material for the hot phase (evaporation, mechanical ablation) thereby increasing the rate of direct radiative losses from the hot matrix gas. In the picture of the SDC-ISM presented in §3 it is precisely this 'symbiotic' relationship between clouds and SNR which is invoked as the primary determiner of the equilibrium properties of the ISM.

The nature of the mechanisms involved guarantee significant departures from thermal and pressure equilibrium at the level of individual clouds. For conditions in the solar neighbourhood the timescales governing the essential physical processes (SNR shock repetition time, cloud dynamical response time, radiative cooling time, ionisation and recombination times, evaporation timescale etc.) are all similar and close to $\sim 10^5$-10^6 years (see Table 3.2-1). The state of any given cloud at any instant will then be a complex function of its

past history as well as the nature of its present surroundings.

In view of this it seems necessary to examine the problem of the interaction of a cloud with an SNR blast wave in rather more detail than in §3; the very simple (although in the final analysis surprisingly good) treatment given there begs several important questions, such as how is the evaporation rate affected by the severe deformation and perhaps partial disruption of the cloud, or rather it lumps all of them into a single highly uncertain parameter ϕ.

In this chapter I attempt to follow the response of individual clouds to their changing environment. In particular I will be concerned with the determination of some sort of average or 'typical' cloud state. This is important both for improving estimates of the parameters of the global model such as ϕ and for making eventual comparison with observation. In the next section I assemble a highly simplified model for the interaction of an isolated cloud with a single SNR blast wave, generalised from published numerical computations. In §5.3 I ennumerate a number of the complicating factors associated with the 'real world' of an SDC-ISM and establish the domain of validity of this simple model. In § 5.4 I discuss a number of consequences of the model for theories of the ISM in general and the work of the earlier chapters in particular. § 5.5 summarises the principle results.

While the cloud model presented was constructed with application to the SDC-ISM specifically in mind attention is focussed throughout on scale invariant properties of the problem. It is thus applicable under a much wider range of circumstances. Obviously it has direct relevance to the problem of shock induced star formation irrespective of whether the shocks are driven by SNR, stellar winds or a global density wave. On a more esoteric level it may also be relevant to process in the line emitting regions of active galactic nuclei or perhaps even the formation of galaxies in a 'violent intergalactic medium.'

5.2 Basic Cloud Model

A number of authors have addressed the problem of the dynamical response of an interstellar cloud to being overrun by a shock wave (e.g. Bychcov & Pikel'ner 1975; McKee & Cowie 1975; Sgro 1975; Dyson & Gulliford 1975). At the time this work was performed (Heathcote & Brand 1983) the most 'realistic' calculations available were those of Woodward (1976, 1979, hereinafter W76 and W79) who employed a 2-D hydrodynamic code to follow the cloud evolution in considerable detail. These computations were carried out for essentially only one set of model parameters chosen for their relevance to the problem of star formation in massive clouds, imploded by density wave shocks. The formidable scale of the computing problem involved precluded any attempt at a parameter study. Subsequently, a few further computations of similar quality have become available (Nittmann 1981; Nittmann et al 1982 - NFG; Krebs & Hildebrandt 1983); for the most part these confirm the main features of Woodward's study, but some new features are revealed, while others are further illuminated. Consequently these results will be mentioned as appropriate in the development of the model; our major conclusions (Heathcote & Brand 1983) are, however, in no way modified.

For the present purposes it is necessary to extend the applicability of these calculations to encompass the large volume of parameter space appropriate to the interaction of clouds

with SNR blast waves. To accomplish this I employ the numerical results to identify the important physical processes which can be expected to occur and I then attempt to model these with simple highly approximate analytic calculations. In this way it is possible to assemble a crude model of the interaction dynamics capable of reproducing the gross features of the detailed computations which then forms the basis for a plausible extrapolation to other conditions. A few points about this procedure are worth noting at the outset.

(i) I will not hesitate to sacrifice numerical accuracy in favour of analytical simplicity. The uncertainties in the initial conditions inherent in our current understanding of the three phase ISM are sufficient that a factor of two or so is unlikely to prove of vital importance.

(ii) Although throughout I will be guided by physical principles, the justification for the selection of the important processes and my approximate treatment of them rests heavily on the numerical models.

(iii) I am fully aware that processes not apparent in the computed models may become important in other regions of parameter space. Some of these will be discussed in §5.3, and their consequences in §5.4.

I begin the discussion of the approximate model with a brief summary of the important results of the numerical computations.

5.2.1 Numerical Results

In W76 the collision of a plane parallel shock of mach number $M_b \sim 2.6$ with an initial spherical cloud having a density ~ 80 times that of the pre-shock intercloud medium (ICM) was studied. The cloud was initially at rest in, and in pressure equilibrium with, the ICM. The equation of state of the ICM was a $\gamma = 5/3$ adiabat while that of the cloud was effectively isothermal.* In W79 the parameters of the cloud were unchanged, but an isothermal equation of state was used for the ICM. This had the important dynamical effect that the post shock flow was supersonic with respect to the cloud and so a bow shock formed upstream of the cloud. The evolution was also followed to a considerably later stage in this case. The main features of the interaction are, however, similar in both studies. These are (see also figures 5.2-1 and 5.2-2):

---

*More precisely the equation of state was chosen to represent that expected for an interstellar cloud in the two phase model of Field et al (1969). It consisted of an isobaric segment at $\tilde{P} = 210$ Kcm^{-3} for densities $\lesssim 1.5$ cm^{-3} (temperatures $\gtrsim 140$K) joined smoothly to an isothermal segment with T = 26K for densities $\gtrsim 20$cm^{-3} ($\tilde{P} \gtrsim 520$ Kcm^{-3}). Consequently in some respects the cloud behaves like an isothermal cloud with an initial density ~ 8cm^{-3} (420 times that of the ICM) with a radius ~ 0.57 times the actual radius.

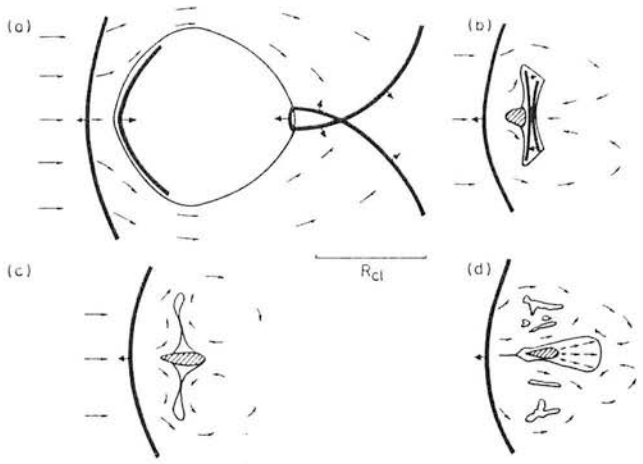

Figure 5.2-1 A schematic representation of the clouds structure at various stages during its collapse and subsequent re-expansion. Heavy lines represent shocks; broad tipped arrows attached to these indicate the downstream side of the shock. The cross hatched areas indicate the zone of enhanced density associated with the axial clump. Narrow tipped arrows depict the flow of the gas around the cloud. (a) $\tilde{t} \sim 3A/M_b$ ($t \sim 0.01$Myr for the typical cloud of Table 5.2-1). The various segments of the external shock have just met at the back of the cloud. (b) $\tilde{t} \sim 0.6/M_b$ ($t \sim 0.5$ Myr). The shocks driven into the front and back of the cloud are about to collide. (c) $\tilde{t} \sim 0.6/M_b$ the re-expansion of the cloud in the downstream direction has commenced. (d) $\bar{t} \sim 0.6/M_b + 0.5$ ($t \sim 1.6$Myr) a typical stage during the re-expansion.

(1) As the external shock (S_o) overruns the cloud its ram pressure drives a strong shock (S_1) into the front face of the cloud (Sgro 1975, Silk & Solinger 1975). Subsequently, when steady flow around the cloud is established, this shock is driven by the high pressure in the vicinity of the front stagnation point.

(2) Having swept over the cloud, the various segments of the shock meet almost head-on at the back of the cloud and are reflected leading to a transiently high pressure there. This drives a somewhat weaker shock (S_2) into the back of the cloud. The pressure behind the cloud falls rapidly as the intersection point of the external shock segments moves downstream and the angle of incidence increases. However, the flow around the cloud conspires with the sideways flow of the reflected shocks to set up a vortex system the pressure of which, combined with the thermal pressure of the ICM, continues to drive S_2. (Figure 5.2-1a).

(3) The shock driven into the sides of the cloud (S_3) is quite weak and the lateral compression of the cloud is only moderate. Together with points (1) and (2) this implies that the cloud collapse is essentially one dimensional and for much of the time it can, in fact, be treated as approximately plane parallel.

(4) In the subsonic case, the sides of the cloud are Kelvin-Helmholtz (KH) unstable. The instability grows rapidly and is later amplified by the Rayleigh-Taylor (RT) instability. When the flow over the cloud is strongly

supersonic the KH instability is supressed (Gerwin 1968).

(5) The convergence of the shock S_1 causes it to accelerate (Zel'dovich & Raizer 1968) and leads to the front face of the cloud being RT unstable. The resulting flow of cloud gas towards the symmetry axis leads to the formation of a dense clump of material there. In the subsonic case this collection process is limited to the zone between the KH tongues closest to the symmetry axis (Figure 5.2-1b).

(6) Eventually S_1 and S_2 collide. The shock reflected towards the back of the cloud is much stronger than that reflected towards the front. The cloud at this stage is strongly flattened so this shock reaches the back of the cloud very soon after the interaction (Figure 5.2-1c).

(7a) At the back of the cloud a weak shock is propagated into the ICM and a strong rarefaction wave is reflected back into the cloud. This 'engulfs' most of the material near the symmetry axis including the dense clump and a fan of quite dense material expands rapidly in the downstream direction. Any expansion upstream is prevented by the pressure at the forward stagnation point.

(8a) The remaining cloud material is confined to an extremely thin sheet. This also begins to re-expand but is quite rapidly fragmented by KH instability before this process has progressed very far. (Figure 5.2-1d).

As noted above the cloud equation of state employed by Woodward was essentially isothermal. At the time of our original work the only calculation available for the case of an adiabatic cloud was that of Thorogood (1979) which was performed for a situation identical to that considered in W76, except that the equation of state of the cloud, as well as the ICM was a simple $\gamma = 5/3$ adiabat. The main dynamical features discussed above in (1) - (3) and (6) are reproduced in this calculation, except that the cloud is substantially less flattened. This latter difference is a direct consequence of the different equation of state for the cloud as is shown in the plane parallel calculations shown below. Unfortunately, Thorogood's calculation was terminated just before the start of the re-expansion phase and more seriously the low resolution and large numerical viscosity in his scheme completely supressed the surface instabilities discussed in (4) and (5). Because of the important role of the dense axial clump in the re-expansion phase we were only able to reach tentative conclusions about the late time evolution in this case.

The subsequent calculation of NFG for an adiabatic cloud of initial density 25 times that of the pre-shock ICM struck by a shock of the same strength ($M_b \sim 2.6$) in part fills this gap. Surface instabilities <u>do not</u> occur in their main computation either. However, in a subsidiary calculation they demonstrate the amplification of pre-existing large

amplitude irregularities and argue that this constitutes sufficient proof that the cloud would have been unstable. In their main computation the clouds early evolution again follows the pattern described above (apart from the absence of surface instabilities). However, in their case the final stages of the clouds evolution were:

(7b) the ram pressure of the vortex system at the back of the cloud is sufficient to prevent much re-expansion at the back of the cloud, and the fan shaped tail so characteristic of Woodward's computation does not develop.

(8b) Instead the cloud re-expands laterally the vortex flow helping to "whirl matter off" the back of the cloud which consequently takes up a 'saucer-shaped' appearance.

With hindsight this result is understandable as a consequence of the much weaker compression suffered by an adiabatic cloud together with the smaller initial density contrast. These considerations enable a distinction to be drawn between those clouds which will develop tails and those which do not (§ 5.2.5). Had a dense axial clump been allowed to form in this case, the backward expansion of the cloud would have been somewhat greater, but not sufficiently for the formation of the tail. The material whirlled off the cloud would probably be fragmented by the KH instability.

The phases outlined in (1) - (8) above seem to be

inevitable parts of a shocked cloud's evolution phases (4) and (5) cause the greatest difficulty, since they represent highly non-linear processes, namely the interactions between surface instabilities and the complex flow regime outside the cloud.

In the following subsections I will approximate each of the phases by an analytical solution, or by a fit to data derived by reasonable extrapolation from the numerical computations.

5.2.2 The Collapse Phase

To the extent that self gravity may be neglected, and provided cooling and heating of the gas occur on timescales either very long or very short compared to the dynamical timescale, then it is possible to scale results obtained for a cloud of given size to yield those appropriate to a cloud of different size, by simply multiplying all lengths and times by a common factor. It is thus convenient to introduce the dimensionless lengths times and velocities defined by

$$\tilde{R} = R/R_{cl} \quad \tilde{t} = C_{cl}t/R_{cl} \quad \tilde{u} = u/C_{cl} \qquad 5.2\text{-}1$$

Here R_{cl} and C_{cl} are respectively the initial scale length and sound speed of the undisturbed cloud. The problem then reduces to one containing essentially only two parameters, namely the Mach number, M_b of the incident shock and the ratio A of C_{cl} to the sound speed of the undisturbed ICM, C_{ic}. The polytropic indices describing the equation of state of the cloud and the ICM, γ_{cl} and γ_{ic} respectively, must also be specified. In the case of infinite cooling times I take $\gamma = 5/3$ while in the opposite case of infinitessimal cooling times I take $\gamma = 1$.

The approximation made is that the front cloud shock S_1 and the back cloud shock S_2 are plane parallel and are driven by the front stagnation point pressure, P_1 and the pressure at the back of the cloud, P_2 (see Figure 5.2-2). I also ignore the influence of the lateral cloud shock, S_3 upon the motion of these shocks. In reality, although as noted above S_1

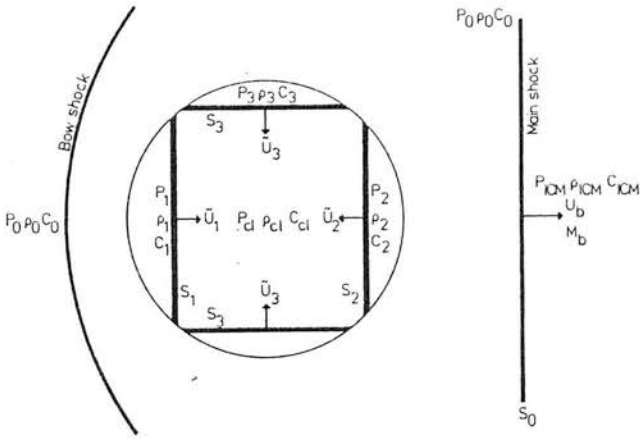

Figure 5.2-2 A schematic representation of the cloud during the collapse phase showing my notation for the several shocks and their velocities and for the pressures, P, densities and sound speeds C in the various zones.

and S_2 are almost plane, their strengths decrease with distance from the symmetry axis (the distinction between S_1, S_3 and S_2 is of course purely artificial) so this approximation is only strictly valid near the symmetry axis. However, comparison with Woodward's model suggests that this approximation is a good one.

The calculation of P_1 is straightforward. Following the impact of the external shock, S_o with the front of the cloud, a strong shock S_1 is transmitted into the cloud and a weak shock S_4 is reflected back into the ICM. Near the symmetry axis, if the curvature of both the cloud boundary and the SNR shock can be neglected, the problem reduces to that of the reflection and transmission of a shock wave, normally incident upon the interface between two fluids, which is treated in several elementary texts on fluid mechanics (e.g. Zel'dovich & Raizer 1968; Bradly 1962: See also Appendix A of Brand 1982 for extensions to isothermal fluids). The jump conditions across S_1 determine completely the conditions in the newly shocked cloud gas through which it has travelled, in terms of its strength; (either pressure jump or Mach number); similarly conditions in the twice shocked gas between S_4 and the cloud boundary are determined by successively applying the jump conditions across the external shock S_o and the reflected shock S_4. Imposing the condition that the pressure and fluid velocity must be continuous across the cloud boundary then leads to transcendental equations relating the strengths of S_1 and S_4 to M_b and A. Solutions to

these equations are depicted in Figure 5.2-3. For various values of M_b and A. a similar analysis for the restricted case of a strong external shock and $\gamma_{ic} = \gamma_{cl} = 5/3$ has been given by Sgro (1975) and Silk & Solinger (1973).

The very high pressure developed at the front of the cloud in this way is only transient. The external shock S_4 propagates upstream with steadily decreasing speed and strength. If the flow behind S_o is supersonic with respect to the (moving) cloud boundary S_4 eventually becomes a standing Bow shock; otherwise it continues to propagate away from the cloud and eventually decays into a weak sound wave. In either case steady flow will be set up around the cloud on a timescale comparable with the cloud crossing time for the external shock $\sim A/M_b$. The duration of this phase is sufficiently short that no serious error is incurred by neglecting it all together; for instance the distance travelled by S_1 and the cloud boundary during this time is also only $O(A/M_b)$.

Once steady flow has been established, the situation is that considered by McKee and Cowie (1975). Straightforward application of Bernoullis'equation (together with the jump conditions across S_4 when the flow behind S_o is supersonic) leads to an expression for the pressure P_1 at the front stagnation point. For $\gamma_{ic} = 5/3$ this is,

$$P_1/P_o = (1 + M^2/3)^{5/2} \qquad M \leq 1$$

$$P_1/P_o = 1.5\, M^2(1 - 1/(5M^2))^{-3/2} \qquad M \geq 1 \qquad \text{5.2-2a}$$

Similarly, for $\gamma_{ic} = 1$.

$$P_1/P_o = \text{EXP}\,(M^2/2) \qquad M \lesssim 1$$

$$P_1/P_o = M^2\ \text{EXP}(1/(2M^2)) \qquad M \gtrsim 1 \qquad \text{5.2-2B}$$

Here, P_o is the pressure behind S_o, while M is the <u>local</u> Mach number of the flow behind S_o relative to the cloud boundary. Note that this result is essentially independent of the clouds shape, provided it can be treated as a bluff body.

If V_o and V_1 denote respectively the gas velocities behind S_o and S_1 in the rest frame of the undisturbed gas and if C_o is the <u>post shock</u> sound speed in the ICM (See Figure 5.2-2) Then (recalling that M_b and $\tilde{U}_1$ are the Mach numbers of S_o and S_1, and that $A = C_{c1}/C_{ic}$) the jump conditions for S_o and S_1 imply,

$$M = \frac{V_o - V_1}{C_o} = \left[\frac{2}{(\gamma_{ic}+1)}\frac{(M_b^2-1)}{M_b} - \frac{2A}{(\gamma_{c1}+1)}\frac{(\tilde{U}_1^2-1)}{\tilde{U}_1}\right]\frac{C_{IC}}{C_o} \qquad \text{5.2-3}$$

and,

$$\frac{C_{ic}}{C_o} = (\gamma_{ic}+1)M_b\left\{\left[2\gamma_{ic}M_b^2 - (\gamma_{ic}-1)\right]\left[(\gamma_{ic}-1)M_b^2 + 2\right]\right\}^{-\frac{1}{2}} \qquad \text{5.2-4}$$

Finally, since the cloud and ICM are supposed initially to be in pressure equilibrium,

$$\tilde{U}_1^2 = \frac{P_1}{P_o}\frac{\gamma_{ic}}{\gamma_{c1}}\frac{(\gamma_{c1}+1)}{(\gamma_{ic}+1)}\left[M_b^2 - \frac{(\gamma_{ic}-1)}{2\gamma_{ic}}\right] - \frac{(\gamma_{c1}-1)}{2\gamma_{c1}} \qquad \text{5.2-5}$$

Again Equations 5.2-2, 5.2-3 and 5.2-4 together reduce to a transcendental equation for $\tilde{U}_1$ as a function of M_b and A. Figure 5.2-4 shows values of $\tilde{U}_1$ obtained from this as a function of M_b for various values of A. McKee and Cowie (1975) obtained an approximate expression for P_1/P_o when $\gamma_{ic} = 5/3$ under the assumption that both S_o and S_1 are strong. From this one obtains,

$$(\tilde{U}_1/M_b) = (\gamma_{c1} + 1)\, A^{-1} \left[1.4((\gamma_{c1} + 1)\gamma_{c1} A^{-2} - 3.63)^{\frac{1}{2}} - 3.9 \right.$$
$$\times \left[(\gamma_{c1} + 1)\gamma_{c1} A^{-2} - 11.69 \right]^{-1} \qquad 5.2\text{-}6a$$

Similarly when $\gamma_{ic} = 1$ I obtain,

$$(\tilde{U}_1/M_b) = \tfrac{1}{2}(\gamma_{c1}+1)A^{-1} \left[(\tfrac{1}{2}(\gamma_{c1}+1)(AM_b)^{-2})^{\frac{1}{2}} - 1 \right]$$
$$\times \left[\tfrac{1}{2}(\gamma_{c1} + 1)\gamma_{c1}(AM_b)^{-2} - 1 \right]^{-1} \qquad 5.2\text{-}6b$$

These relationships are plotted as broken lines for some representative values of A in Figure 5.2-4. As can be seen although derived for the case of strong shocks expression 5.2.5a errs by less than 50% even when $M_b \sim 1$ while 5.2-5b is everywhere accurate to $\sim$10%. When A is very small as it will be in most cases of interest here I will further simplify by taking the limit $A \rightarrow 0$ which leads to,

$$\tilde{U}_1 \quad 1.4\,((\gamma_{c1} + 1)/\gamma_{c1})^{\frac{1}{2}} M_b \qquad \gamma_{ic} = 5/3 \qquad 5.2\text{-}7a$$

$$\tilde{U}_1 \quad 0.71((\gamma_{c1} + 1)/\gamma_{c1})^{\frac{1}{2}} M_b^2 \qquad \gamma_{ic} = 1 \qquad 5.1\text{-}7b$$

In the meantime the external shock S_o propagates past the cloud with barely diminished velocity, until a point is

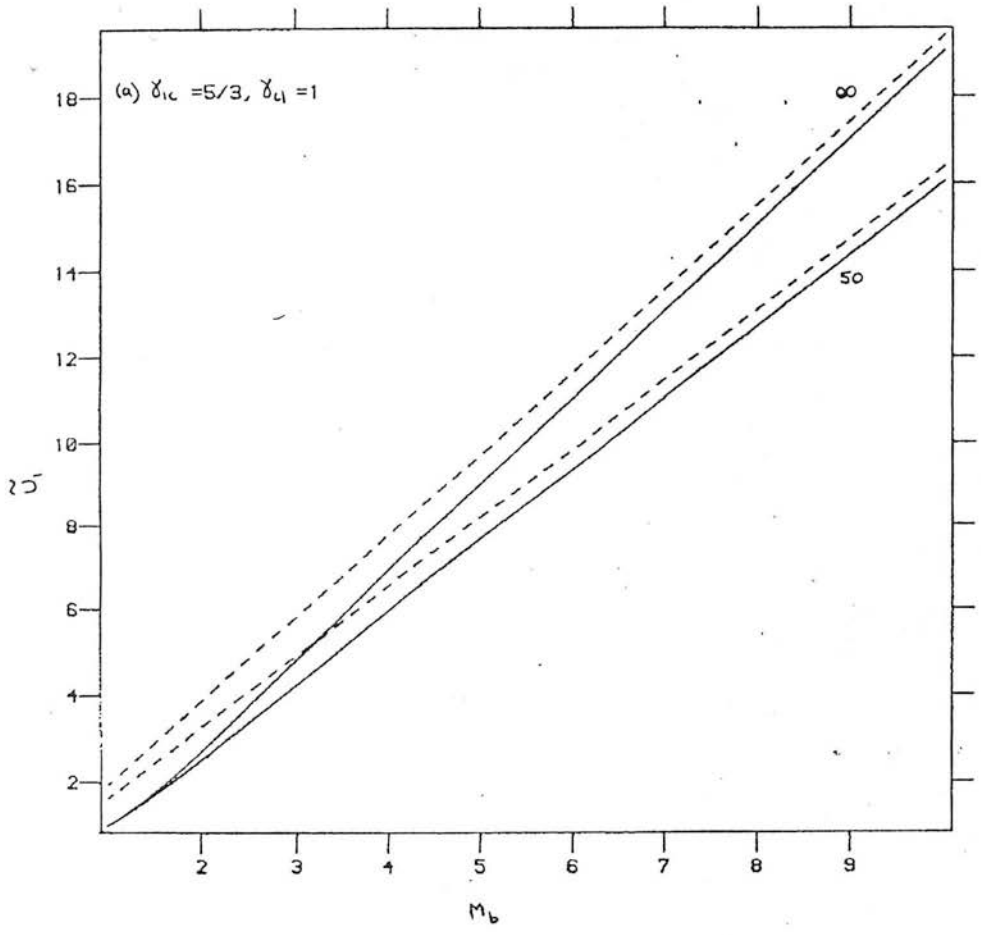

Figure 5.2-4: The Mach number of the main cloud shock $\tilde{U}_1$ as a function of the Mach number of the external shock M_b in the steady flow case. Solid lines show the exact results while the dashed lines show the predictions of the strong shock approximations given in the text. The various curves are labelled by the value of the cloud-intercloud density ratio = $(\gamma_{ic}/\gamma_{cl}A)^{\frac{1}{2}}$. The values of γ_{ic} and γ_{cl} used are (a) $\gamma_{ic} = 5/3$ $\gamma_{cl} = 1$, (b) $\gamma_{ic} = 5/3$, $\gamma_{cl} = 5/3$ (c) $\gamma_{ic} = 1$, $\gamma_{cl} = 1$.

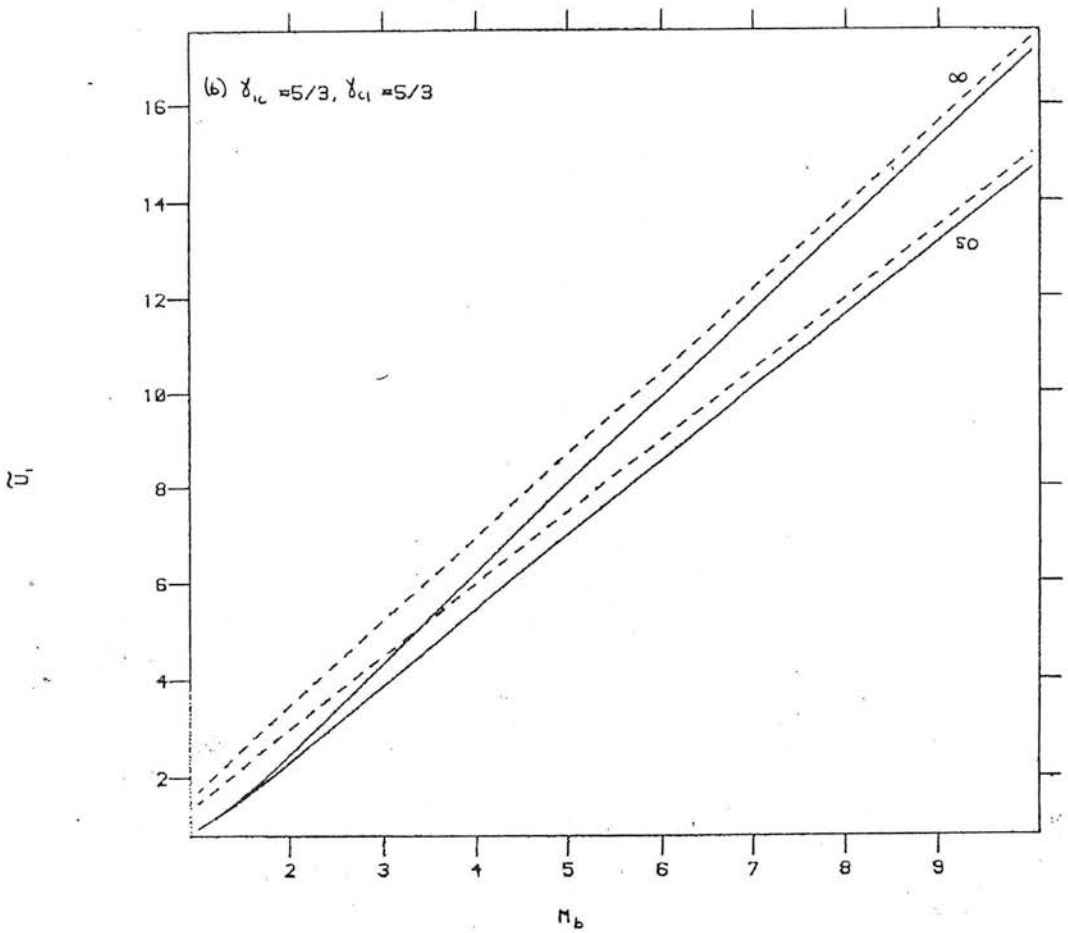
(b) γ_{1c} =5/3, γ_{c1} =5/3
∞
50
$\tilde{v}_1$
M_b

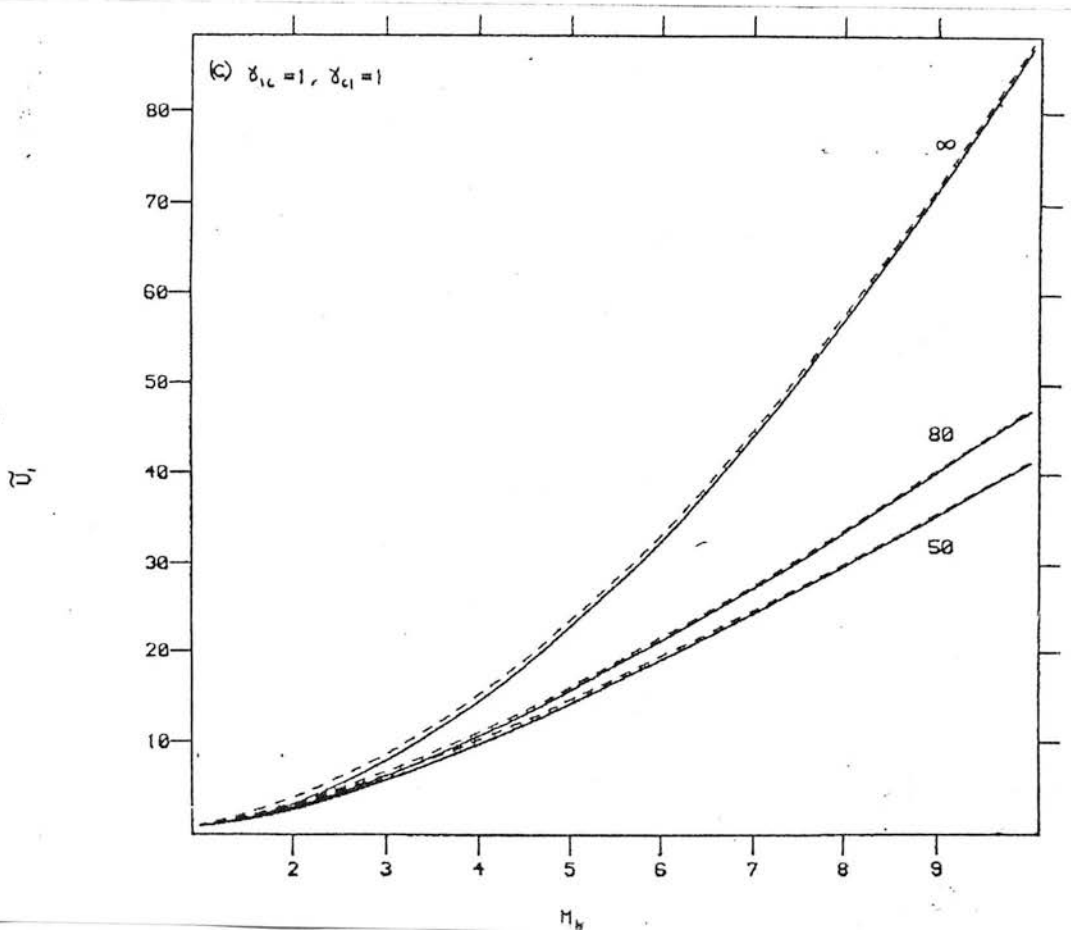
(c) γ_{1c} =1, γ_{c1} =1
∞
80
50
$\tilde{v}_1$
M_b

reached where the post shock gas begins to rush inward behind the cloud. The various segments of the shock that have travelled around the cloud collide almost head on at the symmetry axis leading to an almost cylindrical reflected shock. This leads to a transiently high pressure at the back of the cloud the magnitude of which can be estimated from the standard results for the head on collision of two shocks of strength M_b. For $\gamma_{ic} = 5/3$ this leads to $(P_2/P_o) \simeq (6M_b^2 - 2)/(M_b^2 + 3) \sim 6$ which results in a value $\sim$1.6 times the peak value obtained by Woodward probably because of a slight retardation of the shock as it passes over the cloud. For $\gamma_{ic} = 1$ the corresponding result is $(P_2/P_o) \simeq M_b^2$. As the reflected shock travels outward from the symmetry axis it weakens and eventually decays to a pressure wave. At the same time the colliding segments of the external shock meet at an increasingly oblique angle as their point of intersection moves downstream. Consequently P_2 falls quite rapidly and again this transient initial phase is relatively unimportant for the propagation of the cloud shock S_2.

The outward flow of the reflected shock from the symmetry axis, is however, responsible for the generation of the vortex system, the ram pressure from which does play a long term role in driving S_2. Because of this ram pressure contribution it is not possible to derive the value of P_2 precisely from analytic considerations. Analogy with the situation at the front stagnation point together with careful examination

of the flow patterns in the various numerical models suggests that an adequate approximation is $P_2 = \xi P_1$ subject to the requirement that $(P_o/P_1) < \xi < 1$. Note that $P_2 = P_1$ is precisely the result obtained from the usual potential flow solution for a rigid sphere immersed in a steadily flowing incompressible, irrotational fluid (e.g. Currie 1974). For the cases described by Woodward I estimate $\xi \sim 0.75$ for $\gamma_{ic} = 5/3$ and $\xi \sim 0.5$ for $\gamma_{ic} = 1$. None of the results obtained here depend critically on the value chosen for ξ. Consequently $\tilde{U}_2$ the Mach number of the rear cloud shock S_2 is given by,

$$\tilde{U}_2 = \tilde{U}_1 \left[\xi + \frac{(\gamma_{cl} - 1)}{2\gamma_{cl}} \frac{1 - \xi}{\tilde{U}_1^2} \right]^{\frac{1}{2}} \qquad 5.2\text{-}8$$

In the limit of small M the pressure P_3 at the sides of the cloud may again be estimated from the potential flow solution for a rigid sphere; to lowest order in M this leads to $P_3/P_o \simeq 1 - (\gamma_{ic} M^2/4)$. This result can be crudely extended to the case of finite but still subsonic flow by means of the Prandtl-Glauert rule (Currie 1974). These approximate subsonic calculations together with the results of the numerical calculations suggest that a sufficient approximation to the value of P_3 is $P_3 \simeq \zeta P_o$ with $\zeta \sim 0.5$. Hence the Mach number of the shock S_3 will be given by,

$$\tilde{U}_3^2 = \zeta \frac{\gamma_{ic}}{\gamma_{cl}} \frac{(\gamma_{cl}+1)}{(\gamma_{ic}+1)} \left[M_b^2 - \frac{(\gamma_{ic}-1)}{2\gamma_{ic}} \right] - \frac{(\gamma_{cl}-1)}{2\gamma_{cl}} \qquad 5.2\text{-}9$$

The collapse phase ends when S_1 and S_2 collide after a time

$$\tilde{t}_{col} = (2/\tilde{U}_1) \quad (1 + \tfrac{1}{2}\tilde{t}_{inj}\tilde{U}_2/\tilde{U}_1) \; / \; (1 + \tilde{U}_2/\tilde{U}_1) \qquad 5.2\text{-}10$$

where $\tilde{t}_{inj}$ is the time of injection of S_2 into the back of the cloud which I estimate to be $\sim 3A/M_b$. Employing the strong shock, small A approximations for $\tilde{U}_1$ and for $\tilde{U}_1/\tilde{U}_2$ then leads to,

$$\tilde{t}_{col} \simeq 1.4 \left[\frac{\gamma_{c1}}{\gamma_{c1}+1}\right]^{\frac{1}{2}} \Big/ \left[M_b(1 + \xi^{\frac{1}{2}})\right] \qquad \gamma_{ic} = 5/3$$

$$\tilde{t}_{col} \simeq 1.4 \left[\frac{\gamma_{c1}}{\gamma_{c1}+1}\right]^{\frac{1}{2}} \Big/ \left[M_b^2 (1 + \xi^{\frac{1}{2}})\right] \qquad \gamma_{ic} = 1 \qquad 5.2\text{-}11$$

Comparison with W76 and W79 suggests that these estimates are $\sim$40% too small. When $\tilde{U}_1$ is obtained from the exact solutions to equations 5.2-2, 5.2-3 and 5.2-4 I obtain a result $\sim$11% too small.

Obviously if the cloud w ere initially very elongated in the direction of travel of the external shock the cloud might collapse laterally faster than it collapses longitudinally; clearly this can only happen if the major to minor axis ratio of the cloud exceeds the value of P_1/P_o given by equation 5.2-2. For the typical SNR shock with $M_b \sim 3$ considered in §5.3 clouds with major to minor axis ratios $\lesssim 3$ for $\gamma_{ic} = 5/3$ and $\lesssim 8$ for $\gamma_{ic} = 1$ will collapse predominantly parallel to the direction of travel of the external shock, even when this lies along their major axis.

5.2.3 Surface Instabilities and the Growth of the Dense Axial Clump

As mentioned in §5.2.1 and extensively discussed in W 76 the development of the surface instabilities and the consequent growth of a dense clump of gas near the axis of symmetry presents the greatest difficulties, both for numerical and analytical methods.

First consider the rather idealised case of an initially unpurturbed cloud considered by Woodward. At first sight it would seem that the assumed spherical symmetry is rather special as well as highly improbable. However, in fact this is not so. There are two features of the symmetry axis which cause it to play a special role in clump growth : (1) it coincides with the location of the stagnation point in the external flow near which the KH instability will grow very slowly; (2) convexity of the cloud surface there, leads to convergent flow of the cloud gas behind S_1, producing a density enhancement. The first feature only requires that the cloud be a bluff body; the second requires that the front face of the cloud is bi-laterally convex on scales comparable with its dimensions. These conditions are both much more likely to be met with in reality.

Given that they are, then two factors determine what fraction of the cloud's mass can be accumulated into the dense clump: (1) The effective area of the front surface of the cloud

from which material may be collected. If the flow is subsonic this is determined by the lateral distance to the KH tongues closest to the stagnation point.

(2) The rate at which the RT instability can collect the available material.

Following W 76, when the density of the cloud greatly exceeds that of the ICM (i.e. when A is small) I find for the growth time of the KH mode of wavenumber $(\tilde{K}/R_{cl})$,

$$\tilde{t}_{KH} \sim (\gamma_{ic}/\gamma_{cl})^{\frac{1}{2}} (C_{cl}/C_1) (\tilde{K}M_{slip})^{-1} \qquad 5.2\text{-}12$$

where M_{slip} is the local Mach number of the flow at the cloud boundary and C_1 is the sound speed in the gas behind S_1. Again employing the solution for incompressible flow about a rigid sphere, I find $M_{slip} \sim M\sin\phi$ where ϕ is the polar angle of a given point on the cloud surface measured from the symmetry axis. Using this together with the exact solution to equation 5.2-2 - 5.2.5 I find that the ratio of $\tilde{t}_{KH}$ to $\tilde{t}_{col}$ for any $\tilde{K}$ and ϕ is independent of M_b for $M_b \gtrsim 2$ (γ_{ic} = 1 or 5/3). Thus for incident shocks stronger than this, but weak enough that the post shock flow is still subsonic with respect to the cloud, the general form of the KH ripples will be very similar to those found in W 76. Since I will generally be concerned with $M_b \gtrsim 2$ the surface area over which material can be collected to form the clump will be roughly constant in the subsonic regime. For A = 0 ('rigid' cloud) the flow behind S_o is subsonic with respect to the

cloud when $M_b < 2.7$ for $\gamma_{ic} = 5/3$ and $M_b < 1.62$ for $\gamma_{ic} = 1$. However, for non-zero A this limit can be appreciably raised. Once the flow around the cloud is supersonic, as noted above, the Kelvin-Helmholtz instability is suppressed (Gerwin 1968) and effectively the whole area of the front face of the cloud is available for the collection of clump material.

The growth of the dense clump is a straightforward consequence of the convexity of the cloud surface (Rictmeyer 1960; Chevalier & Theys 1975; Nittman et al 1982)*. The shock transmitted into the cloud is forced to converge while the reflected shock is forced to diverge. Consequently the flow behind S_1 is everywhere directed toward the stagnation point leading to a growing density and pressure there. This buildup of the past shock pressure causes S_1 to accelerate and the cloud boundary to deform, as the post shock gas is squeezed toward the axis.

Richtmeyer (1960) has discussed the growth of the RT instability under these circumstances. He finds that after an initial period of very rapid growth the amplitude grows linearly with time until the instability enters the non-linear regime. The normalised growth time of a mode of wave number $(\tilde{K}/R_{cl})$ is (again assuming A small)

$$\tilde{t}_{RT} \sim \tfrac{1}{2} \quad (\gamma_{cl} + 1)\ (1 + \tilde{U}_1^{-2})^{-1}\ (\tilde{K}\,\tilde{U}_1)^{-1} \qquad 5.2\text{-}13$$

---

*I follow Richtmeyer (1960) in referring to this process as the Rayleigh-Taylor instability although the physical situation is rather different from that considered by Taylor (1950).

Again for M_b sufficiently large that S_1 is strong the ratio of $\tilde{t}_{RT}$ to $\tilde{t}_{col}$ is independent of M_b for all $\tilde{K}$. The efficiency of clump collection is then also crudely constant.

Obviously departures of the cloud from sphericity will affect the growth rate of both modes; M_{slip} will increase more rapidly with distance from the stagnation point as 'the radius of curvature' of the surface decreases, while the more the cloud departs from being plane parallel the earlier clump formation will be complete. However, these effects can probably be neglected at the present level of approximation. The fraction of the clouds mass which can be collected into the clump can then be estimated from careful inspection of Woodward's models. At the end of the computation for the subsonic case (W 76) just before the collision of S_1 and S_2 the clump contained $\sim$5% of the clouds mass but was still growing. If all the available material was incorporated into the clump before the re-expansion of the cloud commenced then I estimate that the fraction of the cloud mass contained in the clump would be $F \simeq 0.1$. Careful 'planimetry' of the diagrams for the supersonic case (W 79) suggests that there $F \simeq 0.5$. Although I will take these values as being representative of the subsonic and supersonic regimes in numerical examples, F will be retained as a free parameter to illustrate the sensitivity of the results to the value adopted.

Next consider the more realistic case treated by NFG where

the cloud surface is initially highly corrugated on scales only slightly less than R_{cl}*. These corrugations will be amplified by the RT instability and if they have even a modest initial amplitude they can collect a considerable amount of material before the mode responsible for the formation of the axial clump can develop. They thus play a role similar to the KH modes at the sides of the cloud in restricting the area over which material can be gathered into the central clump. Hence, rather than a single clump there will be several, whose number and size is dictated by the scale length of the initial perturbations. Nevertheless the end result obtained by NFG is strikingly similar to that of W 76. In particular the region of the stagnation point is still most favourable for clump development - the initial perturbation(s) nearest to it achieve the greatest and most rapid growth. Equally, initial perturbations of wavelength much smaller than those considered by NFG would ultimately be engulfed by the main axial clump. Thus it seems that quite generally the end product of the RT instability will be the formation of one or a few dense clumps at the front face of the cloud with those nearest the stagnation point achieving the greatest size.

---

*Modes for which $\tilde{k} \ll 1$ need not be considered since they grow into the non-linear regime very rapidly and will constitute small perturbations upon the larger $\tilde{k} \sim 1$ mode which forms the axial clump.

5.2.4 The Collision of Shocks S_1 and S_2

To the extent that S_1 and S_2 are very nearly parallel at the time of their collision we may employ simple shock tube theory (Bradley 1962; Brand 1981) to calculate the effect of the collision. When $\gamma_{cl} = 1$ (the isothermal case) the consequences of the collision are straightforward. The shocks S_1 and S_2 'pass through' each other, their Mach numbers being unaffected, although of course they now travel into a medium of higher density which has already passed through the other shock (the sound speed in this gas is still C_{cl} however). Overall the pressure and density of the twiced shocked material between S_1 and S_2 are increased by a factor of $\sim\tilde{U}_1^2\ \tilde{U}_2$ relative to their values in the undisturbed cloud. For the cases considered by Woodward this leads to a final density of $\sim 100\ cm^{-3}$ for $\gamma_{ic} = 5/3$ and $\sim 2000 cm^{-3}$ for $\gamma_{ic} = 1$. (When $n_{cl} \sim 8cm^{-3}$ see footnote on page 193) which are to be compared with the maximum densities $\sim 340 cm^{-3}$ and $\sim 4140 cm^{-3}$ quoted by Woodward. The difference of a factor $\sim 2 - 3$ can readily be understood in terms of the slight lateral compression of the cloud which has been ignored in the analytic estimate.

When $\gamma_{cl} = 5/3$ the properties of the resultant shocks can only be found from a complete analysis. Nevertheless a procedure which is sufficient to determine the resulting density, given that S_1 and S_2 are not of drastically different strengths, is to employ the result for the collision

of two identical shocks of strength $\tilde{U} = (\tilde{U}_1 + \tilde{U}_2)/2$. The resulting density of the twice shocked material is then $\rho_f \sim 2\,\tilde{U}^2\,(5\tilde{U}^2 - 1)/\left[(\tilde{U}^2 + 3)(\tilde{U}^2 + 1)\right]\rho_{cl}$. At most the cloud material can be compressed by a factor 10 in this case. This leads to densities in good agreement with those found by NFG. Under the same assumptions the pressure between S_1 and S_2 is $P_f \sim \frac{1}{2}(15\tilde{U}^4 - 8\tilde{U}^2 + 1)/(\tilde{U}^2 + 3)P_{cl}$ which is at most $\sim 7.5\tilde{U}^2 P_{cl}$.

In the plane parallel idealization the thickness of the cloud at the end of the collapse phase is $\sim R_{cl}\ (\rho_{cl}/\rho_f)$; clearly an isothermal cloud becomes very highly flattened while the adiabatic cloud becomes somewhat less so. Nevertheless, even for $\gamma_{cl} = 5/3$ the flattening of the cloud is sufficiently great that the time elapsed between the collision of S_1 and S_2 and the arrival of the rearward moving shock at the back of the cloud can be neglected by comparison with $\tilde{t}_{col}$. I will consequently take $\tilde{t}_{col}$ to be a measure of the total duration of the collapse phase.

5.2.5 The Re-Expansion Phase

The large difference in the amount of compression and flattening suffered by adiabatic and isothermal clouds is primarily responsible for the differences between the late time evolution in the computations of NFG ($\gamma_{cl} = 5/3$) and Woodward ($\gamma_{cl} = 1$). The degree of compression is important for two reasons. Firstly, since an adiabatic cloud will be, at the very most over pressured by a factor ~ 6 relative to the ICM at the rear stagnation point (including the ram pressure of the vortex system) it need only expand very slightly in order to achieve pressure equilibrium. Conversely an isothermal cloud must expand very much more in order to relieve its much greater overpressure. Secondly, because the outer regions of an isothermal cloud have a thickness very much less than the lateral extent of the cloud they can be fragmented by instabilities which are still in the linear regime. Conversely for an adiabatic cloud surface instabilities would have to grow well into the non-linear regime before reaching an amplitude comparable with the cloud thickness.

It then follows that whenever, as a result of being shocked a cloud is appreciably flattened it will follow the evolutionary pattern found by Woodward; while in the converse case it will behave as discussed by NFG. It is not possible to determine the exact value of the compression factor which divides these two regimes but one might guess at a value ~ 8.

This is easily realised for isothermal clouds especially when the ICM is also isothermal. For adiabatic clouds this dividing line occurs roughly at $\tilde{U}_1 \sim 4$ corresponding to $M_b \sim 2.75$ and ~ 2.25 for $\gamma_{ic} = 5/3$ and 1 respectively in the limit of rigid clouds (See Figure 5.2-4).

Again to the extent that the curvature of the main cloud shock S_1 and the cloud boundary can be neglected, the initial stages of the clouds expansion can be approximated by the usual solution for the interaction of a plane shock with a plane contact discontinuity (Bradley 1962; Brand 1981). This time the shock is incident from the high density side. Therefore a weak shock is transmitted and a strong rarefaction wave is 'reflected' into the cloud.

However, although the outflow behind the rarefaction wave is initially plane parallel, as the cloud 'tail' develops it expands laterally and the plane parallelism quickly disappears. Comparison with W 79 suggests that the ensuing motion is more nearly spherically symmetric. In my approximate treatment of the tail's evolution I therefore treat it as forming a segment of a gas sphere expanding freely into vacuum.

For $\gamma_{cl} = 1$ the density profile and equation of motion are (Kahn, 1972, Imshenik, 1960).

$$\rho(r,t) = \rho_c(t) \exp\left[-r^2/2R(t)\right]$$
$$P(r,t) = C_{c1}^2 \rho(r,t)$$
$$v(r,t) = \sqrt{2}\, C_{c1} \left[\mathrm{Ln}\,(R(t)/R(o))\right]^{\frac{1}{2}} r/R(t) \qquad 5.2\text{-}13$$
$$C_{c1}t/R(o) = \sqrt{2}\; R(t)/R(o)\; D\left(\left[\mathrm{Ln}\,(R(t)/R(o))\right]^{\frac{1}{2}}\right)$$

Here,

$$D(x) = e^{-x^2} \int_o^x e^{-y^2}\, dy,$$

and the boundary conditions $R(t) = \dot{R}(o)$, $R(t) = 0$ at $t=0$ have been imposed. Note that the value of Dawsons integral $D(x)$ is almost proportional to x for $x \lesssim 0.4$, passes through a maximum value of 0.54 at $x = 0.92$ and is $\sim (2x)^{-1}$ for large x (Abramowitz & Stegun). Consequently over the range of values of x of relevance here $D(x)$ is almost a constant $\sim 0.4 - 0.54$. Obviously, the validity of this solution requires that the above density profile should hold at all times including the initial instant. Although this is patently not true it is to be expected that at times sufficiently great that the initial conditions have been forgotten, the evolution for the case of an arbitrary initial density distribution will not differ greatly from equation 5.2-13. Furthermore, comparison with W 79 shows that the actual density profile, velocity profile and evolutionary timescale do not differ grossly from that given by this solution even at quite early times.

For $\gamma_{c1} = 5/3$ the corresponding density profile and equation of motion are (Zeldovich and Raizer 1968)

$$\rho(r,t) = \rho_c(t)\left[1 - (r/R(t))^2\right]^{3/2}$$
$$P(r,t) = P_c(t)\left[1 - (r/R(t))^2\right]^{5/2}$$
$$v(r,t) = \sqrt{3}\, C(o)\left[1 - (R(o)/R(t))^2\right]^{\frac{1}{2}} r/R(t) \qquad 5.2\text{-}14$$
$$C(o)\, t/R(o) = \left\{\tfrac{1}{3}\left[(R(t)/R(o))^2 - 1\right]\right\}^{\frac{1}{2}}$$

here $C(o)$ is the sound speed of the tail gas at the beginning of the expansion and the same boundary conditions as above have been employed.

To complete the solution in either case it is necessary to obtain the value for the initial scale length, $R(o)$. To do this I require that the mass of the conical segment representing the tail should equal the mass of the dense clump from which I obtain

$$R(o) = R_{cl}\left\{(\rho_{cl}/\rho_c(o))\, F\ominus(\theta)\right\}^{\frac{1}{3}} \qquad 5.2\text{-}15$$

Where

$$\ominus(\theta) = \left[2 + \sin^2\theta\cos\theta + \cos^3\theta - 3\cos\theta\right]^{-1}$$

and θ is the semi-angle of the conical segment. From W 79 I estimate $\theta \sim 20^o$ so that $\ominus \sim 8$, for $\gamma_{cl} = 1$. In the computation of NFG the expansion of the back of the cloud is only very slight making it difficult to estimate θ, however $\theta \sim 90^o$ is probably appropriate implying $\ominus \sim \frac{1}{2}$, for $\gamma_{cl} = 5/3$.

The expansion phase ultimately ends when the tail reaches pressure equilibrium with its surroundings. I take $P_c(t)/e$ as the typical pressure in the tail (this is obtained at $r = 2R(t)$ and $r \sim \frac{1}{3}R(t)$ for the isothermal and adiabatic

cases respectively. The expansion timescale is then

$$\tilde{t}_{exp} \approx 2F^{\frac{1}{3}} D\left\{\left[\tfrac{1}{3}\mathrm{Log}\ (0.4P_c(o)/P_{ext})\right]^{\frac{1}{2}}\right\} \quad \gamma_{cl} = 1$$

$$\tilde{t}_{exp} \approx \left[\zeta_{cl}/C(o)\right] F^{\frac{1}{3}} \left\{1 - 1.5\left[P_{ext}/P_c(o)\right]^{2/5}\right\}^{\frac{1}{2}} \quad \gamma_{cl} = 5/3 \qquad 5.2\text{-}16$$

where P_{ext} is the external pressure. For a plane incident shock as considered in all the numerical computations the appropriate value of P_{ext} will be the pressure at the rear stagnation point P_2. For a cloud struck by an SNR both the thermal pressure and ram pressure exerted by the external medium decline as the SNR expands so that for very late times a value closer to P_{ic} may be more appropriate.

In the isothermal case the insensitivity of D(x) to its argument leads to $\tilde{t}_{exp} \sim 0.9F^{\frac{1}{3}}$ and $[R(t_{exp})/R(o)] \sim \sqrt{2}\,\Theta^{-\frac{1}{3}}\tilde{U}_1^2\tilde{U}_2^2$ independent of M_b or the choice of P_{ext} provided $\tilde{U}_1 \gtrsim 3$. Correspondingly for the adiabatic case, $\tilde{t}_{exp} \sim 1.7F^{\frac{1}{3}}$ $\left[1 - 0.73(P_{ext}/P_2)^{2/5}\right]^{\frac{1}{2}}$ and $[R/t_{exp})/R(o)] \lesssim \left\{1 + 14\right.$ $\left.\left[1 - 0.73(P_{ext}/P_2)^{2/5}\right]\right\}^{\frac{1}{2}}$.

5.2.6 Summary of Cloud Model: A Representative Case

To provide a better feel for the results of this section I give values for the cloud dimensions and timescales for a 'representative' cloud at various phases during its evolution in table 5.2-1. The parameters chosen for this 'representative' cloud are $R_{cl} = 2$ pc $C_{cl} = 0.8$ kms^{-1}, $C_{ic} = 120$ kms^{-1}, $M_b = 3.5$ $\gamma_{cl} = 1$ and $\gamma_{ic} = 5/3$. The term 'typical' in the table is used to describe times half way through the collapse and half way through the re-expansion.

TABLE 1

Values for the critical phases of evolution of a 'representative cloud', showing the scaling with the controlling parameters A and M_b

$R_{cl} = 2$ pc $C_{cl} = 0.8$ kms^{-1} $t_{cl} = R_{cl}/C_{cl} = 2.5$ Myr

$A = C_{cl}C_{ic} = 6.67 \times 10^{-3}$ $M_b = 3.5$ $\gamma_{cl} = 1$ $\gamma_{ic} = 5/3$

PHASE	EPOCH		EXTENT				
			Lateral		Axial		
	t/t_{cl}	Myr	Y/R_{cl}	pc	Z/R_{cl}	pc	
Shock reaches front of cloud	0		2.0	4.0	2.0	4.0	
External shock reaches back of cloud	$3A/M_b$	0.014	2.0	4.0	2.0	4.0	(i)
'Typical' stage during collapse		0.23		3.0		1.0	(ii)
Shocks S_1 and S_2 collide	$0.64/M_b$	0.46	0.98	2.0	$0.9M_b^{-2}$	0.15	(iii)
'Typical' stage during re-expansion		1.6		0.55		1.2	(iv)
End of re-expansion pressure equilibrium	$0.72+0.64/M_b$	2.3	0.55	1.1	1.2	2.4	(v)

Notes:

(i) Shock is slowed by cloud boundary. Fig 1(a)

(ii) Time is $t_{col}/2$

(iii) Time is t_{col} eq (8a) Extents calculated from U_i eq (6a) and U_2 eq (7).. Fig. 1(b).

(iv) Time is $t_{col} + t_{exp}/2$ Fig. 1(d)

(v) Time is $t_{col} + t_{exp}$ eq (12a). t_{exp} is nearly independent of M_b. Length is scale length of tail $R(t_{exp})$ eq (9c): Width from 20° opening angle.

5.3 The 'Real World' of the SDC-ISM

So far I have considered a highly idealised model of the cloud shock wave interaction. This model is an over-simplification in a number of respects:

(i) the initial conditions were that the cloud was in pressure equilibrium with and at rest in the ICM.

(ii) the cloud was initially spherically symmetric and structuraly homogeneous.

(iii) the equation of state was taken to be a simple polytrope throughout its evolution.

In addition, a number of potentially important physical processes have so far been neglected. In this section I will concentrate on establishing the timescales of these various processes to compare with the clouds evolution timescale. The effects that the processes have on the cloud evolution will be discussed in §5.4. The processes considered are: multiple shocks, cloud evaporation, ionisation, H_2 formation, cloud-cloud collisions and self-gravity.

As discussed above the dynamics of the cloud are specified by essentially three parameters; the cloud radius, R_{cl}; the ratio of its sound speed to that of the ICM, A, and the Mach number of the incident shock, M_b. Furthermore, when A is small, as it often is in the cases of interest, the problem ceases to be sensitive to its value. However,

TABLE 5.3-1

Adopted values of various ISM parameters for the solar neighbourhood. After McKee and Ostriker (1977) and Brand and Heathcote (1981).

PARAMETER	VALUE
Intercloud Medium	
Sound speed	$C_{ic} \sim 95\sqrt{\gamma}_{ic}$ kms^{-1}
Temperature	$T_{ic} \sim 7 \times 10^{5}$ K
Density	$n_{ic} \sim 2 \times 10^{-3}$ cm^{-3}
'Cold Clouds'	
Sound Speed	$C_{cl} \sim 0.8\sqrt{\gamma}_{cl}$ kms^{-1}
Temperature	$T_{cl} \sim 10^{2}$ K
Density	$n_{cl} \sim 30$ cm^{-3}
$A = C_{cl}/C_{ic}$	$A \sim 8.4 \times 10^{-3}\sqrt{\gamma_{cl}/\gamma_{ic}}$
'Warm Clouds'	
Sound speed	$C_{cl} \sim 10\ \gamma_{cl}$ kms^{-1}
Temperature	$T_{cl} \sim 10^{4}$ k
Density	$n_{cl} \sim 0.2$ cm^{-3}
Ionisation fraction	$x_{cl} \sim 0.5$
$A = C_{cl}/C_{ic}$	$A \sim 0.11\sqrt{\gamma_{cl}/\gamma_{ic}}$

TABLE 5.3-1

Supernova Remnants

Volumetric supernova rate	$S \sim 1 \times 10^{-13} pc^{-3} yr^{-1}$
Energy per supernova	$E_o \sim 1 \times 10^{51}$ ergs
Porosity parameter	$Q_c \sim 0.5$
SNR cooling radius	$r_c \sim 182$ pc
Interior density at r_c	$n_c \sim 5 \times 10^{-3}$ cm^{-3}
Interior temperature	$T_h \sim 4.4 \times 10^5 (M_b/M_{bc})^2$ K
Blast wave mach number at r_c	$M_{bc} \sim 3.5$
Shock repetition time	$t_{sn} \sim 3 \times 10^5$ yr

Miscellaneous

Ambient photoionising UV flux	$J \sim 0.2 \times 10^5$ cm^{-2}s^{-1}
Cloud number density	$N_{cl} \sim 6 \times 10^{-3} pc^{-3}$
Cloud velocity parameter	$\langle R_{cl}^2 V_{cl} \rangle \sim 9.5$ pc^2 kms^{-1}

many of the other processes are dependent on additional parameters of the cloud and its surroundings. For definiteness of presentation I will adopt a single set of values for these various quantities which will be employed in all numerical examples and then indicate the scaling (usually simple) to other cases. These values were chosen on the basis of both observations and the theoretical model of the SDC-ISM discussed in sections 3 and 4 as being appropriate to the solar neighbourhood. For ease of reference they are listed in table 5.3-1. A general feature of any model of the ISM is the existance of two preferred equilibrium cloud temperatures viz $\sim$100K ('cold clouds') and $\sim 10^4$K ('warm clouds'). I will treat these two cases separately.

The boundary of the region of validity in the (M_b, R_{cl}) plane appropriate for cold clouds is shown in figures 5.3-1 to 5.3-3 for the following cases:

Figure 5.3-1 isothermal cloud, adiabatic ICM ($\gamma_{cl} = 1, \gamma_{ic} = 5/3$)

Figure 5.3-2 isothermal cloud, isothermal ICM ($\gamma_{cl} = 1, \gamma_{ic} = 1$)

Figure 5.3-3 adiabatic cloud, adiabatic ICM ($\gamma_{cl} = 5/3\ \gamma_{ic} = 5/3$)

The calculation of the position of this boundary will now be described and the generalisation to other cases will be discussed. The question of what values of γ_{cl} and γ_{ic} are appropriate will also be addressed.

5.3.1 Shock Repetition

Quite generally the time between successive SNR having radii r smaller than some value r' is

$$t_{sn}\ (r \lesssim r') \simeq 2.4 \times 10^6 \text{yr} (100\ \text{pc}/r)^3\ (10^{-13}\text{pc}^{-3}\text{yr}^{-1}/S)$$

Figure 5.3-1 The domain of validity of the simplified model in the initial cloud radius (R_{cl}), incident shock Mach number (M_b) plane for 'cold' clouds when γ_{ic} = 5/3 and γ_{cl} = 1. Each labelled line represents one of the various constraints enumerated in Section 5.3. The label is always on the side of the line where the assumptions of the model are violated. For instance, above the line labelled SNR(a) clouds do not have sufficient time to complete their collapse before being overrun by a second shock. For details and the scaling to other conditions, see text. Shading indicates the region within which none of my assumptions is violated.

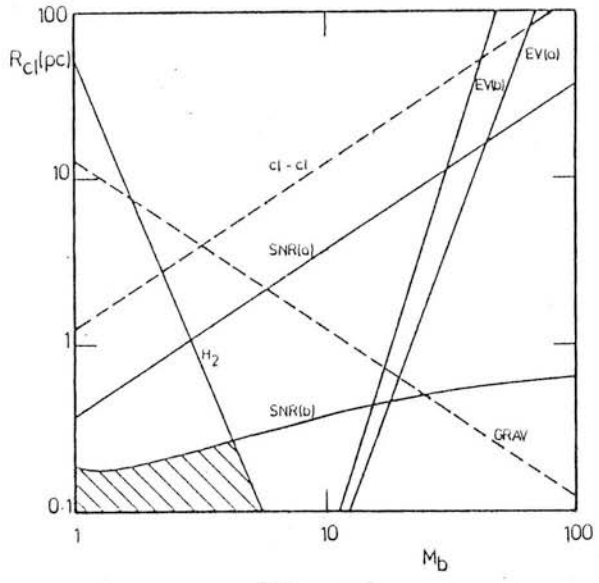

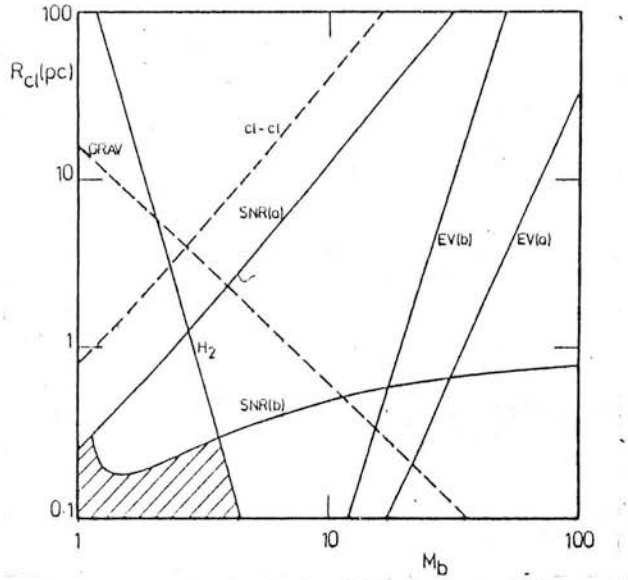

Figure 5.3-2 As Fig. 5.3-1 but $\gamma_{ic} = 1$ and $\gamma_{cl} = 1$

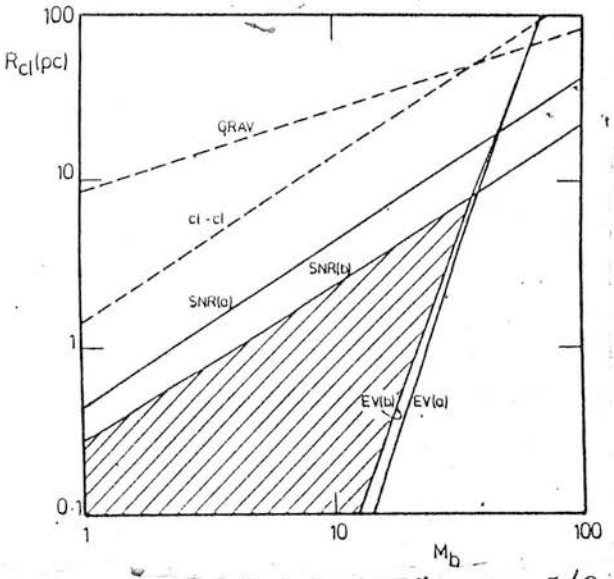

Figure 5.3-3 As Fig. 5.3-1 but $\gamma_{ic} = 5/3$ and $\gamma_{cl} = 5/3$.

where S is the volumetric supernova rate. This may be cast into a more useful form involving the shock Mach number if a specific model of SNR evolution is adopted. As an example I will here use the evolutionary model for evaporative SNR developed in §3.2.2 and will for the sake of definiteness consider the $\omega = 0$ case. If the various theoretical parameters discussed in that section are taken to have their 'standard' values as listed in table 3.5.1 then,

$$t_{sn}\ (M_b > M_b') \simeq 2.4 \times 10^6 \text{yr} (100\text{pc}/r_{bc}) (10^{-13}\text{pc}^{-3}\text{yr}^{-1}/S) (M_b'/M_{bc})^{9/2} \quad M_b > M_{bc}$$

$$5.5 \times 10^6 \text{yr} (100\text{pc}/r_{bc}) (10^{-13}\text{pc}^{-3}\text{yr}^{-1}/S) (M_b'/M_{bc})^{1.92} \quad M_b > M_{bc}$$

Here M_{bc} is the Mach number of the blast wave just before the SNR cools to form a dense shell of radius r_{bc} (c.f. Table 3.2-2),

$$M_{bc} \simeq 2.1\ (E_o/10^{51}\text{ergs}) Q_c^{-0.75} (S/10^{-13}\text{pc}^{-3}\text{yr}^{-1})^{0.75}$$

$$r_{bc} \simeq 200\ (E_o/10^{51}\text{ergs}) Q_c^{0.23} (S/10^{-13}\text{pc}^{-3}\text{yr}^{-1})^{0.23}$$

where E_o is the initial explosion energy and Q_c is the porosity parameter, $0 \leq Q_c \leq 1$. Because of the strong dependence of t_{sn} on M_{bc}, a cloud will typically only encounter a shock of Mach number greater than ~ 10 $(3M_{bc})$ once in the time it takes to pass from one spiral arm to the next. During the same time it would interact with ~ 900 SNR shocks of all strengths.

The line labelled SNR (a) in Figures 5.3-1 to 5.3-3 shows

the locus of points for which $t_{sn} = t_{col}$. Similarly, the line labelled SNR(b) shows the locus of points for which $t_{sn} = (t_{col} + t_{exp})$ when F, the axial clump mass fraction equals 0.5. The curves for other values of F are displaced parallel to the R_{cl} axis by a factor $(F/0.5)^{\frac{1}{3}}$. The value of t_{sn} used in these figures has been calculated assuming all SNR, up to the maximum radius at which the remnants overlap and come into pressure equilibrium, contribute to the compression of the clouds. Changing the value of t_{sn} simply displaces these curves parallel to the R_{cl} axis such that $t_{sn}C_{cl}/R_{cl}$ = constant. So long as the cloud dynamical timescales are insensitive to A ($A \lesssim 0.1$, $\gamma_{ic} = 5/3$; $A \lesssim 0.05$ $\gamma_{ic} = 1$) the same is true if C_{cl} is changed. In particular, the scaling to the case of warm clouds, may be made to sufficient accuracy by displacing these lines vertically upward by ~ 1 dex.

5.3.2 Cloud Evaporation

As discussed in § 3.2-1 the evaporation timescale of a static spherical cloud undergoing classical evaporation is (Cowie & McKee 1977),

$$t_{ev} \sim 3 \times 10^5 \text{yr}\, n_{cl} (R_{cl}/\text{pc})^2 / \phi_m (T_h/10^6\text{K})^{5/2}$$

where T_h is the temperature of the surrounding medium and ϕ_m is an uncertain correction factor $\sim \frac{1}{3}$. To apply this to the case of a collapsing and (except at the initial instant) non-spherical cloud I multiply by a term $(\tilde{a}\phi_g)^{-1}$ evaluated at a typical stage in the appropriate phase of the clouds

TABLE 5.3.2

The evaporative reduction factor $(\tilde{a}\phi_g)$ (Section 5.3.2) at a typical point during the collapse, at the end of the collapse and at a typical point during re-expansion as functions of M_b.

γ_{cl}	γ_{ic}	$(a\phi_g)$		
		$t_{col}/2$	t_{col}	$t_{exp}/2$
1	1	$[1-0.7/(M_b + 1)]^{\frac{2}{3}}$	$M_b^{-1}\left[1-1.4/(M_b + 1)\right]^{\frac{2}{3}}$	$0.2\ F^{\frac{1}{3}}$
1	5/3	0.7	$0.5\ M_b^{-\frac{2}{3}}$	$0.2\ F^{\frac{1}{3}}$
5/3	1	$0.9\left[1-(0.5/(M_b + 1))\right]^{\frac{2}{3}}$	$0.6\left[1-(M_b + 1)^{-1}\right]^{\frac{2}{3}}$	$0.2\ F^{\frac{1}{3}}(C_c(o)/C_{cl})^{\frac{1}{3}}$
5/3	5/3	0.7	0.4	$0.2\ F^{\frac{1}{3}}(C_c(o)/C_{cl})^{\frac{1}{3}}$

evolution. The term $\tilde{a}$ is the radius of a sphere having the same volume as the collapsed cloud (in units of R_{cl}) while ϕ_g is the geometrical connection factor defined by equation 3.2-3 and illustrated in Figure 3.2-1. During the collapse phase I evaluate $(\tilde{a}\phi_g)^{-1}$ when $\tilde{t} = \tilde{t}_{col}/2$ and similarly during the expansion phase when $\tilde{t} = \tilde{t}_{col} + \tilde{t}_{exp}/2$. The values of $(\tilde{a}\phi_g)$ derived in the strong shock small A limit are listed in table 5.3-2.

The line labelled EV(a) in figures 5.3-1 to 5.3-3 is the locus of points for which t_{ev} evaluated for the cloud as a whole equals t_{col} while that labelled EV(b) is evaluated for the axial clump when F = 0.5. The curves for other values of F are displaced parallel to the R_{cl} axis by a factor $(F/0.5)^{4/3}$. Again in so far as the results are independent of A scaling to other values of T_h can be achieved by displacing these lines parallel to the R_{cl} axis by a factor $(T_h/4.4\times10^5 K)^{5/2}$ or correspondingly by an amount $(M_b/3.5)^5$. Since $n_{cl} \propto C_{cl}^2$ it follows that $t_{ev} \propto (R_{cl}/C_{cl})^2$. Thus we may scale to other values of C_{cl} by displacing the plotted curves parallel to the R_{cl} axis such that $t_{ev}C_{cl}/R_{cl}$= Constant. In particular, the scaling to the case of warm clouds is obtained by shifting the lines shown upward by ~1 dex.

5.3.3 Ionisation

I will show in §5.4.3 that the time required for the complete

ionisation of an initially neutral, static, spherical cloud exposed to a steady, isotropic flux J, of ionising photons is given by

$$t_{ion} \simeq 3 \times 10^5 \text{yr } n_{cl} R_{cl} (10^5 \text{cm}^{-2}\text{s}^{-1}/J)$$

As in section 5.3.2above I correct to the case of a collapsing cloud by multiplying by $(\tilde{a}^2 \Psi_J)^{-1}$ where Ψ_J is again a flattening correction. Notice that since t_{ion} and the cloud dynamical timescales are both proportional to R_{cl} the ratio $t_{ion}/(t_{col} + t_{exp})$ is simply an increasing function of M_b. For the value of J given in Table 5.3.2 t_{ion} is always much larger than the dynamical timescales for either warm or cold clouds. Typically, for t_{ion} to be comparable with $(t_{col} + t_{exp})$ when M_b is 1 requires $J \gtrsim 10^6$ photons $\text{cm}^{-2}\text{s}^{-1}$ for cold clouds and $J \gtrsim 5 \times 10^4$ photons $\text{cm}^{-2}\text{s}^{-1}$ for warm clouds.

5.3.4 H_2 Formation

The formation timescale for H_2 molecules is (Spitzer 1978)

$$t_{H_2} \sim 1.6 \times 10^7 \text{yr } (100 \text{ cm}^{-3}/n)$$

where a cloud temperature $\sim$80K is assumed. The value for n is derived from equations 5.2-13 or 5.2-14. The existence of a significant steady state abundance of H_2 requires that the column density through the cloud should be great enough to provide adequate self-shielding in the Werner bands. An appropriate empirical criterion (Savage et al 1977) is $R(t) \gtrsim (200 \text{ cm}^{-3}/n)\text{pc}$.

There exists a region in figures 5.3-1 to 5.3-3 within which the tails of cold clouds are sufficiently shielded and t_{H_2} is shorter than the expansion time. The boundary of this region which is only weakly dependent on the clump mass fraction is labelled H_2.

5.3.5 Cloud-Cloud Collisions

If the velocity distribution of the clouds is isotropic and remains unaffected by the SNR blast wave then the cloud-cloud collision time is just given by,

$$t_{cl-cl} \sim 0.6 \times 10^5 \text{yr} / \left[(N_{cl}/\text{pc}^{-3}) \langle (R_{cl}/\text{pc})^2 (V_{cl}/\text{kms}^{-1}) \rangle \right]$$

where N_{cl} is the number of clouds per unit volume and V_{cl} is the RMS cloud velocity. The average denoted by $\langle\rangle$ is taken locally over the entire ensemble of interstellar clouds. In reality of course clouds overrun by the blast wave will be accelerated to differing extents depending essentially on the column density through them (McKee et al 1978). Consequently clouds will tend to be struck from downstream by clouds of lower column density overrun at an earlier stage in the remnants expansion. Similarly, they will tend to run into clouds of higher column density overrun at a later stage. This will somewhat decrease the mean collision time but this can easily be compensated for by choosing an appropriate value for V_{cl}. The shapes of the loci along which t_{cl-cl} is equal to the cloud dynamical timescales are of course identical to those found for t_{sn}

above and obey the same scaling relationships. The line for which $t_{cl-cl} = t_{col}$ is labelled cl-cl in figures 5.3-1 to 5.3-3.

5.3.6 Self Gravity

The boundary of the region within which the self-gravity of the axial clump exceeds its thermal energy at the end of the collapse phase is indicated by GRAV in figures 5.3-3 to 5.3-5. The clump is idealised as a sphere of mass F (clump fraction) times the mass of the cloud and radius equal to the thickness of the cloud along the symmetry axis at the end of the collapse phase. F has been taken as 0.5 scaling to other values can be obtained by multiplying by a factor $(F/0.5)^{-\frac{1}{2}}$.

5.3.7 Radiative Cooling

The most useful cooling characteristic for treating the shocks is the cooling column density which can be written entirely in terms of the shock velocity, u_s. An important complication in determining the cooling column density is the ionisation of the pre-shock material by radiation emitted by the shock itself. I employ the following relations from McKee and Holenbach (1980).

$$N_{cool} \sim 10^{19} - 10^{20} \text{ cm}^{-2} \quad 1 \text{ kms}^{-1} \lesssim u_s \lesssim 20 \text{ kms}^{-1}$$

$$N_{cool} \simeq 6.4 \times 10^{23} \, (\text{kms}^{-1}/u_s)^{4.0} \text{ cm}^{-2} \quad 20 \text{ kms}^{-1} \lesssim u_s \lesssim 60 \text{ kms}^{-1}$$

$$N_{cool} \simeq 8.0 \times 10^{8} \, (u_s/\text{kms}^{-1})^{4.2} \text{ cm}^{-2} \quad 60 \text{ kms}^{-1} \lesssim u_s \lesssim 1000 \text{ kms}^{-1}$$

Adopting the standard cold cloud parameters I find that all clouds struck by shocks weaker than $M_b \sim 11$ for $\gamma_{ic} = 5/3$ and $M_b \sim 4.7$ for $\gamma_{ic} = 1$ lie in the first of these three velocity regimes. Consequently the cooling lengths $N_{cool}/n_{cl} \leq R_{cl}$ for all clouds having $R_{cl} \gtrsim 0.1 - 1$ pc and consequently such clouds can be treated as effectively isothermal. Smaller clouds will be more nearly adiabatic. Because the cooling column density decreases so precipitously for $u_s > 20$ kms^{-1} clouds which encounter the rather rare shocks stronger than the above limits will be approximately isothermal.

For the warm clouds u_1 will exceed 60 kms^{-1} when $M_b \sim 2.6$ $\gamma_{ic} = 5/3$ (~ 2.3 $\gamma_{ic} = 1$). Consequently when $\gamma_{ic} = 5/3$ warm clouds as small as 0.1 pc will be adiabatic when struck by shocks stronger than $M_b \sim 3.3$; for clouds as large as 100pc this limit rises to $M_b \sim 17$. For $\gamma_{ic} = 1$ the dividing line between isothermal and adiabatic clouds lies at $M_b \sim 2.6$ for $R_{cl} = 0.1$ pc and at $M_b \sim 5.8$ for $R_{cl} = 100$pc.

For interactions between clouds and SNR in the adiabatic phase the appropriate value of $\gamma_{ic} = 5/3$. For interactions with SNR in the radiative phase $\gamma_{ic} = 1$, when the post shock flow is subsonic with respect to the cloud ($M_b \lesssim 1.6$ for cold clouds and $M_b \lesssim 2.0$ for warm clouds). When the incident flow is supersonic the resulting stationary bow shock will reheat the ICM. The cooling length in the

external flow will then exceed the cloud size so that $\gamma_{ic} = 5/3$ is appropriate for even only slightly supersonic incident flow.

Thus in broad terms the most commonly encountered situation will be the interaction of an adiabatic shock with an isothermal cloud (cold or warm).

5.4 DISCUSSION

As a consequence of the phenomena discussed in Section 5.3 the typical cloud evolution will not be as straight forward as that described in the Woodward model. However, it is possible to use the simple model as a basis for the discussion of these phenomena and their effect on clouds, and to suggest what as a consequence is happening to cloud-like material in the supernova - dominated interstellar medium. Specifically, I discuss the mean pressure and shape of clouds, mass loss rates by shock ablation and evaporation and by warm envelope stripping, and compressional heating of clouds.

5.4.1 Departures from pressure equilibrium

Perhaps the most striking result apparent in figure 5.3-1 to 5.3-3 is the length of the cloud dynamical timescales especially that for the re-expansion of isothermal clouds ($\gamma_{cl} = 1$) by comparison with the SNR shock repetition time. This has the important consequence that interstellar clouds (with the exception of the very smallest) struck by a shock will rarely have time to relax back to pressure equilibrium with their surroundings before encountering a second shock. Furthermore, for clouds of still only modest size, the interaction with this second shock is quite likely to occur during the collapse phase. Clearly then the details of the interaction of any given shock with a cloud will depend

in a most complex way on the past history of the cloud. In particular, they will be strongly dependent on the strength and direction of the previous shock(s) which interacted with the cloud, and how long has passed since that last interaction. Nevertheless, it is possible to speculate about the general features of such an interaction on the basis of the simplified model.

Firstly consider the smaller clouds for which the shock repetition time is only slightly shorter than the expansion timescale, and longer than the collapse time scale. For those clouds which are also adiabatic and hence only weakly flattened, the end product of the interaction is not too unlike the initial state; the cloud will be only slightly overpressured with respect to its surroundings and will be re-expanding fairly slowly. The simple model will then still give quite a good description of the clouds response to a second shock. If the cloud is overpressured with respect to the preshock ICM by a factor η then it is straight forward to show from the analysis of §5.2 that the Mach numbers of the shocks driven into the cloud are reduced by a factor $\eta^{\frac{1}{2}}$ in the strong shock, small A (large cloud-inter-cloud contrast) limit.

The case of the highly flattened isothermal cloud is more troublesome. I will neglect the presence of the highly flattened sheet like outer region of the cloud and just

consider the interaction of an SNR with an entity similar to the rather elongated, highly over-pressured and asymmetrically expanding cloud tail produced by the previous collision. If the new shock wave is very much stronger than the last shock to strike the cloud, then the expansion can be halted and the subsequent evolution of the cloud will be dominated by this new shock and will again be similar to that computed. In the more probable case that both shocks are of similar strength (the majority of shocks have M_b comparable with M_{bc}, (Section 5.3.1) the expansion of the cloud is likely to continue. Nevertheless, shocks will be driven into the cloud in a manner similar to that envisaged, although because the over-pressure is much greater in this case, the shocks will be considerably reduced in strength. Obviously, in this case the collapse and re-expansion of the cloud will be rather less ordered than in the case of a previously undisturbed cloud, but the simple model should still give a rough idea of the type of phenomena to be expected and some idea of the timescales involved.

In the extreme opposite limit of clouds for which the collapse time is very much longer than the shock repetition time I expect an entirely different pattern of events. Such clouds will experience a succession of external shocks of similar strength arriving from (by assumption) random directions. Consequently, they will 'see' an effective external pressure comparable to the sum of the post-shock

thermal plus ram pressure for a typical shock. Any shocks driven into them will be relatively weak. Clouds somewhat smaller than this limiting case will most likely resemble the "irregularly vibrating or writhing clouds" envisioned by Cox (1979) which at all times contain several **shocks of moderate strength.**

5.4.2 Cloud Mass Loss Rates

The disruption of the thin disk like outer regions of isothermal clouds by the Rayleigh-Taylor instability will obviously be a very efficient cloud destruction mechanism. If the mass fraction which is collected into the tail is F, then the clouds mass is reduced by a factor (1 - F)/F during each successive shock passage! I estimated in § 5.3.2 that F is between ~0.1 and ~0.5, depending on whether the flow past the cloud is supersonic or not, while the shock repetition time was estimated in § 5.4.1 to be $\sim 3 \times 10^5$yr for the parameters adopted. Clearly this process of shock ablation is at least of comparable importance with the related process of cloud fission in cloud-cloud collisions (Chiéze & Lazereff). Since clouds whose dynamical timescale is much larger than the shock repetition time probably do not ever have time to become highly flattened (see § 5.4.1) the operation of the process might ~~then~~ be restricted to somewhat smaller clouds. This might then neatly account for the absence of observed cold clouds much smaller than ~1pc (e.g. Greison 1976; Dickey et al 1977, Knude 1979, 1981) for which the dynamical timescale is ~1Myr.

Although as shown in § 5.3.2 thermal evaporation does not play a major role in the dynamics of the cloud-shock interaction under most circumstances, it is a highly important parameter of the SDC-ISM models discussed in the earlier part of this thesis. As discussed in § 5.3.2 the compression and the flattening of the cloud reduce the evaporation rate relative to that of an undisturbed cloud by a factor $\tilde{a}\phi_g$, which was tabulated at typical stages during the clouds evolution (Table 5.3-2). An equally important effect in fixing the nett evaporation rate at late times in the evolution of the smaller clouds is the disruption of the 'disk'. If this process leads to the formation of N_{fr} fragments of approximately equal size and possessing similar geometry to that of the original disk the net evaporation rate for the disk is increased by a factor $N_{fr}^{\frac{2}{3}}$. As a rough estimate of the average evaporation rate over the clouds evolution I write

$$\langle \dot{M}_{ev} \rangle \simeq \frac{\dot{M}_{ev}(Sp) \left\{ (\tilde{a}\phi_g)_{col} \left(t_{col} + N_{fr}^{\frac{2}{3}} t_{exp} \right) + (\tilde{a}\phi_g)_{exp} t_{exp} \right\}}{\left(t_{exp} + t_{col} \right)}$$

where $\dot{M}_{ev}$ (Sp) is the evaporation rate of the original undisturbed cloud and $(\tilde{a}\phi_g)_{col}$ and $(\tilde{a}\phi_g)_{exp}$ are the values of the reduction factors from Table 5.3-2 evaluated during the collapse and re-expansion phases respectively. It is readily apparent that if $N_{fr} \sim 5$, $\langle \dot{M}_{ev} \rangle$ is little different from $\dot{M}_{ev}(Sp)$ so that the cloud dynamics would then not be of major importance in determining the evaporation rate.

5.4.3 Composite clouds; Envelope stripping

In the SDC-ISM model of MO discussed extensively in Chapter 3 the interstellar clouds were supposed to be composite, consisting of a warm partially ionised envelope maintained by the interstellar uv and soft X-ray flux, surrounding a cold neutral core. Subsequently Chiése and Lazereff (1980) have demonstrated that (a) such a cloud envelope is efficiently removed by passing SNR blast waves and (b) that the timescale for the reformation of such an envelope by photo-ionisation is long compared to the shock repetition time. The present work confirms these latter findings.

The first conclusion, that of efficient envelope removal, rests on the very different velocities imparted to the low density material of the envelope and the dense material of the core on passing through an SNR blast wave. An approximate estimate of the velocity imparted to a single density cloud on passage through an adiabatic blast wave is obtained simply by application of momentum conservation,

$$V_{cl} \sim 0.9 \quad (n_c/n_{cl})(r_c/R_{cl}) \quad \left[(r/r_c)^{-4/4} - M_{bc}^{-2}\right] M_{bc}\, C_{cl} \qquad r \lesssim r_c$$

This expression in which n_c is the mean density in the SNR interior just before the remnant cools makes allowance for the enhancement of the interior density by evaporation (MO). In the post-cooling ($r > r_c$) case the remnant evolves with approximately constant momentum so this equation with

$r = r_c$ still applies. Comparison with more careful calculation (McKee et al 1978) suggests that although this certainly gives a slight over-estimate it does give the correct dependence on n_{cl} and R_{cl}. For the standard ISM parameters of table 1 I obtain $V_{cl} \simeq (80\ pc/R_{cl})kms^{-1}$ for warm clouds and $V_{cl} \simeq (0.5\ pc/R_{cl})\ kms^{-1}$ for cold clouds.

These values exceed those obtained by Chiéze and Lazareff from a similar analysis because they used the expression for M_{bc} given by MO which contains a numerical error leading to an underestimate of M_{bc} by a factor of 2.

The time for the regrowth of a warm envelope around an initially wholly neutral static spherical cloud exposed to a steady isotropic flux J of ionising photons (assuming a weak R ionization front and neglecting recombination) is,

$$t_{env} \simeq t_{ion} \quad (n_{env}/n_{cl})(R_{env}/R_{cl})^3$$

where R_{env} and n_{env} are the radius and density in the envelope and t_{ion} is the time required for the total ionisation of the cloud,

$$t_{ion} \simeq 3 \times 10^5 yr \left(\frac{n_{cl}}{cm^{-3}}\right) \quad \left(\frac{J}{10^5 cm^{-2} S^{-1}}\right)^{-1}$$

The inclusion of recombination would of course further increase this growth time. This expression differs slightly from that given by Chiéze and Lazereff (1980) because they considered a plane parallel envelope.

For the value of the ambient UV flux given in Table 5.3-1

this expression gives a value for the envelope growth time a factor of ~100 longer than the SNR shock repetition time for the smallest clouds of M0 which have $R_{env} \sim 2$ pc and $R_{cl} \sim 0.4$ pc. For M0's cloud spectrum (See § 3.4) the quantity R^3_{env}/R^2_{cl} has a minimum for clouds ~1.6 times as massive as the smallest clouds. Even there, however, assuming the average uv field leads to an envelope growth time a factor of ten longer than the repetition time. I have compared the values of the shock repetition time and the envelope growth time for all the galactic SDC-ISM models (described in Chapter 4) and find that this conclusion holds everywhere. I have also considered the effects of the local enhancement of the uv flux in an SNR cavity during the period of shell formation. Even then the envelope growth time remains long compared to the shock repetition time.

It thus seems that cold clouds cannot retain an equilibrium warm envelope if current estimates of the shock repetition rate are correct. If, as I believe, a significant filling factor for warm material is essential to account both for observations (Payne et al 1983) and for a proper theoretical understanding of the global properties of the ISM (§ 3) and perhaps even of spiral structure (§ 4), then it becomes necessary to look for another means of providing it.

Such a source may not be very difficult to find as suggested

by Cox (1981). As reviewed in §3.1 supernova explosion in a cloudy ISM inevitably result in the transfer of a large mass of interstellar gas from the cooler denser phases of the ISM to the hot tenuous matrix; this may occur as a result of thermal evaporation or the process of shock ablation discussed in §5.4.2, and must occur to a greater or lesser extent <u>irrespective</u> of whether there is a warm phase of the ISM or not. If global mass balance is to be achieved this material must ultimately be returned to the dense phase either through radiative cooling in old SNR or through the operation of a galactic fountain. Even in the absence of additional heating sources the time for this gas to cool from $\sim 10^4$K to $\sim 10^2$K is a factor of 10 to 100 times larger than the time to cool from $\sim 10^5$K to $\sim 10^4$K depending on whether the cooling occurs isochorically or isobarically; there are many steady heating sources which might be invoked to further slow down or halt completely the radiative cooling of the gas when its temperature reaches the precipice in the interstellar cooling curve at $\sim 10^4$K (Dalgarno & McCray 1972; Draine 1978; de Jong 1980; Cox 1979; Spitzer 1982). In particular the interstellar ionising flux which in the MO model maintains the equilibrium warm envelopes <u>must</u> act to keep a comparable amount of material in the warm state. Material then tends to build up in the warm phase until the capacity of the available heating sources is reached.

TABLE 4

The PV work done on the cloud during the collapse phase δW_{col} and by the cloud tail during the re-expansion phase δW_{exp} (Section 4.4).

γ_{cl}	γ_{ic}	$\delta W_{col}/(4\pi/3 R_{col}^3 P_o)$	$W_{exp}/(4\pi/3 R_{cl}^3 P_o)$
1	1	$M_b^2 \left[M_b^4 (M_b + 3) + 3M_b + 1\right] /(M_b+1)^3$	0.1 F
1	5/3	$3 M_b^2$	0.1 F
5/3	1	$2 M_b^2 \left[M_b^4(M_b+2) + 2M_b + 1\right] /(M_b+ 1)^3$	0.1 F $(C_c(o)/C_{cl})$
5/3	5/3	$2 M_b^2$	o.1 F $(C_c(o)/C_{cl})$

5.4.4 Cloud Compressional Heating

Cox (1979) has suggested that the PV work done upon clouds when overrun by SNR blast waves may represent an important source of thermal energy for clouds and a significant energy sink for SNR. The compressional work done by the external medium during the collapse phase is particularly simple to work out for the present model since the pressures driving the cloud shocks are assumed constant. If the cloud re-expands the work done back on the external medium by the cloud should be subtracted from this (the cloud re-expands at a pressure near P_{ic}). The results of such calculation are summarised in Table 5.4-1. As is to be expected these results are very similar to those obtained by Cox (1979) for the corresponding case. The values obtained here are slightly higher because Cox assumed the cloud shocks to be driven by the thermal pressure of the external medium while I have included a ram pressure contribution for the main cloud shock which does most of the work.

5.5 Summary

In this chapter I have constructed a highly simplified analytical model of the interaction of an SNR blast wave with an interstellar cloud based on published numerical calculations (Woodward 1976, 1979; Nittmann et al 1983). This model permits extrapolation of the numerical results to other values of the parameters of the shock and the cloud. Under the assumptions made the dynamics of the interaction

are determined completely by three parameters; the Mach number of the incident shock, M_b, the cloud radius, R_{cl}, and the ratio of the cloud to intercloud sound speeds A. Further, when A is small as is often the case the dependence on this parameter is quite weak. The scaling with R_{cl} and M_b is found to be quite simple. Any theoretical advance in this area is likely to require a fully three-dimensional computation with at least as great a resolution as that employed by Woodward in his two-dimensional calculations (the utility of calculations at lower resolution is put in question by the importance of small scale instabilities of the cloud boundary).

I have imposed the conditions believed to prevail in a 'realistic violent' three phase interstellar medium upon this model in order to assess the importance of processes not included in the model (e.g. a high shock repetition rate, thermal evaporation etc.) and to determine the effect of the cloud dynamics on processes important to the global properties of the ISM (evaporation, cloud crushing etc.) I conclude that:

(i) If current estimates of the rate at which a given interstellar cloud encounters SNR shocks are correct, then a shocked cloud is rarely allowed sufficient time to relax back to pressure equilibrium with its surroundings before being overrun by another shock. Large departures from pressure equilibrium are

expected, and the dynamics and properties of a given cloud will generally depend in a complex way on its past history. Nevertheless, I expect the model presented to be qualitatively correct under a wide variety of conditions.

(ii) For isothermal clouds, and adiabatic clouds struck by very strong shocks, the final product of the interaction is a highly flattened disk of material which is easily disrupted by Rayleigh-Taylor instabilities, and a rather extended cloud 'tail' expanding in the downstream direction. Each component is generally expected to contain $\sim\frac{1}{2}$ the mass of the original cloud. This process of shock ablation may represent an important mechanism for cloud disruption. If it is, then the half life of the cloud is comparable to the shock repetition time. Adiabatic clouds struck by typical weak shocks do not become sufficiently flattened to be subject to this disruption mechanism.

(iii) Although the flattening and compression of clouds overrun by SNR shocks reduces the evaporation rate below that for a static spherical cloud this will often be compensated by enhancement of the evaporation rate due to the fragmentation of the disk.

(iv) Warm envelopes are efficiently removed from cold cores by SNR shocks and require a time considerably longer than the shock repetition time for their recreation by ionisation. Nevertheless, a warm low density component of the ISM is observed, and is necessary

for proper theoretical understanding of its global properties. I have suggested some tentative mechanisms by which warm material might be produced, and I believe a solution to this problem is possible. SDC-ISM models, like those discussed in Chapter 3 are almost certainly sufficiently 'robust' to accommodate any consequent changes.

(v) The expected rate of PV work done by SNR on clouds for this model is similar to that found by Cox (1979).

While the assumption of pressure equilibrium is useful in simplifying the study of interstellar conditions, the prevalence of shock waves in the ISM requires that considerable caution be exercised in employing it. Many, or most, clouds should be observed to have structures rendered complex by being associated with 'tails', with shock ablated material, and with partially reformed envelopes, and by having one or more shock waves transversing their interiors.

6. SUMMARY AND CONCLUSIONS

Each of the preceeding chapters is to some extent self contained and in particular contains a summary of the main results obtained within it. Nevertheless, it seems worthwhile to very briefly summarise the main points again.

In Chapter 2 I briefly described each of the main energetic phenomena which have been invoked to account for the highly disturbed state of the 'violent interstellar medium'. Particular emphasis was put on establishing the amount of both kinetic energy and hot phase thermal energy each could supply to provide a basis for establishing their relative importance, and to facilitate a comparison with the systems estimated requirements. The main results of that effort are summarised in Table 2-1. From this it is apparent that in the spiral arms more than 80% of the thermal energy comes from supernovae, the remaining contribution being made by stellar winds blown by the more massive supernova progenitors; supernovae and the expansion of the HII regions around the more massive stars make roughly equal contributions to the kinetic energy supply. In the interarm region essentially the only energy input comes from supernovae of type I. It is also clear that within the fairly large uncertainties of the estimates the total energy supply is adequate to meet the demands. These results are neither very surprising nor particularly new. However, the survey of energy sources presented is more complete than any given elsewhere. The direct comparison made between the energy

input by massive stars through expansion of their HII regions, through the action of their stellar winds and by their explosion as supernovae is as far as I am aware unique; in most previous compilations estimation of the relative contributions is hindered by the large uncertainty in the supernova rate. The results of Chapter 2 provide justification for my contention that the ISM is supernova dominated and for my exclusive concentration on their role in the subsequent chapters.

In Chapter 3 I presented a simple model of the SDC-ISM based on the work of McKee and Ostriker (1977). This model extends on the previous work in three important ways:

(1) By incorporating a highly approximate description of the way a cloud responds to being overrun by an SNR blast wave, I have been able to assess the effects of cloud dynamics on the process of cloud evaporation which forms the keystone of the model.

(2) To assess the effects of the complete suppression of evaporation by the clouds magnetic field I have constructed a varient model in which 'cloud crushing' replaces evaporation enhanced radiation as the dominant sink of SNR energy.

(3) The treatment of the cloud population has been generalised to allow for the possibility of non spherical clouds and changes in the form of the assumed mass spectrum.

The model turns out to be remarkably robust : the results obtained from it do not change grossly when quite drastic changes are made to the description of the cloud dynamics; they are not unduly sensitive to the assumptions made about the dominant energy sink; nor are they greatly altered by changes in the slope of the cloud spectrum or the cloud morphology. The properties of this specific model may therefore be taken, with some confidence, to be typical of SDC-ISM models in general.

The various variants of the model have been subjected to an exhaustive parameter search in order to establish the domain in parameter space within which the model is self consistant and to test the sensitivity of its predictions to the very many uncertain free parameters which enter into its formulation. From this I conclude that:

(1) the model remains self consistant when its main controlling parameters, the supernova rate S, explosion energy E_o mean gas density $\bar{n}$ and the ionising photon emissivity ε_{uv} vary over quite large ranges near the values believed appropriate in the solar neighbourhood.

(2) the qualitative features of the model remains unaffected by quite major changes of the other input parameters; its quantitative predictions are only moderately sensitive to the precise values chosen and depend on them in a readily understandable way.

In Chapter 4 the model of the SDC-ISM developed and validated

in Chapter 3 is combined with a very simple model of the spiral structure of a galaxy like our own, permitting the first investigation of the interrelationship of global aspects of galactic structure and the small scale properties of an SDC-ISM. In addition to the adoption of a specific description of the SDC-ISM the assumptions made were that (1) the pattern of mean total density $\bar{n}$ is similar to that predicted by TASS models and (2) that the local star formation rate and supernova rate are proportional to one another and to some power m, of $\bar{n}$. The principle conclusions from this study are:

(1) Contrary to the expectations of others, whenever the hot phase of the ISM is important in the spiral arms it is also important between them; although the supernova rate is indeed lower in the interarm region this is more than compensated for by the accompanying reduction in the gas density.

(2) My results impose strong constraints on the conditions which must prevail in spiral galaxies if the intercloud medium is to support a strong density wave shock. For our galaxy both the lower estimates of the supernova rate (i.e. $S_{gal} \lesssim 0.02 yr^{-1}$) and the higher estimates of the galactic gas content must both be correct. If these conditions are not met then the spiral shock must be supported by the 'cloud fluid'.

(3) Unfortunately observational studies of external galaxies seem unlikely to provide information on the vital question of the ubiquity of the hot phase in

the near future.

In Chapter 5 I described a detailed investigation of the interaction of an interstellar cloud with an SNR blast wave which was carried out to meet the pressing need for such a study identified as a result of the work described in Chapter 3. Guided by the results of published numerical studies, a simple model of the processes involved in the interaction, has been constructed which permits extrapolation of the numerical results to other values for the parameters of the shock and the cloud. The conditions expected to prevail in the SDC-ISM where then imposed on the model in order to assess the importance of processes not included in it (e.g. a high shock repetition rate, thermal evaporation etc.) and to determine the effect of the cloud dynamics on processes important to the global properties of the ISM. I conclude that:

(1) If current estimates of the rate at which a given interstellar cloud encounters SNR shocks are correct, then a shocked cloud rarely has time to return to pressure equilibrium with its surroundings before being overrun by another shock. Large departures from pressure equilibrium are expected, and the dynamics and properties of a given cloud will generally depend in a complex way on its past history. Nevertheless the simple model presented will probably remain qualitatively correct under a wide variety of conditions.

(2) Isothermal and strongly shocked adiabatic clouds become highly flattened and are subject to efficient disruption by surface instabilities. This process of shock ablation may represent an important mechanism for cloud destruction. If it is then the half life of the cloud is comparable to the shock repetition time.

(3) Although the flattening and compression of clouds overrun by SNR shocks reduces the evaporation rate below that for a static spherical cloud this is probably compensated for by enhancement of the evaporation rate due to fragmentation of the cloud.

(4) Warm envelopes are efficiently removed from cold cores by SNR shocks and require a time considerably longer than the shock repetition time for their re-creation by ionisation. Nevertheless, a warm component of the ISM is observed and as discussed in Chapters 3 and 4 is necessary for the proper theoretical understanding of its global properties and may perhaps be vital for the maintenance of spiral structure.

Several problems are clearly identified in the present thesis as being in particular need of further study. Of these perhaps the most urgent is the problem of how to generate and maintain the warm component of the ISM. As briefly outlined in Chapter 3 a solution may readily be obtained if an energy source or sources can be identified to slow down or halt the radiative cooling of material on its way

tc rejoin the dense phase as part of the inevitable mass cycle of an SDC-ISM. A copious energy supply is potentially available from supernovae (Chapter 2) if ways can be found to harness it. Much of the thermal energy of the hot phase becomes available for heating cooler material as soft X-ray and uv photons. The kinetic energy of SNR is converted into forms which might eventually heat clouds by many processes; Cosmic ray acceleration (Blandford 1982); cloud crushing (Cox 1979, 1981); acoustic wave generation either by scattering from clouds (Spitzer 1982) or when old SNR come into pressure equilibrium with their surroundings; cloud acceleration followed by the generation of turbulence in cloud-cloud collisions. The overall conversion efficiency need not be very high; if the warm component is predominantly neutral and has a density $\sim 0.25 cm^{-3}$ for instance then conversion of the total available supernova energy input with an efficiency of 0.4% - 4% would suffice to keep 30% of the interstellar gas warm. The major problem lies as it always has done in preventing the warm material once formed from either being heated back to coronal temperatures or shock compressed back to cold cloud temperatures by the next SNR shock which passes it. In this respect moving the formation site to the relatively benign environment of the galactic halo via a fountain may help considerably. I believe that this problem can be solved and that when it is SDC-ISM models of the type described here will prove sufficiently robust to withstand the necessary changes.

Another problem of interest concerns the response of clouds to the arrival of interstellar shocks on intervals comparable with or much shorter than their dynamical timescale. To go much beyond the qualitative discussion of § 5.4.1 may require the availability of high resolution 3D hydrodynamic codes. However some aspects of the problem may be amenable to an extension of the sort of analytical procedure discussed in Chapter 5. A particular problem of interest which may be tractable is the excitation of turbulence by the external shocks, the interactions of turbulent eddies with one another and the clouds magnetic field and the eventual conversion of the turbulent energy into heat as envisaged by Cox (1979).

On the larger scale of spiral structure, the fact that the results obtained in Chapter 4 (a) describe the state of our Galaxy (and possibly others) fairly well and (b) indicate a narrow range of viable conditions in which the model sustains itself, suggest the operation of a feedback process to ensure that the constraints are obeyed. Since both the interarm supernovae and the planetary nebulae which provide most of the ionising flux there are old disk population objects such a process must almost certainly operate on the gas density. Supernova overproduction might drive much of the material into the hot phase and eventually reduce the star formation rate, however, the storage capacity of the halo may not be sufficient for this. Alternatively if molecular clouds can be made long lived a large

part of the interstellar gas might become locked up in them and feedback control might then be exercised through their process of formation as discussed by Seiden (1983) in a rather different context.

APPENDIX A : THE EVOLUTION OF AN EVAPORATION-DOMINATED SNR

A1 The Adiabatic Phase

Since the pressure of the ambient medium is assumed negligible the SNR is bounded by a strong shock for which the jump conditions are,

$$\rho_s = x\rho_o \quad u_s = \frac{X-1}{X}\dot{R}_s \quad P_s = \frac{X-1}{X^2}\rho_s \dot{R}_s^2 \quad T_s = \frac{\bar{u}}{K}\frac{X-1}{X^2}\dot{R}_s^2 \qquad (A1)$$

where ρ_s, u_s, P_s and T_s are respectively the density, velocity, pressure and temperature evaluated immediately behind the shock, ρ_o is the density in the ambient medium and $\dot{R}_s$ is the expansion velocity of the remnant. When conduction is unimportant the density jump, $X = 4$ (for $\gamma = 5/3$); if conduction carries a heat flux per unit area $\rho_o \dot{R}_s^3 F/2$ toward the shock then $X = [5 + 3(1 - 16F/9)^{\frac{1}{2}}]/2(1 + F)$ which is greater than (less than) four when F is less than (greater than) zero. It is convenient to introduce the various moments defined by,

$$I_\rho = 3\int_o^1 \hat{\rho}\hat{R}^2 d\hat{R}, \quad I_p = 3\int_o^1 \hat{P}\hat{R}^2 d\hat{R}, \quad I_k = 3\int_o^1 \hat{\rho}\,\hat{u}^2\hat{R}^2 d\hat{R}, \quad I_{ev} = \int_o^1 \hat{\chi}\hat{T}^{5/2}\hat{R}^2 d\hat{R} \qquad (A2)$$

where $\hat{R} \equiv R/R_s$, $\hat{\rho} \equiv \rho/\rho_s$ etc.

Then the total (thermal plus kinetic) energy within the remnant is,

$$E = \left[\frac{3}{2}\frac{X-1}{X^2}\frac{I_p}{I_\rho} + \frac{1}{2}\left(\frac{X-1}{X}\right)^2\frac{I_K}{I_\rho}\right] M \dot{R}^2 = \frac{3}{2}\frac{M}{\varepsilon}\left(\frac{\dot{R}}{\alpha}\right)^2 \qquad (A3)$$

In the second form $\varepsilon = [1 + (X - 1)\, I_K/3\, I_p]^{-1}$, is the ratio

of the thermal energy to the total energy, so that the parameter $\alpha = [X^2 I_\rho / (X-1) I_p]^{\frac{1}{2}}$ simply measures the ratio of the expansion velocity to the mass averaged isothermal sound speed within the remnant. During the adiabatic stage radiative losses are negligible and, by assumption, so are the losses due to interaction with the clouds, so that E is constant and equal to the energy of the supernova explosion.

The secular increase of the mass within the remnant is governed by,

$$\frac{dM}{dt} = \frac{4\pi}{3} R_s^3 \bar{\chi}(R_s) \bar{T}^{5/2} + 4\pi R_s^2 \rho_o \dot{R}_s \qquad (A4)$$

where the first term on the right is $\dot{M}_{ev}$ the rate at which mass is injected by evaporation (equation 4.2-7) and the second term is $\dot{M}_{sw}$ the rate at which ambient gas is swept into the remnant as it expands. Note that in terms of the moments defined above the mass averaged temperature and evaporation parameter are given by,

$$\bar{T} = \frac{I_p}{I_\rho} T_s, \quad \bar{\chi}(R_s) = \chi(\bar{P}) I_\rho^{5/2} I_p^{-(5/2+\omega)} I_{ev} \equiv \chi(\bar{P}) \phi_{SNR} \qquad (A5)$$

In order to solve equations B3 and B4 for the expansion law I assume that α, ε and ϕ_{SNR} are constant. Strictly this requires that the remnants evolution is self similar. As discussed by Chiéze and Lazareff (1981) such a similarity solution can only be found by making the ad hoc assumption

that the density of the ambient medium varies with distance from the explosion site as $\rho_o(R) \propto R^{-5/3}\chi(R)^{\frac{1}{3}}$. The ratio of $\dot{M}_{ev}$ to $\dot{M}_{sw}$ is then a constant. Not surprisingly, Chièze and Lazareff find that for $\dot{M}_{ev} \gg \dot{M}_{sw}$ a limiting solution is obtained in this case, which they argue will hold for evaporation dominated SNR irrespective of the form of distribution of the (vanishingly small) external density. Furthermore as I shall discuss below the numerical values of α, $\mathcal{E}$ and ϕ_{SNR} are quite insensitive to the precise runs of density, pressure and temperature within the remnant. Thus for a remnant evolving into a medium of constant density it is to be expected that as the relative importance of evaporation declines, the values of these constants will change slowly and smoothly from those found in the extreme evaporative limit, ultimately tending toward the (not very different) values found for SNR in the absence of evaporation.

Hence following MO I will rewrite equations B4 and B3 as,

$$\frac{dy}{dz} = \frac{4 + 3\omega}{3}\,\frac{z}{y^2}^{3(1+\omega)} + 3z^2 \qquad \omega \neq 5/3 \qquad (A6)$$

$$\frac{d\tau}{dz} = y^{\frac{1}{2}}$$

where $z = R_s/R_{es}$, $y = M/M_{es}$ and $\tau = t/t_{es}$ with,

$$R_{es} = \left[\frac{3}{4\pi^2}\,\frac{1}{4+3\omega}\left(\frac{\bar{u}}{k}\right)^{5/2}\frac{\chi(R_{es})}{\alpha}\,\frac{(\mathcal{E}E_o)^2}{\rho_o^3}\right]^{1/5},$$

$$M_{es} = \frac{4\pi}{3}R_{es}^3\rho_o, \quad t_{es} = \frac{R_{es}}{\alpha}\left(\frac{3\,M_{es}}{2\,E_o}\right)^{\frac{1}{2}}$$

In writing (A6) the pressure dependence of the evaporation parameter (equation 3.2-4) has been combined with the pressure radius relationship $\bar{P} \propto R_s^{-3}$ to obtain $\chi(\bar{P}) \propto R_s^{3\omega}$. Note that for $\omega < 5/3$ evaporation is the dominant source of mass at early epochs, $z < 1$, and declines in importance as z approaches unity; the condition $z \ll 1$ ensures that both $\dot{M}_{ev}/\dot{M}_{sw} \ll 1$ (Formally $\dot{M}ev/\dot{M}_{sw} = z^{3\omega-5}/(4+3\omega)$ and that the total mass added by evaporation exceeds the swept up mass. For $\omega > 5/3$ the converse is the case and the evaporative limit corresponds to $z \gg 1$.

An approximate solution to equation (A6) which is exact in both the evaporation dominated limit and in the opposite limit of negligible evaporation and provides an adequate interpolation for intermediate values is,

$$y \simeq z^{(4+3\omega)} + z^3 \left[1 - \frac{z^{(3\omega-5)/3}}{1+z^{(3\omega-5)/3}}\right]$$

$$\tau \simeq \frac{6}{10+3\omega} z^{(10+3\omega)/6} + \frac{2}{5} z^{5/2} \left[1 - \frac{15}{10+3\omega} z^{(3\omega-5)/6} \left(1 + \frac{15}{10+3\omega} z^{(3\omega-5)/6}\right)^{-1}\right] \qquad \omega \neq 5/3 \quad (A7)$$

These relationships are shown in Fig. A1 together with the results from numerical integrations of equation (A6) for several values of ω.

For the limiting case $\omega = 5/3$, which satisfies the condition for self similarity, equations (A3) and (A4) can be integrated exactly to give,

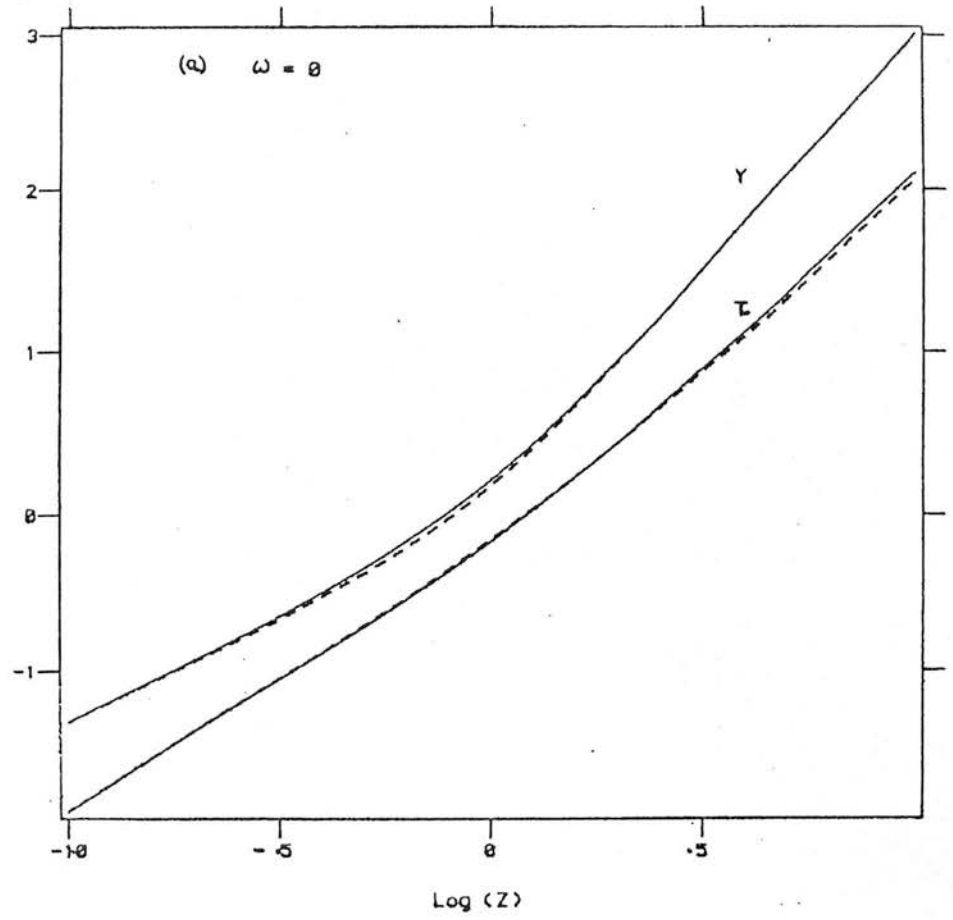

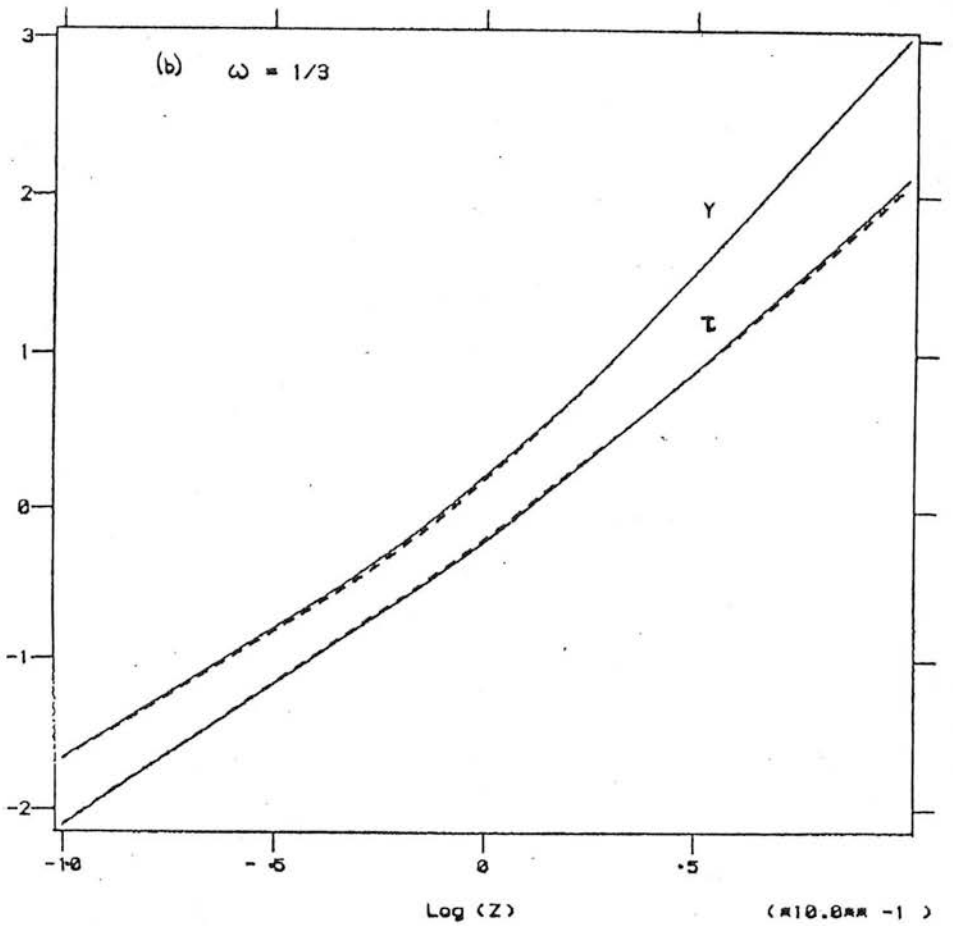

Figure A1 the normalised mass Y and normalised age τ as functions of normalised radius z for an evaporative SNR. Both axes are logarithmic. The solid lines show the exact results while the dashed lines show the results from the approximations given in the text. See text for details. Curves are plotted for four values of ω (a) $\omega = 0$ (b) $\omega = \frac{1}{3}$ (c) $\omega = 5/3$ (d) $\omega = 1.8$.

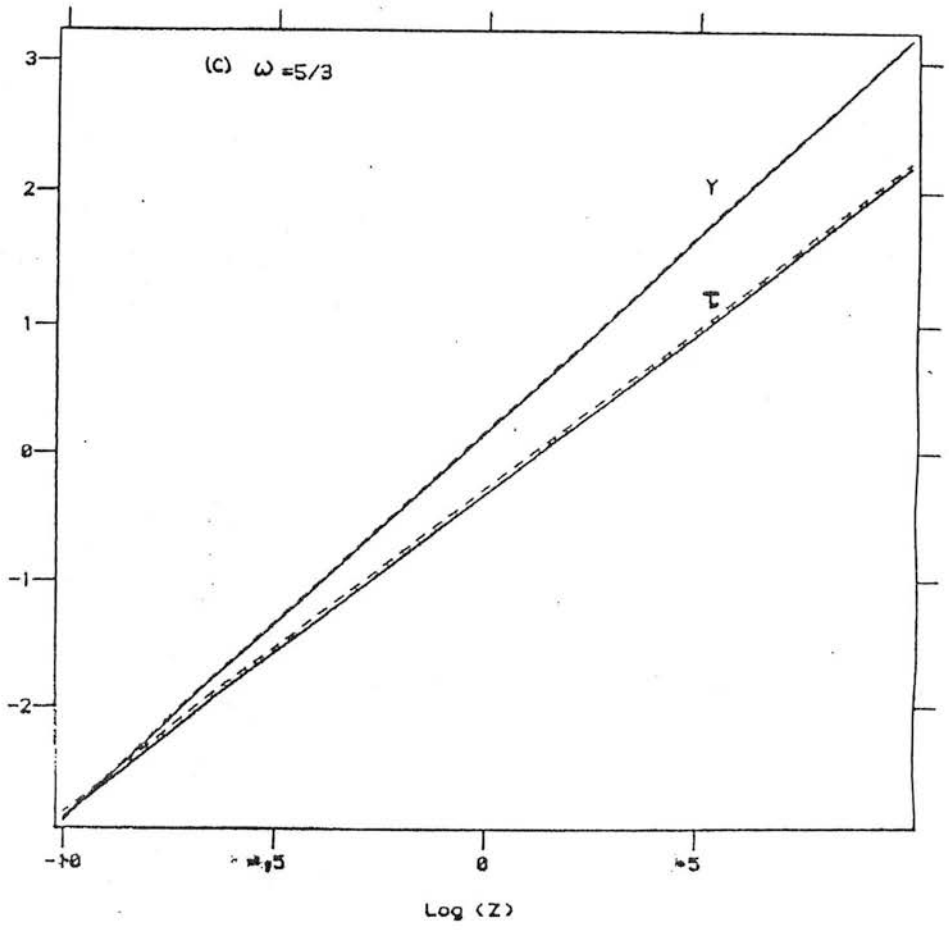
(c) ω =5/3
Y
τ
3
2
1
0
-1
-2
-1.0
-.5
0
.5
Log (Z)

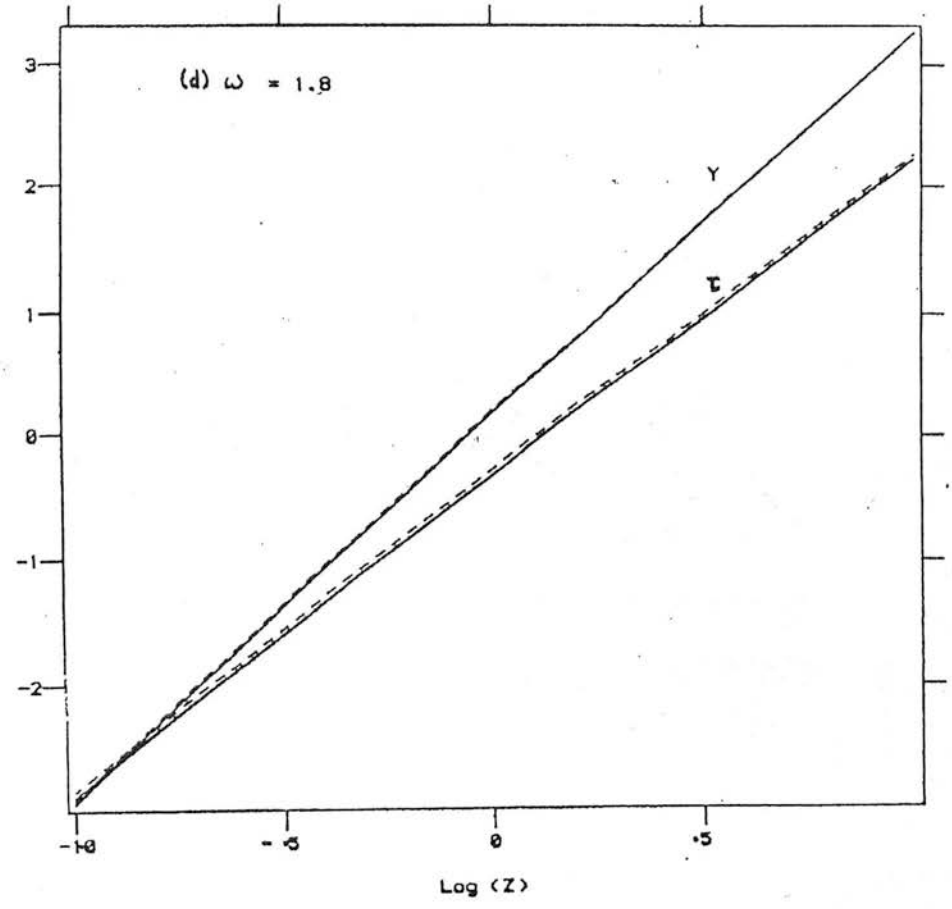
(d) ω = 1.8
Y
τ
3
2
1
0
-1
-2
-1.0
-.5
0
.5
Log (Z)

$$M = \frac{4\pi}{3} R^3 \bar{\rho}, \quad t = \frac{2}{5}\left(\frac{\varepsilon E_o}{2\pi\alpha^2 \rho_o}\right)^{\frac{1}{2}} R^{5/2}, \quad \bar{\rho} = \rho_o \, G\left[\left(\frac{3}{2}\frac{\rho_{ev}}{\rho_o}\right)^3\right]_{\omega=5/3} \quad (A8)$$

where,

$$\rho_{ev} = \left[\frac{1}{3\pi^2}\left(\frac{\bar{\mu}}{\bar{K}}\right)^{5/2} \frac{\bar{\chi}(R_o)}{R_o^5} \frac{(\varepsilon E_o)^2}{\alpha}\right]^{\frac{1}{3}}$$

$$G(\xi) = \frac{1}{3}\left[\left\{(\xi+1) + \left[(\xi+1)^2-1\right]^{\frac{1}{2}}\right\}^{\frac{1}{3}} + \left\{(\xi+1) - \left[(\xi+1)^2-1\right]^{\frac{1}{2}}\right\}^{\frac{1}{3}} + 1\right]$$

Note that, for this case, the importance of evaporation is measured by ρ_{ev}/ρ_o and the evaporative limit corresponds to $\rho_{ev} \gg \rho_o$;

as expected $\bar{\rho} \sim \rho_{ev}$ in this limit and $\bar{\rho} \sim \rho_o$ in the opposite limit.

For all values of ω the solution in the extreme evaporative limit which is employed in the text can be written,

$$M = \left(\frac{\eta}{1-\eta}\pi\left(\frac{\bar{\mu}}{\bar{K}}\right)^{5/2} \frac{\bar{\chi}(R)}{\alpha} (\varepsilon E_o)^2\right)^{\frac{1}{3}} R^{4/3}$$

$$t = \left(\frac{\pi}{(1-\eta)}\left(\frac{\eta}{\alpha}\right)^7\left(\frac{\bar{\mu}}{\bar{K}}\right)^{5/2} \bar{\chi}(R) (\varepsilon E_o)^2\right)^{1/6} R^{4/3} \quad (A9)$$

$$\bar{\chi}(R) = \bar{\chi}(R_o)\left(\frac{R}{R_o}\right)^{3\omega}$$

where R_o is any convenient radial scale (taken to be R_c in the text) and $\eta = 6/(10 + 3\omega)$. Although for the $\omega = 1.8$ case discussed in the text the evaporative limit solution is only applicable at late epochs, for the values of ρ_o and χ considered, the transition to the evaporation dominated regime occurs sufficiently early that equation (A9) is still appropriate.

The determination of the values of α, ε and ϕ_{SNR} requires knowledge of the runs of density, pressure, fluid velocity and cloud number density, which can only be obtained from a complete solution of the problem. However, the coefficient in the SNR expansion law depends on a combination of these quantities, from which most of the structural dependence cancels , raised to a very small power. Consequently, only very approximate values of the moments are required in order to determine the expansion law with high accuracy. It further follows that, even though the various complicating effects neglect in deriving equation (B9) may lead to substantial changes in the remnants structure, it will remain a good approximation.

For the $\omega = 0$ case in the extreme evaporative limit, $\alpha = 2.89$, $\varepsilon = 0.56$ and $\phi_{SNR} = 0.66$ when conduction is unimportant globally ("adiabatic" case) and $\alpha = 2.94$, $\varepsilon = 0.49$ and $\phi_{SNR} \simeq 1$ when conduction is sufficiently effective to render the remnant isothermal (Chiéze and Lazereff 1981). These values differ by $\sim 10\%$ from those obtained in the limit of negligible evaporation despite the considerable difference between the structures obtained in the two cases. For other values of ω I will first obtain limits on the values of the parameters from quite general considerations and then obtain approximate expressions for α and ε by analogy with the $\omega = 0$ solutions.

By symmetry the fluid velocity $\hat{U}$ must be zero at the origin and must increase monotonically and almost linearly with $\hat{R}$. Conduction tends to smooth the temperature profile and even in its absence the strong temperature dependence of the evaporation rate ($\propto T^{5/2}$) is sufficient to ensure that the temperature is almost uniform. From the definition of the moments it then follows that $0 \leqslant I_K/I_\rho \leqslant 1$, $\hat{T}_{min} \leqslant I_p/I_\rho \leqslant \hat{T}_{max}$ $0 \leqslant I_K/I_p \leqslant \hat{T}_{min}^{-1}$ and $\hat{T}_{min}^{5/2-w} \leqslant (I_{ev}/\langle\hat{\rho}^{-\omega}\rangle \leqslant \hat{T}_{max}^{5/2-w}$ $(\omega \leqslant 5/2)$ where $\hat{T}_{min} \leqslant 1$ and $\hat{T}_{max} \geqslant 1$ are the minimum and maximum values of T/T_s which occur within the remnant. Further, from elementary considerations, for values of $\omega > 0$ $\hat{T}_{min}(\omega) \gtrsim \hat{T}_{min}(\omega = 0) \sim 0.5$ for the adiabatic case and $X(\omega) \lesssim x(\omega = 0) \sim 8.5$ in the "isothermal" case. Hence for the "adiabatic" case $2.31\ \hat{T}_{max}^{-\frac{1}{2}} \lesssim \alpha \lesssim 3.26$, $0.5 \lesssim \varepsilon \leqslant 1$ and $(2/T_{max})^{5/2-w} \leqslant (\phi_{SNR}\langle\hat{\rho}\rangle^{-\omega}$ $/\langle\hat{\rho}^{-\omega}\rangle) \leqslant (2T_{max})^{5/2-w}$ while for the "isothermal" case $2 \lesssim \alpha \lesssim 3.1$, $0.28 \lesssim \varepsilon \leqslant 1$ and $\phi_{SNR} \equiv \langle\hat{\rho}^{-\omega}\rangle/\langle\hat{\rho}\rangle^{-\omega}$.

Rough values of α and ε can be obtained by noting that despite the more uniform density profiles, the majority of the mass of an evaporative SNR is still concentrated in a narrow zone near (although not at) the shock. By virtue of the form of $\hat{U}$, the kinetic energy is even more concentrated toward the edge. Consequently the "thin shell" approximation (Cavaliere and Messina, 1976) can still be used to give a crude estimate of the moments. In this the dynamics of the SNR are approximated by treating it as a thin pressure driven shell. Demanding consistancy between the expansion law

derived by integrating the equation of motion (equation A11) and equation (A9) then gives an estimate of I_p/I_ρ ($I_K/I_p = 1$ by assumption). From this I obtain

$$\alpha \sim [24/(4 + 3\omega)]^{\frac{1}{2}}, \quad \varepsilon \sim [1 + 9/(8 + 6w)]^{-1} \quad \text{"adiabatic"} \quad (A10$$

$$\alpha \sim 18/[(4+3w)(14+3w)^{\frac{1}{2}} + (14-3w)/(12+9w)]^{-1} \quad \text{"isothermal"}$$

which for $\omega = 0$ differ by $\lesssim 20\%$ from the exact results. It is rather more difficult to evaluate ϕ_{SNR}, however, since the computed solution show that ρ as well as T is crudely uniform, the limits given above ensure that ϕ_{SNR} does not differ greatly from unity.

Finally, it is straight forward to verify that the reduction of the evaporation rate due to saturation and complete cloud destruction does not seriously affect the remnants evolution. The expansion law when evaporation is saturated everywhere in the SNR can be obtained in exactly the same way as equation (A9). From this it follows that the transition to classical evaporation will occur when the remnant reaches a radius $R_{class} \sim 20_{pc}\ (\bar{\chi}/10^2 gs^{-1}K^{-5/2}pc^{-3})^{-1}(a_{cl}/pc)^{-1}$. The mass enclosed by the remnant and its age are then ~ 0.98 and ~ 1.5 of the values obtained from equation (A9). Similarly when the remnants evolution is limited by complete destruction of the warm clouds the SNR will expand roughly according to the Sedov equation for a uniform medium of density $\sim n_w f_w$. Equation (A9) then becomes appropriate for radii greater than $R_{dest} \sim 30pc\ (E_o/10^{51}erg)^{2/5}$, $(\bar{\chi}/10^2 gs^{-1}K^{-5/2}pc^{-3})^{1/5}(n_w f_w/0.1\ cm^{-3})^{-3/5}$ where the

enclosed mass and age are respectively ~ 0.8 and ~ 1.6 times the values from equation (B9). Since the departures from the evaporative limit solution are quite small and since typically neither transition radius is much larger than the radius at blast wave formation it follows that the neglect of these effects will not seriously vitiate my results.

A2 Snow Plough Solutions

The evolution of a thin, pressure driven shell is governed by the equations of mass and momentum conservation,

$$M = M_c + \frac{4\pi}{3}(R^3 - R_c^3)\rho_o$$
$$\frac{d}{dt}(M\dot{R}) = 4\pi R^2 (P - P_o) \qquad (A11)$$

subject to the boundary conditions $M = M_c$, $\dot{R} = \dot{R}_c$, $P = P_c$ and $R = R_c$ at $t = t_c$. Here P_o and ρ_o are the pressure and density of the gas external to the shell. I will assume that PdV losses dominate over radiative cooling and thermal conduction in the shells' interior so that $P \propto R^{-5}$. Then introducing the dimensionless variables $X = R/R_c$, $\tau = (\dot{R}_c/R_c)t$, $M_* = \left[(3M_c/4\pi R_c^3\rho_o) - 1\right]$ and $X_p = (P_c/P)^{1/5}$ it is readily shown that (A11) has the first integral,

$$(M_* + X^3)\frac{dX}{d\tau} = 3\left(\frac{P_c}{\dot{R}_c^2\rho_o}\right)^{\frac{1}{2}} \frac{1}{X}\left[\Omega X^2 + 2X^3 - M_* - \frac{2}{3}\left(\frac{X}{X_p}\right)^5\left(M_* - \frac{X^3}{4}\right)\right]^{\frac{1}{2}}$$

(A12)

$$\Omega = \frac{1}{3}\frac{\dot{R}_o^2\rho_o}{P_c}(M_* + 1)^2 + (M_* - 2) + \frac{2}{3}\frac{(M_* + \frac{1}{4})}{X_p^5}$$

In general (A12) cannot be integrated in closed form, however, I note the following limiting cases: (1) when M_* is very large so that the forces acting on the shell are negligible compared to its inertia then the shell expands at constant velocity and $R \propto t$; (2) when both P_c and P_o are small compared to the ram pressure, $\dot{R}^2\rho_o$, the right hand side of (A12) tends to zero and the shell expands as a

pure momentum driven snow plow. For small M_* the expansion law then follows the Oort (1951) solution which has the late time asymptote $R \propto t^{\frac{1}{4}}$; (3) when P_o and M_* are small the remnant expands at late times, according to the pressure modified snow plough solution of MC with $R \propto t^{2/7}$.

For the case of the cooled shell at the outer edge of an SNR, if the pre-cooling evolution is described by $R \propto t^{\eta}$ and if the shell contains a fraction δ of the mass within the remnant at the cooling point then $t_c = \eta R_c/\dot{R}_c$ and $P_c/\dot{R}_c^2 \rho_o = (M_* + 1)\left[(1-\delta)/\delta\right]$ are the appropriate boundary conditions. Further, from the results of Appendix B1 $M_* \simeq \left[\delta(R_c/R_{es})^{(5+3w)/3} - 1\right]$ provided the SNR is still evaporation dominated at the cooling point ($R_c \ll R_{es}$). Typically I anticipate $R_c \sim R_{es}$ so that $M_* \sim 0\text{-}10$, while in §4.2.3 I will show that $X_p \sim 1\text{-}2$ for the SDC-ISM.

Figure A2 shows the results of numerical integrations of (A12) for various values of M_* and X_p with $\eta = 5/3$ and $\delta = \frac{1}{2}$ for purposes of illustration. The curves for the case of negligible external pressure show the expected limiting behaviour when $M_* = 0$ and $M_* = \infty$; at intermediate values of M_* the expansion law can approximately be described by $R \propto t^{\eta'}$ with η' slowly changing from ~ 1 to $\sim 2/7$ as X^3 becomes greater than M_*. Because the internal pressure falls so precipitously the external pressure becomes important rather suddenly at $X = X_p$; for $X \sim X_p$ $\eta' \sim \frac{1}{4}$ as expected

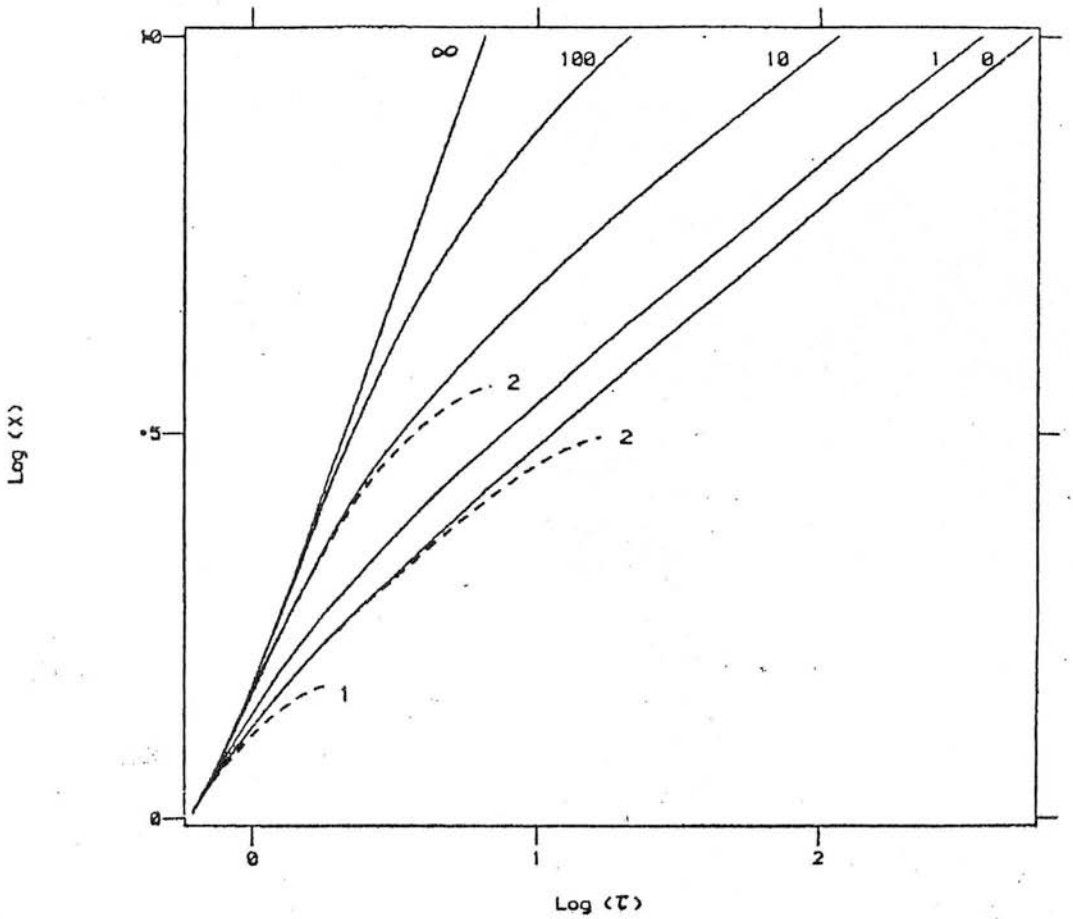

Figure A2 the normalised radius X as a function of normalised age τ for a pressure driven snow plow. The solid lines show the evolution when the external pressure is zero ($X_p = \infty$) and are labelled by the value of M_*. The dashed lines show the modification of representative trajectories brought about by a finite external pressure and are labelled by the value of X_p. Both axes are logarithmic.

from the Oort (1951) solution. The shell continues to expand beyond X_p because of its momentum; if it remains intact the external pressure will eventually halt, and indeed reverse, the shells motion. Since the decelerating shell is Rayleigh-Taylor unstable it is more likely that it breaks up; the resulting fragments will then continue to expand approximately according to the Oort solution until their velocity becomes comparable with the typical random velocity of clouds in the ambient medium.

For the parameter range $1 \lesssim M_* \lesssim 10$, $1 \lesssim X_p \lesssim 2$ anticipated above a reasonable approximation to the expansion law for $X \lesssim X_p$ is therefore $R \propto t^{\eta'}$ with η' a constant in the range $2/7 \lesssim \eta' \lesssim 1$.

REFERENCES

Abbott, D.C., 1978. Astrophys. J., 225, 893.

Abbott, D.C., 1982. Astrophys. J., 263, 723.

Abbott, D.C., Beiging, J.H. & Churchwell, E., 1981. Astrophys. J., 250, 645.

Abbott, D.C., Beiging, J.H., Churchwell, E.& Gassinelli, J.P., 1980. Astrophys. J., 238, 196.

Abramowitz, M. & Stegun, I. 1970 'Handbook of Mathematical Functions' Dover.

Arnaud, M. & Rothenflug, R., 1980. Astr. Astrophys., 87, 196.

Arnett, W.D. & Lerche, I., 1981. Astr. Astrophys., 95, 308.

Balbus, S.A. & McKee, C.F., 1982. Astrophys. J. 252, 529.

Bally, J. 1980, in 'Interstellar Molecules' ed. B.H. Andrew, p. 151.

Barlow, M.J., Smith, L.J. & Willis, A.J., 1981. Mon. Not. R. Astr. Soc. 196 101.

Batchelor, G.K., 1967. 'An Introduction to Fluid Dynamics', CUP, Cambridge.

Biermann, P., Kippenhahn, R., Tscharnutter, W. & Yorke, H., 1972. Astr. Astrophys. 19, 113.

Blaauw, A., 1964. Ann. Rev. Astr. Astrophys., 2, 213.

Blandford, R.D., 1982. In 'Supernovae : A Survey of Current research', eds. M.J. Rees & R.J. Stoneham, Reidel, Dordrecht p 459.

Blandford, R.D. & Cowie, L.L., 1982. Astrophys. J. 260, 625.

Blitz, L., 1978. PhD Thesis University of Columbia.

Blitz, L. & Shu, F.H., 1980. Astrophys. J., 238, 148.

Bodenheimer, P., Yorke, H.W. & Tenorio-Tagle, G. Preprint.

Bradly, J.N., 1962. 'Shock Waves in Chemistry and Physics', Methuen, London.

Brand, P.W.J.L., 1982. Mon. Not. R. Astr. Soc. 197, 217.

Brand, P.W.J.L. & Heathcote, S.R., 1982. Mon. Not. R. Astr. Soc. 198, 545.

Brand, P.W.J.L. & Zealy, W.J., 1975. Astr . Astrophys. 38, 363.

Bregman, J.N., 1980. Astrophys. J. 236, 577.

Brinks, E., 1981. Astron. Astrophys., 95, LI.

Brown, R.H. & Gould, R.J., 1970. Phys. Rev. D., 1, 2252.

Bruhweiler, F.C., Gull, T.R., Kafatos, M & Sofia, S., 1980. Astrophys. J., 238, L 27.

Burstein, P., Borken, R.J., Kraushaar, W.L. & Sanders, W.T., 1977. Astrophys. J., 213, 405.

Burton, W.B., 1976. Ann. Rev. Astr. Astrophys., 14, 275.

Burton, W.B. & Gordon, M.A., 1978. Astron. Astrophys. 63, 1

Bychcov, K.V. & Pikel'ner, S.B. 1975 Sov. Ast. Lett. 1, 14.

Cahn, J.H. & Wyatt, S.P., 1978. in 'Planetary Nebulae', ed. Y. Terzian Reidel Dordrecht P3.

Casinelli, , 1979. Ann. Rev. Astr. Astrophys. 17,

Castor, J., McCray, R. & Weaver, R., 1975. Astrophys. J. 200, L107.

Caswell, J.L. & Lerche , I., 1979(a) Mon. Not. R. Astr. Soc. 187, 201.

Caswell, J.L. & Lerche , I., 1979(b) Proc. Astr. Soc. Australia, 3, 343.

Cavaliere, A & Messina, A., 1976. Astrophys. J. 209, 424.

Chevalier, R.A., 1974. Astrophys. J. 188, 501.

Chevalier, R.A., 1977. Ann. Rev. Astr. Astrophys. 15, 175.

Chevalier, R.A., 1981(a) Fundam. Cosmic Phys. 7, 1.

Chevalier, R.A., 1981(b) Astrophys. J. 246, 267.

Chevalier, R.A. & Theys, J.C., 1975. Astrophys. J. 195, 53.

Chevalier, R.A. & Oergerle, W.R. 1979. Astrophys. J. 227, 398.

Chios i, C., Nasi, E. & Sreenivasan, S.R., 1978. Astr. Astrophys. 63, 103.

Chièze, J.P. & Lazeref, B., 1980. Astr. Astrophys., 91, 290.

Chièze, J.P. & Lazeref, B., 1981. Astr. Astrophys., 95, 194.

Clark, D.H. & Caswell, J.L. 1978. Mon. Not. R. Astr. Soc. 187, 201.

Clark, D.H. & Stevenson, F.R. 1977(a) Mon. Not. R. Astr. Soc. 179, 87p.

Clark, D.H. & Stevenson, F.R. 1977(b) 'The Historical Supernovae' Pergamon, New York.

Clark, D.H. & Stevenson, F.R., 1981. in 'Supernovae : A Survey of Current Research' eds. M.J. Rees & R.J. Stoneham, Reidel, Dordrecht, p. 355.

Cohen, R.S., Cong,H. Dame, T.M. & Thaddeus, P., 1980. Astrophys. J. 239, L53.

Cohen, R.S. & Thaddeus, P., 1977. Astrophys. J. 217, L155.

Coleman, G.D. & Worden, S.P., 1976. Astrophys. J. 205 475.

Coleman, G.D. & Worden, S.P., 1977. Astrophys. J. 218, 792.

Conti, P.S. 1978. Ann. Rev. Astr. Astrophys. 16, 371.

Conti, P.S. 1982 in 'Wolf-Rayet Stars : Observations, Physics, Evolution' eds. C.W.H. deLoore & A.J. Willis Reidel Dordrecht p3.

Conti, P.S. & McCray, R. Science 208, 9.

Contopoulos, G. 1973 in 'Dynamical Structure and Evolution of Stellar Systems', eds. L. Martinet & M. Mayer, Geneva obs., P1.

Cowie, L.L. 1980 Astrophys. J. 236, 868.

Cowie, L.L. 1981 Astrophys. J. 245, 66.

Cowie, L.L., Jenkins, E.B., Songaila, A. & York, D.G., 1979 Astrophys. J., 232, 467.

Cowie, L.L. & McKee, C.F. 1977 Astrophys. J. 211, 135.

Cowie, L.L., McKee, C.F. & Ostriker, J.P., 1981. Astrophys. J. 237, 908.

Cowie, L.L. & Songaila, A., 1977. Nature 266, 501.

Cowie, L.L. & Songaila, A., 1983. cited by Cowie et al. 1981 op. cit.

Cox, D.P., 1972. Astrophys. J. 178, 159.

Cox, D.P., 1979. Astrophys. J. 234, 863.

Cox, D.P., 19 . Astrophys. J. 245, 534.

Cox, D.P. & Anderson, P.R., 1982. Astrophys. J. 253, 268.

Cox, D.P. & Franco, J., 1981. Astrophys. J. 253, 268.

Cox, D.P. & Smith, B.W., 1974. Astrophys. J. 189, L105.

Crovisier J., 1981. Astr. Astrophys., 94, 162.

Currie I.G. 1974. 'Fundamental Mechanics of Fluids'. McGraw-Hill.

Dalgarno, A. & McCray, R.A., 1972. Ann. Rev. Astr. Astrophys. 10, 375.

de Jong, T., 1980. Heighlights of Astronomy. 5, 301.
de Loore, C., 1982 'Wolf-Rayet Stars - Observations, Physics, Evolution' C.de Loore ed P313
de Loore, C., De Greve, J.P. & Lamers, H.J.G.L.M., 1977. Astr. Astrophys., 61, 251.

de Vaucoleurs, G., 1979 in 'The Large Scale Characteristics of the Galaxy' ed. W.B. Burton, Reidel, Dordrecht, P 203.

Dickey, J.M., Salpeter, E.E. & Terzian, Y., 1977. Astrophys. J. 211, L77.

Dickey, J.M., Salpeter, E.E. & Terzian, Y., 1978. Astrophys. J. Suppl. 36, 77.

Dickey, J.M., Salpeter, E.E. & Terzian, Y., 1979. Astrophys. J. 228, 465.

Draine B.T., 1978. Astrophys. J. Suppl. 36, 595.

Dyson, J.E., 1981 in 'Investigating the Universe' ed. F.D. Kahn Reidel, Dordrecht, p 125.

Dyson, J.E. & Gulliford, P. 1975. Astrophys. Space Sci., 37, 477.

Elmegreen, B.G. 1975. Astrophys. J. 198, L31.

Elmegreen, B.G. 1976(a) Astrophys. J. 205, 405.

Elmegreen, B.G. 1976(b) Astrophys. J. Suppl. 32, 147.

Elmegreen, B.G. 1978 in 'Large Scale Characteristics of the Galaxy' eds. F.J. Kerr & B. Zuckerman Reidel Drodrecht.

Elmegreen, B.G. 1979. Astrophys. J. 231, 372.

Elmegreen, B.G. 1982(a). Astrophys. J. 253, 634.

Elmegreen, B.G. 1982(b). Astrophys. J. 253, 655.

Elmegreen, D.M. 1980. Astrophys. J. Suppl. 43, 37.

Elmegreen, D.M. 1981. Astrophys. J. Suppl. 47, 229.

Elmegreen, B.G. & Chiang, H., 1982. Astrophys. J. 253, 666.

Elmegreen, B.G., Dickinson, D.F. & Lada, C.J. 1978. in 'Protostars & Planets' ed. T. Gehrels, University of Arizona Press, Tuscon Arizona.

Elmegreen, B.G. & Elmegreen, D.M., 1983. Mon. Not. R. Astr. Soc.203, 31.

Elmegreen, D.M. & Elmegreen, B.G., 1982. Mon. Not. R. Astr. Soc. 201, 1021.

Elmegreen, B.G. & Lada, C.J. 1977. Astrophys. J. 214, 725.

Falle, S.A.E.G., 1975. Mon. Not. R. Astr. Soc. 172, 55.

Falle, S.A.E.G., 1981. Mon. Not. R. Astr. Soc. 195, 1011.

Falle, S.A.E.G., & Garlick, A.R. 1982. Mon. Not. R. Astr. Soc., 201, 635.

Feitzinger, J.V. & Schmidt-Kaler, Th. , 1980. Astr. Astrophys., 88, 41.

Field, G.B., 1965. Astrophys. J. 142, 531.

Field, G.B., Goldsmith, D.W. & Habbing, H., 1969. Astrophys. J. 155, L49.

Field, G.B. & Hutchings, J., 1968. Astrophys. J. 153, 737.

Field, G.B. & Saslaw, W.C., 1965. Astrophys. J. 153, 737.

Fleck, R.C., 1981. Astrophys. J. 246, L151.

Fujimoto, M. 1968 in 'Non Stable Phenomena in Galaxies' ed V.A. Ambartsumian P 453.

Garmany, C.D., Conti, P.S., & Chiosi, C. 1982. Astrophys. J. 263, 777.

Garmany, C.D., Olson, G.L., Conti, P.S. & Van Steenburg, M.E. 1981 Astrophys. J.

Gerola, H. & Seiden, P.E., 1978. Astrophys. J. 223, 129.

Gerola, H. & Seiden, P.E., 1979. in 'Phometry and Kinematics of Galaxies'.

Gerwin, R.A., 1968. Rev. Mod. Phys., 40, 652.

Gordon, M.A. & Burton, W.B., 1976. Astrophys. J. 208, 346 (GB)

Graham, J.A. & Lawrie, D.G., 1982. Astrophys. J. 253, L73.

Greisen, E.W., 1976. Astrophys. J. 203, 371.

Guibert, J., Lequeux, J. & Viallafond, 1978. Astr. Astrophys. 68, 1 (GLV)

Gull, S.F., 1973. Mon. Not. R. Astr. Soc. 161, 47.

Gull, S.F., 1975. Mon. Not. R. Astr. Soc. 171, 263.

Habe, A, & Ikeuchi, S., 1980. Prog. Theor. Phys., 64, 1995.

Habe, A., Ikeuchi, S. & Tanaka, Y.D., 1981. Pub. Astr. Soc. Japan 33, 23.

Hartquist, T.W. & Snijders, M.A.J., 1982. Nature 299, 783.

Hausman, M.A., 1981. Astrophys. J. 245, 72.

Hausman, M.A., 1982. Astrophys. J. 261, 532.

Heathcote, S.R. & Brand, P.W.J.L., 1983. Mon. Not. R. Astr. Soc. 203, 67.

Heiles, C., 1975. Astrophys. J. Suppl. 20, 37.

Heiles, C., 1979. Astrophys. J. 229, 553.

Heiles, C., 1980. Astrophys. J. 235, 833.
Herbst, W. & Assousa, G.E. 1977 Astrophys. J. 217, 473
Higdon, J.C. & Lingenfelter, R.E., 1980. Astrophys. J. 239, 867.

Hobbs, L.M., 1974a. Astrophys. J. 191, 395.
Hobbs, L.M., 1974b. Astrophys. J. 191, 381.
Hu, E.M., 1981. Astrophys. J. 248, 119.

Hulsbosch, A.N.M., 1975. Astr. Astrophys. 40, 1.

Hulsbosch, A.N.M., 1979. in 'Large Scale Characteristics of the Galaxy' ed. W.B. Burton Reidel, Dordrecht, p 525.

Huntly, J.M. & Gerola, H., 1981 Astrophys. J. 248, L69.

Ikeuchi, S., 1978. Pub. Ast. Soc. Japan, 30, 563.

Imshenik, V.S., 1960, Soviet Phys. Dokl., 5, 523.

Jackson, P.D. & Kellman, S.A., 1974. Astrophys. J. 190, 53.

Jenkins, E.B., 1978(a). Astrophys. J., 219, 845.

Jenkins, E.B., 1978(b). Astrophys. J., 220, 107.

Jenson, E.B., Talbot, R.J. & Dufour, R.J., Astrophys. J., 243, 716.

Jones, E.M., 1973. Astrophys. J. 182, 559.

Jones, E.M., 1975. Astrophys. J. 201, 377.

Jones, E.M., Smith, B.W., Straka, W.C., Kodis, J.W. & Guitar, H., Astrophys. J. 232, 129.

Jura, M., 1976 Astrophys. J. 206, 691.

Kafatos, M., Sofia, S., Bruhweiler, F. & Gull, T. Astrophys. J. 242, 294.

Kahn, F.D., 1972 in 'Interstellar Matter' Geneva Obs. P 343.

Kahn, F.D., 1975 in '14th International Cosmic Ray Conference' 11, 3566.

Kahn, F.D., 1976, Astr. Astrophys. 50, 145.

Kahn, F.D., 1981 in 'Investigating the Universe' ed. F.D. Kahn Redel, Dordrecht, P 1.

Kahn, F.D. & Dyson, J.E., 1965. Ann. Rev. Astr. Astrophys. 3, 47.

Kalnajs, A.J., 1972. Astrophys. J. 175, 63.

Kaufman, M. 1979a Astrophys. J. 232, 707.

Kaufman, M., 1979b Astrophys. J. 232, 717.

Kaufman, M., 1981. Astrophys. J. 250, 534.

Kenicutt, R.C., 1983. Astrophys. J. 272, 54.

Knude, J., 1979. Astr. Astrophys. Suppl. 38, 407.

Knude, J. 1981. Astr. Astrophys. 98, 74.

Kormandy, J. 1982 in 'Morphology and Dynamics of Galaxies' Geneva Obs.

Kormandy, J. & Norman, C.A., 1979. Astrophys. J. 233, 539.

Kraushaar, W.L., 1977 invited lecture at Honolulu AAS Meeting, Wisconsin Preprint.

Kraushaar, W.L., 1979 in 'X-Ray Astronomy' eds. W.A. Baity & L.E. Peterson Pergamon Press P 293.

Krebbs, J. & Hillebrandt, W. 1983 Preprint MPA 60

Kwan, J., 1979 Astrophys. J. 229, 567.

Kwan, J. & Valdes, F., 1983. Astrophys. J. 271, 604.

Larson, R.B., 1979 Mon. Not. R. Astr. Soc. 186, 479.

Larson, R.B., 1982.Mon. Not. R. Astr. Soc. 200, 159.

Lerche, I., 1981 Astrophys. Space Sci. 74, 273.

Lequeux, J. 1980 'Star Formation' SAASFEE Geneva Obs. P77.

Levinson, F.H. & Roberts, W.W. Astrophys. J. 245, 465.

Linn, C.C., 1967 Ann. Rev. Astr. Astrophys. 5, 453.

Lin, C.C. & Shu, F.H., 1964 Astrophys. J. 140, 646.

Lin, C.C. & Shu, F.H., 1966 Proc. Nat. Acad. Sci. 55, 229.

Liszt, H.S., 1982. Astrophys. J. 262, 198.

Lozinskya, T.A., 1980. Astr. Astrophys. 84, 26.

Lynds, B.T., 1980. Astron. J. 85, 8.

Lyne, A.G., 1982 in 'Supernovae : A Survey of Current Research', eds. M.J. Rees & R.J. Stoneham, Reidel, Dordrecht, P. 405.

Maddore, B.F., 1977 Mon. Not. R. Astr. Soc. 178, 1

Mark, J.W-K 1976 Astrophys. J. 205, 363.

Mark, J.W-K 1977 Astrophys. J. 212, 645.

Manchester, R.N., Whiteoak, J.B., Robinson, B.J., Otrupchek, R.E. & Rennie, C.J. CSIRO, Preprint No. RPP 2682.

Mathews, W. & Baker, J. 1971. Astrophys. J. 170, 241.

Mathews, W.G. & O'Dell, C.R., 1967 Ann. Rev. Astr. Astrophys.J.7, 67.

Mathewson, D.S., Van der Kruit, P.C. & Brown, W.N., 1972. Astr. Astrophys. 17, 468.

Mathewson, D.S., Ford, V.L., Dopita, M.A., Tuohy, I.R., Long, K.S. & Helfand, D.J., 1982. Astrophys. J. Suppl. 51, 345.

Maza, J. & Bergh, S. Van Den, 1976 Astrophys. J. 204, 519.

Mazurek, T.J., 1980 Astron. Astrophys., 90, 65.

McCammon, D., Burrows, D.N., Sanders, W.T. & Kraushaar, W.L. 1983 Astrophys. J. 269, 107.

McCray, R. & Snow, T.P. Jr. 1979 Ann. Rev. Astr. Astrophys. 17, 213.

McKee, C.F. 1982 in 'Supernovae : A Survey of Current Research' eds. M.J. Rees & R.J. Stoneham, Reidel, Dordrecht, P 433.

McKee, C.F. & Cowie, L.L., 1975 Astrophys. J. 195, 715.

McKee, C.F. & Cowie, L.L., 1977 Astrophys. J. 215, 213.

McKee, C.F., Cowie, L.L. & Ostriker, J.P., 1978 Astrophys. J. 219, L23.

McKee, C.F. & Holenbach, D.J., 1980. Ann. Rev. Astr. Astrophys. 18, 219.

McKee, C.F. & Ostriker, J.P., 1977. Astrophys. J. 218, 148 (MO)

Meaburn, J., 1983. Highlights of Astronomy 6, 655.

Mebold, V., Winnberg, A., Kalberla, P.M.W. & Goss, W.M. 1982. Astr. Astrophys.

Mezger, P.G., 1978 Astr. Astrophys. 70, 565.

Miller, G.E. & Scalo, J.M., 1979 Astrophys. J. Suppl. 41, 513.

Milne, D.K., 1979 Austr. J. Phys. 32, 83.

Mirabell, I.F., 1981 Astrophys. J. 247, 97.

Mouschovias, T.Ch. 1976. Astrophys. J. 206, 753.

Mouschovias T.Ch., Shu, F.H. & Woodward, P.R., 1974. Astron. Astrophys. 210, 670.

Mouschovias, T.Ch. & Spitzer, L. Jr. 1976 Astrophys. J. 210, 326.

Mueller, M.W. & Arnett, W.D., 1976 Astrophys. J. 210, 670.

Nittman, J., 1981, Mon. Not. R. Astr. Soc. 197, 699.

Nittman, J., Falle, S.A.E.G. & Gaskell,P.H. 1982 Mon. Not. R. Astr. Soc. 201, 833.

Norman, C. & Silk, J. 1980 Astrophys. J. 238, 135.

Nulsen, P.E.J., 1982 Mon. Not. R. Astr. Soc. 198, 1007.

O'Dell, C.R., York, D.G. & Henize, K.G., 1967 Astrophys. J. 150, 835.

Oemler, A. & Tinsley, B.M. 1979 Astr. J. 84, 985.

Olano, C.A., 1982 Astr. Astrophys. 112, 195.

Oort, J.H., 1951 in 'Problems of Cosmical Aerodynamics' Central Air Force Documents Dayton Ohio P 118.

Oort, J.H., 1954. Bull. Astr. Inst. Netherlands 12, 77.

Oort, J.H., 1962 in 'Interstellar Matter in Galaxies' ed. L. Woltjer Benjamin, New York, P 234.

Oort, J.H. & Hulsbosch, A.N.M., 1978 in 'Astronomical Papers Dedicated to Bengt Stromgren' ed. J. Reiz, Copenhagen University Press, Copenhagen, P 409.

Osterbrock, D.E., 1974. 'Astrophysics of Gaseous Nebulae' Freeman.

Pagel, B.E.J. & Edmunds, M.G., 1981 Ann. Rev. Ast. Ap. 19, 77.

Panagia, N. 1973 Astron. J. 78, 929.

Parker, E.N. 1966 Astrophys. J. 145, 811.

Payne, H.E., Salpeter, E.E. & Terzian, Y. Astrophys. J. 272, 540.

Penston, M.V., Munday, V.A., Stickland, D.J. & Penston, M.J. 1969, Mon. Not. R. Astr. Soc. 142, 355.

Priete-Martinez, A., 1981 Astron. Astrophys. 96, 283.

Raymond, J.C., Cox, D.P. & Smith, B.W., 1976, Astrophys. J. 204, 290.

Reid, I.N. & Gilmore, G. Mon. Not. R. Astr. Soc. 200.

Reinhardt, M. & Schmidt-Kaler, Th., 1979 Astrophys. Space Sci., 66, 121.

Reynolds, R.J. & Ogden, P.M., 1979, Astrophys. J. 229, 942.

Richtmeyer, R.D., 1960 Comm. Pure Appl. Math. 13, 297.

Ride, S.K. & Walker, A.B.C Jr., 1977 Astr. Astrophys. 61, 339.

Roberts , W.W. 1969 Astrophys. J. 158, 123.

Roberts , W.W., 1977 Vistas in Astronomy 19, 91.

Roberts , W.W., 1983 in 'Kinematics, Dynamics and Structure of the Milky-Way' ed. W.L. Shuter Reidel Dordrecht.

Roberts , W.W., Hausman, M.A. & Levinson, F.H. in 'Internal Dynamics of Galaxies' ed. E.Athanassoula, Reidel, Dordrecht, P 131.

Roberts , W.W. & Shu, F.H., 1973 Astrophys. Lett. 12, 49.

Robinson, B.J., McCutcheon, W.H., Manchester, R.N. & Whiteoak, J.B., 1983 CSIRO Preprint No. RPP 2641.

Rohlfs, K. 1977, 'Lectures in Density Wave Theory' Springer.

Rosenburg, I., & Scheur, P., 1972 Mon. Not. R. Astr. Soc. 161, 27.

Salpeter, E.E., 1979 in IAU Symp. 84, Large Scale Characteristics of the Galaxy P 245, Ed. Burton, W.B., Reidel, Dordrecht.

Sanders, D.B., Soloman, P.M. & Scoville, N.Z. 1983 Preprint.

Sanders, R.H. & Huntly, J.M., 1976 Astro. J. 209, 53.

Savage, B.D., Bohlin, R.C., Drake, J.F. & Budich, W., 1977 Astrophys. J. 216,291.

Savage, B.D.,& de Boer, K.S., 1981 Astrophys. J. 243, 460.

Scalo, J.M. & Pumphrey, W.A. 1982 Astrophys. J. 258, L 29.

Scott, J.S., Jensen, E.B. & Roberts, W.W., 1977, Nature, 265, 123.

Scoville, N.Z. & Hersh, K., 1979 Astrophys. J. 229, 578.

Scovile, N. & Young, J.S., Astrophys. J. 265, 148.

Scheffler, H. 1967, Zeitschrift fur Astrophys. 65, 30.

Schmidt, M., 1959 Astrophys. J. 129, 245.

Schmidt-Kaler, Th. & Wiegandt, R., 1980. Astr. Astrophys., 89, 67.

Schwartz, J., McCray R. & Stein, R.F. 1972, Astrophys. J. 175, 673.

Schwartz, U.J. & Van Woerden, H., 1974 in 'Galactic Radio Astronomy' eds. Kerr, F.J. & Simonson, S.C.

Schweizer, F., 1976 Astrophys. J. Suppl. 31, 313.

Sedov, L., 1959, 'Similarity & Dimensional Methods in Mechanics. Academic New York

Seiden, P.E., 1983a in 'Kinematics, Dynamics and Structure of the Milky-Way' Ed. Shuter, W.L.H. Reidel Dordrecht, P. 259.

Seiden, P.E., 1083b Astrophys. J. 266, 555.

Seiden, P.E. & Gerola, H., 1979 Astrophys. J. 197, 621.

Seiden, P.E. & Gerola, H., 1982 Fund. Cosmic Phys. 7, 241.

Seward, F.D., Chlebowski, T., 1982. Astrophys. J. 256, 530.

Shapiro, P.R. & Field, G.B., 1976 Astrophys. J. 205, 762.

Sgro, A.G., 1975 Astrophys. J., 197, 621.

Shu, F.H., 1973 American Scientist, 61, 524.

Shu, F.H., 1978. IAU Symp. No. 77 'Structure and Dynamics of Nearby Galaxies' eds. Berkhuijsen, E.M. & Wielebinski, Dordrecht Reidel P 139.

Shu, F.H., Milione, V., Gebel, W., Yuan, C., Goldsmith, D.W. & Roberts, W.W. 1972 Astrophys. J. 173, 557.

Shu, F.H., Milione, V. & Roberts, W.W., 1973. Astrophys. J., 183, 819.

Shull, J.M., 1980a Astrophys. J. 237, 769.

Shull, J.M., 1980b Astrophys. J. 238, 860.

Silk, J. in "star Formation", SAAS FEE 10, Geneva obs. P170, 1980

Silk, J. & Solinger, A., 1973 Nature Phys. Sci. 244, 101.

Smith, B.W., 1977. Astrophys. J., 211, 404.

Smith, L.F., Biermann, P. & Mazger, P.G., 1978. Astr. Astrophys. 66, 65.

Snow, T.P., 1982 Astrophys. J. 253, L 39.

Solomon, P.M., Sanders, D.B. & Scoville, N.Z., 1979 in IAU Symp. 84, Large Scale Characteristics of the Galaxy, P. 35, ed. Burton, W.B., Reidel, Dordrecht.

Solomon, P.M., Barret, J. Sanders, D.B, & De Zafra, R. Astrophys. J. 266 L103 1983

Songaila, A., 1981 Astrophys. J. 248, 945.

Spitzer, L. Jr., 1956 Astrophys. J. 124, 20.

Spitzer, L. Jr., 1978 'Physical Processes in the Interstellar Medium' Wiley, London.

Spitzer, L. Jr. 1982a Astrophys. J. 262, 315.

Spitzer, L. Jr., 1982b 'Searching Between the Stars'

Stark, A.A. & Blitz, L., 1978 Astrophys. J. 225, L 15.

Sturock, P.A. & Stern, R. Astrophys. J. 238, 98.

Taff, L.G. & Savedoff, M.P. 1972 Mon. Not. R. astr. Soc. 160, 89
1973 Mon. Not. R. astr. Soc. 164, 357

Tammann, G.A., 1982 in 'Supernovae : A Survey of Current Research', eds. M.J. Rees & R.J. Stoneham Reidel, Dordrecht, P 371.

Tanaka, Y & Bleeker, J.A.M., 1977 Space Sci. Rev. 20, 815.

Taylor, G.T., 1950 Proc. R. Soc. A. 201, 192.

Taylor, J.H. & Manchester, R.N., 1977 Astrophys. J. 215, 885.

Tenorio-Tagle, G., 1980 Astro. Astrophys. 88, 61.

Tenorio-Tagle, G., 1981 Astr.Astrophys. 94, 338.

Tenorio-Tagle, G., 1982 in 'Regions of Recent Star Formation' eds. R.S. Rodger & P.E. Dewdney, Reidel, Dordrecht, P 1.

Tenorio-Tagle, G., Yorke, H.W. & Bodenheimer, P., 1983 Preprint.

Terlevich, R. & Melnick, J., 1983. ESO Preprint No. 264.

Thorogood, P.J., 1979. PhD Thesis, University of Leeds.
Tinsley, B.M. in 'Planetary Nebulae' IAU 76 Y. Terzian ed. P 341 1978
Tomisaka, K., Habe, A. & Ikeuchi, S., 1980 Prog. Theo. Phys. 64, 1587.

Tomisaka, K., Habe, A. & Ikeuchi, S., 1981 Astrophys. Space Sci. 78, 273.

Toomre, A., 1969 Astrophys. J. 158, 899.

Toomre, A., 1977 Ann. Rev. Astr. Astrophys. 15, 437.

Toomre, A., 1982 in 'The Structure and Evolution of Normal Galaxies' eds. S.M. Fall & D. Lynden-Bell CUP Cambridge P 111.

Torres-Piembert, S., Lazcano-Araujo, A., & Piembert, M., 1974 Astrophys. J. 191, 401.

Twarog, B.A., 1980 Astrophys. J. 242, 242.

Visser, H.C.D., 1980 Astro. Astrophys, 88, 149.

Wayte, R.C., Wynne-Jones, I. & Blades, J.C., 1978 Mon. Not. R. Astr. Soc. 182, 5p.

Weaver, H.F., 1979 in 'The Large Scale Characteristics of the Galaxy' ed. W.B. Burton Reidel, Dordrecht.

Wheeler, J.C., 1981 in 'Fundamental Problems in the Theory of Stellar Evolution' eds. Sugimoto, D., Lamb, D.Q., & Schramm, D.N. Reidell Dordrecht P285.

Wheeler, J.C. & Bash, F.N., 1977 Nature 268, 706.

Wheeler, J.C., Mazureck T.J. & Sivaramakrishnan, Astrophys. J. 237, 781.

Whitworth, A., 1979, Mon. Not. R. Astr. Soc. 186, 59.

Wielen, R., 1974, Pub. Astr. Soc. Pacific, 86, 341.

Woodward, P.R., 1975 Astrophys. J. 195, 61.

Woodward, P.R., 1976, Astrophys. J. 207, 484 (W76)

Woodward, P.R., 1978, Ann. Rev. Astr. Astrophys. 16, 555.

Woodward, P.R., 1979 in 'The Large Scale Characteristics of the Galaxy' ed. W.B. Burton Reidel, Dordrecht, (W79).

York, D.G., 1982 Ann. Rev. Astr. Astrophys. 20, 221

Young, J.S. & Scovile, N., 1982a Astrophys. J. 258, 467.

Young, J.S. & Scovile, N., 1982b Astrophys. J. 260, L 11.

Young, J.S. & Scovile, N., 1982c Astrophys. J. 260, L 41.

Zel'dovich Ya.B. & Raizer Yu. P., 1968. 'Elements of Gasdynamics and the Classical Theory of Shock Waves, Academic Press, New York.

Mon. Not. R. astr. Soc. (1982) 198, 545–562

Spiral arms and a supernova-dominated interstellar medium

P. W. J. L. Brand and S. R. Heathcote *University of Edinburgh, Blackford Hill, Edinburgh EH9 3HJ*

Received 1981 April 15; in original form 1980 December 17

Summary. Models of the interstellar medium (ISM) utilizing the large energy output of supernovae to determine the average kinematical properties of the gas, are subjected to an imposed (spiral) density wave.

The consequent appearance of the ISM is considered. In particular the McKee–Ostriker model with cloud evaporation is used, but it is shown that the overall appearance of the galaxy model does not change significantly if a modification of Cox's mechanism, with no cloud evaporation, is incorporated.

We find that a spiral density wave shock can only be self-sustaining if quite restrictive conditions are imposed on the values of the galactic supernova rate and the mean interstellar gas density.

1 Introduction

Since the work of Cox & Smith (1974) and its subsequent elaboration by McKee & Ostriker (1977, hereafter MO), it has been clear that supernova remnants (SNRs) play a major role in determining the state of the interstellar medium (ISM). Consequently some fraction of its volume must be occupied by a very hot, tenuous plasma. However, observational estimates of this fraction, mostly referring to the solar neighbourhood, vary from 10 per cent (Heiles 1980) to 80 per cent (Dwek & Scalo 1979; Higdon & Lingenfelter 1980). Furthermore, as stressed by Scott, Jensen & Roberts (1977), gas in such a hot state, occupying a large volume fraction throughout the galactic disc, might, by virtue of its high sound speed, prevent the formation of the strong shock waves, often invoked (Roberts 1969) to initiate star formation in spiral arms.

In response to this difficulty various attempts have been made recently, either to explain spiral structure independently of density waves (Seiden & Gerola 1979) or by only indirect appeal to density waves (Cowie 1980). Others have avoided the problem by suggesting that the hot component has a large volume filling factor only in spiral arms, the ISM between the arms remaining in a state capable of supporting density wave shocks (Scott *et al.* 1977; Reinhardt & Schmidt-Kaler 1979; Blitz & Shu 1980). Alternatively as suggested by Schmidt-Kaler & Weigandt (1980) the difficulty may not exist if the effective sound speed in the inhomogeneous medium is determined largely by the 'warm' component. This is discussed in Section 5.

In this paper we investigate, within the framework of the MO model, the consequences of assuming that (1) the pattern of the total mean density is similar to that predicted by two-armed spiral shocks, and (2) that the star formation rate and supernova rate are proportional to each other, and to some power of the local mean density. In Section 2 we shall briefly discuss modifications to the MO model necessary to permit its use in a time-dependent situation and describe the method we employ to calculate the variations of the supernova rate, ionizing photon emissivity and mean density. In Section 3 we describe the results for a spiral galaxy like the Milky Way. In Section 4, we discuss the importance of the cloud evaporation assumption, and by modifying Cox's (1979) discussion, show that similar results are predicted with a non-evaporative model. In the final section we consider the consequences of our results for galactic structure and examine what observational constraints might be imposed on the parameters of the model.

2 Assumptions

MO considered the consequences of the inhomogenous nature of the ISM for SNR evolution, within the framework of the Cox & Smith picture and found that, with the introduction of a number of simplifying assumptions, it was possible to develop a self-consistent model conforming with many of its observational properties. They picture the ISM as consisting of three more or less distinct components: (1) a hot low density plasma (HIM), filling 70–80 per cent of the interstellar volume, (2) cold, dense, neutral clouds (CNM) imbedded within the HIM and (3) warm, intermediate density, photo-ionized cloud coronae enveloping each cloud (WIM). The filling factor of the WIM is ~ 20 per cent while that of the CNM is only ~ 2 per cent although it contains most of the mass in the ISM. All three components are supposed to be in rough pressure equilibrium.

A fundamental ingredient in the MO scheme is the assumption that the thermal evaporation of clouds engulfed by a young SNR is sufficiently rapid for radiation to become important, permitting a transition to the 'snow-plough' phase, before either the external pressure becomes important, or the SNR radius becomes comparable with the scale height of the disc gas. For the time being we will assume that this is in fact the case, discussion of the opposite point of view advanced by Cox (1979) being postponed until Section 4. We will, however, include the effects of cloud geometry and of the dynamical response of the clouds to their surroundings in our model.

2.1 CLOUD DYNAMICS AND THE EVAPORATION RATE

From the work of Cowie & McKee (1977) and Cowie & Songaila (1977) the evaporation rate for a static spheroidal cloud imbedded in a medium of temperature T_h is given by,

$$\dot{M}_{ev} = 10^{4.44}\,\phi_m\,\phi_g(l)\,T_h^{5/2}\,a\,. \tag{1}$$

Here, a(pc) is the radius of a sphere having the same volume as the cloud and $\phi_g(l)$ is a geometrical factor which is unity for spherical clouds and increases with increasing major–minor axis ratio, l, for oblate or prolate spheroids. The constant ϕ_m is introduced to allow for partial quenching of thermal conduction by magnetic fields or turbulence. This equation ceases to be valid if the mean free path for electron energy exchange in the cloud becomes comparable to its dimensions ('saturation'), or if the rate of radiative cooling in the cloud envelope exceeds the rate of conductive heating so that the cloud grows by condensation. The saturated condition will always occur at a sufficiently early epoch in SNR evolution and its neglect leads to an overestimate of the net evaporation rate over the remnant's lifetime.

This effect is, however, relatively unimportant over the range of conditions considered here. Similarly, there are always some larger clouds in which radiative losses are important, however, with the steep cloud mass spectrum implied by observation (e.g. Hobbs 1974) and adopted here this is never important.

The surface pressure experienced by a cloud which is overrun by an SNR blast wave will increase sharply as the shock passes and then slowly decline as the remnant expands. The cloud's response to this changing surface pressure will be extremely complex (*cf.* Sgro 1975; McKee & Cowie 1975; Woodward 1976, 1979; Cox 1979) and large departures from pressure equilibrium are inevitable. Nevertheless, the cloud must relax back toward pressure equilibrium in a few times the cloud soundspeed crossing time τ_{cl}. Cowie & McKee (1977) found that in general the time-scale for evaporative flow in the cloud is very much shorter than τ_{cl} so that the cloud can be treated quasistatically and equation (1) will give the correct instantaneous evaporation rate.

If $\tau_{cl} \gg \tau_{SNR}$ (the mean interval between successive young SNRs overrunning a given cloud) *or* if evaporation plays an important role in SNR dynamics for a period $\tau_{ev} \ll \tau_{cl}$, then we can regard the cloud radius as a constant determined by the time averaged pressure it experiences. Conversely, if $\tau_{ev} \gg \tau_{cl}$ the cloud must remain close to pressure equilibrium with its immediate surroundings. Neglecting magnetic support and assuming the cloud remains isothermal we find in this latter case that the cloud radius a, varies with pressure P, according to

$$a(P) \propto P^{-\gamma}, \tag{2}$$

where $\gamma \simeq 1.8$ if recombination is sufficiently rapid to keep the cloud in ionization equilibrium or $\gamma = 1/3$ if the ionization state remains frozen. In practice we find that τ_{cl}, τ_{ev} and the recombination time-scale, τ_{rec}, are all of comparable magnitude so none of these cases is likely to be applicable in detail. Nevertheless, equation (2) with $\gamma = 0$, 1/3 and 1.8 may provide some general indication of the effects of cloud dynamics on the evaporation rate.

With the evaporation rate given by (1) and (2), a straightforward extension of the work of MO (see Appendix) leads to a system of equations which can be solved iteratively to yield values of several quantities of interest. We have undertaken an extensive series of calculations employing different values for the various constants which enter into the MO model. In the present context we wish to focus attention primarily on those quantities which are expected to change from point to point as a consequence of galactic structure. Consequently we have set the remaining quantities at the values chosen by MO, (these values are tabulated in the Appendix) except that we use supernova energy $E_0 = 5 \times 10^{50}$ erg, half the value used by MO. Our calculations confirm, however, that our results are not unduly sensitive to the choice of these other parameters. In particular we find that the cloud geometry chosen is unimportant and hence consider only the case of spherical clouds. Further, in what follows we will take $\gamma = 1/3$ although our results are not too sensitive to its value.

2.2 THE MODEL OF THE GALAXY

The quantities we have chosen to vary in our model are the local mean total density $\bar{n}$, the emissivity of ionizing photons ϵ_{uv}, and the supernova rate per cubic parsec S. MO selected values for these parameters based on observational data pertaining to the solar neighbourhood. Here we calculate their values by means of a simple semi-empirical galactic model, constructed within the framework of density wave theory.

In the TASS model (Roberts 1969, Shu, Milione & Roberts 1973) the variation of the gas

density along a representative streamline can be approximated by

$$\bar{n}(R, t) = \bar{n}_0(R)\ \{1 + (c - 1)\exp(-t/t_0)\}\ , \tag{3}$$

where t is the time since the last passage through the density wave shock and the decay time t_0 is of the order 3×10^7 yr. For simplicity we take c the density contrast or compression ratio, to be constant.

We obtain $\bar{n}_0(R)$ from the relation

$$\langle \bar{n}(R) \rangle = \int_0^{t_{\rm gal}(R)/2} \bar{n}(R, t)dt \simeq \bar{n}_0(R) \left\{1 + 2(1 - c)\frac{t_0}{t_{\rm gal}(R)}\right\} \equiv \bar{n}(R, \mathrm{H}^0) + 2\bar{n}(R, \mathrm{H}_2),$$

where $\bar{n}(R, \mathrm{H}^0)$ and $\bar{n}(R, \mathrm{H}_2)$ are the observed azimuthally smoothed densities of neutral and molecular hydrogen respectively. Here $t_{\rm gal}$ is the galactic rotation period in a frame rotating at the pattern speed of the spiral potential $\Omega_{\rm p}$, i.e.

$$t_{\rm gal}(R) = 2\pi/[\Omega(R) - \Omega_{\rm p}]\ ,$$

where $\Omega(R)$ is the angular rotation speed of the galaxy. In what follows $\Omega_{\rm p}$ is taken to be 13.5 km s^{-1} kpc^{-1} and we adopt a flat rotation curve such that $\Omega(R) = 250/R$ km s^{-1} kpc^{-1}.

While the galactic distribution of H^0 is quite well established (Burton 1976) that of H_2 must be inferred indirectly from observations of CO. Both the local value of the ratio $\bar{n}(\mathrm{H}_2)/\bar{n}(\mathrm{CO})$ and the question of a possible radial variation of this quantity (due to a galactic abundance gradient) remain controversial (Solomon, Sanders & Scoville 1979 (SSS); Guibert, Lequeux & Viallefond 1978 (GLV); Blitz & Shu 1980). We therefore consider three different H_2 distributions based on (i) the data of SSS, (ii) the data of Gordon & Burton (1976; GB) and (iii) the values obtained by GLV from the data of GB by assuming a smaller value for $\bar{n}(\mathrm{H}_2)/\bar{n}(\mathrm{CO})$ in the solar neighbourhood and incorporating a strong radial gradient of the carbon abundance. For the vertical distribution of both H^0 and H_2 we adopt a Gaussian form with scale heights of 160 and 70 pc respectively (Cohen & Thaddeus 1977).

The relationship between the gas density and the rate of star formation has been a subject of considerable controversy since the classic work of Schmidt (1959) who proposed on empirical grounds that on a large scale the star formation rate varies as some power m of the total gas density. Recently, GLV have used a comparison of the radial and vertical distribution of several tracers of recent massive star formation with that of the interstellar gas and found some justification for adopting $m \simeq 1.3$–2.5. A similar study by Smith, Biermann & Mezger (1978) based primarily on the distribution of giant H II regions led to a somewhat smaller value in the range 0.5–1.0. Conversely from consideration of the past history of star formation in the solar neighbourhood assuming a time independent initial mass function Miller & Scalo (1979) have deduced $m \lesssim 0.5$. We here employ the Schmidt law as a convenient parameterization relating the *local* star formation rate to the *local* mean total density and construct models employing $m = \frac{1}{2}$, 1 and 2. It should, however, be stressed that the observational tests refer only to properties smoothed over large regions.

We thus take the supernova rate to be given by

$$S(R, t) = S_0 \bar{n}(R, t - t_*)^m \qquad m = \tfrac{1}{2}, 1 \text{ or } 2\ , \tag{4}$$

where t_* is the 'lifetime' of the stars which give rise to supernova events, which we take to be of order 10^7 yr, comparable to observational estimates of the delay between the formation of a dust lane and the appearance of the first massive OB stars in external galaxies (Mathewson, van der Kruit & Brouw 1972). To obtain the constant of proportionality, S_0, we equate the integral of $S_0 \bar{n}(R, t)^m$ over the whole disc to the value of the total galactic supernova rate, $S_{\rm gal}$. Estimates for this latter quantity have been obtained by a number of

independent methods, but all are subject to severe selection effects and/or ambiguities of interpretation (see, e.g. Clark & Stephenson 1977, Tammann 1978; Caswell & Lerche 1979a; Lozinskaya 1980; Higdon & Lingenfelter 1980; Taylor & Manchester 1977; Arnaud & Rothenflug 1980). Taken together all the available data appear to be consistent with $S_{gal} \sim 0.01$–$0.1\,yr^{-1}$. Similarly we obtain the emissivity of ionizing photons from the simple relationship

$$\epsilon_{uv}(R, t) = \epsilon_1 S(R, t) + \epsilon_2 , \tag{5}$$

where the term proportional to S represents contribution from SNRs themselves and young hot stars, while the constant term describes the contribution from density bounded planetary nebulae. Observational estimates in the solar neighbourhood suggest that SNRs, unshielded B stars and planetary nebulae each provide $\epsilon \sim 1$–$1.5 \times 10^{-15}\,cm^{-3}\,s^{-1}$ (Salpeter 1979). Potentially the local contribution from unshielded O stars is a factor of 10–20 greater than this; however, Elmegreen (1976) has argued that most of this flux is absorbed within ~ 100 pc of its source. Neglecting this latter contribution and allowing for losses from the galactic disc we take $\epsilon_1 \sim 1.2 \times 10^{61}$ per SNR and $\epsilon_2 \sim 0.7 \times 10^{-15}\,cm^{-3}\,s^{-1}$; however, it must be recognized that a 'leak' of only 10 per cent of the O star flux would double this value.

Equations (3), (4) and (5) define our galactic model. In incorporating it into the three phase scheme we tacitly assume that the ISM remains in a quasi-steady state as S, $\bar{n}$ and ϵ_{uv} vary slowly with time and that the spatial variation of these parameters on length scales very much larger than the typical dimensions of an SNR do not drastically affect local conditions. Smith (1977) found that a quasi-equilibrium state was achieved in his Monte Carlo simulations based on the Cox & Smith (1974) model on a time-scale of order 10^7 yr. This relaxation time and the statistical distribution of supernovae will inevitably somewhat blur the parameter distributions we obtain. Nevertheless, solutions obtained assuming locally uniform values for S, $\bar{n}$ and ϵ_{uv} at each point in the disc, should not represent too severe an approximation except near the discontinuities at the passage of the density wave shock and the 'switch on' of the new generation of supernovae.

3 Results

For purposes of orientation we will begin by considering a specific model incorporating the BG density distribution and having spiral shock compression $c = 5.0$, exponent of star formation rate $m = 1.0$ and $S_{gal} = 0.02\,yr^{-1}$ (note that S_{gal} is the number of supernovae occurring per year in our Galaxy while S is the supernova rate per year per cubic parsec). For this case, Fig. 1 shows the variation of a number of parameters of the ISM with azimuth (θ) in the midplane of the galaxy, at the galactocentric distance of the Sun. The values of the same quantities at points on the loci of maximum supernova rate ('arm') and minimum mean density ('interarm') are shown as functions of galactocentric distance in Fig. 2.

In Table 1(a) we list the 'arm' and 'interarm' values both for $R = 10$ kpc and $R = 5$ kpc, the latter distance being chosen as broadly representative of points in the molecular ring. Column 1 gives Q_c, the porosity parameter, which measures the sum of the fractional volumes of all SNRs still in the pre-cooling phase of their evolution while column 2 gives R_c, the SNR radius at the end of this phase. These quantities, especially the former, increase very rapidly with *both* decreasing $\bar{n}$ *and* decreasing S. This behaviour is a direct consequence of the evaporative feedback mechanism in the MO scheme and is not dependent on the details of our galactic model. When $Q_c \gtrsim 1$, as occurs in the 'interarm' region interior to 4 kpc or exterior to 8 kpc, SNRs frequently overlap before cooling and the basic assumptions of the MO model break down. Similarly if R_c exceeds the scale height of the disc gas, energy losses to the halo may play a dominant role in SNR energy balance invalidating our results.

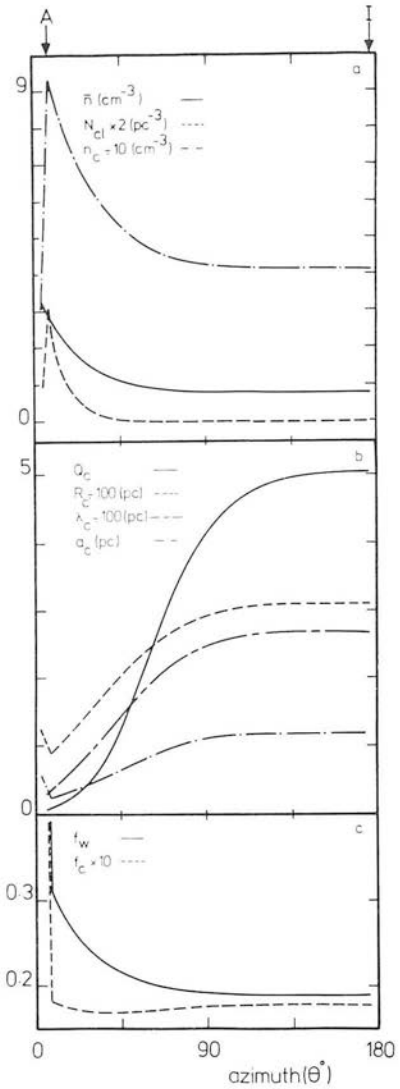

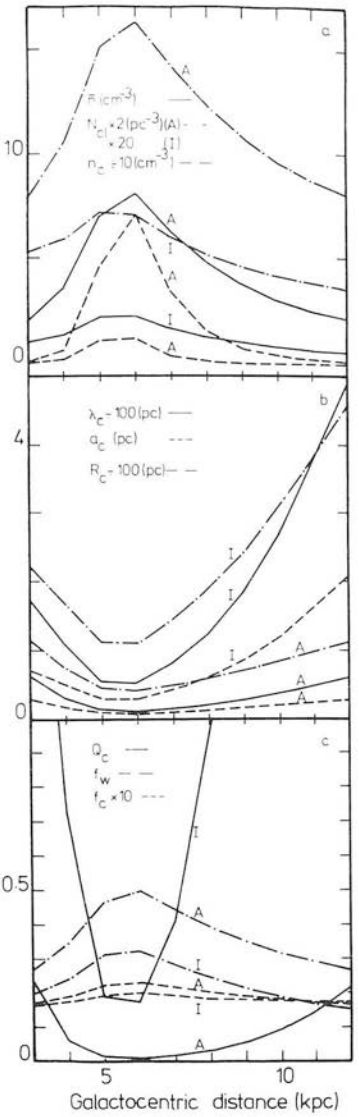

Figure 1. (Left) Calculated quantities as a function of azimuth θ^0, in the midplane of the galaxy at a galactocentric distance of 10 kpc (see text). θ is zero at the position of the density wave shock. The positions at which the 'arm' (A) and 'interarm' (I) properties were evaluated are indicated. The properties of the warm envelopes may be estimated from the relationships in the text while $\langle P \rangle \approx 88 k n_c$.

Figure 2. (Right) The same quantities as in Fig. 1 but plotted as functions of galactocentric distance, R (kpc) along the 'arm' (A) and 'interarm' (I) loci.

The occurrence of either of these conditions is likely to lead to the violation of energy conservation in the disc gas. The excess energy will be transported to the halo where it may assist in driving a galactic wind or a galactic fountain (Shapiro & Field 1976; Chevalier & Oegerle 1979). Further, if dense shell formation is prevented under these circumstances, material will not be returned to the dense phase and the mass of the HIM will grow by evaporation at the expense of the clouds. The critical radius above which clouds begin to condense rather than evaporate decreases with increasing hot phase density (McKee & Cowie 1977). Thus ultimately a new equilibrium state may be achieved with evaporation of the

	R (kpc)	$\bar{n}$ (cm^{-3})	S (10^{-13} pc^{-3} yr^{-1})	Q_c	R_c (pc)	$\langle P\rangle/k$ (10^4 K cm^{-3})	N_{cl} (pc^{-3})	$\langle a_c\rangle$ (pc)	λ_c (pc)	f_c (×100)	n_c (cm^{-3})	$\langle a_w\rangle$ (pc)	λ_w (pc)	f_w	n_w (cm^{-3})
(a) $S_{gal} = 0.02\,yr^{-1}$, $c = 5.0$, $m = 1.0$, GB density law.															
A	5	7.01	10.69	0.01	45	1.32	2.34	0.09	13.5	4.66	150.5	0.28	1.69	0.22	1.04
I	5	2.25	2.86	0.19	112	0.63	0.06	0.30	54.6	3.12	72.1	0.93	6.36	0.19	0.45
A	10	3.04	4.64	0.09	85	0.84	0.18	0.20	38.2	3.17	96.0	0.62	4.52	0.18	0.61
I	10	0.79	0.93	5.06	310	0.37	7.4×10^{-4}	1.19	269.4	1.89	41.6	3.86	28.96	0.18	0.23
(b) $S_{gal} = 0.02\,yr^{-1}$, $c = 10.0$, $m = 1.0$, GB density law.															
A	5	7.79	12.33	0.01	42	1.44	3.27	0.08	12.1	4.76	163.6	0.25	1.51	0.22	1.14
I	5	1.61	2.17	0.48	148	0.56	0.02	0.42	88.4	2.54	63.5	1.32	10.02	0.18	0.38
A	10	4.22	6.68	0.04	65	1.03	0.53	0.14	25.3	3.60	117.3	0.44	3.06	0.19	0.77
I	10	0.57	0.67	18.57	451	0.32	1.4×10^{-4}	2.05	479.6	1.56	36.3	6.70	50.48	0.18	0.19
(c) $S_{gal} = 0.05\,yr^{-1}$, $c = 5.0$, $m = 1.0$, GB density law.															
A	5	7.01	26.73	0.02	39	2.54	4.89	0.06	16.6	2.43	288.3	0.18	2.00	0.12	1.89
I	5	2.25	7.15	0.26	98	1.23	0.11	0.19	69.8	1.62	139.4	0.62	7.89	0.10	0.83
A	10	3.04	11.59	0.13	74	1.63	0.33	0.13	48.9	1.64	185.6	0.41	5.60	0.10	1.12
I	10	0.79	2.32	6.56	266	0.70	1.5×10^{-3}	0.75	335.8	0.99	79.9	2.44	35.70	0.09	0.43
(d) $S_{gal} = 0.02\,yr^{-1}$, $c = 5.0$, $m = 1.0$, SSS density law.															
A	5	16.57	13.38	0.01	28	1.41	16.38	0.06	4.3	10.60	159.5	0.19	0.58	0.43	1.17
I	5	5.32	3.58	0.02	65	0.64	0.49	0.19	16.2	7.32	72.8	0.56	2.04	0.37	0.51
A	10	6.45	5.21	0.02	55	0.81	1.03	0.14	13.3	7.02	91.9	0.43	1.69	0.34	0.65
I	10	1.67	1.04	0.40	168	0.33	0.01	0.63	73.6	4.43	37.7	1.96	8.47	0.31	0.23
(e) $S_{gal} = 0.02\,yr^{-1}$, $c = 5.0$, $m = 2.0$, GB density law.															
A	5	7.01	44.38	0.02	36	3.65	6.90	0.05	18.9	1.69	414.9	0.14	2.24	0.09	2.64
I	5	2.25	3.18	0.20	110	0.68	0.06	0.28	55.9	2.90	77.7	0.88	6.49	0.18	0.48
A	10	3.04	8.34	0.11	77	1.29	0.28	0.15	44.4	2.08	146.3	0.47	5.15	0.12	0.90
I	10	0.79	0.33	6.90	421	0.18	1.7×10^{-4}	2.56	256.9	3.76	20.9	8.31	27.49	0.40	0.11
(f) $S_{gal} = 0.02\,yr^{-1}$, $c = 5.0$, $m = 1.0$, GB density law.				y_{max}	R_{max}										
A	5	7.01	10.69	0.16	79	0.68	1.35	0.14	10.4	9.03	77.7	0.53	0.82	0.86	0.54
I	5	2.25	2.86	0.17	106	0.29	0.02	0.55	44.0	6.82	33.0	2.16	3.21	0.90	0.20
A	10	3.04	4.64	0.18	97	0.42	0.10	0.32	29.5	6.34	48.0	1.22	2.21	0.74	0.31
I	10	0.79	0.93	0.20	140	0.15	1.5×10^{-4}	2.80	234.1	4.54	17.3	11.47	15.67	0.98	0.09

A = Arm condition. I = Interarm condition.

small clouds balanced by condensation on to large clouds. Alternatively, matter may be returned to the cool dense phase by the operation of a galactic fountain.

Column 3 of Table 1(a) contains the volume average contribution to the ISM pressure provided by SNR, $\langle P \rangle$. The properties of the cloud population discussed below are calculated assuming the clouds to be in equilibrium at this pressure rather than at the 'typical' pressure employed by MO (see Appendix). Notice that the behaviour of this parameter is qualitatively similar to that of $\bar{n}$ in this case. In column 4 we give, $N_{\rm cl}$, the number of cloud centres per cubic parsec. This quantity is largest in the arm region of the molecular ring and falls dramatically with decreasing $\bar{n}$ and S. Notice that the distribution of $N_{\rm cl}$ in both R and θ is significantly more sharply peaked than for instance that of $\bar{n}$. Again this behaviour is a consequence of MOs evaporative feedback mechanism.

Columns 5–8 give respectively the mean radius, $\langle a_{\rm c} \rangle$, filling factor $f_{\rm c}$, intercloud distance, $\lambda_{\rm c}$ and density, $n_{\rm c}$, of the cold cores. Notice that the forms of the variation of $\langle a_{\rm c} \rangle$, and $\lambda_{\rm c}$ are very similar, while the assumption of pressure equilibrium dictates that $n_{\rm c}$ is simply proportional to $\langle P \rangle$. Columns 9–12 give the corresponding quantities; $\langle a_{\rm w} \rangle$, $f_{\rm w}$, $\lambda_{\rm w}$ and $n_{\rm w}$ for the warm envelopes. The ratios $\langle a_{\rm c} \rangle / \langle a_{\rm w} \rangle$, $\lambda_{\rm c}/\lambda_{\rm w}$, $f_{\rm c}/f_{\rm w}$ and $n_{\rm c}/n_{\rm w}$ are entirely fixed by the assumption of pressure equilibrium and MOs modelling of the cloud properties, specifically

$$\langle a_{\rm c} \rangle / \langle a_{\rm w} \rangle = 0.38(1 + x_{\rm w})^{-1/3}, \quad \lambda_{\rm c}/\lambda_{\rm w} = 6.25(1 + x_{\rm w})^{2/3},$$

$$n_{\rm w}/n_{\rm c} = 100(1 + x_{\rm w}), \quad f_{\rm w}/f_{\rm c} = 0.02(1 + x_{\rm w})^{-1} \ln(M_u/M_l),$$

where $x_{\rm w}$ is the fractional ionization in the warm envelope and M_u and M_l are the masses of the largest and smallest clouds permitted by the model. Since $x_{\rm w}$ varies only slightly the first three ratios are almost constant, having in the present case the values ~ 0.3, ~ 8.3 and ~ 0.06 respectively. Conversely M_u/M_l is quite sensitive to the local values of $\epsilon_{\rm uv}$ and $\langle P \rangle$ and hence $f_{\rm w}/f_{\rm c}$ varies rather more.

We may now consider the effect on our results of changing the constants in the galactic model from those used to derive Table 1(a). We have performed calculations employing each of the three density distributions discussed in Section 2 for $m = 0.5$, 1 and 2 and with c and $S_{\rm gal}$ having various values in the range 1–10 and 0.01–0.1 $\rm yr^{-1}$, respectively. These show that the gross *qualitative* features exhibited in Figs 1 and 2 are preserved, even though the absolute values of the derived parameters and the magnitudes of their variation with R and θ may change considerably. One important exception to this, however, is that the qualitative behaviour of the filling factors differs significantly according to the value of m. We will return to this point shortly.

3.1 EFFECT OF CHANGING THE SHOCK COMPRESSION RATIO c, AND THE SUPERNOVA RATE $S_{\rm gal}$

Understandably, the larger the value of c, the larger the contrast between the arm and interarm values of the derived parameters. This tendency is particularly pronounced in the cases of $N_{\rm cl}$ and $Q_{\rm c}$ and is least prominent for the filling factors. Rather more surprising is the relative insensitivity to the value of c of conditions in the arm region of the molecular ring. These trends are illustrated by the data in Table 1(b) which were calculated for $c = 10.0$, the other constants being the same as for Table 1(a). The arm–interarm contrasts in $N_{\rm cl}$ and $Q_{\rm c}$ shown in Table 1(b) are respectively 4–15 times and 3–8 times those shown in Table 1(a). Conversely the values of $f_{\rm w}$ and $f_{\rm c}$ at any point are virtually the same in both tables. In the arm region at $R = 5$ kpc the data in these two tables are the same to within ~ 30 per cent and excluding $N_{\rm cl}$ and $Q_{\rm c}$ brings this difference down to $\lesssim 10$ per cent. For

any individual parameter the difference between the values in the two tables is substantially greater at any other point.

Throughout the volume of parameter space examined here if the value of S_{gal} is *increased*, $\langle P \rangle$, N_{cl}, n_c and n_w all increase at any point, while R_c, the cloud radii and cloud filling factors decrease. To a fairly good approximation, the ratio of the values of any of these quantities obtained from models differing only in the value of S_{gal}, is both independent of position and of the values of the other constants. The values of Q_c, λ_c and λ_w are almost independent of S_{gal}. At points for which the local value of S exceeds $1 \times 10^{-13}\,pc^{-3}\,yr^{-1}$ the value of Q_c increases slightly with S_{gal} while below this the converse is true. Similarly the intercloud distances are slowly increasing functions of S_{gal} wherever $S \gtrsim 0.5 \times 10^{-13}\,pc^{-3}\,yr^{-1}$ and are slowly decreasing functions elsewhere. As a specific example Table 1(c) gives the values obtained for the same values for the constants as in Table 1(a) except that $S_{gal} = 0.05\,yr^{-1}$. Dividing the data in Table 1(c) by those in Table 1(a) we obtain the ratios ~ 2 for N_{cl}, ~ 0.65 for $\langle a_c \rangle$ and $\langle a_w \rangle$, ~ 0.53 for f_c and f_w, ~ 1.85 for $\langle P \rangle$, n_c and n_w and ~ 0.85 for R_c. These ratios are broadly typical of those obtained for any other pair of models having $S_{gal} = 0.02\,yr^{-1}$ and $S_{gal} = 0.05\,yr^{-1}$. In this case the corresponding ratio of the values of Q_c is ~ 1.3 while those of the intercloud distances are both ~ 1.2.

3.2 EFFECT OF CHANGING THE MOLECULAR HYDROGEN DENSITIES

Essentially the values of $\bar{n}(H_2)$ obtained by SSS only differ from those of GB in being everywhere ~ 2.5 times larger. Thus since in either case $\bar{n}(H^0) \ll \bar{n}(H_2)$, adopting the SSS values rather than those of GB affects the normalization constant, S_0, of equation (4), in essentially the same way as *decreasing* S_{gal}. The consequences of this for the values calculated at any position is of course complicated by the accompanying increase in the local value of $\bar{n}$. We find that the overall effect of this change is to *increase* the number of clouds, their densities and their filling factors while decreasing Q_c, R_c, the cloud radii and the intercloud distances. Again the ratio of the values obtained from two models differing only in the choice of the density distribution, are approximately independent of the values of the other constants and only change slowly with position. The data in Table 1(d) were obtained with the same constants as for Table 1(a) but using the SSS density distribution. The ratios here are ~ 0.1 for Q_c, ~ 10 for N_{cl}, ~ 0.6 for R_c, $\langle a_c \rangle$ and $\langle a_w \rangle$, ~ 0.34 for λ_w and λ_c and ~ 1.1 for n_c and n_w.

The density values derived by GLV are ~ 0.64 and ~ 0.2 times those of GB at 10 and 5 kpc respectively. The consequence of these considerably lower densities is that the cloud evaporation rate per unit volume is commonly insufficient for cooling to occur before the SNRs either overlap or burst out of the disc even in the arm region.

3.3 EFFECT OF CHANGING THE STAR FORMATION EXPONENT, m

For the case $m = 2$ our results are in general qualitatively similar to those for $m = 1$ except that the magnitudes of the arm–interarm and radial contrasts in the various quantities are substantially greater. However, the behaviour of the filling factors is exceptional in this respect. We find quite generally that if $m \simeq 1.46$ the value of f_w is independent of R and θ, while for f_c the same is true at $m \simeq 1.73$. As we have seen for the case $m = 1$, below these values the filling factors are higher in the arm region than in the interarm region and have a maximum value in the molecular ring. The converse is true for the case $m = 2$. Table 1(e) which gives the results for the same model as Table 1(a) but with $m = 2$ illustrates these trends and broadly typifies the results obtained for other cases. For $m = {}^1/_2$ the basic trends are consistent with those discussed above. However, generally in this case we find that the

value of f_w predicted approaches or exceeds unity everywhere. When f_w is comparable to unity the SNR evolution will be primarily controlled by the cloud component rather than the HIM and the MO scheme is inappropriate. The situation then becomes more reminiscent of the original Cox & Smith (1974) model.

4 A non-evaporative model

Thus far we have assumed that the evaporation of embedded clouds plays a dominant role in the early stages of SNR evolution. However, thermal evaporation can be quenched if the magnetic field in the cloud–HIM interface possesses a suitable geometry. Cox (1979) has examined the evolution of SNRs in a hot, tenuous intercloud matrix in the absence of evaporation. In particular his calculations show that for this case both the external pressure and interaction with the halo will become important prior to the onset of radiative cooling. He suggested that cloud compression might then be the dominant sink for SNR energy and demonstrated that this mechanism could represent an important heat source for the clouds. To assess the consequences of such a situation for our results we have constructed a model in which Cox's scheme for SNR evolution is incorporated into the representation of the cloud population employed in the MO model.

Cox characterized SNR evolution in terms of a normalized volume y defined so that the ambient pressure becomes important when $y = 1$. He then supposed that the remnant evolved until at $y = y_{max}$, all the explosion energy had been dissipated, and calculated the volume average pressure contributed by the ensemble of SNRs as a function of y_{max}. He also obtained an expression for the rate of nett compressional work done by an SNR on the clouds contained within it. Adopting the cloud geometry and size spectrum used in the MO model (*cf.* Appendix) the integral of this latter quantity from $y = 0.1$ to y' can be approximately represented by

$$w_{net}(y') \simeq \frac{0.955\, E_0 (E_0/P_h)^{1/3} n_h^{1/2}}{n_w^{1/2} \langle a_w \rangle + 0.228\, (E_0/P_h)^{1/3} n_h^{1/2}}\, f_w (1 - (10y')^{-1/4}), \tag{6}$$

where n_h is the density in the undisturbed matrix which we subsequently take to be $5 \times 10^{-3}\,\mathrm{cm}^{-3}$. E_0 is the supernova explosion energy in erg and P_h is the pressure in the hot matrix. Equation (6) has been corrected to allow for the complete compression of the smallest clouds. For simplicity we assume that the entire explosion energy is consumed by cloud compression and obtain y_{max} by setting $w_{net} = E_0$ in equation (6). This, together with Cox's expression for the pressure and the usual equations relating the cloud properties to $\bar{n}$ and ϵ_{uv} leads to a system of equations analogous to those obtained in the MO case.

Acceptable solutions to these equations can only be obtained over rather more limited ranges of values for the input parameters than in the case of the MO model. The asymptotic behaviour of the explicit y dependence in equation (6) together with the rapid decrease of f_w with increasing y, consequent upon the increasing pressure, results in $w_{net}(y)/E_0$ possessing a maximum near $y \sim 0.3$. Hence, our requirement that $w_{net}(y_{max})/E_0 = 1$ imposes as an absolute upper limit $S^{2/3}/\bar{n} \leqslant 3.6 \times 10^{-9}$ at any point. Conversely if the ambient pressure is to be sufficient to confine the warm envelopes so that $f_w \leqslant 1$ then $S^{2/3}/\bar{n} \geqslant 1.4 \times 10^{-9}$. The consequences of any failure to meet these conditions will be similar to those discussed for the MO model in the last section.

Wherever these conditions are satisfied for a particular galactic model we find, however, that the behaviour of the derived parameters with R and θ is qualitatively similar to those obtained in the MO model. Quantitatively the 'Cox' calculations lead to pressures typically $\sim 1/2$ those obtained from the MO model for the corresponding case. Consequently, N_{cl},

the cloud densities and intercloud distances are smaller while the cloud radii and filling factors are rather larger in the Cox case. Table 1(f) lists the data for the GB density distribution with $c = 5.0, m = 1.0$ and $S_{gal} = 0.02\ yr^{-1}$ which can be compared directly with the data of Table 1(a). R_{max} is the SNR radius when $y = y_{max}$. The behaviour of f_w is noteworthy in that it is largest where $\bar{n}$ and S are smallest which differs from the behaviour of f_c. The trends exhibited in this case are typical of those for other models using the GB or SSS density laws and with $m = 1$ (bearing in mind the limits discussed above). For models having $m = 2$ one or both of the above limits are invariably violated at some point in the disc while as in the MO case models having $m = {}^1/_2$ generally predict $f_w > 1$ throughout the disc. With the GLV density law the density is too small to permit the complete dissipation of the explosion energy by cloud crushing for any reasonable value of S_{gal}.

5 Discussion

The essential trend exhibited in our results is that in regions where $\bar{n}$ and S are large, the energy deposited in an SNR is dissipated at a much earlier evolutionary epoch than in regions of low $\bar{n}$ and S, irrespective of whether this dissipation occurs predominantly via evaporation-enhanced radiation or via cloud crushing. Consequently, the ensemble of SNRs contribute to a larger volume average pressure in such regions. The natural concomitant of this (given the assumed cloud properties) is that the clouds are smaller, more dense and considerably more numerous under such conditions.

The dramatic decrease in the predicted number of clouds in passing from 'arm' to 'interarm' conditions, raises the important theoretical question of whether the cloud spectrum is capable of adjusting sufficiently rapidly to local conditions, as is assumed implicitly in our model. The bulk of this variation results from the destruction of the smallest and most numerous clouds. In the MO model the putative mechanisms for this are shock sweeping by SNRs in the 'snow-plough' phase and complete evaporation. The time-scale for the former process will be clearly comparable with that for SNR evolution, while we find that the time-scale for the latter process is typically of the same order of magnitude. Likewise the formation of the smallest clouds is supposed to occur by means of the break up of the dense shells of old SNRs and hence will take place on a similar time-scale. Conversely, it is very unlikely that larger clouds can be created and destroyed so rapidly. However, trial calculations employing modified cloud spectra and differing methods for fixing the upper limit to the cloud mass suggest that this will not unduly affect our results. For the Cox model the mechanism of cloud creation and destruction is unknown so we can make no such assurance.

5.1 MACH NUMBER OF THE SPIRAL SHOCK

Clearly the central question and that which initially motivated this study, concerns whether or not the ISM possesses properties consistent with the existence of a density wave shock. The condition for the existence of a strong shock in the gas is that the streaming velocity normal to the spiral pattern, $W_\perp \sim 10$–$20\ km\ s^{-1}$ should exceed the effective acoustic speed in the gas $\bar{c}$. Schmidt-Kaler & Weigandt (1980) have discussed the value of $\bar{c}$ appropriate to a multicomponent medium, in the limit of long wavelengths. Writing their result in a more convenient form we obtain,

$$\bar{c} = \frac{c_w c_h}{[(1-f_w)^2 c_w^2 + f_w^2 c_h^2 + f_w(1-f_w)(c_w^2 + c_h^2)]^{1/2}}, \tag{7}$$

where c_h is the sound speed in the HIM $\sim 120\ km\ s^{-1}$ and c_w is that in the WIM which lies

between 9.2 and 13.2 km s^{-1} depending on the fractional ionization. Even for quite small values of f_w the warm envelopes are remarkably effective in retarding shocks propagating through the medium.

In Fig. 3 we show the value of $\bar{c}$ calculated from equation (7) for the 'interarm' region as a function of R in a number of representative cases. This can be compared with the expected run of $w_\perp$ for the galaxy (Burton 1977; following Roberts, Roberts & Shu 1975). For the MO models if $m = 1$ or 2 only those employing the SSS density distribution satisfy the criterion $W_\perp > \bar{c}$ at any point and then only if $S_{gal} \lesssim 0.02\,yr^{-1}$. For $m = 1$ this only occurs in a rather limited region near $R = 5$ kpc; however, for $m = 2$ the form of the variation of f_w with $\bar{n}$ and S permits the condition to be satisfied over a much larger range in R for a given value of S_{gal}. Similarly, for the Cox models the requirement that all the explosion energy be dissipated, necessitates a sufficiently large value of f_w for the existence of a shock, but can only be satisfied when S_{gal} is small and $\bar{n}$ large. As already noted the models with $m = {}^1/_2$ predict large values of f_w everywhere and consequently will generally satisfy this criterion.

The point is often made (e.g. Scott, Jensen & Roberts 1977; Reinhardt & Schmidt-Kaler 1979; Blitz & Shu 1980) that supernovae of type I which yield a smaller ($\sim {}^1/_2$, Chevalier 1977) energy per explosion than supernovae of type II, probably predominate in the interarm region. To examine the consequences of this we have performed calculations using a reduced explosion energy for all the supernovae in the interarm region. We find that as would be

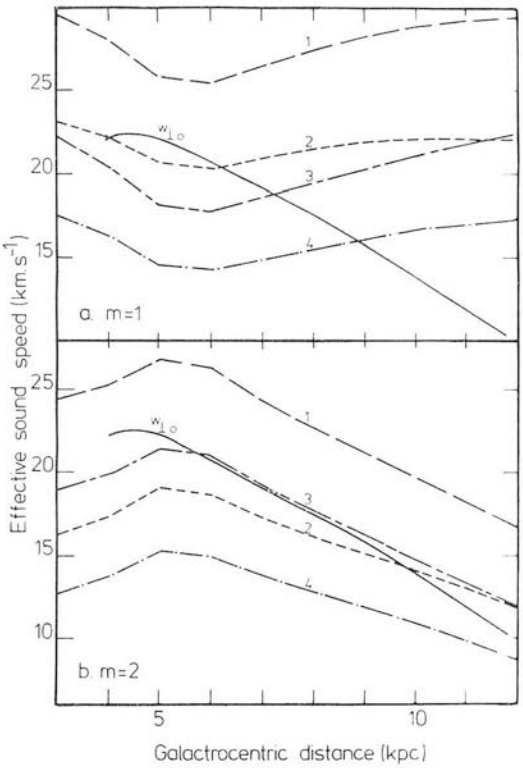

Figure 3. The effective sound speed $\bar{c}$ (km s^{-1}) of the interarm ISM as a function of galactocentric distance. For both panels a compression factor, c of 5.0 and galactic supernova rate, S_{gal} of 0.02 yr^{-1} was employed. For (a) the exponent m of star formation was 1, while for (b) it was 2. The numbered curves were calculated for (1) GB density law $E_0 = 5 \times 10^{50}$ erg, (2) SSS density law $E_0 = 5 \times 10^{50}$ erg, (3) GB density law $E_0 = 2.5 \times 10^{50}$ erg, and (4) SSS density law $E_0 = 2.5 \times 10^{50}$ erg. The solid line shows the streaming velocity perpendicular to the spiral arm $W_{\perp_0}$ (km s^{-1}) after Burton (1976).

expected this reduces $\langle P \rangle$ and hence leads to a modest increase in f_w (typically $\lesssim 70$ per cent if E_0 is halved to 2.5×10^{50} erg). Nevertheless, contrary to the suggestion of these authors the hot phase continues to be an important constituent of the interarm ISM. The increase in f_w does, however, lead to a decrease in $\bar{c}$ as indicated in Fig. 3 and a rather less restricted range of models are then able to satisfy the constraint on $W_\perp/\bar{c}$. In particular it becomes possible for models employing the GB density distribution with $m = 1$ and $S_{gal} \lesssim 0.02$ to satisfy this criterion in the molecular ring.

Even if the intercloud gas is incapable of supporting density wave induced shocks it remains possible that the 'cloud fluid' may be able to do so as has been proposed by Cowie (1980). The details of such a mechanism, however, remain to be worked out. In any case it should be borne in mind that observation both of our own and external galaxies do indicate the existence of a density enhancement associated with spiral arms (e.g. Visser 1980; Cohen *et al.* 1980) so our galactic model may not differ too much from the truth whatever mechanism is ultimately found to be responsible.

5.2 MOLECULAR CLOUDS IN THE MODEL

Another interesting question relates to the status of molecular clouds within our model. In modelling the cloud properties we have not included the presence of molecular cores although in calculating $\bar{n}$ we have included the molecular component. As a rough empirical criterion a cloud possesses sufficient self shielding to contain a significant H_2 content when its column density exceeds $\sim 6 \times 10^{20}\,\mathrm{cm}^{-2}$ (Savage *et al.* 1977), i.e. when its core radius exceeds $\sim 194/n_c$ pc. Consequently the numerous small clouds which primarily control our model never possess molecular cores, so neglecting their presence should not greatly affect our results. Overall, given the cloud spectrum employed ~ 40 per cent of the ISM mass is contained in clouds with sufficient self shielding to possess molecular cores. That this falls short of the molecular fraction actually observed and tacitly assumed is not, however, surprising.

Our cloud spectrum is assumed to terminate at the limiting mass given by Mouschovias & Spitzer (1976), corresponding to a radius typically ~ 10 pc in the spiral arms which as has often been noted falls considerably short of the observed scale length of Giant Molecular Cloud complexes (SSS; Stark & Blitz 1978). On the other hand, the very numerous small clouds found in the arms lead to typical cloud separations very much smaller than the average separation of the early type stars ~ 50 pc responsible for much of the ionization (deduced from Torres-Peimbert, Lazcano-Aruajo & Peimbert 1974). Thus mutual cloud–cloud shielding might become an important effect. Tentatively then we might envisage molecular cloud complexes as being agglomerates of many mutually shielding clouds spaced more closely than the average. The acceleration due to SNRs and stellar winds coupled with the gravitational attraction of the few largest members might provide a natural mechanism for the initial formation of such clumps. Certainly the observational evidence that molecular clouds are inhomogeneous (Silk 1980) provides some encouragement for such a point of view.

5.3 OBSERVATIONAL CONSTRAINTS

It is clearly of considerable interest to examine the observable consequences of our model and to consider what if any constraints can then be imposed upon it. MO compared many predictions of their model with the observed properties of the ISM in the solar neighbourhood, and found reasonable agreement in most respects bearing in mind the highly approximate nature of the model. Here we will concentrate on predictions relating to the larger scale

properties of spiral galaxies. In particular the question of whether the hot component of the ISM is truly ubiquitous or merely a local anomaly can clearly be most easily resolved by studying nearby galaxies.

Ultimately the most unequivocal evidence for a pervasive hot phase in any external galaxy would come from observations of its soft X-ray emission. Following MO the effective soft X-ray opacity of a multiphase medium is approximately given by,

$$k_x \simeq (\lambda_c + 1/n_c\sigma)^{-1} + (\lambda_w + 1/n_w\sigma)^{-1},$$

where σ is the effective cross-section per hydrogen atom (Brown & Gould 1970; the more detailed analysis of Ride & Walker 1977, requires a different cross-section for the CNM and WIM: however, we will neglect this in view of the approximate nature of the calculation). For the MO model we find that the volume average emissivity of the HIM is proportional to S and almost independent of Q_c. It is then straightforward to calculate the relative intensity emitted at a particular energy at each point in our models. In general the S dependence of the emissivity dominates over the increased opacity resulting from larger $\bar{n}$ so that regions of high $\bar{n}$ and S would be expected to be 'bright' at soft X-ray energies. For instance in the Wisconsin groups B band (0.17 keV, Burstein *et al.* 1977) we find from the results of Table 1 that the ratios of the arm to interarm intensities are ~ 1.25 and 1.42 at 5 and 10 kpc respectively. At the higher energy of the M band (0.4–0.85 keV) the corresponding ratios are ~ 2.23 and 1.85. Because most of the soft X-ray flux is emitted by the younger, smaller remnants the actual distribution of flux will inevitably be very irregular. Furthermore, the interpretation of any observations will be complicated by the presence of emission from the galaxies, halo as well as 'contamination' by the emission from our own Galaxy.

Another potential tracer of the hot gas and one for which observations already exist is its non-thermal radio emission. Unfortunately the details of the emission mechanism in SNRs remain unclear and in particular depend critically on the geometry of the magnetic field which is as yet unknown (Caswell & Lerche 1979b). It is therefore not possible to make any useful predictions of its distribution on the basis of our model.

The statistical properties of resolved SNRs may represent a useful probe of the conditions in their vicinity (Higdon & Lingenfelter 1980). Note in particular that our model predicts an increase in the typical remnant size scale with decreasing $\bar{n}$ and S which shows up in our model as an increase in remnant size with increasing galactic radius. Such a trend has already been noted for our galaxy both for radio remnants (Jones 1975) and for the giant H I shells reported by Heiles (1979), (Bruhweiler *et al.* 1980). However, other interpretations of this trend are possible and selection effects are undoubtedly important.

It might seem that observations of the properties of the CNM and WIM in external galaxies might provide a test of our model and hence by inference provide information on the hot phase. Photographic surface photometry can provide information on the distribution of dust and hence gas in nearby galaxies with a linear resolution of tens of parsecs while 21-cm aperture synthesis measurements yield comparable data for H I alone at rather lower resolution. Unfortunately such observations ultimately can only provide a measurement of the local value of $\bar{n}$ at any point and hence while certainly useful for testing our galactic model they provide only limited information on the properties of the cloud population. In principle the statistical fluctuations in the observed column density provide a measure of N_{cl}; however, because of the large volume elements involved we do not expect the effect to be measurable. A statistical study of individual large (resolved) clouds (Elmegreen 1980) can help to elucidate some features of the model but the insensitivity of our results to the details of the cloud spectrum probably render such data of limited value in testing our model. Similar arguments can also be made with regard to Hα observations of the warm envelopes,

in addition to which the emission measure predicted from the WIM is small compared to that from a single normal H II region rendering interpretation difficult.

6 Conclusions

Our initial assumptions were: (1) that SNRs interact with the inhomogenous ISM in the manner proposed by MO; (2) that the pattern of mean total density $\bar{n}$ is similar to that predicted by TASS models; (3) that the local star formation rate and supernova rate are proportional to each other and to some power m, of $\bar{n}$. We have also examined the consequences of relaxing the first of these assumptions to the extent of replacing evaporation enhanced radiation by cloud crushing as the dominant sink of SNR energy as proposed by Cox (1979).

We conclude:

(1) Our results are not strongly dependent on whether we employ evaporation enhanced radiation or cloud crushing, nor are they grossly affected by changes of detail in our model. Consequently we expect similar results to follow from any three phase model.

(2) The theoretical case for a ubiquitous hot phase remains strong. Contrary to previous expectations if the hot phase is important in spiral arms it remains so in the interarm region. This continues to be the case even when due allowance is made for the lower energy of the type I supernovae which predominate in the interarm region.

(3) Our model imposes strong constraints on the condition which must prevail in spiral galaxies if a density wave shock is to be self-sustaining. For our own Galaxy if $m \gtrsim 1$ then we require that both the lower estimates of the galactic supernova rate (i.e. $S_{\text{gal}} < 0.02$) and the higher estimates of $\bar{n}$ (i.e. that of SSS) are both correct. If either requirement is not met then the density wave shock can only be supported if some other mechanism such as that suggested by Cowie (1980) acts to produce a strong density enhancement in the arms. For $m \lesssim {}^1/_2$ our model fails because the warm component becomes predominant everywhere. Such a situation would favour density waves. However, in this instance the star formation rate has such a low arm/interarm contrast that blue spiral arms would be imperceptible, and type II supernovae would occur frequently between the arms. We believe that this provides an observational argument implying that $m > {}^1/_2$. Since observations suggest the existence of a spiral density wave in the galaxy, we must conclude that our requirements are in fact met.

(4) Observationally, it seems unlikely that studies of external galaxies can supply information on the vital question of the importance of the hot phase in the near future.

(5) The high pressure we predict within spiral arms must make the support of giant molecular clouds against self-gravity even more difficult to understand. Conversely, we expect a great many small clouds in the spiral arms. Consequently we tentatively propose a clumpy cloud model similar to that of Norman & Silk (1980). However, instead of T Tauri winds we propose that hot phase material separates, pressurizes and possibly drives the motions of the densely packed small clouds. This will be the subject of a future paper.

(6) The mechanisms we have described in this paper are perhaps subject to feedback, in the sense that for instance, supernova overproduction will drive much of the material into the hot phase and eventually reduce the star formation rate. The fact that our results (a) describe the state of our own Galaxy (and possibly others) fairly well and (b) indicate a narrow range of viable conditions in which the model sustains itself, may be taken as tentative evidence of such feedback. We are currently investigating this possibility.

Theoretical development is urgently required in the dynamics of multicomponent media

both in the large scale (effective sound speed, shocks etc.) and the small scale (cloud collision and collapse etc.)

Acknowledgment

SRH acknowledges the support of an SRC studentship.

References

Arnaud, M. & Rothenflug, R., 1980. *Astr. Astrophys.*, **87**, 196.
Blitz, L. & Shu, F. H., 1980. *Astrophys. J.*, **238**, 148.
Brown, R. H. & Gould, R. J., 1970. *Phys. Rev. D*, **1**, 2252.
Bruhweiler, F. C., Gull, T. R., Kafatos, M. & Sofia, S., 1980. *Astrophys. J.*, **238**, L27.
Burstein, P., Borken, R. J., Kraushaar, W. L. & Sanders, W. T., 1977. *Astrophys. J.*, **213**, 405.
Burton, W. B., 1976. *A. Rev. Astr. Astrophys.*, **14**, 275.
Caswell, J. L. & Lerche, I., 1979a. *Mon. Not. R. astr. Soc.*, **187**, 201.
Caswell, J. L. & Lerche, I., 1979b. *Proc. astr. Soc. Austr.*, **3**, 343.
Chevalier, R. A., 1977. *A. Rev. Astr. Astrophys.*, **15**, 175.
Chevalier, R. A. & Oegerle, W. R., 1979. *Astrophys. J.*, **227**, 398.
Clark, D. H. & Stephenson, F. R., 1977. *Mon. Not. R. astr. Soc.*, **179**, 87P.
Cohen, R. S. & Thaddeus, P., 1977. *Astrophys. J.*, **217**, L155.
Cohen, R. S., Cong, H., Dame, T. M. & Thaddeus, P., 1980. *Astrophys. J.*, **239**, L53.
Cowie, L. L., 1980. *Astrophys. J.*, **236**, 868.
Cowie, L. L. & McKee, C. F., 1977. *Astrophys. J.*, **211**, 135.
Cowie, L. L. & Songaila, A., 1977. *Nature*, **266**, 501.
Cox, D. P., 1979. *Astrophys. J.*, **234**, 863.
Cox, D. P. & Smith, B. W., 1974. *Astrophys. J.*, **189**, L105.
Dwek, E. & Scalo, J. M., 1979. *Astrophys. J.*, **233**, L81.
Elmegreen, B. G., 1976. *Astrophys. J.*, **205**, 405.
Elmegreen, D. M., 1980. *Astrophys. J. Suppl.*, **43**, 37.
Gordon, M. A. & Burton, W. B., 1976. *Astrophys. J.*, **208**, 346 (GB).
Guibert, J., Lequeux, J. & Viallefond, 1978. *Astr. Astrophys.*, **68**, 1 (GLV).
Heiles, C., 1979. *Astrophys. J.*, **229**, 533.
Heiles, C., 1980. *Astrophys. J.*, **235**, 833.
Higdon, J. C. & Lingenfelter, R. E., 1980. *Astrophys. J.*, **239**, 867.
Hobbs, L. M., 1974. *Astrophys. J.*, **191**, 395.
Jones, E. M., 1975. *Astrophys. J.*, **201**, 377.
Lozinskaya, T. A., 1980. *Astr. Astrophys.*, **84**, 26.
Mathewson, D. S., van der Kruit, P. C. & Brouw, W. N., 1972. *Astr. Astrophys.*, **17**, 468.
McKee, C. F. & Cowie, L. L., 1975. *Astrophys. J.*, **195**, 715.
McKee, C. F. & Cowie, L. L., 1977. *Astrophys. J.*, **215**, 213.
McKee, C. F. & Ostriker, J. P., 1977. *Astrophys. J.*, **218**, 148 (MO).
Miller, G. E. & Scalo, J. M., 1979. *Astrophys. J. Suppl.*, **41**, 513.
Mouschovias, T. Ch. & Spitzer, L., 1976. *Astrophys. J.*, **210**, 326.
Norman, C. & Silk, J., 1980. *Astrophys. J.*, **238**, 158.
Reinhardt, M. & Schmidt-Kaler, Th., 1979. *Astrophys. Space Sci.*, **66**, 121.
Ride, S. K. & Walker, A. B. C. Jr, 1977. *Astr. Astrophys.*, **61**, 339.
Roberts, W. W., 1969. *Astrophys. J.*, **158**, 123.
Roberts, W. W., Roberts, M. S. & Shu, F. H., 1975. *Astrophys. J.*, **196**, 381.
Salpeter, E. E., 1979. In *IAU Symp. 84, The Large Scale Characteristics of the Galaxy*, p. 245, ed. Burton, W. B., Reidel, Dordrecht.
Savage, B. D., Bohlin, R. C., Drake, J. F. & Budich, W., 1977. *Astrophys. J.*, **216**, 291.
Schmidt, M., 1959. *Astrophys. J.*, **129**, 243.
Schmidt-Kaler, Th. & Wiegandt, R., 1980. *Astr. Astrophys.*, **89**, 67.
Scott, J. S., Jensen, E. B. & Roberts, W. W., 1977. *Nature*, **265**, 123.
Seiden, P. E. & Gerola, H., 1979. *Astrophys. J.*, **233**, 56.
Sgro, A. G., 1975. *Astrophys. J.*, **197**, 621.
Shapiro, P. R. & Field, G. B., 1976. *Astrophys. J.*, **205**, 762.

Shu, F. H., Milione, V. & Roberts, W. W., 1973. *Astrophys. J.*, **183**, 819.
Silk, J., 1980. In *Star formation*, p. 133, eds Maeder, A. & Martinet, L., Saas Fee.
Smith, B. W., 1977. *Astrophys. J.*, **211**, 404.
Smith, L. F., Biermann, P. & Mezger, P. G., 1978. *Astr. Astrophys.*, **66**, 65.
Solomon, P. M., Sanders, D. B. & Scoville, N. Z., 1979. In *IAU Symp. 84, Large Scale Characteristics of the Galaxy*, p. 35, ed. Burton, W. B., Reidel, Dordrecht.
Stark, A. A. & Blitz, L., 1978. *Astrophys. J.*, **225**, L15.
Tammann, G. A., 1978. *Mem. Soc. astr. ital.*, **49**, 315.
Taylor, J. H. & Manchester, R. N., 1977. *Astrophys. J.*, **215**, 885.
Torres-Peimbert, S., Lazcano-Araujo, A. & Peimbert, M., 1974. *Astrophys. J.*, **191**, 401.
Visser, H. C. D., 1980. *Astr. Astrophys.*, **88**, 149.
Woodward, P. R., 1976. *Astrophys. J.*, **207**, 484.
Woodward, P. R., 1979. In *IAU Symp. 84, The Large Scale Characteristics of the Galaxy*, p. 159, ed. Burton, W. B., Reidel, Dordrecht.

Appendix

Following MO we introduce the evaporation parameter Σ, which measures the efficiency of evaporation and is defined by

$$\Sigma(r) = \alpha/[4\pi N_{\rm cl} < a(r_{\rm c}) > \phi_{\rm g}(l)\,\phi_{\rm m}]\ [P(r)/P(r_{\rm c})]^{-\gamma}\,. \tag{A1}$$

Unlike the MO case Σ is here a function of the SNR radius r because of the pressure dependence of the cloud radius (equation 2). In this expression $r_{\rm c}$ is the remnant radius at the cooling point and $\langle a(r_{\rm c})\rangle$ is the average over the cloud spectrum of the cloud radius evaluated at $r_{\rm c}$. α denotes the constant ratio of the blast wave velocity to the isothermal sound speed in the remnant interior. $N_{\rm cl}$ is the number of clouds per unit volume. The remaining terms are defined in equation (2).

Hence in the evaporative limit as discussed by MO we find for the dependence of the remnant age t upon r

$$t({\rm yr}) = 7.17\times10^{-2}(\eta/\alpha)\ [\eta^{-1}(1-1.625\,\eta)E_0\ \Sigma(r)]^{1/6}\,R^{5/3}({\rm pc}), \tag{A2}$$

where E_0(erg) is the initial explosion energy and $\eta = 6/(10+3\gamma)$. (The overall time dependence of r is given by $r \propto t^{\eta}$. For $\gamma = {}^1/_3$ as adopted in the text $\eta = 6/11$.) The determination of the cooling radius $r_{\rm c}$, the calculation of the dependence of the remnant pressure, temperature, etc. upon r and the computation of their global average values, then proceeds exactly as in MO. In particular we obtain

$$\Sigma(r_{\rm c}) = 5.37\times10^{3}\eta^{1.57}(1+3\eta)^{0.48}(1-1.625\eta)\,\alpha^{-0.57}\beta^{1.04}E_0^{0.04}(Q_{\rm c}/S)^{0.48} \tag{A3}$$

and

$$P(r_{\rm c})/k = 7.6\times10^{-51}(1+3\eta)^{0.69}(\eta/\alpha)^{0.58}\beta^{-0.11}E_0^{0.89}(Q_{\rm c}/S)^{-0.69}\,, \tag{A4}$$

where $Q_{\rm c}$ is the remnant porosity parameter, $S({\rm pc^{-3}\,yr^{-1}})$ is the volumetric supernova rate and β is the radiative enhancement factor.

Our treatment of the cloud properties follows that of MO except that we assume the clouds to be in pressure equilibrium at the average pressure $\langle P\rangle$ rather than the 'typical' pressure employed by MO, since $Q_{\rm c}$ may differ substantially from 0.5 in our models. Like MO we write $\langle P\rangle = P(r_{\rm c})(Q/Q_{\rm c})^{\chi}$, where χ is determined by power law fits to the computed volume average pressure and depends on both γ and the range of values of $Q_{\rm c}$ under consideration.

Using the mass and ionization balance relations together with the definition of the radius $a_{\rm wb}$ of the smallest cloud possessing a cold core, and of the radius a_{0l} of the smallest cloud,

(equations 38, 45, 41 and 37 of MO respectively) and equation (A1) leads directly to

$$\Sigma(r_c) = 0.912\,\phi_g(l)\,\phi_m\,\alpha^{-1}\,a_{wb}^2\,K_l(1+x_w)^{-1}\ln(a_{0u}/a_{0l})\,(\langle P\rangle/\bar{n}k\,T_w)\,[P(r_c)/\langle P\rangle]^{\gamma} \tag{A5}$$

$$(1-x_w)^2/(1+x_w) = 2.96\times10^{-2}\,\phi_g(l)\,\phi_m\,\alpha^{-1}\,K_l\ln(a_{0u}/a_{0l})\,(kT_w/\bar{n}\langle P\rangle)\,[P(r_c)/\langle P\rangle]^{-\gamma}\Sigma(r_c), \tag{A6}$$

$$\ln(a_{0u}/a_{0l}) = 4.9\times10^{-17}\langle P\rangle\bar{n}\,x_w^2/[K_l(1+x_w)\,k\,T_w^{1.8}\,\epsilon_{uv}] \tag{A7}$$

and

$$a_{wb} = [(1+x_w)(T_w/T_c)\,K_l^{-1}]^{1/3}\,a_{0l}\,. \tag{A8}$$

These correspond to equations (46)–(48) and (37) of MO respectively. Here $\bar{n}$ and ϵ_{uv} are respectively the mean gas density and mean volume emissivity of ionizing radiation, T_w and T_c are the temperatures of the warm and cold cloud components and x_w is the fractional ionization in the warm envelopes. K_l is the ratio of the smallest cloud mass to that of the largest fully ionizable cloud. We take a_{0u} the radius of the largest cloud to be that of the most massive magnetically supported cloud as given by Mouschovias & Spitzer (1976). Given values of S, E_0, ϵ_{uv} and $\bar{n}$ and adopting values for T_w, T_c, α, β, γ, $\phi_g(l)$, ϕ_m and K_l the equations (A3)–(A8) can be solved iteratively to obtain values of Q_c, a_{wb}, a_{0u}, a_{0l}, $\langle P\rangle$ and x_w. Thence, we may obtain values for the cloud filling factors and other parameters discussed in the text by means of the equations given by MO.

The corresponding problem for the non-evaporative solution is solved in an analagous manner but with equation (6) and Cox's (1979) expression for $\langle P\rangle$ replacing equations (A3) and (A4).

For convenience of reference we list below the values of the various parameters adopted from MO together with the ranges of the galactic model parameters discussed in the text.

c	Density jump across density wave shock = 5, 10
E_0	Explosion energy per supernova = 2.5×10^{50} erg, 5×10^{50} erg
K_l	Ratio of smallest cloud mass to mass of largest wholly ionizable cloud = 2
m	Exponent of star formation = $^1/_2$, 1, 2
$\bar{n}$	Total mean density of interstellar gas (cm^{-3})
S_{gal}	Galactic supernova rate = 0.02, 0.05 galaxy^{-1} yr^{-1}
T_w	Temperature of warm envelopes = 8000 K
T_c	Temperature of cold cores = 80 K
t_0	Full width at $1/e$ height of spiral shock in units of time = 3×10^7 yr
t_*	Time delay between star formation and first supernova = 1×10^7 yr
α	Blast wave velocity divided by isothermal sound speed in remnant interior = 2.5
β	Radiative cooling enhancement factor = 10
γ	Cloud compression exponent = $^1/_3$
ϵ_{uv}	Mean volume emissivity of ionizing photons ($cm^{-3}\,s^{-1}$)
ϕ_m, ϕ_g	Magnetic and geometrical efficiency constants for evaporation = $^1/_3$, 1
Ω_p	Density wave pattern speed = 13.5 km s^{-1} kpc^{-1}
$\Omega(R)$	Galactic rotation curve = $250/R$ km s^{-1} kpc^{-1}

Mon. Not. R. astr. Soc. (1983) **203**, 67–86

The state of clouds in a violent interstellar medium

S. R. Heathcote and P. W. J. L. Brand *University of Edinburgh, Blackford Hill, Edinburgh EH9 3HJ*

Received 1982 May 17; in original form 1982 January 14

Summary. A highly approximate but simple model of the interaction of a supernova blast wave with an interstellar cloud is described. This is used to explore the behaviour of a cloud when exposed to conditions prevalent in a violent interstellar medium. We find that having been shocked a cloud is rarely allowed sufficient time to return to pressure equilibrium with its surroundings before encountering a second shock. Significant departures from pressure equilibrium are therefore inevitable. The disruption of a cloud by its passage through a blast wave is quite effective and the half life of clouds cannot greatly exceed the mean interval between shocks striking a given cloud. In particular, we find that composite core-envelope clouds are not viable under typical conditions. Results for the net rates of thermal evaporation and PV work are also presented.

1 Introduction

Interaction between supernova remnants (SNR) and interstellar clouds play a central role in our present conception of the interstellar medium (ISM). In the three-phase model (hot, warm and cool material, McKee & Ostriker 1977; Cox 1981; Brand & Heathcote 1982) SNRs generate a pervasive hot but tenuous medium, whose pressure is responsible for the confinement of cooler and denser cloud components. In addition SNRs are a major source of cloud energy both in the form of bulk motions and thermal energy (cosmic-ray, UV and soft X-ray heating, 'cloud crushing'). Conversely, interstellar clouds dissipate SNR energy both in their direct role as energy sinks and by providing a source of new material for the hot phase (evaporation, mechanical ablation) thereby increasing the efficiency of direct radiative losses from the hot gas. This 'symbiotic' relationship between clouds and SNRs determines the equilibrium properties of the ISM. The nature of the mechanisms involved guarantee significant departures from thermal and pressure equilibrium at the level of individual clouds. For conditions in the solar neighbourhood the time-scales governing the essential physical processes (SNR shock repetition time, cloud dynamical response time, radiative cooling time, ionization and recombination times, evaporation time-scale etc) are all similar, and close to $\sim 10^5$–10^6 yr. The state of any given cloud will then be a complex function of its past history as well as the nature of its present surroundings.

In the present paper we attempt to follow the response of individual clouds to their changing environment. In particular we will be concerned with the determination of some sort of average cloud state. This is important both for the construction of global theoretical models and for comparison with observation. In the next section we assemble a highly simplified model for the interaction of an isolated cloud with a single SNR blast wave, generalized from the numerical example by Woodward (1976).

In Section 3 we enumerate a number of the complicating factors associated with the 'real world' of a three-phase ISM and establish the domain of validity of this simple model. In Section 4 we discuss a number of the consequences of our model for theories of the ISM while in the final section we summarize our principal results.

2 Basic cloud model

A number of authors have addressed the problem of the dynamical response of an interstellar cloud to being overrun by a shock wave (e.g. Bychcov & Pikel'ner 1975; McKee & Cowie 1975; Sgro 1975; Dyson & Gulliford 1975). The most 'realistic' calculations available to date are those of Woodward (1976, 1979, hereinafter W76 and W79) who employed a two-dimensional hydrodynamic code to follow the cloud evolution in considerable detail. These computations were carried out for essentially only one set of model parameters chosen for their relevance to the problem of star formation in massive clouds, imploded by density wave shocks. The formidable scale of the computing problem involved precluded any attempt at a parameter study. For our purposes it is necessary to extend the applicability of these calculations to encompass the large volume of parameter space appropriate to the interaction of clouds with SNR blast waves. To accomplish this we employ Woodward's results to identify the important physical processes which can be expected to occur and we then attempt to model these with simple highly approximate analytic calculations. In this way it is possible to assemble a crude model of the interaction dynamics capable of reproducing the gross features of the detailed computations which then forms the basis for a plausible extrapolation to other conditions. A few points about this procedure are worth noting at the outset.

(i) We will not hesitate to sacrifice numerical accuracy in favour of analytical simplicity. The uncertainties in the initial conditions inherent in our current understanding of the three-phase ISM are sufficient that a factor of 2 or so is unlikely to prove of vital importance.

(ii) Although throughout we will be guided by physical principles, the justification for our selection of the important processes and our approximate treatment of them rests heavily on the numerical models.

(iii) We are aware that processes not apparent in the computed models may become important in other regions of parameter space. Some of these will be discussed in Section 3, and their consequences in Section 4.

We begin the discussion of our approximate model with a brief summary of the important results of Woodward's computations.

2.1 WOODWARD'S RESULTS

In W76 the collision of a plane parallel shock of mach number $M_b \sim 2.6$ with an initially spherical cloud having a density ~ 80 times that of the pre-shock intercloud medium (ICM) was studied. The cloud was initially at rest in, and in pressure equilibrium with, the ICM.

The equation of state of the ICM was a $\gamma = 5/3$ adiabat while that of the cloud was effectively isothermal. In W79 the parameters of the cloud were unchanged, but an isothermal equation of state was used for the ICM. This had the important dynamical effect that the post-shock flow was supersonic with respect to the cloud and so a bow shock formed upstream of the cloud. The evolution was also followed to a considerably later stage in this case. The main features of the interaction are, however, similar in both studies. These are (see also Fig. 1):

(i) As the external shock (S_0) overruns the cloud its ram pressure drives a strong shock (S_1) into the front face of the cloud (Sgro 1975; Silk & Solinger 1973). Subsequently, when steady flow around the cloud is established, this shock is driven by the high pressure in the vicinity of the front stagnation point.

(ii) Having swept over the cloud, the various segments of the shock meet almost head-on at the back of the cloud and are reflected leading to a transiently high pressure there. This drives a somewhat weaker shock (S_2) into the back of the cloud. The pressure behind the cloud falls rapidly as the intersection point of the external shock segments moves downstream and the angle of incidence increases. However, the flow around the cloud conspires with the sideways flow of the reflected shocks to set up a vortex system the pressure of which, combined with the thermal pressure of the ICM, continues to drive S_2 (Fig. 1a).

(iii) The shock driven into the sides of the cloud (S_3) is quite weak and the lateral compression of the cloud is only moderate. Together with points (i) and (ii) this implies that the cloud collapse is essentially one-dimensional and for much of the time it can, in fact, be treated as approximately plane parallel.

(iv) In the subsonic case, the sides of the cloud are Kelvin–Helmholtz unstable. The instability grows rapidly and is later amplified by the Rayleigh–Taylor instability. When the flow over the cloud is strongly supersonic the Kelvin–Helmholtz instability is suppressed (Gerwin 1968).

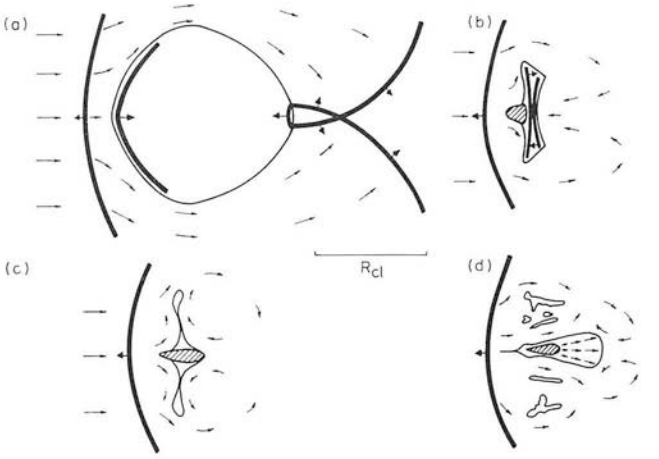

Figure 1. A schematic representation of the clouds structure at various stages during its collapse and subsequent re-expansion. Heavy lines represent shocks; broad tipped arrows attached to these indicate the downstream side of the shock. The cross hatched areas indicate the zone of enhanced density associated with the axial clump. Narrow tipped arrows depict the flow of the gas around the cloud. (a) $\tilde{t} \simeq 3A/M_b$ ($t \sim 0.01$ Myr for the typical cloud of Table 1). The various segments of the external shock have just met at the back of the cloud. (b) $\tilde{t} \simeq 0.6/M_b$ ($t \sim 0.5$ Myr). The shocks driven into the front and back of the cloud are about to collide. (c) $\tilde{t} > 0.6/M_b$ the re-expansion of the cloud in the downstream direction has commenced. (d) $\tilde{t} \sim 0.6/M_b + 0.5$ ($t \sim 1.6$ Myr) a typical stage during the re-expansion.

(v) The convergence of the shock S_1 causes it to accelerate (Zel'dovich & Raiser 1968) and leads to the front face of the cloud being Rayleigh–Taylor unstable. The resulting flow of cloud gas towards the symmetry axis leads to the formation of a dense clump of material there. In the subsonic case this collection process is limited to the zone between the Kelvin–Helmholtz tongues closest to the symmetry axis (Fig. 1b).

(vi) Eventually S_1 and S_2 collide. The shock reflected towards the back of the cloud is much stronger than that reflected towards the front. The cloud at this stage is strongly flattened so this shock reaches the back of the cloud very soon after the interaction (Fig. 1c).

(vii) At the back of the cloud a weak shock is propagated into the ICM and a strong rarefaction wave is reflected back into the cloud. This 'engulfs' most of the material near the symmetry axis including the dense clump and a fan of quite dense material expands rapidly in the downstream direction. Any expansion upstream is prevented by the pressure at the forward stagnation point.

(viii) The remaining cloud material is confined to an extremely thin sheet. This also begins to re-expand but is quite rapidly fragmented by Kelvin–Helmholtz instability before this process has progressed very far (Fig. 1d).

As noted above, the cloud equation of state employed by Woodward was essentially isothermal. Fortunately, a calculation for the same case as W76 but with an adiabatic equation of state has been performed by Thorogood (1979). The main dynamical features discussed above in (i)–(iii) and (vi) are reproduced in this calculation except that the cloud is substantially less flattened. This latter effect can be entirely understood in terms of plane parallel calculations discussed below. Unfortunately, the resolution of the computation was insufficient to show the instability in (iv) and (v) although Thorogood estimates that they should have occurred. Because of the important role played by the dense axial clump in the re-expansion phase, we cannot be confident of the details of the re-expansion phase in adiabatic clouds.

The phases outlined in (i)–(viii) above seem to be inevitable parts of a shocked cloud's evolution. Phases (iv) and (v) cause the greatest difficulty, since they represent highly non-linear processes, namely the interactions between surface instabilities and the complex flow regime outside the cloud. In the following subsections we shall approximate each of the phases either by an analytical solution, or by a fit to the data derived by reasonable extrapolation from Woodward's model.

2.2 THE COLLAPSE PHASE

To the extent that we may neglect self-gravity, and provided cooling and heating of the gas occur on time-scales either very long or very short compared to the dynamical time-scale then we may scale results obtained for a cloud of given size to yield those appropriate to a cloud of different size by simply multiplying all lengths and times by a common factor. It is thus convenient to introduce the dimensionless lengths times and velocities defined by

$$\tilde{R} = R/R_{\mathrm{cl}} \qquad \tilde{t} = C_{\mathrm{cl}}\, t/R_{\mathrm{cl}} \qquad \tilde{u} = u/C_{\mathrm{cl}}. \tag{1}$$

Here R_{cl} and C_{cl} are respectively the initial scale length and sound speed of the undisturbed cloud. The problem then reduces to one containing essentially only two parameters, namely the Mach number, M_{b} of the incident shock and the ratio A of C_{cl} to the sound speed of the undisturbed ICM, C_{ic}. We must also specify the polytropic indices describing the equation of state of the cloud and the ICM, γ_{cl} and γ_{ic} respectively. In the case of infinite cooling times we take $\gamma = 5/3$ while in the opposite case of infinitesimal cooling times we take $\gamma = 1$.

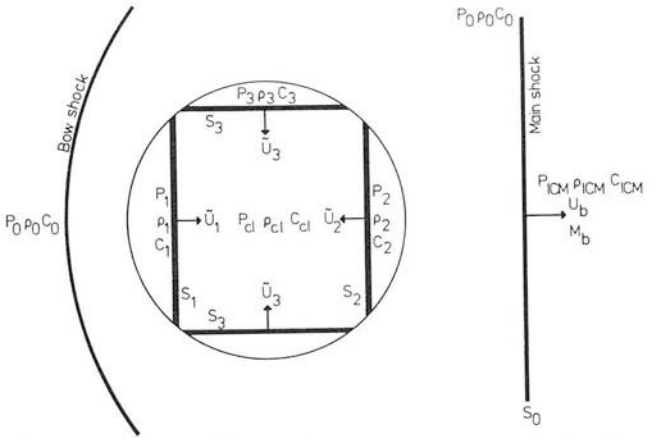

Figure 2. A schematic representation of the cloud during the collapse phase showing our notation for the several shocks and their velocities and for the pressures P, densities ρ and sound speeds C in the various zones.

Our approximation is to assume that the front cloud shock S_1 and the back cloud shock S_2 are plane parallel and are driven by the front stagnation point pressure, P_1 and the pressure at the back of the cloud, P_2 (see Fig. 2). We also ignore the influence of the lateral cloud shock, S_3 upon the motion of these shocks. In reality, although as noted above S_1 and S_2 are almost plane, their strengths decrease with distance from the symmetry axis (the distinction between S_1, S_3 and S_2 is of course purely artificial) so our results will only be approximately true on the symmetry axis. However, comparison with Woodward's model suggests that this approximation is a good one.

The calculation of P_1 is straightforward. Following the impact of the external shock, S_0, with the front of the cloud, a strong shock is transmitted into the cloud and a weak shock is reflected back into the ICM. There then follows a transient phase (Silk & Solinger 1973; Sgro 1975) during which steady flow becomes established around the cloud. The reflected shock either disappears upstream, if the flow behind S_0 is subsonic with respect to the cloud, or else forms a standing bow shock. This phase only lasts for a time comparable with the cloud crossing time for the external shock $\sim A/M_b$ and can be shown to have only minor importance for the cloud dynamics.

Subsequently, the situation is that discussed by McKee & Cowie (1975). They found that for $\gamma_{ic} = 5/3$,

$$\begin{aligned} P_1/P_0 &= (1 + M^2/3)^{5/2} && M \leqslant 1, \\ P_1/P_0 &= 1.5\, M^2\,[1 - 1/(5M^2)]^{-3/2} && M \geqslant 1. \end{aligned} \tag{2a}$$

Similarly, we find for $\gamma_{ICM} = 1$,

$$\begin{aligned} P_1/P_0 &= \exp(M^2/2) && M \leqslant 1, \\ P_1/P_0 &= M^2 \exp[1/(2M^2)] && M \geqslant 1. \end{aligned} \tag{2b}$$

Here, P_0 is the pressure behind S_0, while M is the local Mach number of the flow behind S relative to the cloud boundary. Applying the jump conditions for normal shocks to obtain the velocities of the gas behind S_0 and S_1 we find that in either case (remembering M_b is the Mach number of the initial shock and $A = C_{cl}/C_{ic}$)

$$M = (M_b^2 - 1)\ \{[\gamma_{ic} M_b^2 - {}^1\!/_2(\gamma_{ic} - 1)]\ [{}^1\!/_2(\gamma_{ic} - 1)M_b^2 + 1]\}^{1/2}\ \{1 - [A(\gamma_{ic} + 1)/(\gamma_{cl} + 1)\ (\tilde{u}_1^2 - 1)\,(M_b^2 - 1)(M_b/\tilde{u}_1)]\}\ . \tag{3}$$

Finally, since the cloud and ICM are supposed initially to be in pressure equilibrium the normal shock jump conditions imply that the velocity $\tilde{u}$, behind S_1 is given by

$$\tilde{u}_1^2 = \{(P_1/P_0)(\gamma_{cl}+1)/[(\gamma_{ic}+1)\gamma_{cl}]\ [\gamma_{ic}M_b^2 - {}^1/_2(\gamma_{ic}-1)]\} + {}^1/_2(\gamma_{cl}-1)/\gamma_{cl}. \quad (4)$$

Equations (2), (3) and (4) together reduce to a transcendental equation for $\tilde{u}_1$ as a function of M_b and A. McKee & Cowie (1975) obtained an approximate solution for the case $\gamma_{ic} = 5/3$ under the simplifying assumption that both S_0 and S_1 are strong. From this an expression can be derived for $\tilde{u}_1$ in terms of M_b and A which errs from the exact solution by less than 50 per cent even near $M_b \sim 1$. Similarly, for $\gamma_{ic} = 1$ we have derived an expression for $\tilde{u}_1$, which is everywhere accurate to ~ 20 per cent. When A is very small as it will be in all cases of interest here we may further simplify by taking the limit $A \to 0$ which leads to,

$$\tilde{u}_1 \sim 1.4\,[(\gamma_{cl}+1)/\gamma_{cl}]^{1/2}M_b \qquad \gamma_{ic} = {}^5/_3 \quad (5a)$$

$$\tilde{u}_1 \sim 0.71\,[(\gamma_{cl}+1)/\gamma_{cl}]^{1/2}M_b^2 \qquad \gamma_{ic} = 1. \quad (5b)$$

The pressure at the back of the cloud just after the collision of the external shock segments can be estimated from the standard results for the head-on collision of two plane shocks. Again this pressure is only transient and we may neglect its effects on the motion of S_2. Because of the contribution from the ram pressure of the vortex system behind the cloud an exact calculation of the value of P_2, during the subsequent evolution of the cloud would be extremely complex. However, comparison with Woodward's results suggests that an adequate approximation is $P_2 = \xi P_0$ with ξ of order unity. Thus, in the strong shock limit we may write

$$\tilde{u}_2^2 \simeq \xi(\gamma_{ic}/\gamma_{cl})\,[(1+\gamma_{cl})/(1+\gamma_{ic})]\,M_b^2. \quad (6)$$

In the limit of very low M we may estimate the pressure at the sides of the cloud from the solution for the steady flow of an incompressible fluid around a rigid sphere (e.g. Currie 1974). The results may then be crudely extended for finite, but still subsonic incident flow speeds by means of the Prandtl–Glauert rule (Currie 1974). For our purposes a sufficient approximation to the value of $\tilde{u}_3$ for arbitrary M, which is in agreement with both these approximate subsonic calculation and Woodward's results, is obtained from equation (6) with $\xi \sim 0.25$.

The collapse phase ends when S_1 and S_2 collide after a time

$$\tilde{t}_{col} = (2 + \tilde{u}_2\tilde{t}_{inj})/(\tilde{u}_1 + \tilde{u}_2) \quad (7)$$

where $\tilde{t}_{inj}$ is the time of injection of S_2 into the back of the cloud which we estimate to be $\sim 3A/M_b$. Employing the strong shock and small A approximations we obtain

$$\tilde{t}_{col} \sim [\gamma_{cl}/(\gamma_{cl}+1)]^{1/2}M_b^{-1} \qquad \gamma_{ic} = {}^5/_3, \quad (8a)$$

$$\tilde{t}_{col} \sim 3\,[\gamma_{cl}/(\gamma_{cl}+1)]^{1/2}\,[M_b\,(M_b+1)]^{-1} \qquad \gamma_{ic} = 1. \quad (8b)$$

Comparison with W76 and W79 suggests that these estimates are ~ 40 per cent too small. The more exact calculation using equation (4) for $\tilde{u}_1$ gives a result ~ 11 per cent too small.

2.3 THE DEVELOPMENT OF THE DENSE AXIAL CLUMP

What fraction of the clouds mass can be accumulated into the dense clump created by the Rayleigh–Taylor initiated lateral collapse of material behind the front shock S_1? This depends on:

(i) The effective area of the front surface of the cloud from which material may be collected. If the incident flow is subsonic this is determined by the lateral distance to the Kelvin–Helmholtz tongues closest to the symmetry axis.

(ii) The rate at which the Rayleigh–Taylor instability can collect the available material.

Following W76 we obtain for the ratio of the growth time of a given Kelvin–Helmholtz mode to the dynamical time-scale of the cloud,

$$t_{KH}(\tilde{K})/t_{dyn} \sim (\gamma_{ic}/\gamma_{cl})^{1/2}\tilde{K}^{-1}(\tilde{u}_1/M_{slip})(C_{cl}/C_1)$$

where $\tilde{K}$ is the wave number of the mode in units of R_{cl}^{-1}, M_{slip} is the local Mach number of the flow at the cloud boundary and C_1 is the sound speed in the gas behind S_1. If we again employ the solution for incompressible flow about a rigid sphere, we find $M_{slip} \sim M \sin\phi$ where ϕ is the polar angle of a given point on the cloud surface measured from the symmetry axis. Using this together with the exact solutions to equations (2)–(4) we find that the ratio of the time-scales for fixed ϕ becomes almost independent of M_b for $M_b \gtrsim 2$ ($\gamma_{ic} = 1$ or $5/3$). Thus for incident shocks stronger than this but weak enough that the post-shock flow is still subsonic with respect to the cloud, the general form of the Kelvin–Helmholtz ripples will be very similar to those found in W76. Since we will generally be interested in $M_b \gtrsim 2$ we can therefore assume a roughly constant collecting area for the axial clump in the subsonic regime.

For $A = 0$ ('rigid' cloud) the flow behind S_0 is subsonic with respect to the cloud when $M_b < 2.7$ for $\gamma_{ic} = 5/3$ and $M_b < 1.62$ for $\gamma_{ic} = 1$. However, for non-zero A this limit can be appreciably raised. Once the flow around the cloud is supersonic, as noted above, the Kelvin–Helmholtz instability is suppressed (Gerwin 1968) and effectively the whole area of the front face of the cloud is available for the collection of clump material.

As discussed in W76 the ratio of the growth rate of the Rayleigh–Taylor instability to the dynamical time-scale is only weakly dependent on M_b in an indirect manner through changes in the degree of flattening of the front face of the cloud. There is thus no simple way of determining the relationship between M_b and the efficiency with which material is collected to form the clump, and we estimate the fraction collected by inspection of Woodward's models.

At the end of the computation for the subsonic case (W76) just before the collision of S_1 and S_2 the clump contained ~ 5 per cent of the cloud's mass but was still growing. If all the available material was incorporated into the clump before the re-expansion of the cloud commenced then we estimate that the fraction of the cloud mass contained in the clump would be $F \simeq 0.1$. Careful 'planimetry' of the diagrams for the supersonic case (W79) suggests that there $F \simeq 0.5$. We will take these two values as representative of the subsonic and supersonic regimes, although possible weak dependence of F on M_b through the collection efficiency should be borne in mind.

2.4 THE COLLISION OF SHOCKS S_1 AND S_2

To the extent that S_1 and S_2 are very nearly parallel at the time of their collision we may employ simple shock tube theory (Bradley 1962) to calculate the effect of the collision. When $\gamma_{cl} = 1$ (the isothermal case) the consequences of the collision are straightforward. The shocks S_1 and S_2 'pass through' each other, their Mach numbers being unaffected, although of course they now travel into a medium of higher density which has already passed through the other shock (the sound speed in this gas is still C_{cl}, however). The density of the twice shocked material between S_1 and S_2 becomes $\sim \tilde{u}_1^2\tilde{u}_2^2\rho_{cl}$.

Conversely, when $\gamma_{cl} = 5/3$ the properties of the resultant shocks can only be found from a complete analysis. Nevertheless, a procedure which is sufficient to determine the resulting density, given that S_1 and S_2 are not of drastically different strengths is to employ the result for the collision of two identical shocks of strength $(\tilde{u}_1 + \tilde{u}_2)/2$. Comparison with the exact calculation shows that this procedure gives a value for the resulting density which errs by $\lesssim 30$ per cent from the true mean density in the cases of interest.

Since as we have seen the cloud becomes considerably flattened for quite moderate shock strengths, the time between the collision of S_1 and S_2 and the arrival of the rearward moving shock at the back of the cloud is quite short compared to t_{coll}. In what follows we will therefore neglect it and take the re-expansion phase as starting immediately after the collision of S_1 and S_2.

2.5 THE RE-EXPANSION PHASE: TAIL GROWTH

Although the outflow behind the rarefaction wave is initially plane parallel, as the cloud 'tail' develops it expands laterally and the plane parallelism quickly disappears. Comparison with W79 suggests that the ensuing motion is more nearly spherically symmetric. In our approximate treatment of the tail's evolution we therefore treat it as forming a segment of a gas sphere expanding freely into vacuum.

For $\gamma_{cl} = 1$ the density profile and equation of motion are (Kahn 1972; Imshenik 1960).

$$\rho(r, t) = \rho_c(t) \exp[-r^2/2R(t)] \tag{9a}$$

$$P(r, t) = C_{cl}^2 \rho(r, t) \tag{9b}$$

$$v(r, t) = \sqrt{2}\, C_{cl} \{\ln[R(t)/R(0)]\}^{1/2} r/R(t) \tag{9c}$$

$$C_{cl}\, t/R(0) = \sqrt{2}\, R(t)/R(0) D\, \langle \{\ln[R(t)/R(0)]\}^{1/2} \rangle. \tag{9d}$$

Here,

$$D(x) = \exp(-x^2) \int_0^x \exp(-y^2) dy\,,$$

and the boundary conditions $R = R(0)$, $\dot{R}(t) = 0$ at $t = 0$ have been imposed. Obviously, the validity of this solution requires that the above density profile should hold at all times including the initial instant. Although this is patently not true it is to be expected that at times sufficiently great that the initial conditions have been forgotten, the evolution for the case of an arbitrary initial density distribution will not differ greatly from equation (9). Furthermore, comparison with W79 shows that the actual density profile, velocity profile and evolutionary time-scale do not differ grossly from that given by this solution even at quite early times.

For $\gamma_{cl} = 5/3$ the corresponding density profile and equation of motion are (Zel'dovich & Raizer 1968)

$$\rho(r, t) = \rho_c(t) \{1 - [r/R(t)]^2\}^{3/2} \tag{10a}$$

$$P(r, t) = P_c(t) \{1 - [r/R(t)]^2\}^{5/2} \tag{10b}$$

$$v(r, t) = \sqrt{3}\, C(o) \{1 - [R(o)/R(t)]^2\}^{1/2} r/R(t) \tag{10c}$$

$$C(0)t/R(0) = \langle 1/3 \{[R(t)/R(0)]^2 - 1\} \rangle^{1/2} \tag{10d}$$

here $C(0)$ is the sound speed of the tail gas at the beginning of the expansion and the same boundary conditions as above have been employed.

To complete the solution in either case we must obtain the value for the initial scale length, $R(0)$. To do this we require that the mass of the conical segment representing the tail should equal the mass of the dense clump from which we obtain

$$R(0) = R_{cl}\{[\rho_{cl}/\rho_c(0)]\, F\Theta(\theta)\}^{1/3} \qquad \gamma_{cl} = 1 \tag{11a}$$

$$R(0) = R_{cl}\{[\rho_{cl}/\rho_c(0)]\, F\Theta(\theta)\}^{1/3} \qquad \gamma_{cl} = 5/3 \tag{11b}$$

where

$$\Theta(\theta) = [2 + \sin^2\theta\cos\theta + \cos^3\theta - 3\cos\theta]^{-1}$$

and θ is the semi-angle of the conical segment. From W79 we estimate $\theta \sim 20^\circ$ so that $\Theta \sim 8$.

The expansion phase ultimately ends when the tail reaches pressure equilibrium with its surroundings. We take $P_c(t)/2.7$ as the typical pressure in the tail (this is obtained at $r = 2R$ and $r \sim {}^1/_3 R$ for the isothermal and adiabatic cases respectively). We also take the pressure of the surroundings to be the pre-shock pressure P_{ic} rather than the post-shock pressure P_0. Hence, we obtain for the expansion time-scale

$$\tilde{t}_{exp} \approx 2F^{1/3}D\langle{}^1/_3 \ln\{[0.4P_c(0)/P_{ic}]\}\rangle^{1/2} \qquad \gamma_{cl} = 1 \tag{12a}$$

$$\tilde{t}_{exp} \approx [C_{cl}/C(0)]\, F^{1/3}\{1-1.5\,[P_{ic}/P_c(0)]^{2/5}\}^{1/2} \qquad \gamma_{cl} = 5/3\,. \tag{12b}$$

Table 1. Values for the critical phases of evolution of a 'representative cloud', showing the scaling with the controlling parameters A and M_b. $R_{cl} = 2$ pc $C_{cl} = 0.8\,\mathrm{km\,s^{-1}}$, $t_{cl} = R_{cl}/C_{cl} = 2.5$ Myr, $A = C_{cl}/C_{ic} = 6.67\times10^{-3}$, $M_b = 3.5$, $\gamma_{cl} = 1$, $\gamma_{ic} = 5/3$.

Phase	Epoch		Extent				Comments
			Lateral		Axial		
	t/t_{cl}	Myr	Y/R_{cl}	pc	Z/R_{cl}	pc	
Shock reaches front of cloud	0		2.0	4.0	2.0	4.0	
External shock reaches back of cloud	$3A/M_b$	0.014	2.0	4.0	2.0	4.0	Shock is slowed by cloud boundary. Fig. 1(a)
'Typical' stage during collapse		0.23		3.0		1.0	Time is $t_{col}/2$
Shocks S_1 and S_2 collide	$0.64/M_b$	0.46	0.98	2.0	$0.9M_b^{-2}$	0.15	Time is t_{col} equation (8a). Extents calculated from $\bar{U}_1$ equation (6a). and $\bar{U}_2$ equation (7). Fig. 1(b).
'Typical' stage during re-expansion		1.6		0.55		1.2	Time is $t_{col} + t_{exp}/2$ Fig. 1(d).
End of re-expansion pressure equilibrium	$0.72 + 0.64/M_b$	2.3	0.55	1.1	1.2	2.4	Time is $t_{col} + t_{exp}$ equation (12a). t_{exp} is nearly independent of M_b. Length is scale length of tail $R(t_{exp})$ equation (9c): Width from 20° opening angle.

2.6 SUMMARY OF CLOUD MODEL: A REPRESENTATIVE CASE

To provide a better feel for the results of this section we give values for the cloud dimensions and time-scales for a 'representative' cloud at various phases during its evolution in Table 1. The parameters chosen for this 'representative' cloud are $R_{cl} = 2$ pc, $C_{cl} = 0.8\,\mathrm{km\,s^{-1}}$, $C_{ic} = 120\,\mathrm{km\,s^{-1}}$, $M_b = 3.5$, $\gamma_{cl} = 1$ and $\gamma_{ic} = 5/3$. The term 'typical' in the table is used to describe times half way through the collapse and half way through the re-expansion.

3 The 'real world' of a three-phase ISM

So far we have considered a highly idealized model for a cloud shock wave interaction. Our model is an over-simplification in a number of respects:

(i) Our initial conditions were that the cloud was in pressure equilibrium with, and at rest in, the ICM.

(ii) Our cloud was initially spherically symmetric and structurally homogeneous.

(iii) We employed a simple polytropic equation of state for the cloud throughout its evolution.

In addition, a number of potentially important physical processes have so far been neglected. In this section we will concentrate on establishing the time-scales of these various processes to compare with the clouds evolution time-scale. The effects that the processes have on the

Table 2. Adopted values of various ISM parameters for the solar neighbourhood. After McKee & Ostriker (1977) and Brand & Heathcote (1982).

Parameter	Value
Intercloud medium	
Sound speed	$C_{ic} \simeq 95\sqrt{\gamma_{IC}}\,\mathrm{km\,s^{-1}}$
Temperature	$T_{ic} \simeq 7\times10^{5}\,\mathrm{K}$
Density	$n_{ic} \simeq 2\times10^{-3}\,\mathrm{cm^{-3}}$
'Cold clouds'	
Sound speed	$C_{cl} \simeq 0.8\sqrt{\gamma_{cl}}\,\mathrm{km\,s^{-1}}$
Temperature	$T_{cl} \simeq 10^{2}\,\mathrm{K}$
Density	$n_{cl} \simeq 30\,\mathrm{cm^{-3}}$
$A = C_{cl}/C_{ic}$	$A \simeq 8.4\times10^{-3}\sqrt{\gamma_{cl}/\gamma_{IC}}$
'Warm clouds'	
Sound speed	$C_{cl} \simeq 10\sqrt{\gamma_{cl}}\,\mathrm{km\,s^{-1}}$
Temperature	$T_{cl} \simeq 10^{4}\,\mathrm{K}$
Density	$n_{cl} \simeq 0.2\,\mathrm{cm^{-3}}$
Ionization fraction	$x_{cl} \simeq 0.5$
$A = C_{cl}/C_{ic}$	$A \simeq 0.11\sqrt{\gamma_{cl}/\gamma_{IC}}$
Supernova remnants	
Volumetric supernova rate	$S \simeq 1\times10^{-13}\,\mathrm{pc^{-3}\,yr^{-1}}$
Energy per supernova	$E_0 \simeq 1\times10^{51}\,\mathrm{erg}$
Porosity parameter	$Q_c \simeq 0.5$
SNR cooling radius	$r_c \simeq 182\,\mathrm{pc}$
Interior density at r_c	$n_c \simeq 5\times10^{-3}\,\mathrm{cm^{-3}}$
Interior temperature	$T_h \simeq 4.4\times10^{5}(M_b/M_{bc})^2\,\mathrm{K}$
Blast wave mach number at r_c	$M_{bc} \simeq 3.5$
Shock repetition time	$t_{sn} \simeq 3\times10^{5}\,\mathrm{yr}$
Miscellaneous	
Ambient photoionizing UV flux	$J \simeq 0.2\times10^{5}\,\mathrm{cm^{-2}\,s^{-1}}$
Cloud number density	$N_{cl} \simeq 6\times10^{-3}\,\mathrm{pc^{-3}}$
Cloud velocity parameter	$\langle R_{cl}^2 V_{cl}\rangle \simeq 9.5\,\mathrm{pc^2\,km\,s^{-1}}$

cloud evolution will be discussed in Section 4. The processes considered are: multiple shocks, cloud evaporation, ionization, H_2 formation, cloud–cloud collisions and self-gravity.

As discussed above the dynamics of the cloud are specified by essentially three parameters; the cloud radius, R_{cl}; the ratio of its sound speed to that of the ICM, A, and the Mach number of the incident shock, M_b. Furthermore, when A is small, as it often is in the cases of interest, the problem ceases to be sensitive to its value. However, many of the other processes are dependent on additional parameters of the cloud and its surroundings. For definiteness of presentation we will adopt a single set of values for these various quantities which will be employed in all numerical examples and then indicate the scaling (usually simple) to other cases. The values, selected on the basis of both observation and theoretical models of the three-phase ISM (McKee & Ostriker 1977; Brand & Heathcote 1982) as being appropriate to the solar neighbourhood, are listed for ease of reference in Table 2. A general feature of any model of the ISM is the existence of two preferred equilibrium cloud temperatures viz $\lesssim 100\,K$ ('cold clouds') and $\sim 10^4\,K$ ('warm clouds'). We will treat these two cases separately.

The boundary of the region of validity in the (M_b, R_{cl}) plane appropriate for cold clouds is shown in Figs 3–5 for the following cases;

Fig. 3. Isothermal cloud, adiabatic ICM ($\gamma_{cl} = 1, \gamma_{ic} = 5/3$).
Fig. 4. Isothermal cloud, isothermal ICM ($\gamma_{cl} = 1, \gamma_{ic} = 1$).
Fig. 5. Adiabatic cloud, adiabatic ICM ($\gamma_{cl} = 5/3, \gamma_{ic} = 5/3$).

The calculation of the position of this boundary will now be described and the generalization to other cases will be discussed. At the end of the next section the question of which γ_{cl} to use is also settled.

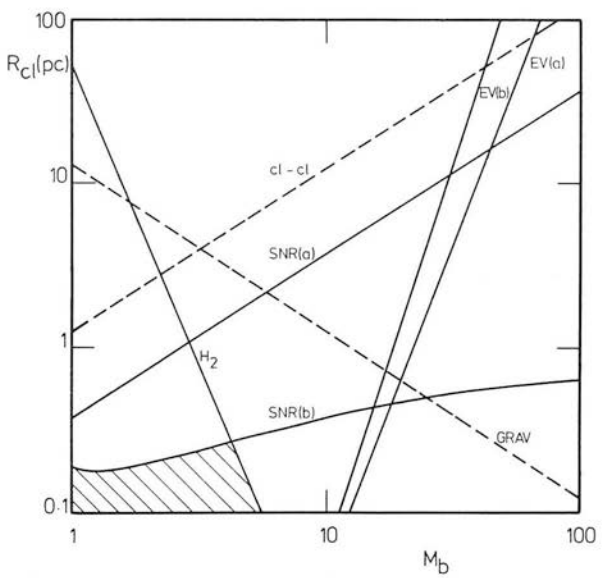

Figure 3. The domain of validity of our simplified model in the initial cloud radius (R_{cl}), incident shock Mach number (M_b) plane for 'cold' clouds when $\gamma_{ic} = 5/3$ and $\gamma_{cl} = 1$. Each labelled line represents one of the various constraints enumerated in Section 3. The label is always on the side of the line where the assumptions of the model are violated. For instance, above the line labelled SNR(a) clouds do not have sufficient time to complete their collapse before being overrun by a second shock. For details and the scaling to other conditions, see text. Shading indicates the region within which none of our assumptions is violated.

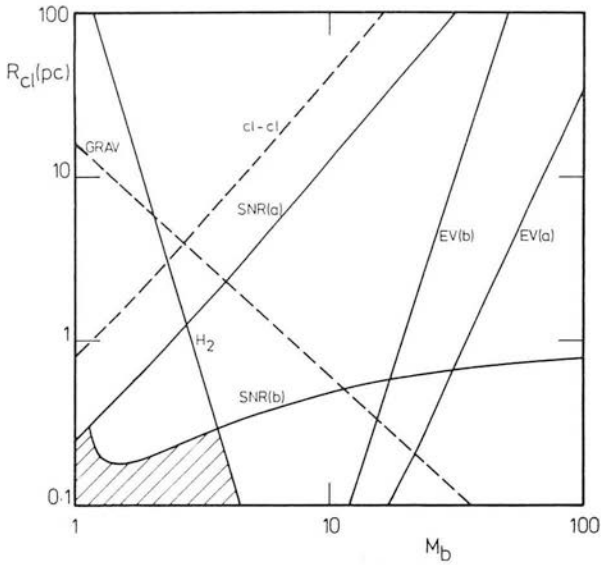

Figure 4. As Fig. 3 but $\gamma_{ic} = 1$ and $\gamma_{cl} = 1$.

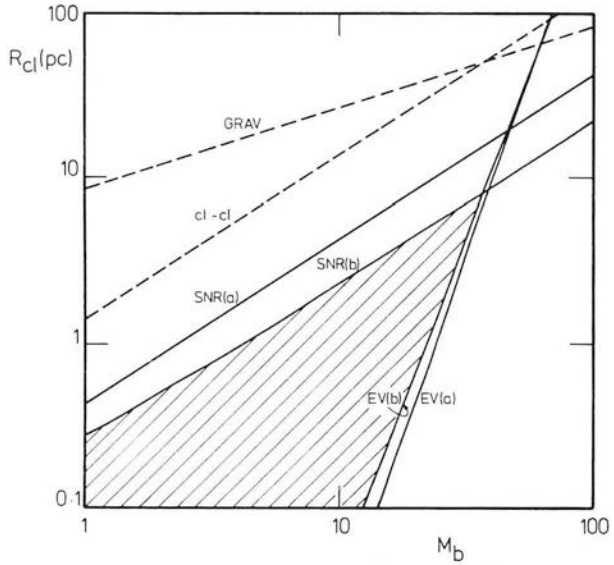

Figure 5. As Fig. 3 but $\gamma_{ic} = {}^5/_3$ and $\gamma_{cl} = {}^5/_3$.

3.1 SHOCK REPETITION

Quite generally the time between successive SNR having radii r smaller than some value r' is

$$t_{sn}(r \leqslant r') \simeq 2.4 \times 10^6 (100\,\mathrm{pc}/r)^3\,(10^{-13}\,\mathrm{pc^{-3}\,yr^{-1}}/S)\,\mathrm{yr}$$

where S is the volumetric supernova rate. By adopting a specific model of SNR evolution we may re-express this in a more useful form involving the shock Mach number. For instance if the standard evaporative model of McKee & Ostriker (1977, see also Brand & Heathcote 1982) is appropriate then

$$t_{sn}(M_b > M_b') \simeq 2.4 \times 10^6 (100\,\mathrm{pc}/r_{bc})(10^{-13}\,\mathrm{pc^{-3}\,yr^{-1}}/S)(M_b'/M_{bc})^{9/2}\,\mathrm{yr} \quad M_b' > M_{bc}$$

$$\simeq 5.5 \times 10^6 (100\,\mathrm{pc}/r_{bc})(10^{-13}\,\mathrm{pc^{-3}\,yr^{-1}}/S)(M_b'/M_{bc})^{1.92}\,\mathrm{yr} \quad M_b' < M_{bc}.$$

Here M_{bc} is the Mach number of the blast wave just before the SNR cools to form a dense shell of radius r_{bc},

$$M_{bc} \simeq 2.1\,(E_0/10^{51}\,\mathrm{erg})\,Q_c^{-0.75}\,(S/10^{-13}\,\mathrm{pc^{-3}\,yr^{-1}})^{0.75}$$

$$r_{bc} \simeq 200\,(E_0/10^{51}\,\mathrm{erg})\,Q_c^{0.23}\,(S/10^{-13}\,\mathrm{pc^{-3}\,yr^{-1}})^{0.23}$$

where E_0 is the initial explosion energy and Q_c is the porosity parameter, $0 \leqslant Q_c \leqslant 1$. Notice that because of the very strong dependence of t_{sn} on M_{bc}, the weaker shocks are by far the most common. Clouds have an almost negligible probability of interacting with SNR having $M_b \gtrsim 3M_{bc}$.

The line labelled SNR (a) in Figs 3–5 shows the locus of points for which $t_{sn} = t_{col}$. Similarly, the line labelled SNR(b) shows the locus of points for which $t_{sn} = (t_{col} + t_{exp})$ when F, the axial clump mass fraction equals 0.5. The curves for other values of F are displaced parallel to the R_{cl} axis by a factor $(F/0.5)^{1/3}$. The value of t_{sn} used in these figures has been calculated assuming all SNR, up to the maximum radius at which the remnants overlap and come into pressure equilibrium, contribute to the compression of the clouds. Changing the value of t_{sn} simply displaces these curves parallel to the R_{cl} axis such that $t_{sn}\,C_{cl}/R_{cl}$ = constant. So long as the cloud dynamical time-scales are insensitive to A ($A \lesssim 0.1$, $\gamma_{ic} = 5/3$; $A \lesssim 0.05$, $\gamma_{ic} = 1$) the same is true if C_{cl} is changed. In particular, the scaling to the case of warm clouds, may be made to sufficient accuracy by making an appropriate vertical displacement.

3.2 CLOUD EVAPORATION

Following Cowie & McKee (1977) the evaporation time-scale for a static spherical cloud is

$$t_{ev} \sim 3 \times 10^5\,n_{cl}\,(R_{cl}/\mathrm{pc})^2/\phi_m\,(T_h/10^6\,\mathrm{K})^{5/2}\,\mathrm{yr}$$

where T_h is the temperature of the surrounding medium and ϕ_m is an uncertain correction factor $\simeq 1/3$. To apply this to the case of our collapsing and (except at the initial instant) non-spherical cloud we multiply by a term $(\tilde{a}\,\phi_g)^{-1}$ evaluated at a typical stage in the appropriate phase of the clouds evolution. The term $\tilde{a}$ is the radius of a sphere having the same volume as the collapsed cloud (in units of R_{cl}) while ϕ_g is a correction for the flattening of the cloud estimated from the results of Cowie & Songaila (1977) for spheroidal clouds. During the collapse phase we evaluate $(\tilde{a}\,\phi_g)^{-1}$ when $\tilde{t} = \tilde{t}_{col}/2$ and similarly during the expansion phase when $\tilde{t} = \tilde{t}_{col} + \tilde{t}_{exp}/2$. The values of $(\tilde{a}\,\phi_g)$ derived in the strong shock small A limit are listed in Table 3.

The line labelled EV(a) in Figs 3–5 is the locus of points for which t_{ev} evaluated for the cloud as a whole equals t_{coll} while that labelled EV(b) is evaluated for the axial clump

Table 3. The evaporative reduction factor $(\tilde{a}\,\phi_g)$ (Section 3.2) at a typical point during the collapse, at the end of the collapse and at a typical point during re-expansion as functions of M_b.

γ_{cl}	γ_{ICM}	$(\tilde{a}\,\phi_g)$		
		$\tilde{t}_{col}/2$	$\tilde{t}_{col}$	$\tilde{t}_{exp}/2$
1	1	$[1 - 0.7/(M_b + 1)]^{2/3}$	$M_b^{-1}\,[1 - 1.4/(M_b + 1)]^{2/3}$	$0.2\,F^{1/3}$
1	5/3	0.7	$0.5\,M_b^{-2/3}$	$0.2\,F^{1/3}$
5/3	1	$0.9\,\{1 - [0.5/(M_b + 1)]\}^{2/3}$	$0.6\,[1 - (M_b + 1)^{-1}]^{2/3}$	$0.2\,F^{1/3}\,[C(0)/C_{cl}]^{1/3}$
5/3	5/3	0.7	0.4	$0.2\,F^{1/3}\,[C(0)/C_{cl}]^{1/3}$

when $F = 0.5$. The curves for other values of F are displaced parallel to the R_{cl} axis by a factor $(F/0.5)^{4/3}$. The scaling to other values of T_h is exactly as discussed in the case of t_{SN} (Section 3.1). Since $n_{cl} \propto C_{cl}^2$ it follows that $t_{ev} \propto (R_{cl}/C_{cl})^2$. Thus we may also scale to other values of A (in particular that appropriate to warm clouds) by displacing the plotted curves parallel to the R_{cl} axis such that $t_{ev} C_{cl}/R_{cl} = \text{constant}$.

3.3 IONIZATION

We estimate the time required for the ionization of an initially neutral static spherical cloud exposed to a steady isotropic flux J of ionizing photons to be (assuming a weak R ionization front and neglecting recombination)

$$t_{ion} \simeq 3 \times 10^5 n_{cl} R_{cl} (10^5 \text{cm}^{-2}\text{s}^{-1}/J) \text{yr}.$$

As in Section 3.2 above we correct to the case of a collapsing cloud by multiplying by $(\tilde{a}^2 \psi)^{-1}$ where ψ is again a flattening correction. Notice that since t_{ion} and the cloud dynamical time-scales are both proportional to R_{cl} the ratio $t_{ion}/(t_{col} + t_{exp})$ is simply an increasing function of M_b. For the value of J given in Table 2, t_{ion} is always much large than the dynamical time-scales for either warm or cold clouds. Typically, for t_{ion} to be comparable with $(t_{col} + t_{exp})$ when M_b is 1 requires $J \gtrsim 10^6$ photons $\text{cm}^{-2}\text{s}^{-1}$ for cold clouds and $J \gtrsim 5 \times 10^4$ photons $\text{cm}^{-2}\text{s}^{-1}$ for warm clouds.

A closely related time-scale which will be of interest in Section 4 is the time required for the formation of an equilibrium warm envelope around a cold core as envisaged by McKee & Ostriker (1977). Under the same assumptions we estimate this to be

$$t_{env} \simeq t_{ion} (n_{env}/n_{cl}) (R_{env}/R_{cl})^3$$

where R_{env} is the envelope radius.

3.4 H_2 FORMATION

The formation time-scale for H_2 molecules is (Spitzer 1978)

$$t_{H_2} \sim 1.6 \times 10^7 (100 \text{cm}^{-3}/n) \text{yr}$$

where a cloud temperature ~ 80 K is assumed. The value for n is derived from equations (9) or (10). The existence of a significant steady-state abundance of H_2 requires that the column density through the cloud should be great enough to provide adequate self-shielding in the Werner bands. An appropriate empirical criterion (Savage *et al.* 1977) is $R(t) \gtrsim (200 \text{cm}^{-3}/n)$pc.

There exists a region in Figs 3–5 within which the tails of cold clouds are sufficiently shielded and t_{H_2} is shorter than the expansion time. The boundary of this region which is only weakly dependent on the clump mass fraction is labelled H_2.

3.5 CLOUD–CLOUD COLLISIONS

We estimate

$$t_{cl-cl} \sim 0.6 \times 10^5 / [(N_{cl}/\text{pc}^{-3}) \langle (R_{cl}/\text{pc})^2 (V_{cl}/\text{km s}^{-1}) \rangle] \text{ yr}$$

where N_{cl} is the number of clouds per unit volume and V_{cl} is the rms cloud velocity. The average denoted by $\langle\rangle$ is taken locally over the entire ensemble of interstellar clouds. Because clouds overrun by the blast wave are accelerated to differing extents depending essentially

on their column density (McKee, Cowie & Ostriker 1978) clouds will tend to be struck from downstream by clouds of lower column density overrun at an earlier stage in the remnants expansion. Similarly, they will tend to run into clouds of higher column density overrun at a later stage. The shapes of the locii along which t_{cl-cl} is equal to the cloud dynamical time-scales are of course identical to those found for t_{sn} above, and obey the same scaling relations. The line for which $t_{cl-cl} = t_{col}$ is labelled cl–cl in Figs 3–5.

3.6 SELF-GRAVITY

The boundary of the region within which the self-gravity of the axial clump exceeds its thermal energy at the end of the collapse phase is indicated by GRAV in Figs 3–5. The clump is idealized as a sphere of mass F (clump fraction) times the mass of the cloud and radius equal to the thickness of the cloud along the symmetry axis at the end of the collapse phase. F has been taken as 0.5 scaling to other values can be obtained by multiplying by a factor $(F/0.5)^{-1/2}$.

3.7 RADIATIVE COOLING

The most useful cooling characteristic for treating the shocks is the cooling column density which can be written entirely in terms of the shock velocity, u_s. An important complication in determining the cooling column density is the ionization of the pre-shock material by radiation emitted by the shock itself. We employ the following relations from McKee & Hollenbach (1980).

$$N_{cool} \simeq 10^{19}\text{–}10^{20}\,\mathrm{cm^{-2}} \qquad 1\,\mathrm{km\,s^{-1}} \lesssim u_s \lesssim 20\,\mathrm{km\,s^{-1}}$$

$$N_{cool} \simeq 6.4 \times 10^{23}\,(\mathrm{km\,s^{-1}}/u_s)\,\mathrm{cm^{-2}} \qquad 20\,\mathrm{km\,s^{-1}} \lesssim u_s \lesssim 60\,\mathrm{km\,s^{-1}}$$

$$N_{cool} \simeq 8.0 \times 10^{8}\,(u_s/\mathrm{km\,s^{-1}})^{4.2}\,\mathrm{cm^{-2}} \qquad 60\,\mathrm{km\,s^{-1}} \lesssim u_s \lesssim 1000\,\mathrm{km\,s^{-1}}.$$

Adopting the standard cold cloud parameters we find that for $M_b \lesssim 11$ clouds having $R_{cl} < 0.1$–1 pc have cooling lengths N_{cool}/n_{cl} greater than R_{cl} and hence are 'adiabatic' while outside this region all cold clouds are more nearly isothermal. Conversely, for warm clouds having the standard parameters the cooling length is longer than R_{cl} when $M_b \gtrsim 4.7$ so that warm clouds struck by shocks stronger than this are effectively adiabatic.

4 Discussion

As a consequence of the phenomena discussed in Section 3, the typical cloud evolution will not be as straightforward as that described in the Woodward model. However, it is possible to use the simple model as a basis for the discussion of these phenomena and their effect on clouds, and to suggest what as a consequence is happening to cloud-like material in the supernova-dominated interstellar medium. Specifically, we discuss the mean pressure and shape of clouds and compressional heating of clouds. We also discuss mass-loss rates by shock ablation and evaporation and by warm envelope stripping.

4.1 DEPARTURES FROM PRESSURE EQUILIBRIUM

Perhaps the most striking result apparent in Figs 3–5 is the length of the cloud dynamical time-scales especially that for the re-expansion of isothermal clouds ($\gamma_{cl} = 1$) by comparison with the SNR shock repetition time. This has the important consequence that interstellar

clouds (with the exception of the very smallest) struck by a shock will rarely have time to relax back to pressure equilibrium with their surroundings before encountering a second shock. Furthermore, for clouds of still only modest size, the interaction with this second shock is quite likely to occur during the collapse phase. Clearly then the details of the interaction of any given shock with a cloud will depend in a most complex way on the past history of the cloud. In particular, they will be strongly dependent on the strength and direction of the previous shock(s) which interacted with the cloud, and how long has passed since that last interaction. We may, nevertheless, speculate about the general features of such an interaction on the basis of our simplified model.

First, consider the smaller clouds for which the shock repetition time is only slightly shorter than the expansion time-scale, and longer than the collapse time-scale. We will neglect the presence of the highly flattened sheet like outer region of the cloud and just consider the interaction of an SNR with an entity similar to the rather elongated, over-pressured and asymmetrically expanding cloud tail produced by a previous collision. If this new shock wave is very much stronger than the last shock to strike the cloud, then the expansion can be halted and the subsequent evolution of the cloud will be dominated by this new shock and will be similar to that computed. In the more probable case that both shocks are of similar strength (the majority of shocks have M_b comparable with M_{bc} Section 3.1), the expansion of the cloud is likely to continue. Nevertheless, shocks will be driven into the cloud in a manner similar to that envisaged. If the cloud tail is over-pressured with respect to the pre-shock ICM by a factor η, the 'velocities' of the cloud shocks will be reduced by a factor of $\eta^{1/2}$ in the strong shock, small A (large cloud–intercloud contrast) limit. Obviously, in this case the collapse and re-expansion of the cloud will be rather less ordered than that considered here but our results will still give a rough approximation.

In the extreme opposite limit of clouds for which the collapse time is very much longer than the shock repetition time we expect an entirely different pattern of events. Such clouds will experience a succession of external shocks of similar strength arriving from (by assumption) random directions. Consequently, they will 'see' an effective external pressure comparable to the sum of the post-shock thermal plus ram pressure for a typical shock. Any shocks driven into them will be relatively weak. Clouds somewhat smaller than this limiting case will most likely resemble the 'irregularly vibrating or writhing clouds' envisioned by Cox (1979) which at all times contain several shocks of moderate strength.

4.2 CLOUD MASS-LOSS RATES

As discussed in Sections 2.1 and 2.3 when the flow of the gas behind the external shock is supersonic with respect to the cloud ($M_b \gtrsim 3$, $\gamma_{ic} = 5/3$. $M_b \gtrsim 1.6$, $\gamma_{ic} = 1$ for the 'cold' clouds considered here and correspondingly $M_b \gtrsim 6.0$ or $M_b \gtrsim 2.0$ for the 'warm' clouds) a fraction, $F \sim 0.5$ of the clouds mass is collected into the cloud 'tail' while the remainder is left in a thin 'disc' which is rapidly fragmented by Rayleigh–Taylor instability. This process of shock ablation is a very effective mass-loss mechanism; the mass halving time is roughly the SNR shock repetition time (Section 4.1) $t_{sn} \sim 3 \times 10^5$ yr for the parameters adopted here, making it at least comparable in importance with the related process of cloud fission in cloud–cloud collisions (Chièze & Lazereff 1980).

If the incident flow is subsonic only ~ 0.1 of the cloud mass is confined to the tail. If the flattened disc is still disrupted as seems likely this effectively leads to the complete destruction of the cloud after only one shock passage. Although as shown in Section 3.2 thermal evaporation does not play a major role in the dynamics of the cloud-shock interaction under most circumstances, the evaporation rate is an important parameter in theoretical models

of the ISM as discussed in Section 1. As discussed in Section 3 the compression and flattening of the cloud reduce the evaporation rate relative to that of an undisturbed cloud by a factor $\sim \tilde{a}\phi_g$, which was tabulated at typical stages during the cloud's evolution (Table 3). An equally important effect in fixing the net evaporation rate at late times in the cloud's evolution is the disruption of the 'disc'. If this process leads to the formation of N_{fr} fragments of approximately equal size and possessing similar geometry to that of the original sheet the net evaporation rate for the 'sheet' is increased by a factor $N_{fr}^{2/3}$. As a rough estimate of the average evaporation rate over the cloud's evolution, we write

$$\langle \dot{M}_{ev} \rangle \simeq \dot{M}_{ev}(Sp)\,[(\tilde{a}\phi_g)_{col}\,(t_{col} + N_{fr}^{2/3} t_{exp}) + (\tilde{a}\phi_g)_{exp}\, t_{exp}]\,/(t_{exp} + t_{col})$$

where $\dot{M}_{ev}(sp)$ is the evaporation rate of the original undisturbed cloud and $(\tilde{a}\phi_g)_{col}$ and $(\tilde{a}\phi_g)_{exp}$ are respectively the values of the reduction factors from Table 3 evaluated during the collapse phase and the expansion phase. It is readily apparent that for $N_{fr} \sim 5\,\langle \dot{M}_{ev} \rangle$ is little different from $\dot{M}_{ev}(Sp)$ so that the cloud dynamics may not be of major importance in determining the net evaporation rate.

4.3 COMPOSITE CLOUDS; ENVELOPE STRIPPING

McKee & Ostriker (1977) proposed that interstellar clouds were composite consisting of a warm partially ionized envelope maintained by the interstellar UV and soft X-ray flux, surrounding a cold neutral core. Subsequently, Chièze & Lazereff (1980) have demonstrated that (a) such a cloud envelope is efficiently removed by passing SNR blast waves and (b) that the time-scale for the reformation of such an envelope by photoionization is long compared to the shock repetition time. Our work confirms both these latter findings.

The first conclusion, that of efficient envelope removal, rests on the very different velocities imparted to the low density material of the envelope and the dense material of the core on passing through an SNR blast wave. An approximate estimate of the velocity imparted to a single density cloud on passage through an adiabatic blast wave is obtained simply by application of momentum conservation,

$$V_{cl} \sim 0.9\,(n_c/n_{cl})\,(r_c/R_{cl})\,[(r/r_c)^{-4/3} - M_{bc}^{-2}]\,M_{bc}\,C_{cl} \qquad r \leqslant r_c\,.$$

This expression in which n_c is the mean density in the SNR interior just before the remnant cools makes allowance for the enhancement of the interior density by evaporation (McKee & Ostriker 1977). In the post-cooling ($r > r_c$) case the remnant evolves with approximately constant momentum so this equation with $r = r_c$ still applies. Comparison with more careful calculation (McKee *et al.* 1978) suggests that although this certainly gives a slight overestimate it does give the correct dependence on n_{cl} and R_{cl}. For the standard ISM parameters of Table 1 we obtain $V_{cl} \simeq (80\,\mathrm{pc}/R_{cl})\,\mathrm{km\,s^{-1}}$ for warm clouds and $V_{cl} \simeq (0.5\,\mathrm{pc}/R_{cl})\,\mathrm{km\,s^{-1}}$ for cold clouds.

These values exceed those obtained by Chièze & Lazareff from a similar analysis because they used the expression for M_{bc} given by McKee & Ostriker (1977) which contains a numerical error, leading to an underestimate of M_{bc} by a factor of 2.

We expect this to give a reasonable estimate of the differential velocity imparted to a cloud envelope relative to the core. This clearly indicates that any warm envelope can be removed completely from the average cold cloud of McKee & Ostriker (1977) in a time shorter than the shock repetition time unless some agency such as a magnetic field acts to retain it. Some of the warm material might be trapped at the front of the cloud but this material is likely to be compressed and collected into the dense clump.

We have already given an expression for the growth time of an equilibrium warm envelope in Section 3.3. This differs slightly from that given by Chièze & Lazereff (1980) since they assumed a plane parallel envelope. For the value of the ambient UV flux given in Table 1 this expression gives a value for the envelope growth time a factor of ~ 100 longer than the SNR shock repetition time for the smallest clouds of McKee & Ostriker (1977) which have $R_{env} \sim 2$ pc and $R_{cl} \sim 0.4$ pc. For McKee & Ostriker's cloud spectrum (see their Appendix B) the quantity R_{env}^3/R_{cl}^2 has a minimum for clouds ~ 1.6 times as massive as the smallest clouds. Even there, however, assuming the average UV field leads to an envelope growth time a factor of 10 longer than the repetition time. We have compared the values of the shock repetition time and the envelope growth time for all our galactic three-phase ISM Models (Brand & Heathcote 1982) and find that this conclusion holds everywhere. We have also considered the effects of the local enhancement of the UV flux in an SNR cavity during the period of shell formation. Even then the envelope growth time remains long compared to the shock repetition time.

It thus seems that cold clouds cannot retain an equilibrium warm envelope if current estimates of the shock repetition rate are correct. If, as we believe, a significant filling factor for warm material is essential, both to account for observations and for a proper theoretical understanding of the global properties of the ISM we must look for another means of providing it. Cox (1979) has already pointed out that compressional heating of clouds can convert some cold clouds into warm clouds. He has also (Cox 1981) suggested that if a galactic fountain operates, material returned to the disc will generally be warm. We further note that the cooling time from ~ 10^4 to 10^2 K for the quite tenuous material which forms the 'cool dense' shells of SNRs which evolve in a three-phase ISM is very long. Hence, we tentatively suggest these shells as an alternative site for warm cloud formation. This will be discussed further in a future paper.

4.4 CLOUD COMPRESSIONAL HEATING

Cox (1979) has suggested that the PV work done upon clouds when overrun by SNR blast waves may represent an important source of thermal energy for clouds and a significant energy sink for SNR. The compressional work done by the external medium during the collapse phase is particularly simple to work out for our model since the pressures driving the cloud shocks are assumed constant. If the cloud re-expands the work done back on the external medium by the cloud should be subtracted from this (the cloud re-expands at a pressure near P_{ic}). The results of such calculation are summarized in Table 4. As is to be expected these results are very similar to those obtained by Cox (1979) for the corresponding case. Our values are slightly higher because Cox assumed the cloud shocks to be driven by the thermal pressure of the external medium while we have included a ram pressure contribution for the main cloud shock which does most of the work.

Table 4. The PV work done on the cloud during the collapse phase δW_{col} and by the cloud tail during the re-expansion phase δW_{exp} (Section 4.4).

γ_{cl}	γ_{ic}	$\delta W_{col}/(4\pi/3 R_{cl}^3 P_o)$	$\delta W_{exp}/(4\pi/3 R_{cl}^3 P_o)$
1	1	$M_b^2 [M_b^4 (M_b + 3) + 3M_b + 1]/(M_b + 1)^3$	$0.1 F$
1	$5/3$	$3 M_b^2$	$0.1 F$
$5/3$	1	$2 M_b^2 [M_b^4 (M_b + 2) + 2M_b + 1]/(M_b + 1)^3$	$0.1 F[C(0)/C_{cl}]$
$5/3$	$5/3$	$2 M_b^2$	$0.1 F[C(0)/C_{cl}]$

5 Conclusion

We have constructed a highly simplified analytical model of the interaction of an SNR blast wave with an interstellar cloud based on the detailed numerical calculations of Woodward (1976, 1979). This model permits extrapolation of Woodward's results to other values of the parameters of the shock and the cloud. Under the assumptions made the dynamics of the interaction are determined completely by three parameters; the Mach number of the incident shock, M_b, the cloud radius, R_{cl}, and the ratio of the cloud to intercloud sound speeds A. Further, when A is small as is often the case the dependence on this parameter is quite weak. The scaling with R_{cl} and M_b is found to be quite simple.

Any theoretical advance in this area is likely to require a fully three-dimensional computation with at least as great a resolution as that employed by Woodward in his two-dimensional calculations (the utility of calculations at lower resolution is put in question by the importance of small-scale instabilities of the cloud boundary).

We have imposed the conditions believed to prevail in a 'realistic violent' three-phase interstellar medium upon our model in order to assess the importance of processes not included in the model (e.g. a high shock repetition rate, thermal evaporation etc) and to determine the effect of the cloud dynamics on processes important to the global properties of the ISM (evaporation, cloud crushing etc). We conclude that:

(i) If current estimates of the rate at which a given interstellar cloud encounters SNR shocks are correct, then a shocked cloud is rarely allowed sufficient time to relax back to pressure equilibrium with its surroundings before being overrun by another shock. Large departures from pressure equilibrium are expected, and the dynamics and properties of a given cloud will generally depend in a complex way on its past history. Nevertheless, we expect our model to be qualitatively correct under a wide variety of conditions.

(ii) The final product of the interaction is a highly flattened disc of material which is easily disrupted by Rayleigh–Taylor instabilities, and a rather extended cloud 'tail' expanding in the downstream direction. Each component is generally expected to contain ~ ½ the mass of the original cloud. This process of shock ablation may represent an important mechanism for cloud disruption. If it is then the half life of the cloud is comparable to the shock repetition time.

(iii) Although the flattening and compression of clouds overrun by SNR shocks reduces the evaporation rate below that for a static spherical cloud this is probably compensated by enhancement of the evaporation rate due to the fragmentation of the disc.

(iv) Warm envelopes are efficiently removed from cold cores by SNR shocks and require a time considerably longer than the shock repetition time for their recreation by ionization. Nevertheless, a warm low density component of the ISM is observed, and is necessary for proper theoretical understanding of its global properties. Three-phase models of the ISM are almost certainly sufficiently 'robust' to overcome this difficulty (we have suggested some tentative mechanisms for the production of warm material, and will pursue this matter further in a future paper).

(v) The expected rate of PV work done by SNR on clouds for our model is similar to that found by Cox (1979).

While the assumption of pressure equilibrium is useful in simplifying the study of interstellar conditions, the prevalence of shock waves in the ISM requires that considerable caution be exercised in employing it. Many, or most, clouds should be observed to have structures rendered complex by being associated with 'tails', with shock ablated material, and with partially reformed envelopes, and by having one or more shock waves traversing

their interiors. It appears that the 'warm envelope' of the three-phase model does not exist, but that if warm material is created elsewhere – as it must be – then despite these complications a three-phase model can adequately explain the current state of the ISM.

References

Bradley, J. N., 1962. *Shock Waves in Chemistry and Physics,* Methuen, London.

Brand, P. W. J. L. & Heathcote, S. R., 1982. *Mon. Not. R. astr. Soc.,* **198,** 545.

Bychcov, K. V. & Pikel'ner, S. B., 1975. *Sov. Astr. Lett.,* **1,** 14.

Chièze, J. P. & Lazereff, B., 1980. *Astr. Astrophys.,* **91,** 290.

Cowie, L. L. & McKee, C. F., 1977. *Astrophys. J.,* **211,** 135.

Cowie, L. L. & Songaila, A., 1977. *Nature,* **266,** 501.

Cox, D. P., 1979. *Astrophys. J.,* **234,** 863.

Cox, D. P., 1981. *Astrophys. J.,* **245,** 534.

Currie, I. G., 1974. *Fundamental Mechanics of Fluids.* McGraw-Hill.

Dyson, J. E. & Gulliford, P., 1975. *Astrophys. Space Sci.,* **37,** 477.

Gerwin, R. A., 1968. *Rev. Mod. Phys.,* **40,** 652.

Imshenik, V. S., 1960. *Soviet Phys. Dokl.,* **5,** 253.

Kahn, F. D., 1972. In *Interstellar Matter, Second Advanced Course of the Swiss Society of Astrophysics and Astronomy,* p. 343, Geneva Observatory.

McKee, C. F. & Cowie, L. L., 1975. *Astrophys. J.,* **195,** 715.

McKee, C. F., Cowie, L. L. & Ostriker, J. P., 1978. *Astrophys. J.,* **219,** L23.

McKee, C. F. & Hollenbach, D. J., 1980. *A. Rev. Astr. Astrophys.,* **18,** 219.

McKee, C. F. & Ostriker, J. P., 1977. *Astrophys. J.,* **218,** 148.

Savage, B. D., Bohlin, R. C., Drake, J. F. & Budich, W., 1977. *Astrophys. J.,* **216,** 291.

Sgro, A. G., 1975. *Astrophys. J.,* **197,** 621.

Silk, J. & Solinger, A., 1973. *Nature Phys. Sci.,* **244,** 101.

Spitzer, L. Jr., 1978. *Physical Processes in the Interstellar Medium,* Wiley, New York.

Thorogood, P. J., 1979. *PhD thesis,* University of Leeds.

Woodward, P. R., 1976. *Astrophys. J.,* **207,** 484 (W76).

Woodward, P. R., 1979. *The Large Scale Characteristics of the Galaxy, IAU Symp. 84,* p. 159, ed. Burton, W. B., Reidel, Dordrecht, Holland (W79).

Zel'dovich, Ya. B. & Raizer, Yu. P., 1968. *Elements of Gasdynamics and the Classical Theory of Shock Waves,* Academic Press, New York.